Design, analysis, testing and applications of two-body and three-body kinematic mounts

PAR

Johannes Richard Cornelis Geerit KRUIS

To my family, friends and love

Blazing gratefulness

From every nook and cranny of my fiery beating heart. It is with blazing gratefulness that I impart.
That the winding paths I have travelled, and uncharted waters on which I am yet to embark.
With south of me the splendor of the white Alps and north the boundless flat orange horizons that ignited my spark.
All of this would merely be but a smoldering ember without the smiles, candor, love and warmth that you upon me bestow.
Therefore it is to you, my radiant family, friends and love, that the increasingly brilliant burning of my flame I owe.
Hence it is with a glistening smile and ardent thank you that I desire.
To briefly stand still and let you know how much I appreciate and marvel at our dazzling bonfire.

Abstract

Kinematic couplings are used when two rigid bodies need to be repeatedly and accurately positioned with respect to each other. They allow for sub-micron positioning repeatability by suppressing play and reducing strains in the bodies. Typical applications are lens mounts, work piece mounts and docking interfaces for astrophysics, semiconductor and metrology applications. This thesis generalizes the well-known concept of two-body kinematic couplings to three-body kinematic mounts. The goal of the thesis is:

To pave the way for high precision assembly using kinematic mounts by providing an exhaustive catalogue of all two-body and three-body kinematic mounts and to test key configurations experimentally.

The main contributions of this thesis are:

- State of the art survey of essential knowledge in the field of kinematic couplings.

- Rigorous problem statement for the design of two-body and three-body kinematic mounts.

- Rigorous limitation of the scope of research to three-body kinematic mounts whose contact points lie exclusively on three convergent orthogonal lines and whose constraint lines are parallel to these lines.

- An exhaustive catalogue of three-body kinematic mounts consisting of seven configurations in 3D and nine configurations in 2D.

- An exhaustive set of four conditions satisfied by three-body 3-dimensional kinematic mounts.

- An exhaustive set of seven conditions satisfied by three-body 2-dimensional kinematic mounts.

- Realization of a two-body kinematic mount and a three-body kinematic mount in metal, and precise measurement of their positioning accuracy on a 3D coordinate measurement machine at the Swiss Federal Institute of Metrology. Positioning error of 0.2 microns and 5 μradian achieved with two-body kinematic mounts. Positioning error of 1 micron and 50 μradian achieved with three-body kinematic mounts.

- Realization of three-body kinematic mounts in Silicon by Deep Reactive Ion Etching processes (DRIE) and experimental measurement of their positioning error.

- Physical implementation of nesting forces and assembly methods allowing for the physical construction of kinematic mounts.

- Physical realizations in robotics, optics and aerospace using our new kinematic mounts.

Keywords: Kinematic coupling, Kinematic mount, Contact point, Exact constraint, Constraint line, Alignment method, Precision fixturing, Precision engineering, Kinematic design, Micron-level positioning error.

Version abrégée

Les montures cinématiques isostatiques servent au positionnement précis et univoque de deux corps rigides, l'un par rapport à l'autre. Elles permettent d'obtenir des répétabilités de positionnement submicroniques en éliminant tout jeu et en réduisant les efforts mécaniques dans les corps. Elles sont utilisées typiquement pour la fixation de composants optiques comme des lentilles ou des miroirs, ou aux interfaces d'amarrage des mécanismes de précision utilisés en métrologie dimensionnelle et dans les machines de production des semi-conducteurs. Cette thèse généralise le concept bien connu des montures cinématiques isostatiques entre deux corps, au cas encore inexploré de trois corps en contacts mutuels.

L'objectif principal de cette thèse est le suivant :

Ouvrir la voie à l'assemblage isostatique de haute précision de corps multiples en contacts mutuels, en fournissant un catalogue exhaustif de toutes les montures cinématiques isostatiques à deux corps et à trois corps, et tester expérimentalement certaines configurations clés.

Les principales contributions de la thèse sont les suivantes :

- Une revue de l'état de l'art dans le domaine des montures cinématiques isostatiques.

- L'énonciation rigoureuse de la problématique de la conception des montures cinématiques isostatiques à deux corps et à trois corps.

- Une limitation rigoureuse du champ de recherche aux montures cinématiques isostatiques à trois corps dont chacun des points de contact sont localisés sur l'une de trois lignes orthogonales convergentes et dont les chacune des lignes de contrainte sont parallèles à l'un des axes de ce trièdre.

- Un catalogue exhaustif de montures cinématiques isostatiques à trois corps constitué de sept configurations tridimensionnelles (espace) et neuf configurations en bidimensionnelles (plan).

- La liste exhaustive des quatre conditions que doivent satisfaire les montures cinématiques isostatiques tridimensionnelles à trois corps.

- La liste exhaustive des sept conditions que doivent satisfaire les montures cinématiques isostatiques bidimensionnelles à trois corps.

- La réalisation de deux montures cinématiques à deux et trois corps en matériaux métalliques, ainsi que la mesure de leur précision de positionnement, à l'Institut Fédéral de Métrologie (METAS) sur une machine de mesure dimensionnelle équipée d'un palpeur 3D dont la précision est de 50 nm. Une erreur de positionnement de 0.2 micron et 5 microradians a été mesurée sur la monture à deux corps. Une erreur de positionnement de 1 micron et 50 microradians a été mesurée sur la monture à trois corps.

- La réalisation de montures cinématiques isostatiques à trois corps en silicium par gravure profonde (Deep Reaction Ion Etching, DRIE) et la mesure expérimentale de leur erreur de positionnement.

- L'implémentation physique des forces de précharge et des méthodes d'assemblage permettant la construction physique des montures cinématiques isostatiques.

- L'application de ces nouvelles montures cinématiques isostatiques innovantes à des prototypes réels dans les domaines de la robotique, de l'optique et de l'aérospatial.

Mots-clés: Monture cinématique, Monture isostatique, Point de contact, Ligne de Contrainte, Méthode d'alignement, Montage de précision, Mécanique de précision, Conception cinématique.

Zusammenfassung

Kinematische Kopplungen werden verwendet, um zwei starre Körper mit hoher Wiederholgenauigkeit in Bezug zueinander zu positionieren. Durch die Unterdrückung jeglichen Bewegungsspiels und der Reduktion von körperinternen Spannungen können wiederholgenaue Positionierungen im Submikrometerbereich erreicht werden. Typische Anwendungen sind Linsenfassungen, Werkstückhalterungen und Docking-Schnittstellen für Astrophysik, Halbleiter und Metrologie Anwendungen. Diese Dissertation verallgemeinert das bekannte Konzept der kinematischen Kopplung zweier Körper, und erweitert dieses auf die gegenseitige kinematische Kopplung dreier Körper (→ Kinematic Mounts). Es werden Fälle sowohl in der Ebene, wie auch im Raum behandelt. Das Ziel der Arbeit kann wie folgt formuliert werden:

Diese Dissertation soll im Bereich der hochpräzisen Montage mit kinematischen Befestigungen dienen, durch die Bereitstellung eines vollständigen Kataloges aller kinematischen Zwei-Körper-und Drei-Körper Mounts, sowie der experimentellen Prüfung der wichtigsten Konfigurationen.

Die wichtigsten Beiträge dieser Arbeit sind:

- Einen Überblick der Stand der Technik der wesentlichen Kenntnisse im Bereich der kinematischen Kopplungen zu verschaffen.

- Eine präzise Problemstellung für die Gestaltung von kinematischen Zwei-Körper- und Drei-Körper-Mounts zu erörtern.

- Den Themenumfang auf kinematische Drei-Körper Mounts zu beschränken, deren Kontaktpunkte ausschließlich auf drei konvergenten orthogonalen Linien liegen, und deren Constraint-Linien parallel dazu sind.

- Einen umfassenden Katalog von sieben Konfigurationen mit kinematischen Drei-Körper-Mounts im Raum und von neun Konfigurationen mit kinematischen Drei-Körper-Mounts in der Ebene.

- Einen umfassenden Katalog von vier Konditionen, die durch kinematische Drei-Körper-Mounts im Raum erfüllt werden.

- Einen umfassenden Katalog von sieben Konditionen, die durch kinematische Drei-Körper-Mounts in der Ebene erfüllt werden.

- Die praktische Implementation eines kinematischen Zwei-Körper-Mounts und eines Drei-Körper-Mounts aus Metall, sowie dessen präzisen Ausmessung der Positioniergenauigkeit auf einer 3D-Koordinatenmessmaschine am „Eidgenössischen Institut für Metrologie" (METAS). Positionierungsfehler von 0,2 Mikrometer und 5 Mikroradian wurden mit einem kinematischen Zwei-Körper-Mount gemessen. Positionierungsfehler von 1 Mikrometer und 50 Mikroradian wurden mit einem kinematischen Drei-Körper-Mount gemessen.

- Die praktische Implementation von kinematischen Drei-Körper-Mounts aus Silizium mit „Deep Reactive Ion Etching Processes" (DRIE) gefertigt, inklusive Genauigkeitsmessung ihrer wiederholbaren Positionierung.

- Methoden zur Erzeugung der Andruckkräfte und Montagevorschläge für den praktischen Aufbau eines kinematischen Mounts.

- Anwendungsbeispiele in den Bereichen der Robotik, der Optik und der Luft- und Raumfahrt, welche neue, innovative kinematische Mounts verwenden könnten.

Stichworte: Kinematische Kopplung, Kinematische Mount, Constraintbedingungen, Zwangsbedingungen, Präzisionsmechanik, Wiederholgenauigkeit, Submikrometer, Präzisionsengineering

Acknowledgements

Acknowledgements

Table of contents

Chapter 1   Introduction

This thesis consists of novel contributions to the field of *kinematic mounts* which consist of an arbitrary number of bodies *aligned* with respect to each other. Within the scope of the thesis, *alignment* is defined as the positioning of rigid parts with respect to each other. Figure 1.1. shows the successive phases of an *assembly process*: *manipulation*, *alignment*, *attachment* and *assessment*. Manipulation is the action of placing parts with respect to each other in order to bring them into an aligned state. To keep the parts in their aligned state after manipulation, a *nesting force* is required. Attachment is the action fastening the bodies to each other. When parts are attached, the nesting force can be suppressed. Assessment is the action of verifying via a practical inspection if a set of bodies assembled correctly. In the case of kinematic mounts assessment consists in verifying that all the contact points are effectively in physical contact. This thesis addresses exclusively the alignment and attachment phases.
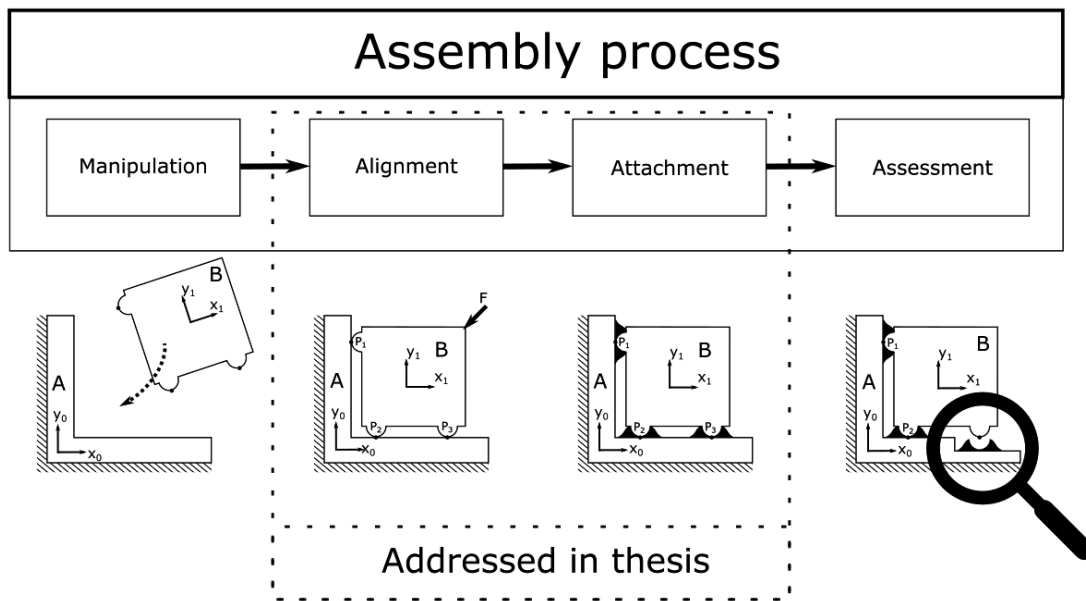
Figure 1.1: The four successive phases of an assembly process. This thesis addresses exclusively the alignment and attachment phases.

In 1830, André-Marie Ampère published his **"Essai sur la philosophie des sciences"** where he introduced the word *Kinematics* (after the Greek word for movement "kínima") as the branch of classical mechanics that focuses on the motion of points, bodies and configurations of multiple bodies. *Kinematic design* is the use of kinematics for conceiving instruments, devices and machinery. The central concept behind kinematic design is that every rigid body has a limited set of independent movements, called *degrees of freedom* (DOFs).

The term *Degree of Freedom* was first defined in Thomson and Tait's 1867 book "Treatise on natural philosophy." In their work the authors noted that a point and body in 3-dimensional space have, respectively, three and six DOFs. Both the point and the body have three perpendicular translations as DOFs. The body has an additional three rotational DOFs, e.g., around three perpendicular axes. If we constrain the movement of a body or point we call this a *Degree of Constraint (DOC)*. We use of *contact points* and *nesting forces* for the DOCs. Contact points are the points where two bodies touch and kept touching by nesting forces. A contact point can either add one degree of constraint or result in a redundant constraint if other contact points exist.

Kinematic design is the art of choosing DOCs and allowing desired DOFs of a configuration of rigid bodies, without any redundant constraints. The advantages of kinematic design are the following: stresses are well-defined by nesting forces, thermal centers are known (a point in space which does not vary in position under homogeneous thermal expansion [1]), accurate and repeatable alignment is possible, sensitivity to manufacturing tolerances is reduced as are manufacturing costs. The merits of kinematic design have made it an essential tool in the field of precision engineering. The principle of kinematic design has been discussed extensively in scientific articles and textbooks [1]–[13].

A notable example of kinematic design is the *kinematic coupling*. A kinematic coupling is obtained when kinematic design is used to constrain exactly once each relative motion between a *pair* of rigid bodies. A kinematic coupling therefore defines exactly the position of the two bodies with respect to each other. The origin of kinematic design and kinematic couplings is not clearly known [14], however, two of the earliest mentions of kinematic couplings are by Maxwell [2] and by Thomson and Tait's 1879 edition of their "Treatise on natural philosophy"[12]. The two different kinematic couplings (Figure 1.2) are: the Three-Vee coupling and the Tetrahedron-Vee-Flat coupling.

This thesis extends for the first time the concept of kinematic coupling to *triples* of rigid bodies. The more general concept of *kinematic mount* is introduced to designate the kinematic assembly of two *or more* parts in such a manner that each of the relative DOFs of all the parts is constrained exactly once.
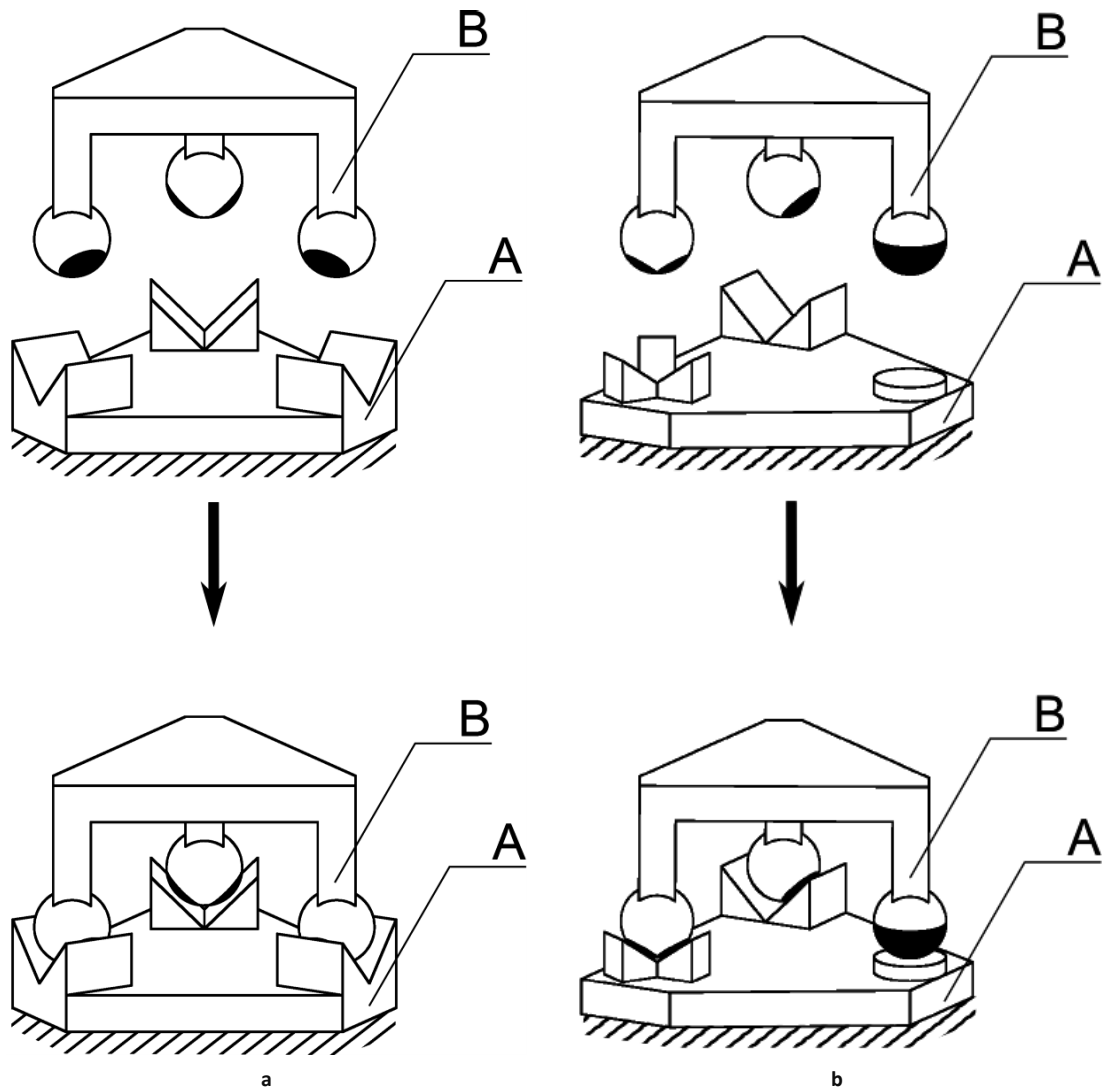
Figure 1.2: a) Three-Vee kinematic coupling between rigid bodies A and B. b) Tetrahedron-Vee-Flat coupling between rigid bodies A and B.

1.1 Benefits of kinematic mounts

The benefits of kinematic mounts are illustrated by comparing them with other classical alignment methods such as dowel pins, elastic averaging and actuated alignment. To explain these concepts, we give a set of illustrative examples. An over-constrained configuration has more constraints than the minimum required (Figure 1.3).

<div align="center">a   b</div>
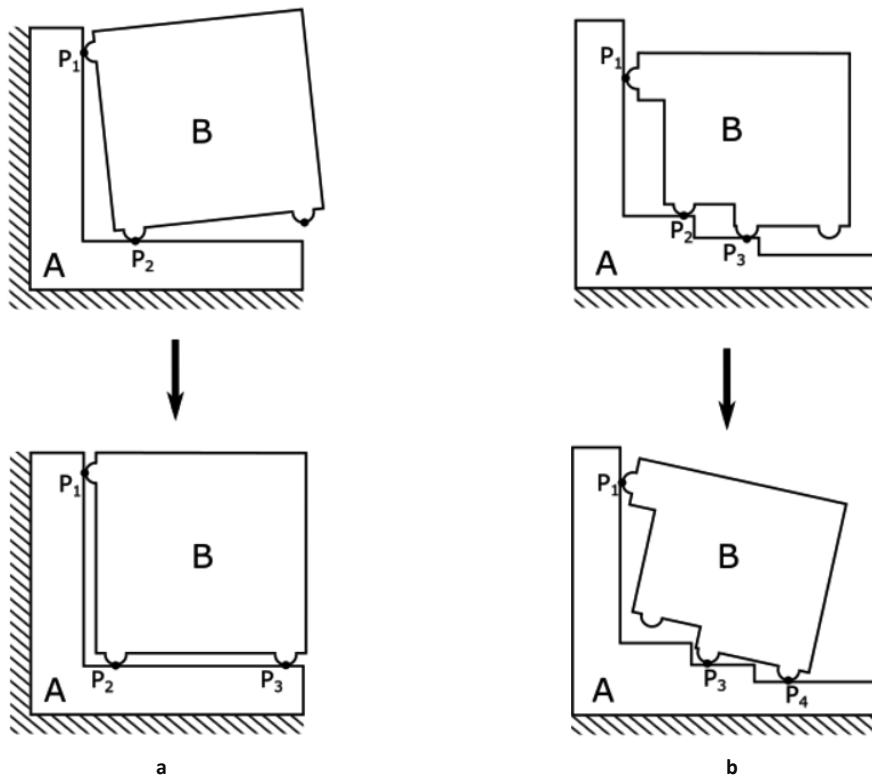
Figure 1.3: a) Exactly-constraint configuration (valid kinematic coupling): all contact points are able to make contact, assuming the bodies are infinitely rigid. b) Over-constrained configuration: if the bodies are infinitely rigid, all contact points cannot be in contact at the same time (not a kinematic coupling).

Dowel pins usually involve tight fit; this means that, by definition, they are redundantly constrained assemblies (Figure 1.4a). This means that tolerances on the dowel pin and hole are tighter and additional stress is induced on the assembly. Elastic averaging (Figure 1.4b) usually makes use of a large series of compliant elements which align the part by; a famous example of elastic averaging is LEGO®. Actuated alignment typically involves a closed-loop feedback to control the DOFs between two parts -- though this can be quite efficient, it typically adds cost and complexity to the design.

1.1.1 Benefits of kinematic mounts compared to over-constrained assemblies

Sub-micron position error: The work of Slocum [15] and Ziegert [16], among others, shows that kinematic couplings can achieve sub-micron positioning error over thousands of assembly cycles.

Exact-constraint design: Since kinematic mounts are exactly constrained they lead to a deterministic positioning of rigid bodies, i.e. if the position of the contact points is known, then the position of the bodies is known.

Localized mechanical assembly stresses: When the nesting force is known the stress at the contact points can be calculated using Hertzian contact theory. The stress effects are concentrated in the vicinity of the contact points. Exact constraint and well-defined local stress are crucial for assembly of optical components for example whose optical properties must not be affected by the assembly process.

Well defined thermal center: As kinematic couplings are exactly constrained they allow for an exact determination of the *thermal center* [1] of the coupling. The thermal center of a body is the point in space associated to the body which undergoes no displacement with respect to a fixed external frame as the assembly undergoes thermal expansion or contraction. For example, locating the thermal center of an optical component onto its optical axis decreases significantly the sensitivity of the optical properties of an opto-mechanical system to temperature changes.

Reduced risk of blocking or jamming during assembly: The assembly of a kinematic mount can be seen as a step by step decrease of the DOFs of the assembly bodies. This means that each contact point exactly removes one degree of freedom. Therefore, kinematic mounts allow for easy assembly of bodies. Typical problems that can occur during assembly, such as parts blocking or jamming half way along the trajectory to the desired position, can thus be avoided. As with classical assembly, the main non-repeatability is surface to surface friction at the contact point. However, when the interfaces are carefully considered and lubrication is used, then sub-micron positioning errors can be achieved [15].

Reduced sensitivity to manufacturing tolerances: Designs using too many constraints require tight tolerances to allow the parts to fit. Kinematic mounts put the minimal number of constraints on a rigid assembly and relax tolerances of designs. Typically, this results in parts with lower manufacturing cost.

Scalability: Kinematic mounts can be applied to scales ranging from millimeters up to meters. The main limitations are the Hertzian stress of the contacts and assuring that the nesting force is the dominant force so that the mounts are aligned properly.

Disadvantages of kinematic mounts compared to classical assembly methods (Figure 1.4 a & b)
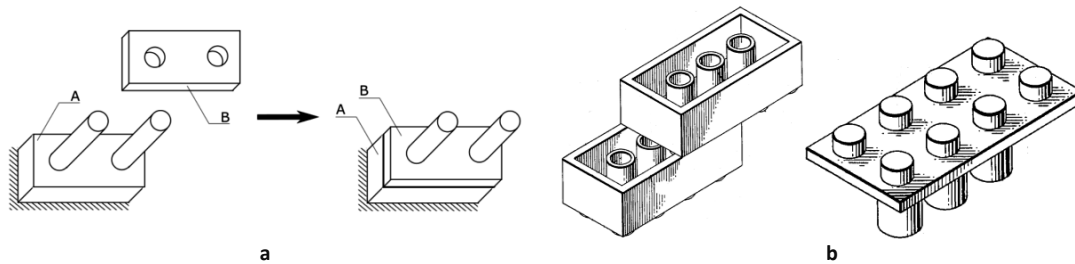
Figure 1.4: a) A dowel pin assembly, b) An assembly making use of elastic averaging, as used in LEGO®, image adapted from [17].

Lower loading capability: As the stress is concentrated in the vicinity of contact points, heavy loads or shocks can lead to plastic deformation of the contact areas. Stress can thus become a limiting factor in the design of kinematic couplings. *Quasi-kinematic mounts,* where contact lines and arcs are used instead of contact points [18] lead to reduced local contact stresses. Elastic averaging assembly methods lead to even wider distributions of loads, and therefore lower local stress levels.

Complex assembly: Kinematic mounts are sometimes considered more complex than classical dowel pin assemblies. The latter is preferred in cases where the positioning tolerances are not too stringent. This thesis describes kinematic mounts where the contact points are directly integrated during manufacturing (Chapter 13) thus considerably reducing the complexity of assembly.

Summary

Though kinematic mounts can sometimes be more complex and can permit lower loads than classical assembly methods, they have shown to be a very versatile and simple concept for achieving micron and sub-micron positioning errors. Their deterministic positioning yields a well-defined thermal center [1], reduces risk of blocking and jamming, and reduces sensitivity to manufacturing tolerances. Moreover, they provide a scalable design concept. The final decision of whether to apply kinematic mounts primarily depends on the specifications and manufacturing methods of the application.

1.2   Goal of thesis

The main objective of this thesis is

> **To pave the way for high precision assembly by providing an exhaustive catalogue of all two-body and three-body kinematic mounts and to test key configurations experimentally.**

This thesis provides engineers and scientists with the tools to enable them to apply kinematic mounts to their own work. These tools allow them to easily align three bodies as well as more complex assemblies using kinematic mounts. These tools consist of a set of conditions and a catalogue of solutions.

The pursuit of this objective has also resulted in several demonstrators pushing the limits of Silicon assembly. Kinematic mounts are interesting for Silicon since contact points can be directly incorporated during DRIE thus allowing simple and repeatable assembly of Silicon bodies. The results of this thesis can be used to design interfaces for assembly at the millimeter scale and upwards and provide the necessary tools for repeatable positioning.

1.3   Scope of the thesis

Kinematic mounts: This thesis addresses exclusively kinematic designs in which each degrees of freedom of each individual part is constrained exactly once. Other alignment methods, in particular kinematic design incorporating redundant constraints or degrees of freedom, are excluded from the scope of the thesis.

Contact points: The physical elements used to create contact points are exclusively solid spheres resting on a flat surface. Contact points concern exclusively pairs of bodies. Contact points shared by three bodies or more are excluded from the scope of the thesis.

Nesting forces: Nesting forces are not addressed in the theoretical part of this thesis. The practical implementation of nesting forces required to perform the experiments is described in Chapter 11, covering the experimental part of this thesis.

Number of bodies: The thesis addresses exclusively two-body and three-body kinematic mounts.

Orthogonal constraint lines: For 2-dimensional configurations, all constraint lines are either parallel or orthogonal to each other. For 3-dimensional configurations, all constraint lines are parallel to any one of the three orthogonal convergent lines on which the contact points lie.

Location of the contact points: For three-body 3-dimenional kinematic mounts, the thesis is limited to cases where all contact points lie on three orthogonal convergent lines. If A, B and C are the three rigid bodies, and α, β and γ are the three convergent lines, then all contact points between A and B lie on α, all contact points between B and C lie on β and all contact points between A and C lie on γ. Moreover, contact points lying on the intersection of the three convergent lines are excluded.

Manufacturing process: The primary focus is on implementing these approaches to the assembly of Silicon components. In addition, we show some applications of this work that are manufactured using classical machining.

Materials: The material used throughout this work is primarily Silicon. 3-D printed plastics and two demonstrators based on classically machined metals are also presented.

Applications: The applications given in this work are mostly related to out of plane MEMS assemblies. Our approach can nevertheless be applied in all domains where kinematic mounts are used. It is specifically useful for parts made with 2D and 2.5D manufacturing processes[1]. Two specific fields of application of kinematic mounts are reconfigurable robotics and reconfigurable optical systems.

Friction: Friction effects are neglected in the theoretical part of the thesis. Though friction is a very important part of kinematic mount non-repeatability, no direct experiments were made with respect to it in the context of this work.

---

[1] By a 2D manufacturing process we refer to processes that are unable to machine in the third dimension. 2.5D manufacturing processes usually manufacture by stacking layers of 2D parts, but are significantly limited in the number of layers.

Stiffness: The stiffness of the rigid bodies and of the contact points is considered to be infinite.

1.4 Thesis overview

The thesis is divided into two parts:

The first part is **theory** (Chapters 3 to 9) which starts with definitions then considers 2-dimensional and 3-dimensional configurations first presented as explanatory figures. We then introduce the conditions and conjectures required to obtain these configurations and classify all solutions in terms of a limited set of kinematic mounts. This structure was chosen to get directly to a description of the results.

The second part of the thesis is **applications** (Chapters 10 to 13). The applications start with a set of 3-D printed demonstrators used as an illustration and first verification of the configurations discussed in the theory part. Chapter 11 discusses several examples of assembly methods by applying nesting forces or fixing bodies. Chapter 12 describes the experiments and evaluates statistically the positioning error of the configurations. Chapter 13 finishes up the thesis with a discussion of applications of the theory.

Chapter 2 State of the art

2.1 Chapter overview

This chapter presents an overview of prior art including historically significant work and the more recent advances in the field of kinematic design, kinematic couplings, kinematic analysis and their applications.

2.2 Kinematic design

The concepts of kinematic design have been applied for the last 250 years, but there are also indications that they were known long before [14]. There is a large literature discussing classical kinematic design [1-13]. Here we first offer an overview of three classical applications of kinematic design, the three point support, the five point linear guide and the five point rotational guide. We recall some of the most recent works attempting to characterize all possible kinematic interfaces. Lastly we discuss work on kinematic assembly in general.

2.2.1 The three contact point support

The three contact point support is a well-known concept in present-day precision engineering. The commonly used example is a wobbly rigid four-legged table having one leg not touching the ground. In this case one of the legs is always too short with respect to the three others leading to a wobbly table. With only three legs this would not be the case thereby illlustrating the concept of a three contact point support.

A three contact point support blocks two rotations and one translation, without redundancy, thus avoiding play or undesired stress. According to Evans [14], three contact point supports were common in early scientific instruments and horological tools. A historical example that benefited from three contact point supports is the marking of graduations in measuring instruments, typically made laboriously by hand. This meant that instruments such as sextants had to be necessarily large (typically 400 mm radius) to allow accurate markings. The European magazine and London review of February 1789 [65] describes the problem as follows:

"The reflecting quadrant, or sextant of Hadley, so much used by English seamen, appeared to Mr Ramsden the most useful instrument of its kind; but it was at this time extremely imperfect. The essential parts of it had not a sufficient degree of solidity; the friction at the center was too great, and in general the alidada[1] might be moved several minutes without any change in the position of the mirror; the divisions were commonly very inaccurate, and Mr Ramsden found that Abbé de la Caille[2] did not exceed the truth in estimating at five arcminutes[3] the error to which an observer was liable in taking the distance between the moon and a star; an error capable of producing a mistake of fifty leagues[4] in the longitude."

---

[1] Alidada is also known as the index arm of a sextant allowing to move the index mirror of a sextant and index the angle of an object of interest with respect to the horizon mirror. The word comes from the Arabic word "al idada", meaning "ruler"
[2] Nicolas Louis de la Caille a French astronomer and priest.
[3] One arcminute equals one sixtieth of a degree.
[4] One league is approximately 5.5 kilometers.

In 1777, Jesse Ramsden addressed the problem with his circular dividing engine (Figure 2.1), a device to mark graduations on measuring instruments. The instrument allowed for the mass production of smaller, lighter and more accurate sextants and octants. The design of the circular dividing engine makes use of two three contact point supports by having a three-legged frame and having three friction rollers, indicated by the W in Figure 2.1. This avoids play and thus errors in marking the graduations.

a	b
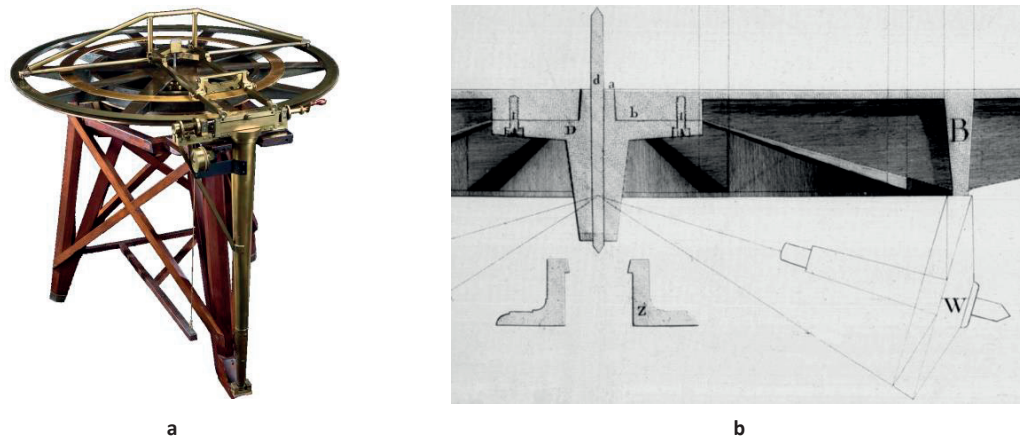
Figure 2.1: The three-legged circular dividing engine. a) shows an overall displaying the three-legged mount of the setup (This image is reprinted with the permission and is courtesy of the time and navigation collection, Division of Medicine & Science, National Museum of American History, Smithsonian Institution [68]), b) shows a cross-sectional view displaying one of the friction rollers W and its contact with the wheel B of the dividing engine (This image is reprinted from [69]).

2.2.2 The five contact point linear guide

A second example of kinematic design is the five contact point linear guide illustrated in Figure 2.2.

a	b	c
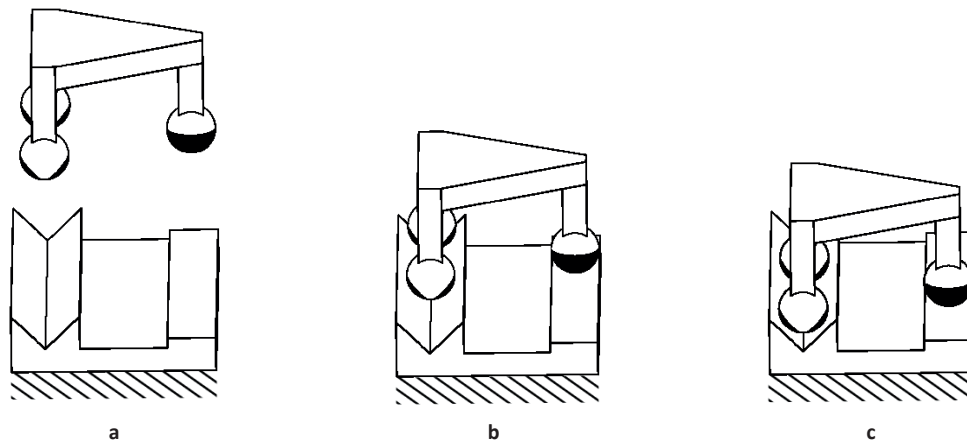
Figure 2.2: Linear guide mechanisms (see Bassière and Gaignebet [8] for more of such examples). a) The unassembled linear guide as applied to the Wilkinson lathe[5]. b) The assembled linear guide in one position c) The linear guide in another position.

An early example of the application of the five contact point linear guide is the Wilkinson lathe[5] for cutting screw threads. According to Robert S. Woodbury in his study of the history of machine tools [19]: "We may credit David Wilkinson with being the founder of the American machine-tool industry." The Wilkinson lathes were a success; in 1848 US government workshops alone had more than 200 such lathes. A principle feature of Wilkinson's lathe was a linear guide patented by Wilkinson in 1794 [20], this linear guide is a key example of early kinematic design. The linear guide consists of a Vee slideway with a total of four contact points and a flat slideway with one contact point. These kind of mechanisms were discussed by many including Maxwell [2] and Thomson & Tait [12].

---

[5]A lathe is a machine in which a piece of wood or metal is rotated around a horizontal axis while being shaped by a sharp fixed tool.

2.2.3   The five contact point rotational guide

In Bassière and Gaignebet's work [8], several examples of five contact point rotational guides are given, here illustrated in Figure 2.3.
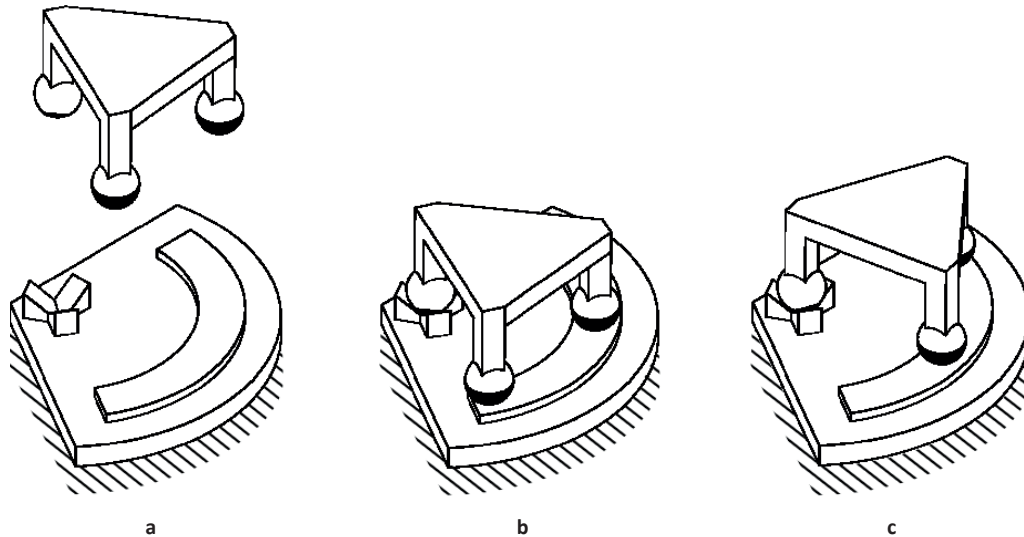
Figure 2.3: Rotational guide mechanisms based on contact points (see Bassière and Gaignebet [8] for more of such examples). a) An unassembled tetrahedron and two flats rotation guide. b) The assembled rotational guide c) The assembled displaced rotational guide.

2.2.4   Characterization of possible interfaces

Efforts have recently been made to characterize all possible interfaces between two bodies, with resulting degrees of freedom (DOFs) ranging from 0 to 5. Though this work was started by Blanding [10] and Philips [7], a more recent effort made by Hopkins [21] offers a full overview of all possible interfaces, and, using Screw Theory [22], he classified all possible families of constraints naming his exhaustive catalogue Freedom and Constraint Topologies (FACT). The resulting topologies of his work are illustrated in Figure 2.4. This figure has six columns each divided in a right and left part. The right part always contains the constraint topologies indicated by blue lines. The left part contains topologies consisting of green and red lines and black arrows. The blue colored lines indicate constraint lines, the red colored lines axes of rotation, the green lines screw motions (a combination of a rotation and translation) and the black arrows indicate allowed translations. For every constraint topology indicated in blue lines there is a freedom topology. Though the generic examples are the drawings using screws, indicated in green lines, Hopkins also indicates whenever possible the freedom topology of as many as possible rotational constraints. The black arrows in the freedom topologies indicated allowed translations. This limited set of options excludes constraints applied by friction so lends itself ideal for the constraints imposed by contact points. And thus can be viewed as an exhaustive set of possible interfaces of contact points between two bodies in 3D.
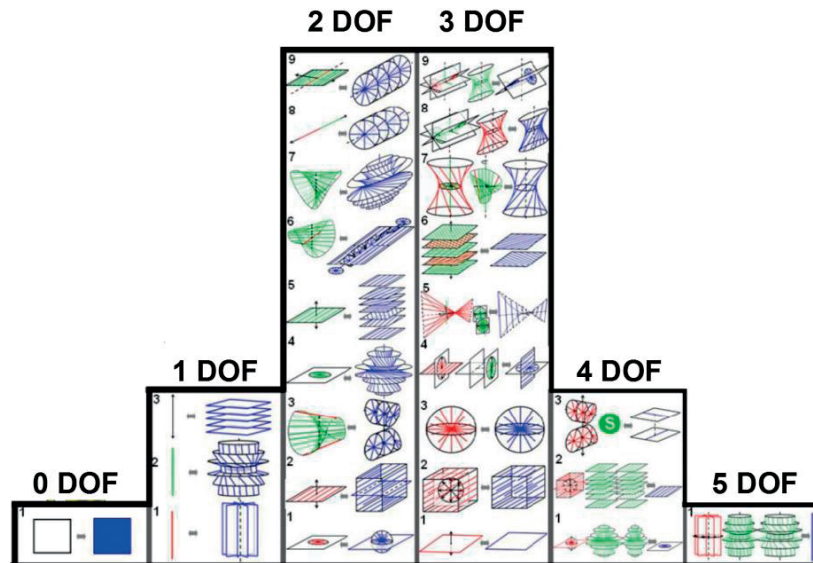
Figure 2.4: FACT, The possible Freedom and Constraint topologies of an interface between 2 bodies ranging from 0 to 5 DOFs. The figure consists of a total of 6 columns indicating the degrees of freedom of the topologies presented. The left hand side of the column illustrates the freedom topology consisting of a combination of red and green lines and black arrows. The red lines indicate rotational axes along which the parts are allowed to rotate with respect to each other. The green lines indicate lines in which a screw motion can be realized by the bodies with respect to each other. The black lines indicate pure translations that the bodies can make with respect to each other. The right-hand side of each column illustrates the constraint space spanned by constraint lines between the two bodies. This graphic can be further simplified by realizing that every rotation is a screw with a pitch of 0 and every translation is a screw with an infinite pitch. This chart offers an exhaustive set of the possible options of freedom and constraint topologies between two bodies. Image reprinted from Precis. Eng., vol. 38, no. 3, J. B. Hopkins, J. J. Vericella, and C. D. Harvey, Modeling and generating parallel flexure elements, pp. 525–537, 2014, with permission from Elsevier [71].

2.2.5   Kinematic assemblies

An interesting method going beyond kinematic couplings was proposed by Whitney [23], where he discusses using screw theory in the context of verifying the constraints of an assembly and then applies it to assemblies. Though he doesn't develop this into an exhaustive solution catalogue, the principal idea is to make assemblies that, from a kinematic point of view, are thought through. This is an interesting example of applying kinematic design to realize static complex assemblies.

2.3   Kinematic couplings

The first written examples of kinematic couplings were given by James Clerk Maxwell and William Thomson (Lord Kelvin). The well-known configurations are illustrated in Figure 2.5. The idea is to fix body B by means of six contact points, in other words, a kinematic design with zero degrees of freedom and six contact points.
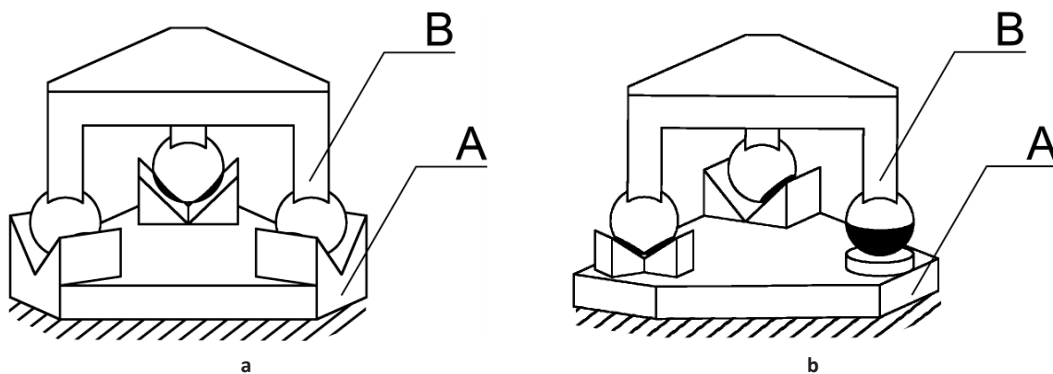
Figure 2.5: The two well-known kinematic couplings: a) shows a three-Vee kinematic coupling and b) displays the tetrahedron, Vee, flat coupling.

2.3.1   Design

Maxwell [3] compares two kinematic couplings stating that the Three-Vee coupling has the advantage of being symmetric. For the Tetrahedron-Vee-flat he states that it is easy to put the right feet at the right contact and avoid erroneously changing the contact pairs.

Research regarding the Tetrahedron-Vee-flat coupling appears to be rather limited. The only result reference found was by Sherrington & Smith [24] where they constructed a kelvin clamp made of bright annealed mild steel. To realize the tetrahedral hole they used a couple of 3 pointed set screws. The average position error they obtained ranged from 1.8 micron to 3.5 micron. The 3σ bounds on the position error (three times the standard deviation) ranged from 6.2 µm to 10 µm. They were limited by the quality of their measurement equipment, as they used image correlation techniques with an unspecified sensor to determine position.

In his work, Maxwell introduced the following condition for optimizing a kinematic coupling:

> *"Each constraint should be aligned to the local direction of motion allowed by the five other constraints, assuming that they remain in contact and are free to slide."*

Maxwell also referred to R.S. Ball's Treatise on screw theory [22] for a better understanding of this condition. In Figure 2.6 we illustrate Maxwell's condition applied to two bodies in 2D. In the correct example Figure 2.6a we see that no matter which contact point we remove, the local motion at the removed contact point is exactly aligned with the constraint line of the point. In the incorrect example Figure 2.6b this is not the case. This becomes clear if one removes contact point 1 the local motion direction illustrated by the two-sided arrow is not collinear with the constraint line that contact point P_1 has.
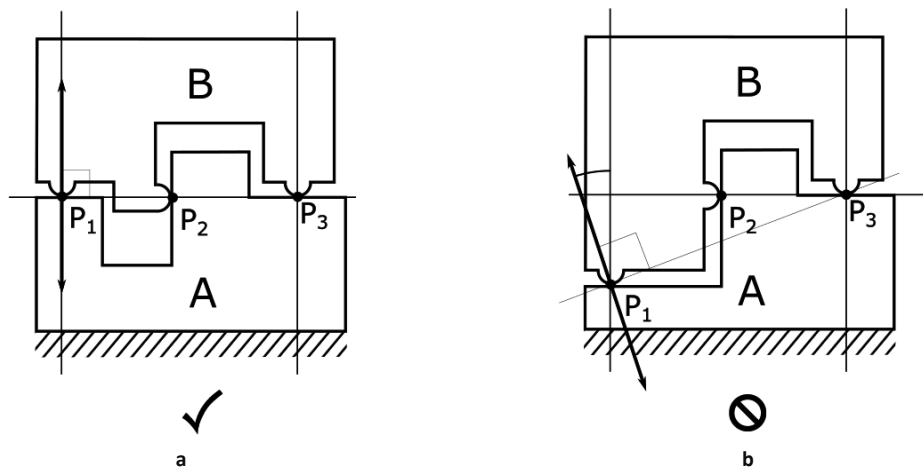
Figure 2.6: a) Maxwell's condition applied correctly. The motion allowed when contact point 1 is removed indicated by the two-sided arrow is collinear with the constraint line of contact point P_1 (the solid line that traverses body A and B at P1), b) Maxwell's criterion applied incorrectly, this is still a kinematic mount but is not optimal, the two-sided arrow is not collinear with the constraint line originating from contact point P_1.

The stability of kinematic couplings with friction is given in Soemers [1]. For three-dimensional couplings, Slocum [18] provides a graphical criterion based on the planes containing the constraint lines of Vee grooves. Figure 2.7 illustrates this for a vertical Three-Vee kinematic coupling, where, for visibility reasons, body B connecting the three spheres B_1, B_2 and B_3 is omitted. The most stable configuration occurs when the contact point is in between the intersection lines of the planes containing the contact forces. This is shown in Figure 2.7a where a small triangle illustrates the planes of the contact forces. In Figure 2.7b a marginally stable variant is shown, the planes of this coupling are intersecting in three lines of which one is at infinity. Figure 2.7c shows the least stable variant where the planes defined by the constraint lines of spheres B_2 and B_3 have all intersections on a single side of the sphere.
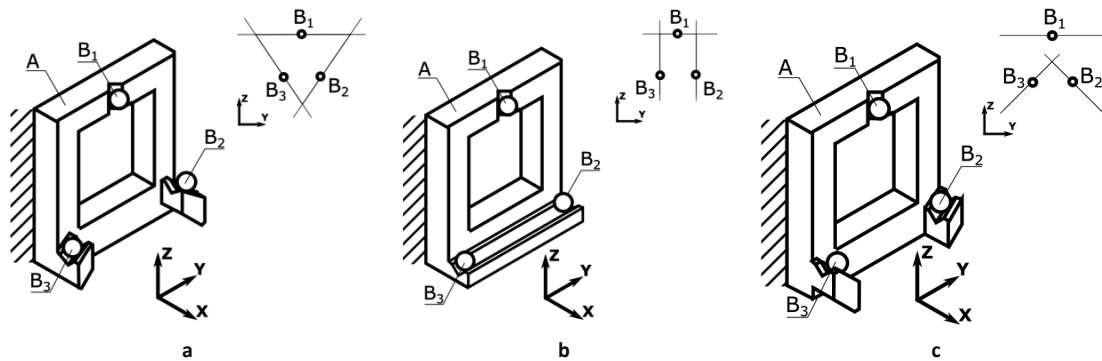
Figure 2.7: a) The most stable variant of the kinematic coupling. The small figure in the top right corner illustrates a view on the YZ plane on the planes defined by the constraint lines of the spheres. As the contact point is in between the intersection lines of the planes defined by the constraint lines, this variant is considered stable. b) A marginally stable kinematic coupling. Here the planes of B_2 and B_3 are parallel (intersect at infinity). The least stable variant where the contact points of B_2 and B_3 are not located in between the intersection lines of the planes. This image is reprinted from Precis. Eng., vol. 14, no. 2, A. H. Slocum, Design of three-groove kinematic couplings, pp. 67-76, 1992, with permission from Elsevier [25].

Slocum [25] discusses that to obtain the most optimal stiffness of a coupling in all directions the normal to the planes containing the constraint lines should be parallel to the angle bisectors of the lines between the balls. If this is not taken into account non-equal stiffness will be the result.
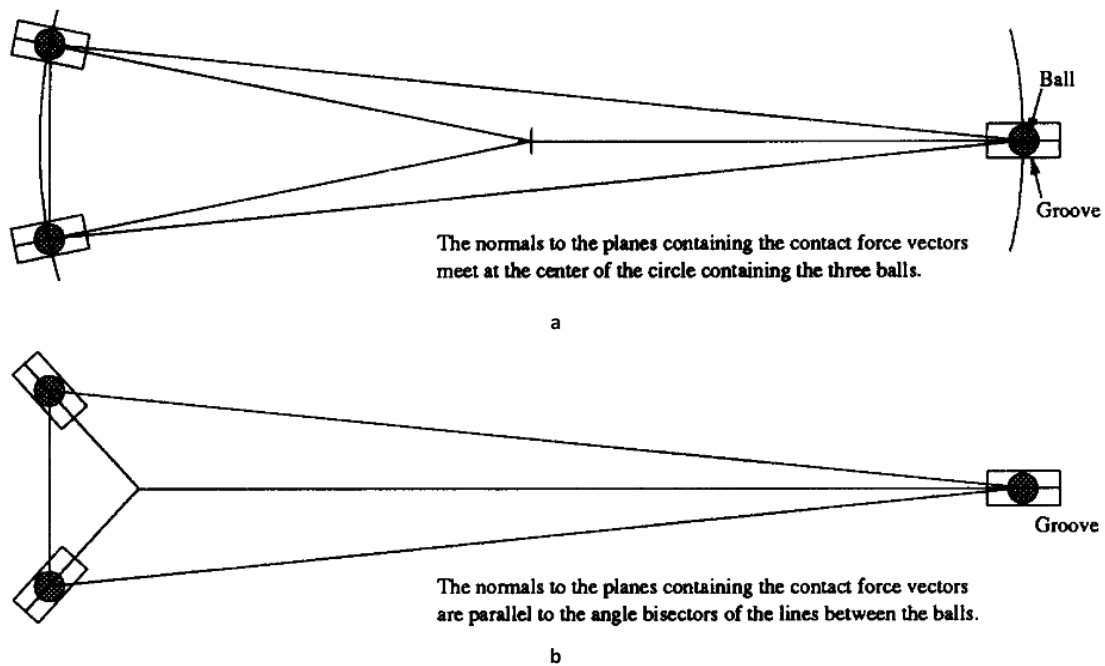
Figure 2.8: a) A coupling with a non-equal stiffness as the normal of the planes of the constraint lines intersect at the center of the circle containing the three balls. b) A coupling with equal stiffness as the normal of the planes containing the contact forces are parallel to the angle bisectors of the lines between the balls. This image is reprinted from Precis. Eng., vol. 14, no. 2, A. H. Slocum, Design of three-groove kinematic couplings, pp. 67-76, 1992, with permission from Elsevier [25].

The paper continues to offer the formulas for determining the contact forces, contact stresses and the deflections at the contact points and the six error motion terms of three groove couplings based on the force and moment equilibrium

More work on the design of kinematic couplings was done by Slocum [26], [27] and Hale [13, 70]. Hale [70] presents interesting recent results optimizing kinematic mounts by defining four criteria for the optimization of kinematic couplings. Applying these criteria to a symmetric Three Vee kinematic coupling, he then optimizes Vee groove angles to balance these criteria. The first is Maxwell's criterion, illustrated in Figure 2.6, which states that the inner product of a vector along the

constraint line and the direction of motion for each contact point should be maximized to 1. Hale also maximizes modal frequency, minimizes frictional non-repeatability and maximizes the limiting coefficient of friction.

The performance of kinematic couplings is given by Slocum [15] and Ziegert et al. [16]. We offer an overview of the performance of both their systems by comparing them in terms of specifications and performance in Table 2.1.

Table 2.1: Two different papers discussing measurements on Kinematic couplings

Reference	[15]		[16]	
Title	Kinematic couplings for precision fixturing part 2: experimental determination of repeatability and stiffness		Air bearing kinematic couplings	
Author	A. Slocum		J. Ziegert, V. Tymianski	
Type	Three-Vee	Three-Vee	Three-Vee Floating	Three-Vee Air bearing no float.
Contact point sphere diameter	28.6 mm	28.6 mm	25 mm	284 mm
Contact point material	Silicon Nitride balls Hardened steel gothic arc inserts. (17.15 mm radius)		Steal balls Steel flats	N.A.
Part size (distance between two contact points with parallel constraint lines)	Diameter 356 mm		143 mm 116 mm 143 mm	143 mm 116 mm 143 mm
Part material	Thick cast iron discs	Thick cast iron discs	Aluminum Weight 20 kg	Aluminum Weight 20 kg
Number of measurement cycles	600	3000	60	2000
Positioning error	Axial: 0.9μm 3σ Radial: 1.4 μm 3σ Tilt-x ~5 μrad 3σ Tilt-y ~5 μrad 3σ	Axial: 0.3μm 3σ Radial: 0.3 μm 3σ Tilt-x ~1.6 μrad 3σ Tilt-y ~2.8 μrad 3σ	N.A.	N.A.
Maximum linear position variation	Axial 1.3 μm Radial: 1.8 μm	Axial: 1 μm Radial: 0.6 μm	5 μm	2 μm
Maximum angular variation	Tilt-x 7 μrad Tilt-y 7 μrad	Tilt-x: 4.2 μrad Tilt-y: 1 μrad	N.A.	4 μrad
Lubrication	No	Yes	No	No
Nesting force	5800 N	5800 N	180N	180N
Stiffness	Axial: 109 N/μm Radial:158 N/μm	Axial: 109 N/μm Radial:158 N/μm	41 N/ μm	250 N/μm
Noise floor and sensor type	Not mentioned LVDT		18 nm Capacitive	
Comments	+/-1 C temperature stability. Disc raised 13 mm. Used LVDTs for measuring the structural loop. Using relative measurement the thermal expansion is minimized Trihedral holes used with epoxied balls	600 measurements wear in on the lubricated system 0.76 μm axial 0.68 μm radial	Sensor issues over 60 measurements No standard deviation computed. Total number of measurements 1000. Lifted 5 mm.	Lifted 5 mm between cycles Cone shaped holes with balls used

Another improvement of positioning error of kinematic couplings is described by Schouten et al. [28]. They compare the use of a standard Vee groove (Figure 2.5a) to the use of a Vee groove using notch hinges (Figure 2.5b). The principal concept is that the hysteresis caused by friction limits the positioning error of a Three-Vee coupling. The use of notch hinges comes at the cost of the stiffness of the kinematic coupling, in their case by a factor two; however the notch hinges help to increase positioning error by a factor of 14. They illustrate the model of a typical ball in a Vee-groove by a set of springs and a friction element, see Figure 2.5a. They measure the position of their coupling as a function of applied preload and they obtain, for unspecified number of experiments, a hysteresis of 0.42 micron for a standard Vee-groove and a hysteresis of 0.03 micron for a Vee-groove using notch hinges. The number of measurements is not specified. For their experiment they use steel cemented carbide balls and glue steel cemented carbide tiles on the surfaces of the Vee-grooves. They record preload versus vertical displacement as illustrated in Figure 2.5c.
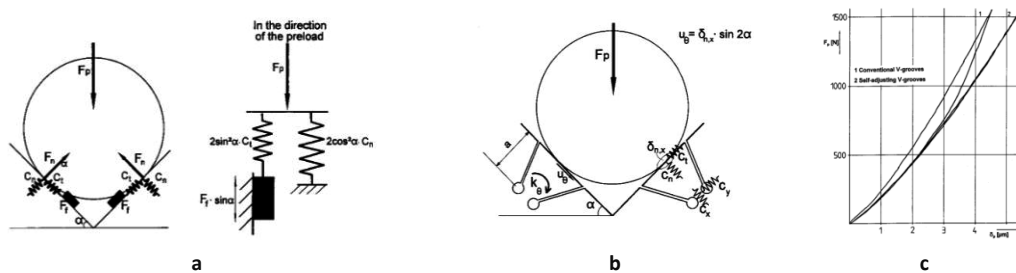
Figure 2.9: a) A model illustrating the position non-repeatability of a single contact as a function of tangential stiffness, axial stiffness and friction. b) They propose to reduce the effects of the friction by implementing notch hinges attached to the contact surfaces. c) shows the force displacement curve of a kinematic coupling with grooves without and with notch hinges. These images are reprinted from Precis. Eng., vol. 20, no. 1, C. H. Schouten, P. C. J. N. Rosielle, and P. H. J. Schellekens, Design of a kinematic coupling for precision applications, pp. 46-52, 1997, with permission from Elsevier [28].

The work of Vallance et al. [29] compares the use of a split groove kinematic coupling, a variant of the Three Vee kinematic coupling, to dowel pins and holes. Their result is that the split groove kinematic coupling obtained +/- 5 micron positioning errors whereas with a similar system using dowel pins and tight fit holes he obtained +/- 50 micron position errors.

Tolerancing of kinematic couplings has been discussed by Barraja et al [30]. Their paper uses multivariate error analysis and nonlinear constrained optimization on Monte Carlo simulation of kinematic couplings. The eventual goal is to minimize the production cost whilst optimizing performance.

In addition to kinematic coupling, the notion of *quasi-kinematic coupling* has been used. The difference is that a quasi-kinematic coupling is typically designed to have contact lines or arcs rather than points. Though in a clean and controlled environment this typically results in slightly worse positioning errors the advantage is that it is less costly and typically easier to machine. A variant of such a quasi-kinematic coupling is Hale's three tooth coupling [13]. Culpepper [18] further expanded the research on quasi-kinematic couplings. The three-tooth coupling and the variants using contact-arcs by Culpepper are illustrated in Figure 2.10.
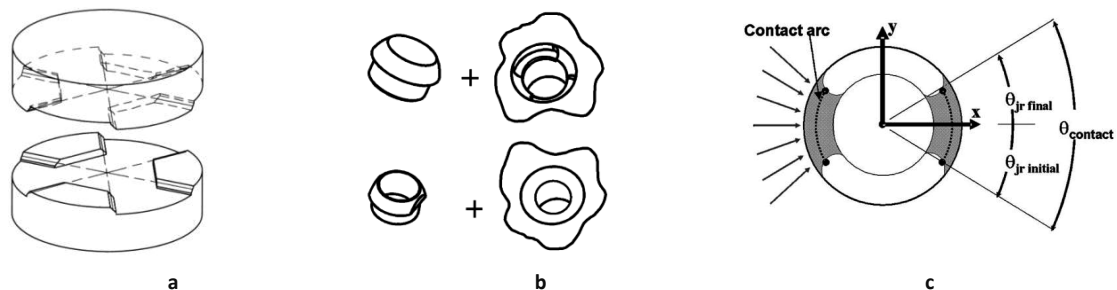
Figure 2.10: a) An illustration of the three tooth coupling with its lines of contact. This image is reprinted from Precis. Eng., vol. 25, no. 2, L. C. Hale and A. H. Slocum, Optimal design techniques for kinematic couplings, pp. 114-127, 2001, with permission from Elsevier [13]. b) An illustration of the contact arcs that are used by Culpepper. This image is reprinted from Precis. Eng., vol. 28, no. 3, M. L. Culpepper, Design of quasi-kinematic couplings, pp. 338-357, 2004, with permission from Elsevier [18] c) illustrates the contact arcs that are applicable to the contacts in Figure 2.20b. This image is reprinted from Precis. Eng., vol. 28, no. 3, M. L. Culpepper, Design of quasi-kinematic couplings, pp. 338-357, 2004, with permission from Elsevier [18].

Other topics such as kinematic coupling interchangeability, for interchanging kinematic couplings in multiple workstation assembly, have been researched by Hart et al. [31]. They concluded that quasi-kinematic couplings provide an equally good performance in environments where cleanliness and variation of preload are less controlled.

In addition, *actuated kinematic couplings,* where the planes or balls are actuated to decrease positioning errors, have been explored by Culpepper [32].

2.4   Kinematic analysis

Kinematic analysis determines the number of DOFs and/or DOCs of a system. A detailed review of kinematic analysis is beyond the scope of this thesis. A summary of some well-known principles of kinematic analysis is given by Spinnler [33]. In his book Spinnler provides equations for the number of Degrees of Freedom of mechanisms in series, mechanisms consisting of closed chains and mechanisms with complex chains. These formulas are inspired by works of Chebyshev, Grübler and Kutzbach. Unfortunately, these equations cannot be used to determine whether a system is a kinematic mount since, for a kinematic mount, the number of constraints must be exactly equal to the number of possible degrees of freedom, while the inherent assumption to derive these formulas is that the constraints are not redundant, which cannot be proven a priori.

An alternative method is screw theory, as discussed by Whitney [23]. This method verifies both over and under constraint separately and takes into account the geometry of a configuration. The existence of over and under constraint is found by examining whether or not two matrices containing screws are full rank. In other words whether the screws span all necessary constraints required to block all movements of the bodies.

Another method is given by Aarts, et al [34]. A finite element based multibody modelling approach is used, considering elements of low stiffness free and those of high stiffness rigid. In the case of a kinematic mount, the constraint lines of contact points would be considered rigid. They calculate the rank of the Jacobian matrix obtained from a Singular Value Decomposition and when the matrix has full rank, they can determine whether there is a kinematic mount. In the case of an over-constrained system, a statically indeterminate stress distribution is derived. In their paper they show the example of a linear guide mechanism which has both an under and an over constraint.

2.5   Applications

There is a wide spectrum of application of kinematic couplings to the semiconductor industry, as discussed in [35]- [49]. One of these applications is the alignment of wafer pods, the containers used to transport wafers. The reliable alignment of these pods is important as the manufacturing conducted with the wafers in these pods is fully automated. Other notable examples are electrically conductive kinematic coupling grooves [50] [51], in which case verifying that a kinematic coupling is in contact is done by simply measuring whether resistance is finite.

In the field of metrology, kinematic couplings are also quite common. For example in the works of Stein [52] and Werner [53], kinematic couplings are used as sample holders of metrological AFMs used by bureaus of standards in order to allow traceability of other metrological instruments.

In addition, Kinematic couplings have been used as segmented and shielded structures for the high precision microscope project, as described by Hart [54]. Here they serve as thermal insulators (for reducing thermal-expansion induced tilt errors), thermal shielding from outside influences, structural stiffness, a reconfigurable opto-mechatronic assembly and an alignment method with a micron level positioning errors. As the modules are pre-calibrated, they can be easily and quickly interchanged between experiments.
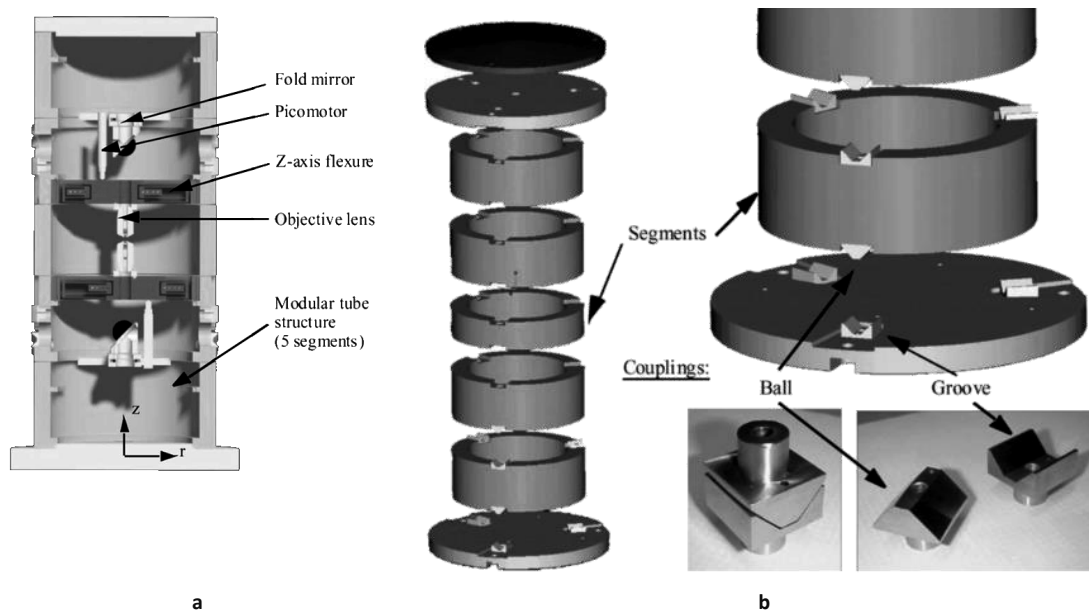
Figure 2.11: a) A set of five segments used for the high precision microscope. b) An exploded view and detail view of the contacts illustrating the stacks of couplings. These images are reprinted from Precis. Eng., vol. 28, no. 4, A. J. Hart, A. Slocum, and J. Sutin, Segmented and shielded structures for reduction of thermal expansion-induced tilt errors, pp. 443–458, 2004, with permission from Elsevier [54].

Also many other optical applications make use of kinematic mounts. Yu et al. [55] discuss using a kinematic mount for the mounting of a lens element.

2.6 Chapter summary

This chapter presented the state of the art of the theory and practice of kinematic couplings from the viewpoint of kinematic design and kinematic analysis. This prior work only considers kinematic couplings of two bodies or stacks of kinematic couplings of two bodies, as compared to this thesis which expands the field of kinematic couplings to more than two bodies (which are not necessarily stacks).

2.7 Closing remark

In their Treatise on Natural Philosophy [12], Thomson and Tait made the following remark about kinematic couplings:

"There is much room for improvement by the introduction of linear guides and kinematic couplings, in the mechanism of mathematical, optical, geodetic, and astronomical instruments: which as made at present are remarkable for disregard of geometrical and dynamical principles in their slides, micrometer screws, and clamps. Good workmanship cannot compensate for bad design, whether in the safety-valve of an ironclad[6], or the movements and adjustments of a theodolite[7]."

Precise and repeatable alignment is to this day an important specification in engineering, robotics, metrology and micro technology applications. The kinematic mounts presented in this work will help to further address these needs.

---

[6]An ironclad is a steam propelled wooden warship or ship of composite construction protected by iron or steel armor plates typically used in the second half of the 19th century.
[7]A theodolite is a precision instrument for measuring angles in the horizontal and vertical planes. Theodolites are mainly used for surveying applications.

Chapter 3   Definitions

This chapter introduces the set of definitions used in this thesis. These definitions are based on elementary point-set topology of standard Euclidean space, as found in any introductory analysis text, for example, [56] .

3.1   Body and configuration

3.1.1   Body

A *body* is defined to be a bounded, open, connected, simply connected set. Bodies are not self-touching, (see §3.2.4 below). Pathological cases will not arise, and bodies are considered to be finite concave unions of finite intersections of the interior of rectangles and open disks (2-D) or cuboids and open balls (3-D). In general, "finite" will actually mean that there will be less than 10 unions and intersections. The boundary consists of a finite number of line segments and arcs of circles and is a simple continuous closed curve and infinitely differentiable (may not be differentiable for a finite set of points, where "finite" means 16 or less) in 2-D and a closed, infinitely differentiable closed surface (possibly not differentiable at a finite set of points). The boundary is therefore considered to be differentiable and a normal is well defined except for the few exceptional points where there is no derivative. A set of bodies is illustrated in figure 3.1.1.
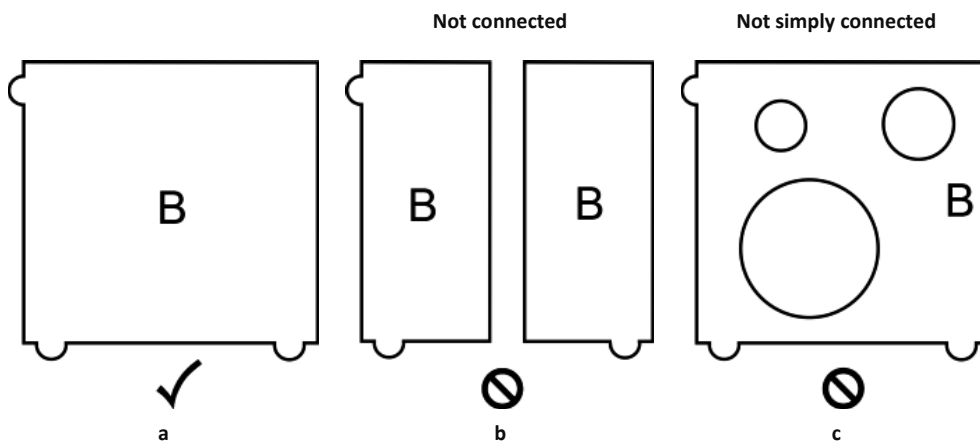
Figure 3.1.1: a) A body consists solely of the interior enclosed by the black line. Bodies are composed of rectangles and open disks (2-D) or cuboids and open balls (3-D); b) A body must be connected, a body such as in this figure is thus not considered in this thesis; c) A body must be simply connected, a body as such as in this figure is not considered in this thesis because it has holes.

3.1.2 Overlap

Bodies do not overlap. Since bodies are open sets, this means that distinct bodies are disjoint, as illustrated in figure 3.1.2a.
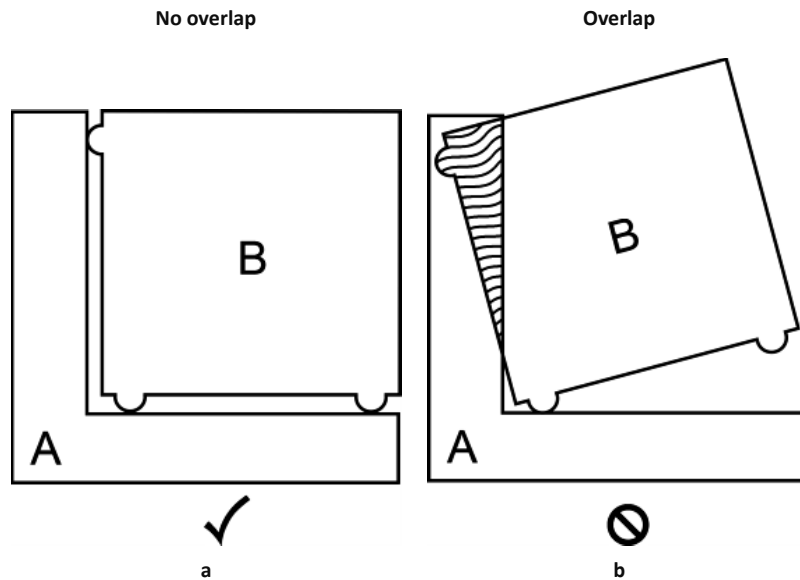
No overlap   **Overlap**

Figure 3.1.2: a) Illustrates two bodies which do not overlap; b) Illustrates two bodies with overlap this does not occur further throughout this thesis.

3.1.3 General configuration

A *general configuration* is a finite collection of bodies, usually considered to be modified as a function of a parameter, which can be taken to be time. An example of a general configuration is offered in figure 3.1.3.
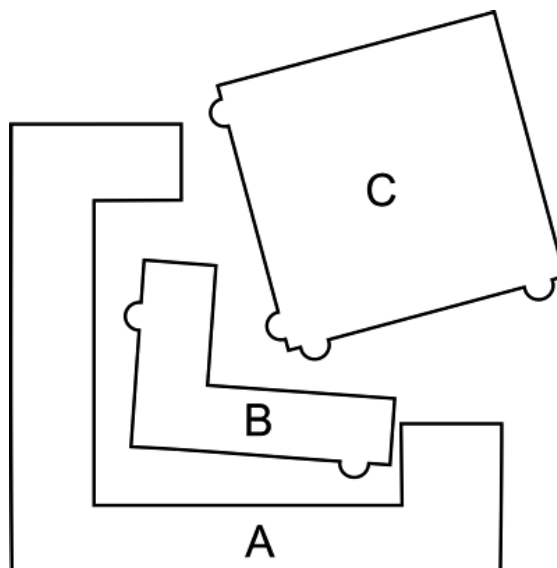
Figure 3.1.3: An example of a general configuration consisting of 3 bodies, A, B and C. The positions of the bodies can be modified in time.

3.1.4   Rigid body

Only *rigid bodies* are considered. That is, for any transformation of a general configuration, represented by a transformation function T_{01}, taking points from the original configuration (t_0) to the modified configuration (t_1), then for any two points, a_1 and a_2, of a body A, one has d=distance(a_1, a_2) = distance($T_{01}(a_1)$, $T_{01}(a_2)$). In all of the cases considered, only orientation preserving transformations will be allowed, that is, bodies will be rotated and translated but not reflected (or possibly all will be reflected). An illustration depicting this is offered in figure 3.1.4.
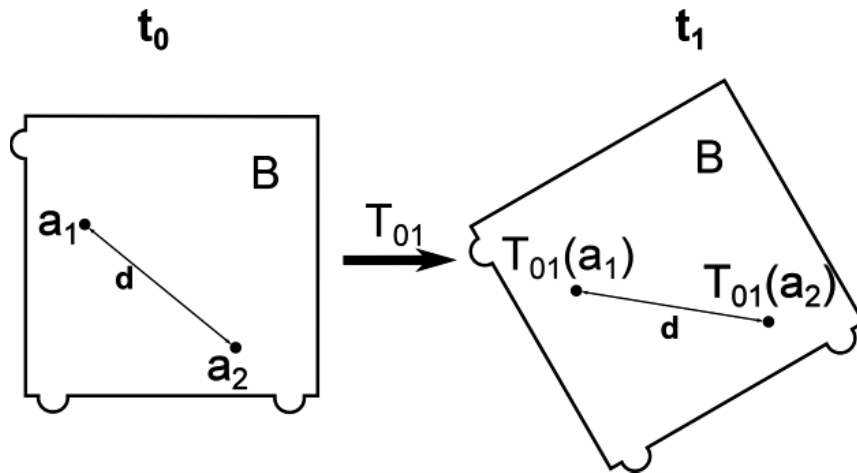
Figure 3.1.4: The bodies considered in this thesis are rigid bodies. That implies that any distance d between two points remains unchanged regardless of the transformation applied to the general configuration.

3.1.5   Fixed base

A body is said to be a *fixed base* when it is unable to change its position for all possible general configurations. In this work we use a hashed marking as depicted in figure 3.1.5.
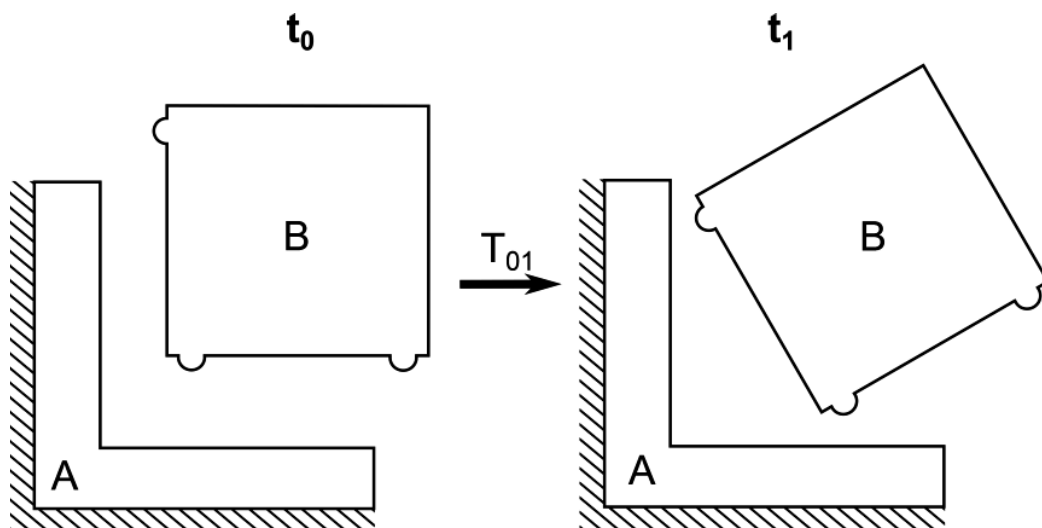
Figure 3.1.5: Fixed base A and body B in two general configurations, regardless of the transformation performed on the configuration fixed base A remains unchanged in position.

3.1.6   (Relative) configuration

A *relative configuration,* or simply *configuration* when no confusion is possible, is defined to be a general configuration in which there is one fixed base. Figure 3.1.6 depicts a relative configuration, as body A is a fixed base.
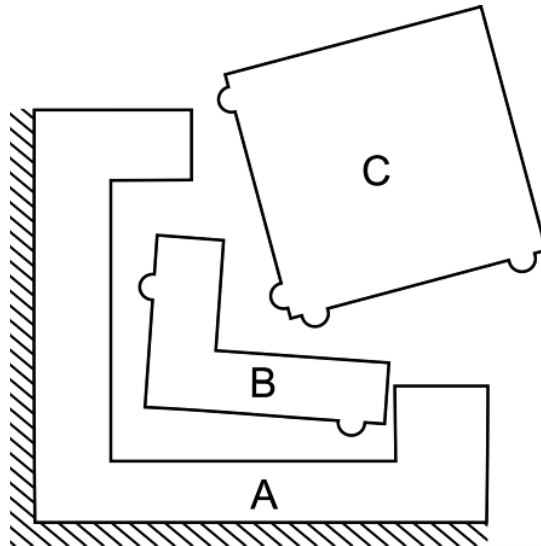
Figure 3.1.6: A (relative) configuration, as body A is a fixed base.

3.2   Contact

3.2.1   Contact point

P is a *contact point* for two distinct bodies, A and B, if P belongs to the closure of A and to the closure of B. In other words, A and B share P as a boundary point. Except for the finite set of points described in 3.1.1 above, the normals of each body at a contact point are collinear. Figure 3.2.1 offers an example of a contact point.
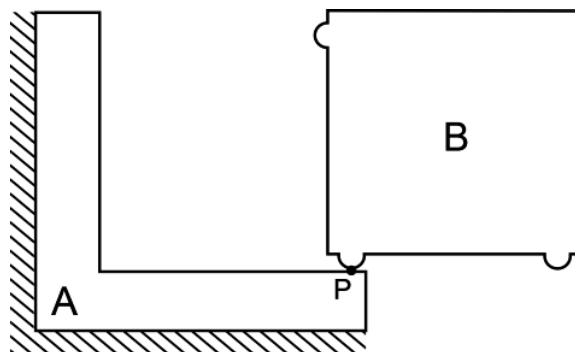
Figure 3.2.1: A contact point P between the bodies A and B.

3.2.2 Contact region

The set S is a *contact region* for two distinct bodies, A and B, if S is a connected set consisting entirely of contact points of A and B. Thus, S is a subset of the boundaries of A and of B. Contact regions are assumed to be simply connected sets, and in practice each simply connected set can be contracted to a point, therefore the contact region will always be considered to be a contact point. Figure 3.2.2 illustrates a contact region.
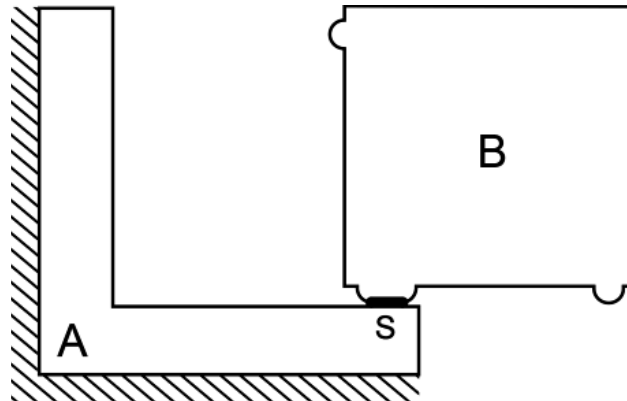
Figure 3.2.2: The contact region S for two bodies A and B, consisting of simply connected set of contact points.

3.2.3 Interface

The set of all contact regions between two bodies, A and B, is the *interface* I_{AB} (Figure 3.2.3).The interface I_{BA} and I_{AB} are the same.

$I_{AB}=\{P_1,P_2,P_3\}$
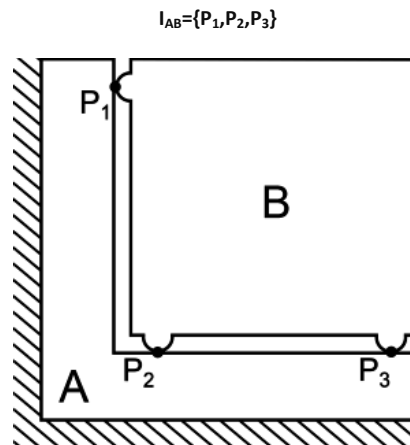
Figure 3.2.3: A general configuration of two bodies A and B having three contact points in interface I_{AB}.

3.2.4 Self-touching

A body D is *self-touching at a point* P in its boundary, if it can be written as the union of two sets B and C, and there is a neighborhood N of P such that B ∩ N and C ∩ N are two distinct bodies having contact point P.

A body is self-touching if there is a point P in its boundary such that the body is self-touching at P. Figure 3.2.4 illustrates this definition.
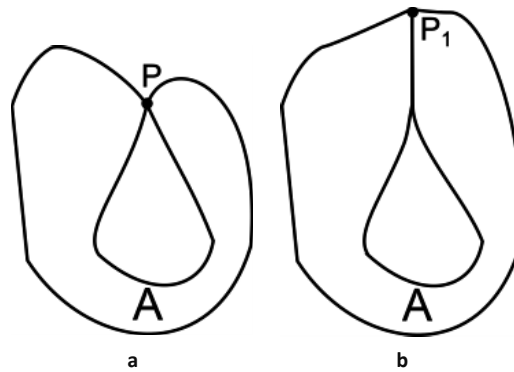
Figure 3.2.4: a) A body A, which is self-touching in P, this is not allowed in this thesis; b) A body A self-touching along a line of contact points, this is not allowed in this thesis either.

3.3 Freedom and constraint

3.3.1 General degree of freedom (GDOF)

The *general degree of freedom (GDOF)* is the number of independent parameters required to uniquely determine a general configuration. The *maximum general degree of freedom* of an n-body general configuration is 3n in 2D and 6n in 3D (Figure 3.3.1).

9 GDOF
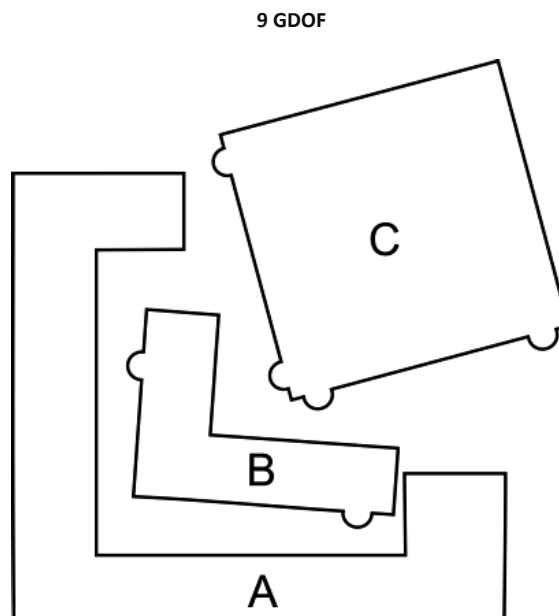
Figure 3.3.1: A general 2D configuration with 9 general degrees of freedom (3 per body).

3.3.2 (Relative) degree of freedom (DOF)

The *relative degree of freedom,* or simply *degree of freedom (DOF)* when no confusion is possible, is the number of independent parameters required to uniquely determine a relative configuration (configuration), with respect to a fixed base (Figure 3.3.2).
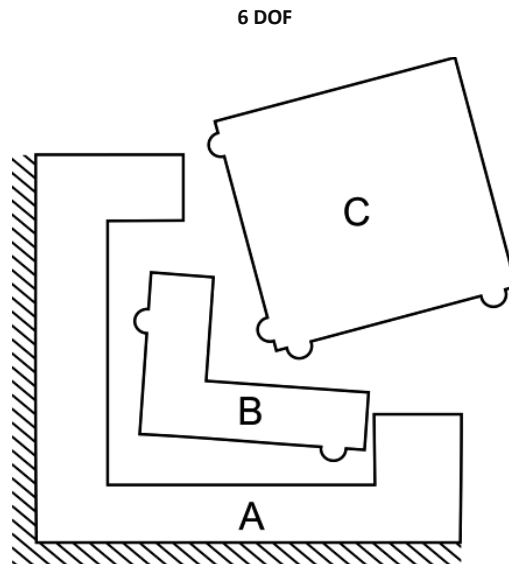
6 DOF

Figure 3.3.2: A relative configuration with fixed base A. This configuration has 6 relative degrees of freedom (6 DOF).

3.3.3 Maximum degree of freedom (MDOF)

The *maximum relative degree of freedom,* or simply *maximum degree of freedom (MDOF)* when no confusion is possible, is the number of independent parameters required to uniquely determine a general configuration (configuration). Fixed bases do not matter for the MDOFs of a system. The MDOF of an n-body configuration is, 3(n-1) in 2D and 6(n-1) in 3D (Figure 3.3.3).
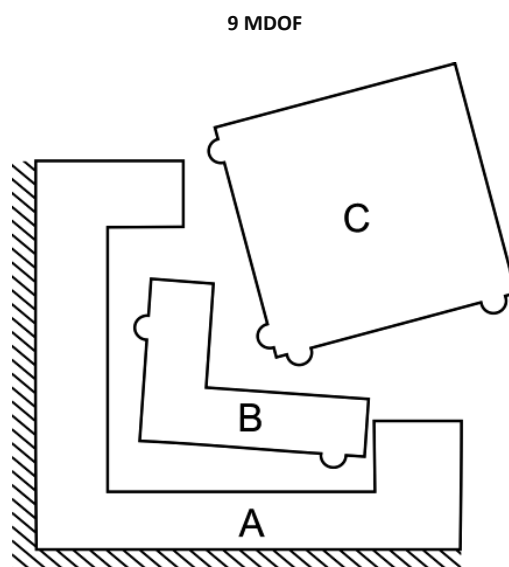
9 MDOF

Figure 3.3.3: A general configuration with fixed base A. This configuration has 9 maximum degrees of freedom (9 MDOF).

3.3.4   Degree of constraint (DOC)

The *degree of constraint* is the reduction in degree of freedom of an n-body configuration from 3(n-1) in 2D or 6(n-1) in 3D. In our case all constraints follow from the specification of an interface, i.e., a set of contact points. Figure 3.3.4 illustrates this definition.
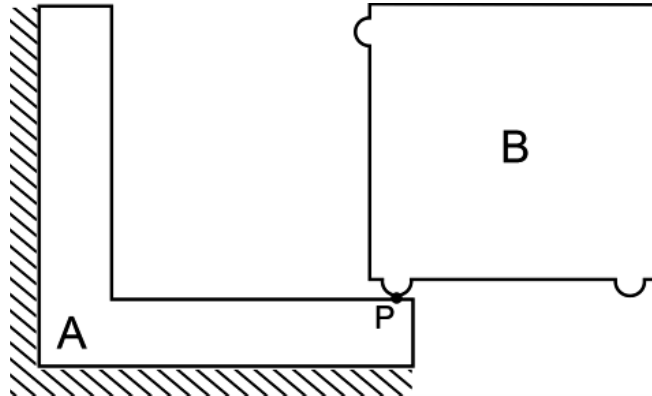
Figure 3.3.4: A relative configuration with body A as a fixed base. This configuration has 1 degree of constraint provided by contact point P.

3.3.5   Constraint line

If P is a contact point of two bodies A and B, then the common line of their normals at P is called the *constraint line* at P of bodies A and B. Figure 3.3.5 illustrates two bodies with a constraint line.
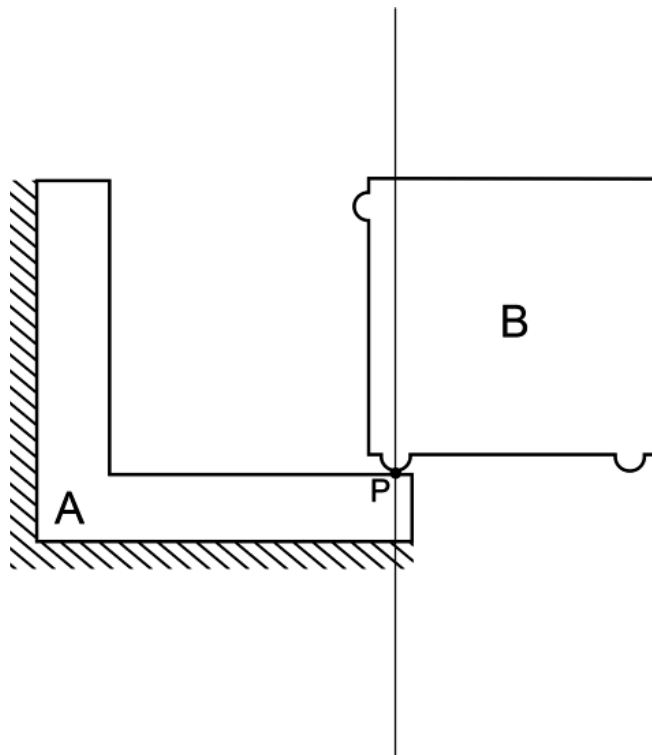
Figure 3.3.5: Two bodies A and B with a contact point P and the constraint line at P.

3.3.6 Virtual pivots

If all constraint lines of an interface I_{AB} intersect in a single point, then the intersection of these constraint lines is called a *virtual pivot* V_1. Figure 3.3.6 illustrates two bodies with a virtual pivot.
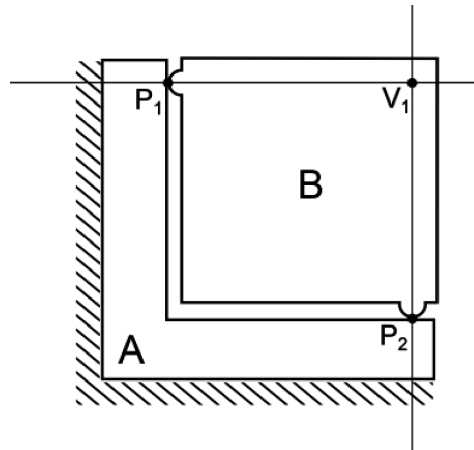
Figure 3.3.6: Two bodies A and B with two constraint lines intersecting at virtual pivot V_1.

3.3.7 Infinite pivots

When all constraint lines of an interface are parallel they intersect at infinity and thus have a virtual pivot at infinity, we name these pivots, *infinite pivots*. Parallel lines intersecting at a point at infinity is discussed in projective geometry, a detailed review on projective geometry can be found in an elementary text such a [57]. Figure 3.3.7 illustrates two bodies with an infinite pivot $V_1^{(\infty)}$
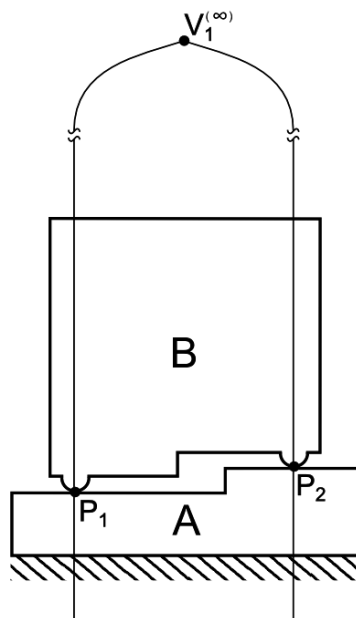
Figure 3.3.7: Two bodies A and B with two parallel constraint lines intersecting at $V_1^{(\infty)}$.

3.3.8 Constraint imposed by a single contact point

The *constraint imposed by a single contact point* P of two bodies, A and B, is a degree of constraint 1, by eliminating a relative translation of the two touching points of bodies A and B along the constraint line at P. We illustrate this in figure 3.3.8. This is made precise as follows:

Consider two bodies A and B with contact point P and assume that A and B have collinear normals at P. By assumption, this holds except for a finite set of points. Let the rigid motion exerted on A and B be represented by two functions, F_a and F_b, with F_a taking A to $F_a(A)$ and F_b taking B to $F_b(B)$.

Since P is a limit point of both A and B, there are sequences $a_1, a_2, \ldots$ in A and $b_1, b_2, \ldots$ in B such that $P = \lim a_i = \lim b_i$.

Let $PF_a = \lim F_a(a_i)$ and $PF_b = \lim F_b(b_i)$. Now, any rigid body motion is a combination of a translation then a rotation. Therefore, F_a can be considered as a translation taking the point P to the point PF_a, then a rotation about PF_a. Similarly, F_b can be considered as a translation taking the point P to the point PF_b, then a rotation about PF_b. One can therefore characterize F_a by (x_a, y_a, θ_a), where x_a, y_a, θ_a are real numbers, the translation is x_a N + y_a N' and the rotation is by angle θ_a. One similarly defines (x_b, y_b, θ_b). We will now consider $x_a, y_a, \theta_a, x_b, y_b, \theta_b$, to be continuously differentiable functions of the real variable t, and that $x_a(0) = y_a(0) = \theta_a(0) = x_b(0) = y_b(0) = \theta_b(0) = 0$, i.e., t = 0 corresponds to the initial configuration.

The constraint can finally be expressed as $x_a'(0) = x_b'(0)$, where f'(t) represents the derivative of f(t) with respect to t. The 3-D is similar. Note: In the 3-D case, one replaces θ_a and θ_b by R_a, R_b which are elements of SO(3)[1], or more explicitly by 6 angles, θ_a, φ_a, ψ_a, θ_b, φ_b, ψ_b, because Euler angle parametrization is possible since this is a local definition.
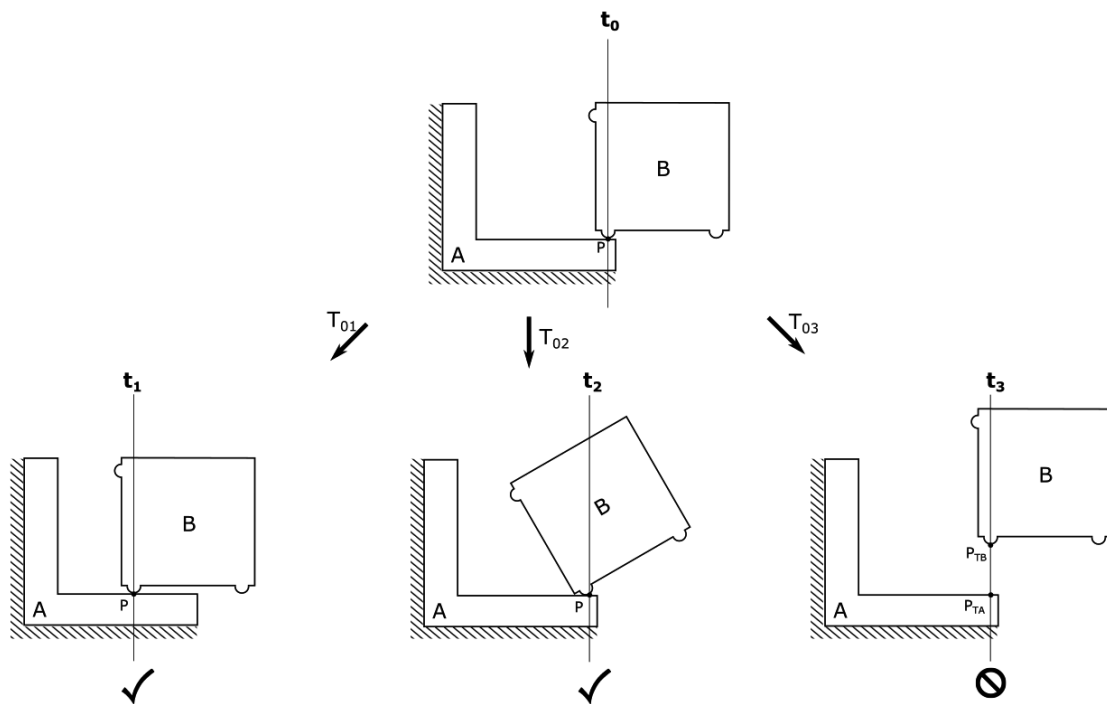
Figure 3.3.8: The definition of the constraint imposed by a single contact point. A contact point allows for a transformation tangential to the constraint line T_{01}. A transformation T_{02}, which is a rotation around the contact point P is also allowed. However a transformation T_{03} which is a vertical translation which results in body B and fixed base no longer sharing a contact point is not allowed.

3.3.9   Redundantly constrained

When the number of contact points is greater than the degree of constraint, the set of all bodies is *redundantly constrained*. This is illustrated in figure 3.3.9

DOC < 3
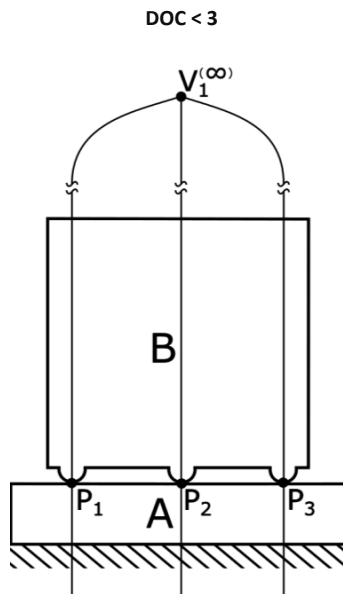
Figure 3.3.9: A configuration of two bodies, A and B, with three contact points providing 2 Degrees of Constraint. The number of contact points is greater than the degree of constraint, resulting in a redundantly constrained configuration.

3.3.10 Non-redundantly constrained

When the degree of constraint equals the number of contact points, the set of all bodies is *non-redundantly constrained*. This is illustrated in figure 3.3.10.

DOC = 2
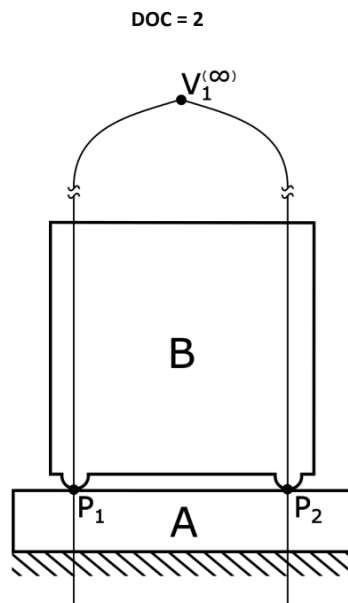
Figure 3.3.10: A non-redundantly constrained configuration of two bodies consisting of two contact points which each provide a Degree of constraint.

3.3.11 Kinematic mount

A *kinematic mount* is a maximal non-redundantly constrained set of bodies and interfaces. In other words, a set of bodies and interfaces, for which the number of contact points is equal to the maximum relative degrees of freedom and all contact points are non-redundantly constraining the bodies. A kinematic mount for two bodies is called a *kinematic coupling*. To refer to a kinematic mount or coupling in 2D, we use the adjective *2-dimensional*. Examples of both a *2-dimensional kinematic coupling* and *2-dimensional kinematic mount* are displayed in figure 3.3.11.
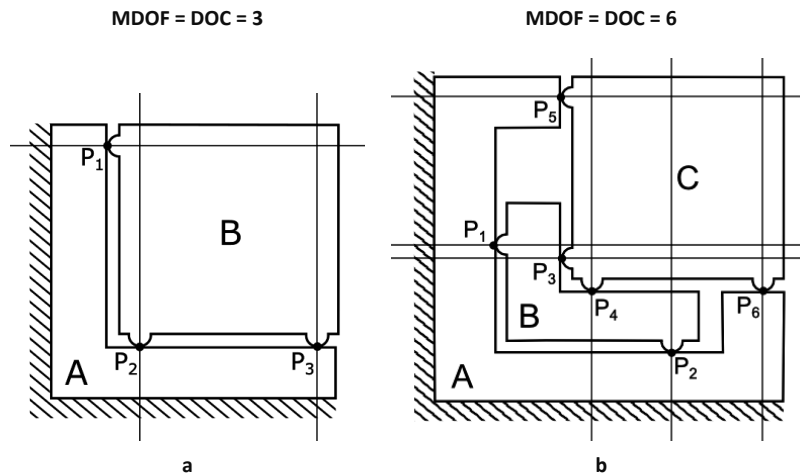
Figure 3.3.11: Both mounts illustrated have a maximum degree of freedom (MDOF) equal to the degree of constraint (DOC) equal to the number of contact points. a) A 2-dimensional kinematic coupling; b) A 2-dimensional three-body kinematic mount.

3.4 Nesting force

The force which is exerted, at an interface I_{AB} of two bodies A and B, along the constraint line at a contact point P_i, by body B on body A is called the *nesting force* $\vec{f}_i$. The sum of all nesting forces, exerted by body B on body A, at an interface I_{AB}, is called the *net nesting force* $\vec{F}_i$. These definitions are illustrated in figure 3.4.1.
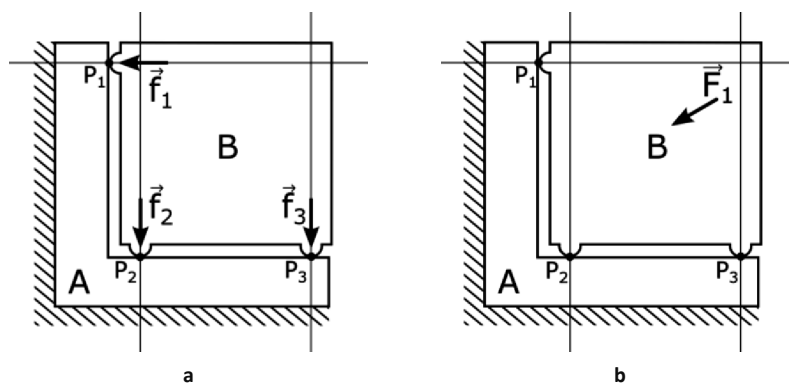
Figure 3.4.1: a) a 2-dimensional kinematic coupling consisting of two bodies, A and B, with their interface I_{AB}. The interface contains three contact points P_1 P_2 and P_3, defining three constraint lines. Along the constraint lines three nesting forces, $\vec{f}_1$, $\vec{f}_2$, $\vec{f}_3$ are exerted by body B on body A. b) the same 2-dimensional kinematic coupling but now with the net nesting force $\vec{F}_i = \sum_{i=1}^{i=3} \vec{f}_i$ exerted by body B on body A.

3.5 Chapter summary

This chapter introduced a rigorous set of geometric definitions in order to provide a firm foundation for the problem statements of the subsequent theoretical chapters.

Chapter 4 Examples of two-body and three-body 2-dimensional kinematic mounts

4.1 Problem statement

The problem statement of this chapter is:

> *Propose examples of 2-dimensional kinematic mounts consisting of two and three bodies whose constraint lines are either parallel or perpendicular to each other.*

4.2 Examples of 2-dimensional kinematic mounts

A set of examples of configurations is presented. For two bodies the example is shown in Table 4.2.1.1. For three bodies the examples are shown Table 4.2.2.1. We conjecture that these examples are exhaustive with respect to this chapters problem statement (§4.1).

4.2.1 Example of two-body 2-dimensional kinematic mounts

Table 4.2.1.1: Two-body 2-dimensional overview
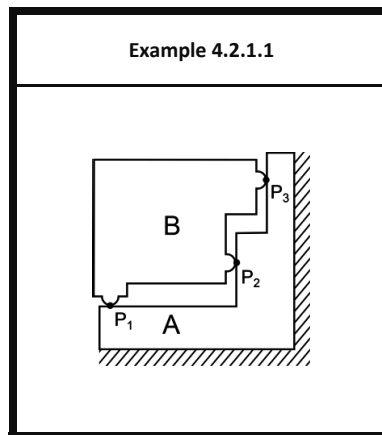
4.2.2 Examples of three-body 2-dimensional kinematic mounts

Table 4.2.2.1: Three-body 2-dimensional overview

Example 4.2.2.1	Example 4.2.2.2	Example 4.2.2.3
Example 4.2.2.4	**Example 4.2.2.5**	**Example 4.2.2.6**
Example 4.2.2.7	**Example 4.2.2.8**	**Example 4.2.2.9**

Chapter 5 Some conditions for two and three-body 2-dimensional kinematic mounts

5.1 Problem statement

Identify necessary conditions for the kinematic mounts of Chapter 4.

5.2 Some conditions for two-body kinematic mounts

Condition 5.2.1:

A two-body 2-dimensional kinematic mount requires three contact points (Figure 5.2.1).

a

b
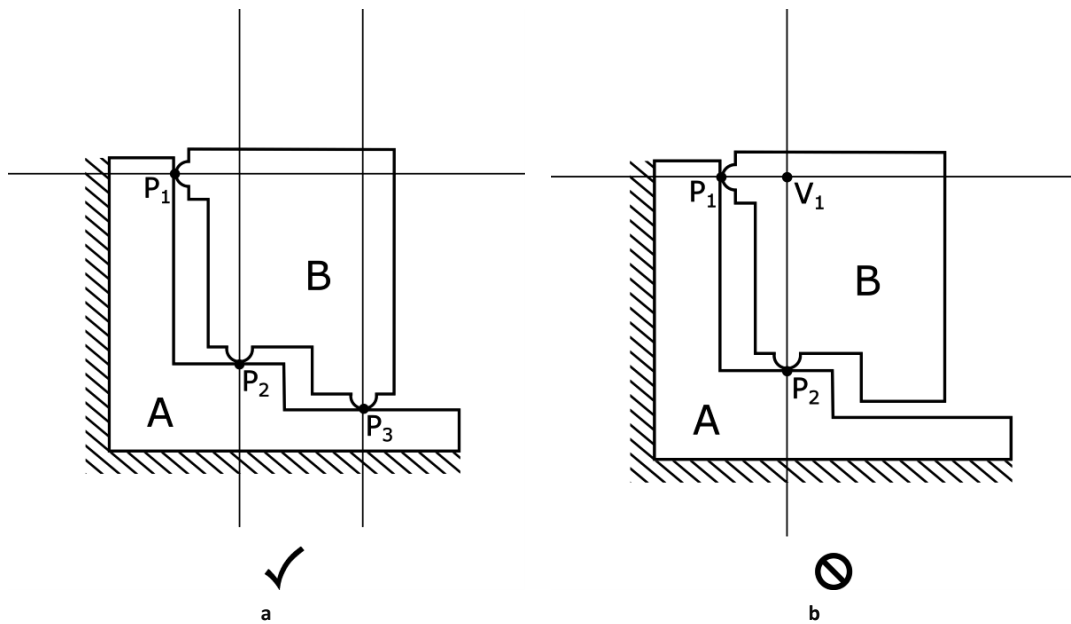
Figure 5.2.1: a) This two-body configuration has three contact points, therefore in accord with Condition 5.2.1. b) This two-body configuration has only two contact points, therefore it is not a kinematic mount.

Condition 5.2.2:

An interface cannot have collinear constraint lines (Figure 5.2.2).
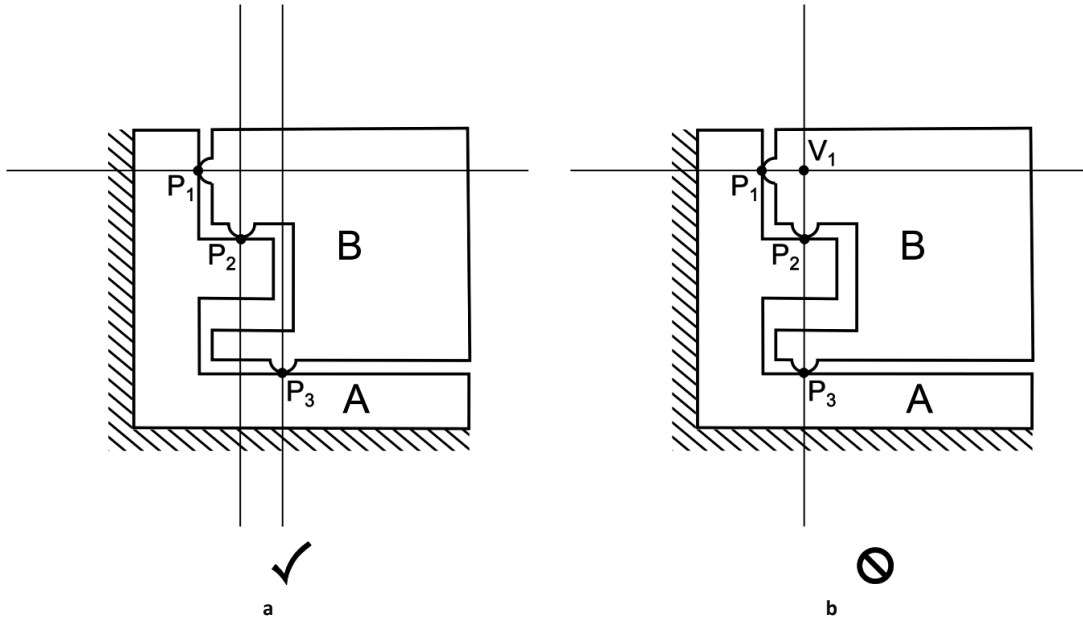
Figure 5.2.2: a) A two-body configuration with no collinear constraint lines, therefore in accord with Condition 5.2.2. b) A configuration where P_2 and P_3 have collinear constraint lines, resulting in a virtual pivot (as described in §3.3.5). This configuration therefore is not a 2-dimensional kinematic mount.

Condition 5.2.3:

The interface of a 2-dimensional configuration cannot have more than two parallel constraint lines (Figure 5.2.3).
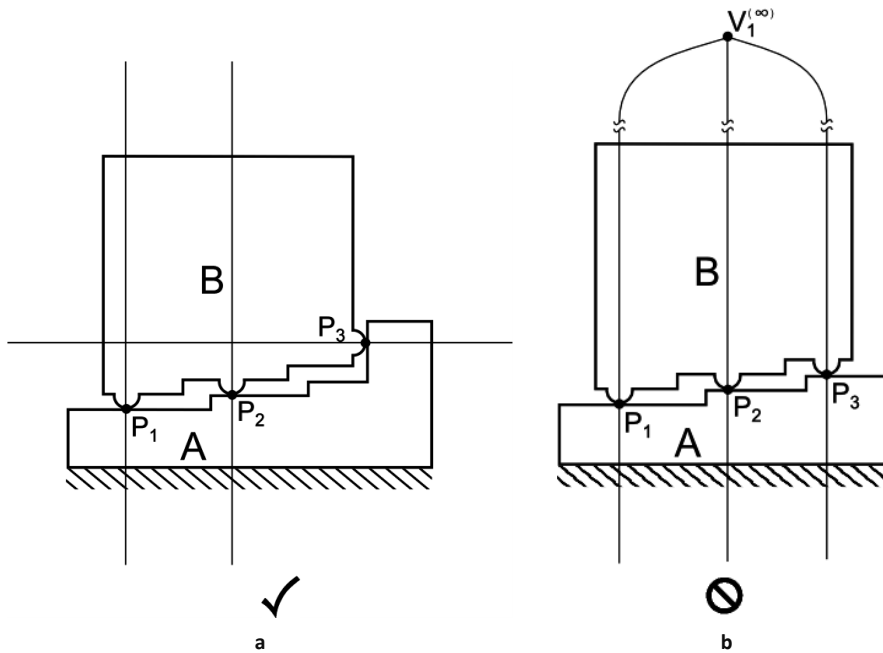
Figure 5.2.3: a) Interface of a 2-dimensional configuration with two parallel constraint lines in accord with condition 5.2.3. b) A configuration that is not a kinematic mount because it has an interface with three parallel constraint lines.

5.3   Some conditions for three-body kinematic mounts

Condition 5.3.1:

A three-body 2-dimensional kinematic mount requires 6 contact points (Figure 5.3.1).
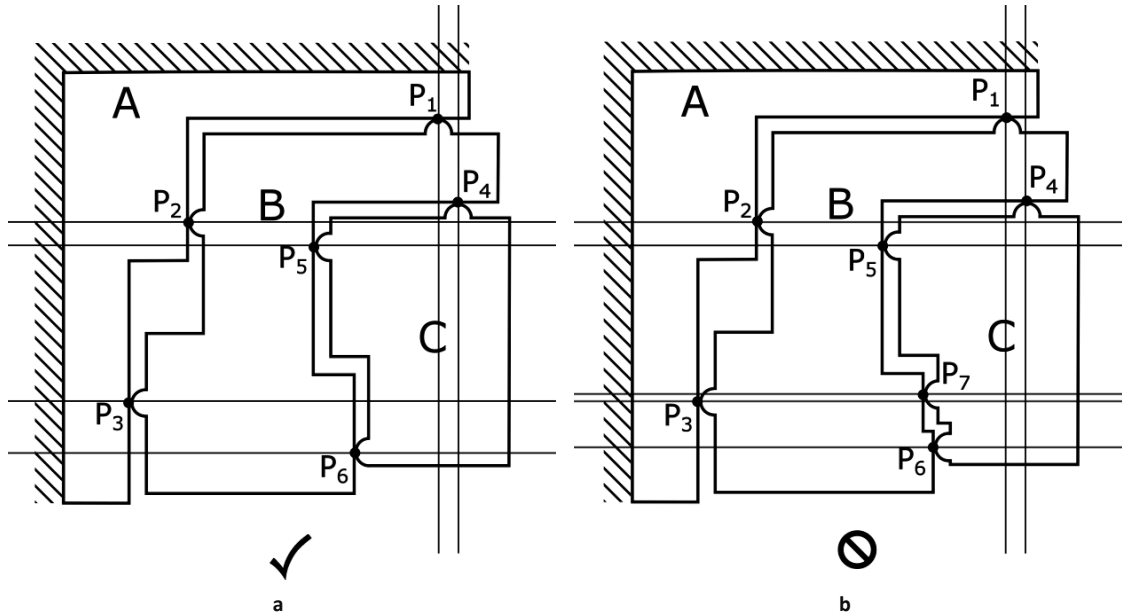
Figure 5.3.1: a) A three-body 2-dimensional configuration with six contact points in accord with Condition 5.3.1. b) This configuration is not a kinematic mount because it has seven contact points and therefore is not a 2-dimensional kinematic mount.

Condition 5.3.2:

An interface cannot have more than three contact points (Figure 5.3.2).
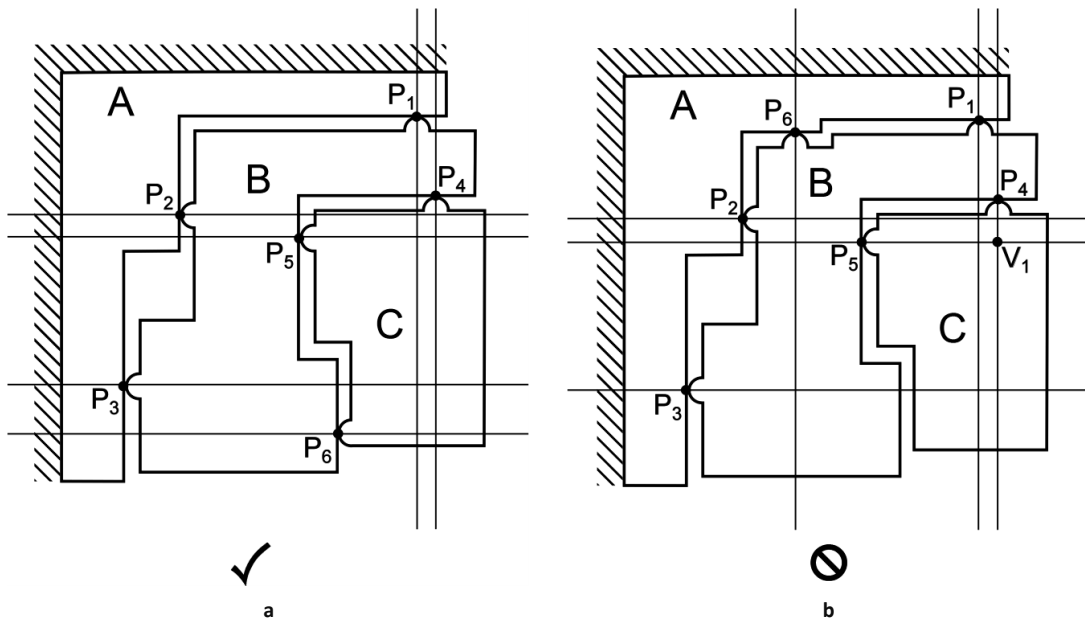
Figure 5.3.2: a) Two interfaces with each 3 contact points, in accord with Condition 5.3.2. b) In this configuration interface I_{AB} has 4 contact points, because the configuration is not a 2-dimensional kinematic mount.

Condition 5.3.3:

An interface cannot have collinear constraint lines (Figure 5.3.3).
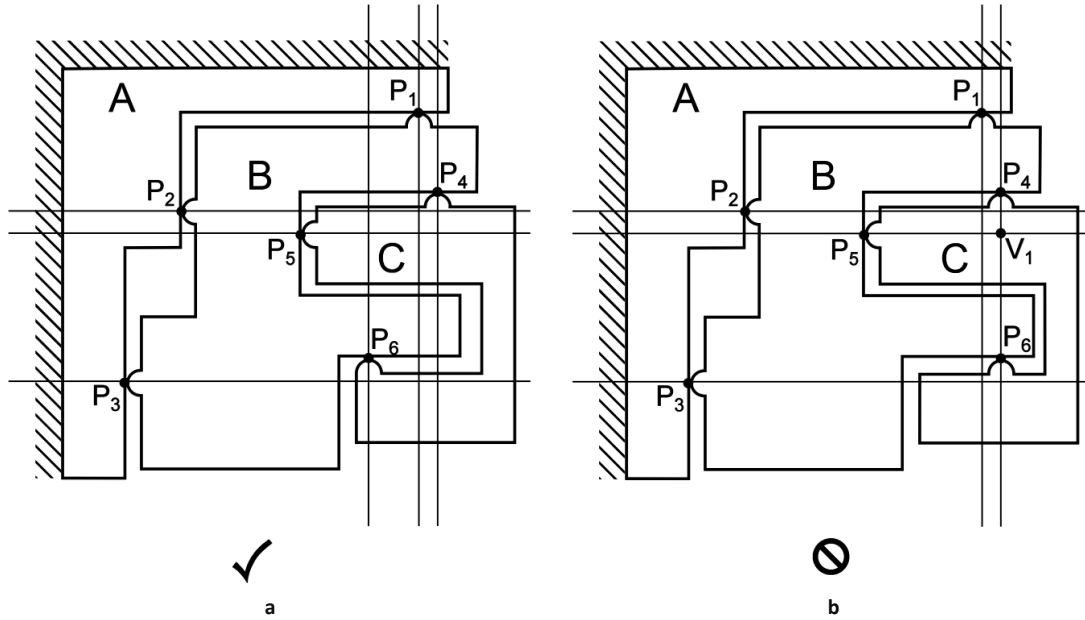
Figure 5.3.3: a) A configuration where no interface has collinear constraint lines, therefore in accord with Condition 5.3.3. b) A configuration that is not a kinematic mount because P_4 and P_6 have collinear constraint lines, resulting in a virtual pivot.

Condition 5.3.4:

An interface of a 2-dimensional configuration cannot have more than two parallel constraint lines (Figure 5.3.4).
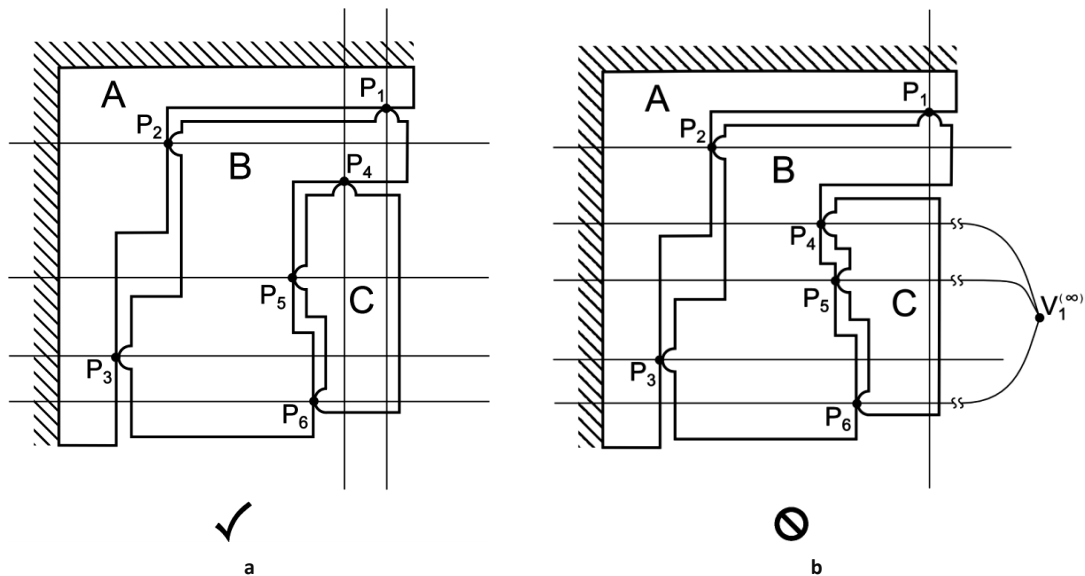
Figure 5.3.4: a) The 2-dimensional configuration has a maximum of two parallel constraint lines and therefore is in accord with Condition 5.3.4. b) A configuration that is not a kinematic mount because, Interface I_{BC} has three parallel constraint lines.

Condition 5.3.5:

Two non-empty interfaces with three constraint lines in total cannot have collinear constraint lines (Figure 5.3.5).

a   **b**

Figure 5.3.5: a) This three-body configuration its Interfaces I_{BC} and I_{AC} have three constraint lines in total of which none are collinear, and thus is in accord with Condition 5.3.5. b) This three-body configuration is not a kinematic mount because its interfaces I_{BC} and I_{AC} have three constraint lines in total of which P_4's and P_5's are collinear.

Condition 5.3.6:

If all interfaces have virtual pivots, these pivots cannot be collinear (Figure 5.3.6.1 - Figure 5.3.6.4).

a   **b**
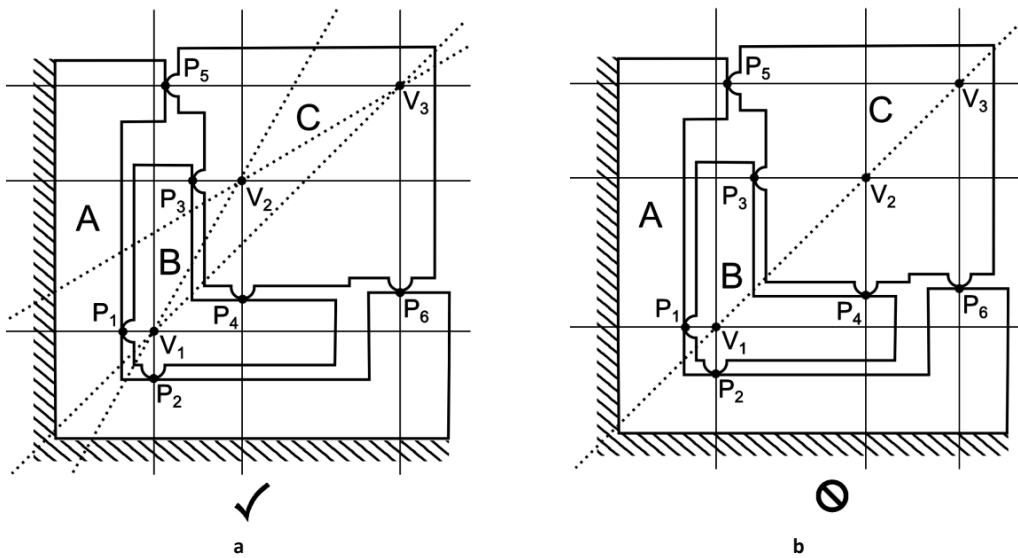
Figure 5.3.6.1: a) This configuration has three non-collinear virtual pivots V_1, V_2 and V_3, in accord with Condition 5.3.6. b) This configuration is not a kinematic mount because it has three collinear virtual pivots V_1, V_2 and V_3. These virtual pivots are instantaneous meaning that as soon as there is a slight movement the virtual pivots are no longer collinear, resulting in a singularity.
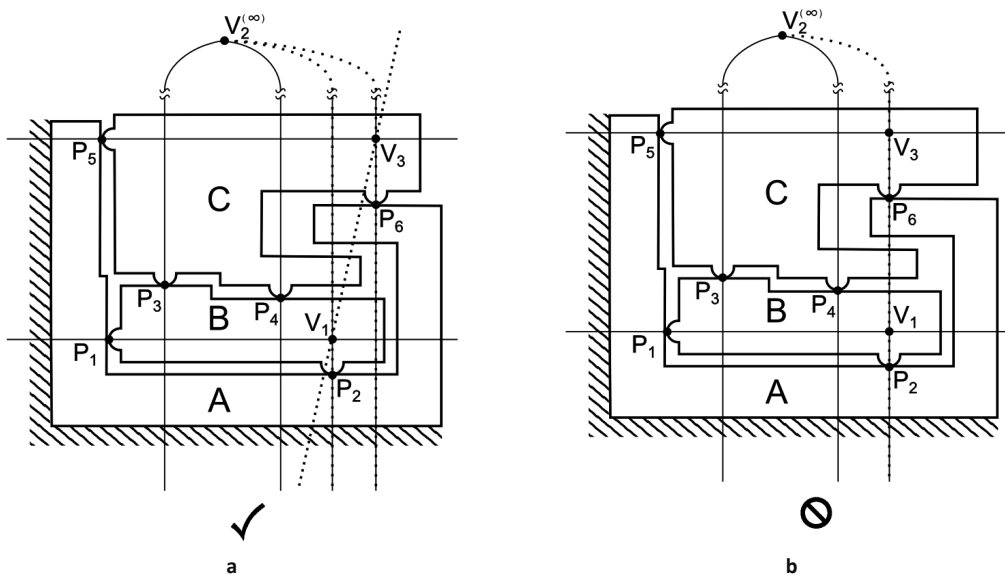
Figure 5.3.6.2: a) A configuration with three non-collinear virtual pivots V_1, V_3 and a virtual pivot V_2 at infinity, in accord with Condition 5.3.6. b) A configuration that is not a kinematic mount because it has three collinear virtual pivots V_1, V_3 and a virtual pivot V_2 at infinity.
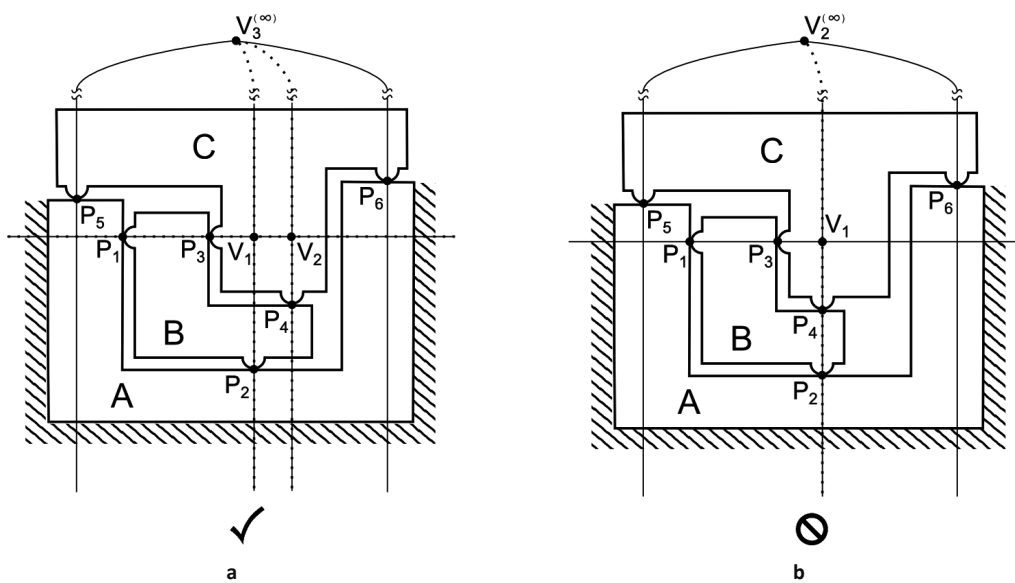
Figure 5.3.6.3: a) A configuration with three non-collinear virtual pivots V_1, V_2 and a virtual pivot V_3 at infinity, in accord with Condition 5.3.6 b) This configuration is not a kinematic mount because it has only has two distinct virtual pivots.
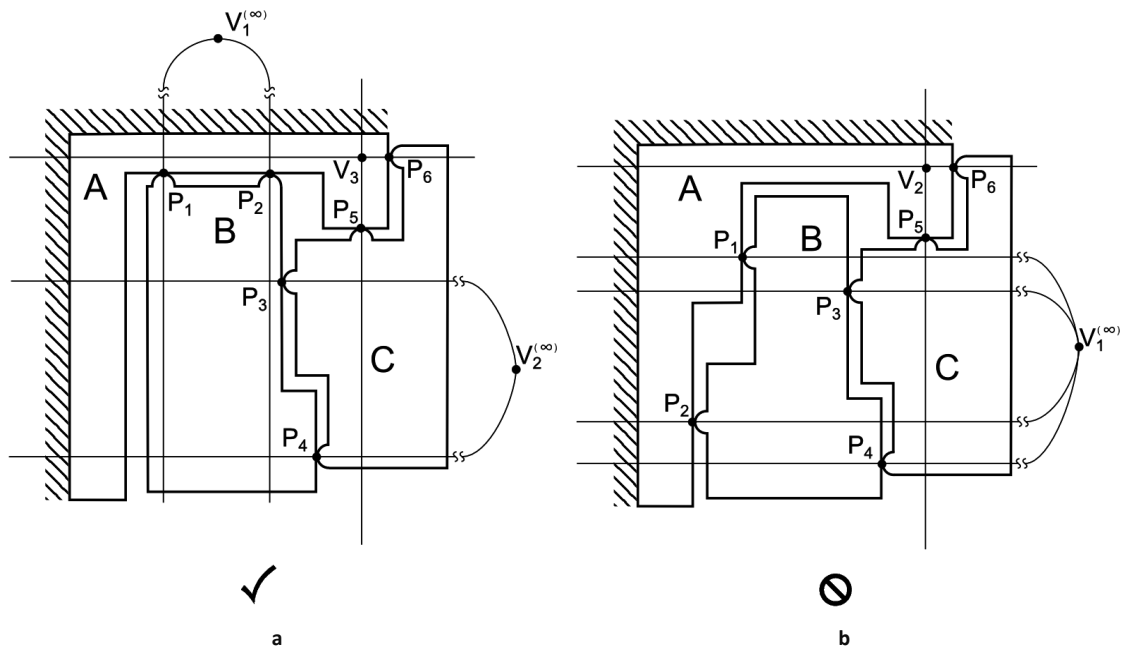
Figure 5.3.6.4: a) A configuration with three virtual pivots that are non-collinear, two different virtual pivots at infinity (V_1 and V_2) and one virtual pivot not at infinity V_3, in accord with Condition 5.3.6. b) A configuration that is not a kinematic mount because it has two distinct virtual pivots.

Condition 5.3.7:

The constraint lines of two interfaces cannot all be parallel (Figure 5.3.7).
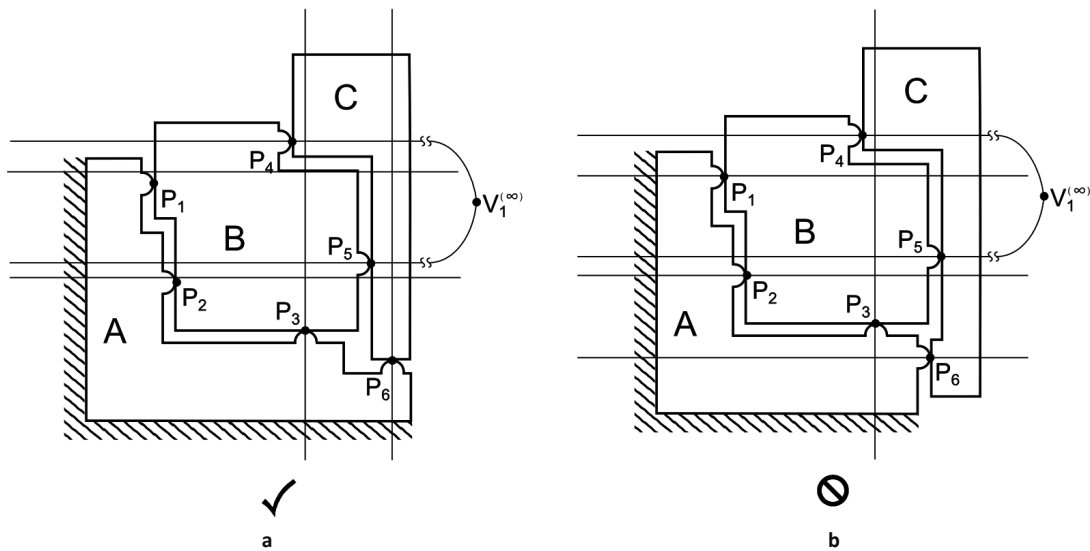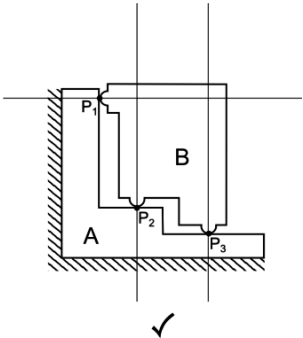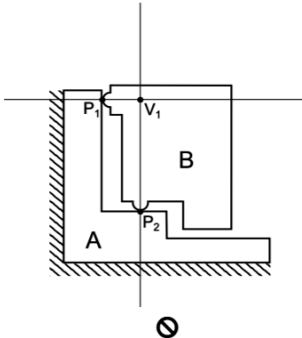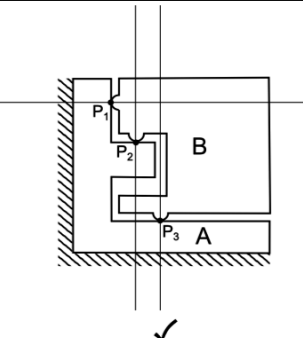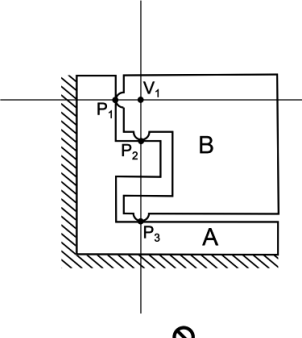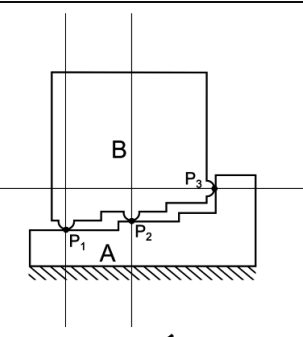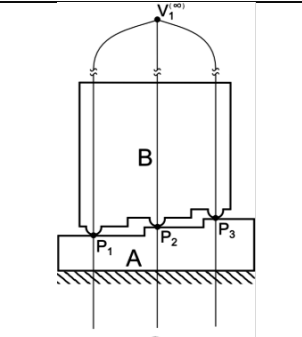
Figure 5.3.7. a) A configuration where there is no combination of interfaces that share only parallel constraint lines, in accord with Condition 5.3.7. b) A configuration that is not a kinematic mount because interface I_{BC} and I_{AC} only have parallel constraint lines.

5.4 Overview
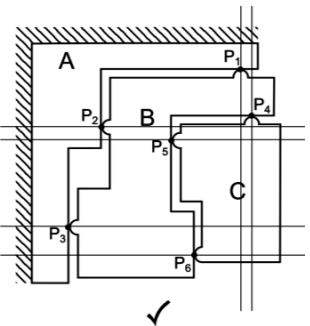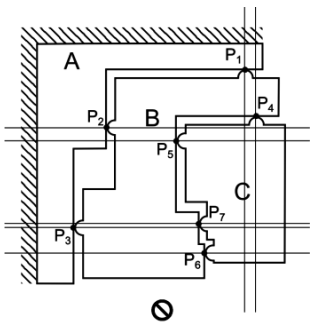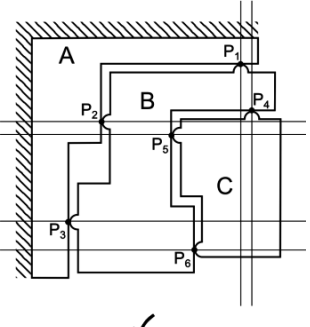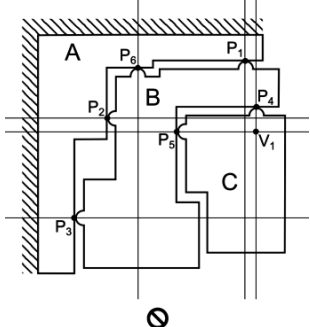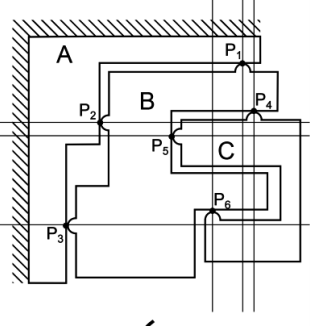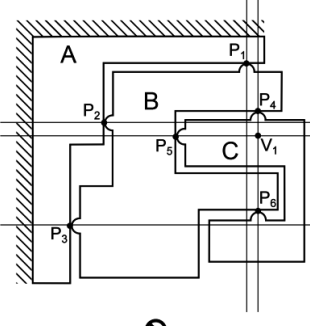
In this section we offer an overview of all the conditions in Table 5.1 to 5.5

Table 5.1: 2-dimensional two-body conditions overview.

|	
Condition 5.2.1: A two-body kinematic mount requires three contact points.	
Figure 5.2.1a	Figure 5.2.1b
Condition 5.2.2: An interface cannot have collinear constraint lines.	
Figure 5.2.2a	Figure 5.2.2b
Condition 5.2.3**:** An interface of a 2-dimensional configuration cannot have more than two parallel constraint lines	
Figure 5.2.3a	Figure 5.2.3b
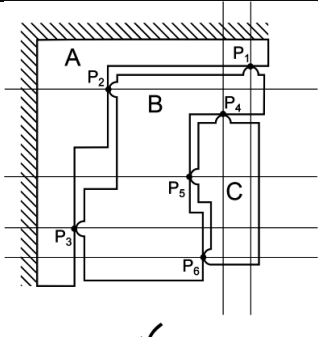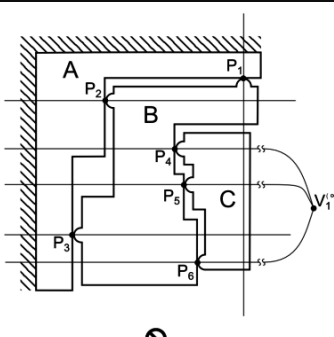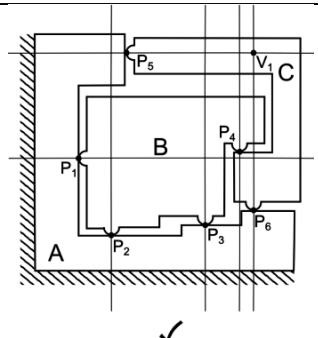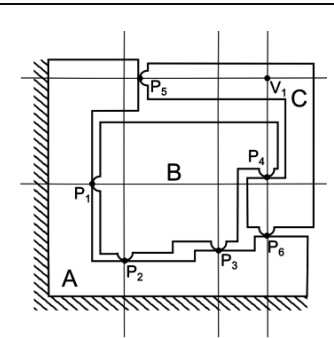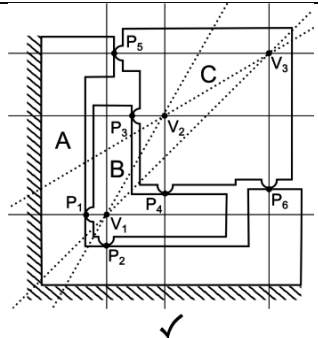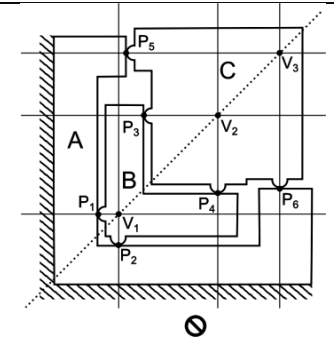
Table 5.2: 2-dimensional three-body conditions overview 1 of 4.

Condition 5.3.1: A three-body kinematic mount requires 6 contact points.

| Figure 5.3.1a | Figure 5.3.1b |

Condition 5.3.2: An interface cannot have more than three contact points.

| Figure 5.3.2a | Figure 5.3.2b |

Condition 5.3.3: An interface cannot have collinear constraint lines.

| Figure 5.3.3a | Figure 5.3.3b |

Table 5.3: 2-dimensional three-body conditions overview (2 of 4).

Condition 5.3.4: An interface of a 2-dimensional configuration cannot have more than two parallel constraint lines.

| Figure 5.3.4a | Figure 5.3.4b |

Condition 5.3.5: Two non-empty interfaces with three constraint lines in total cannot have collinear constraint lines.
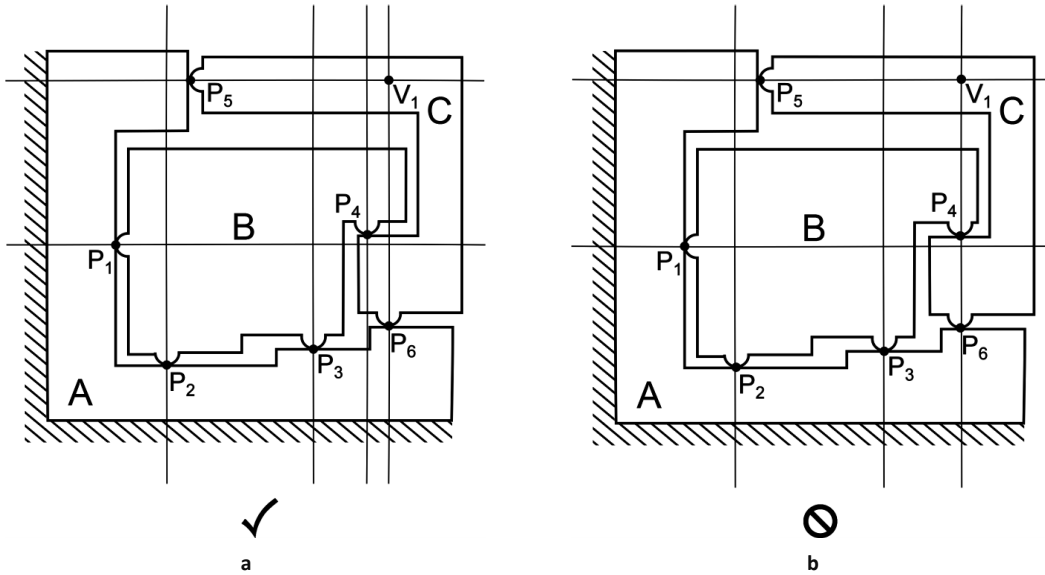

| Figure 5.3.5a | Figure 5.3.5b |

Condition 5.3.6: If all interfaces have virtual pivots they cannot be collinear.

| Figure 5.3.6.1a | Figure 5.3.6.1b |

Table 5.4: 2-dimensional three-body conditions overview (3 of 4).

Condition 5.3.6: If all interfaces have virtual pivots they cannot be collinear.
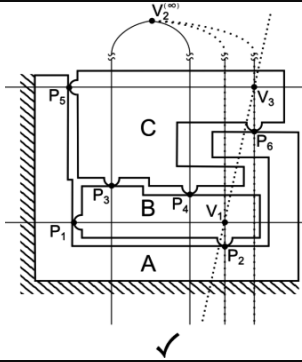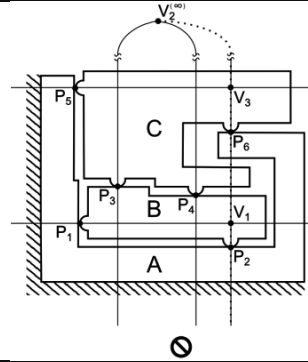
Figure 5.3.6.2a	Figure 5.3.6.2b
Figure 5.3.6.3a	Figure 5.3.6.3b
Figure 5.3.6.4a	Figure 5.3.6.4b
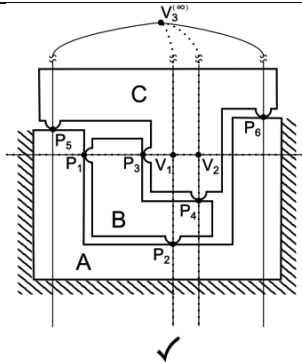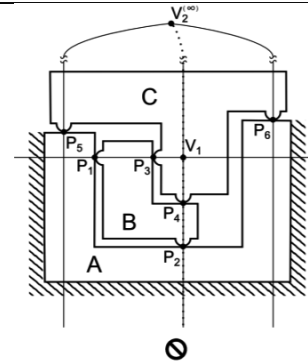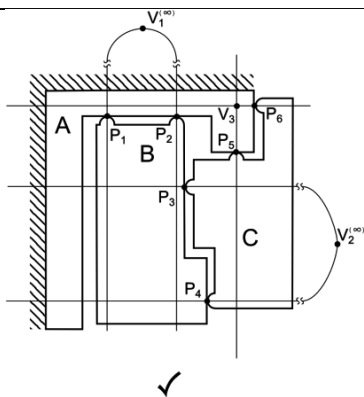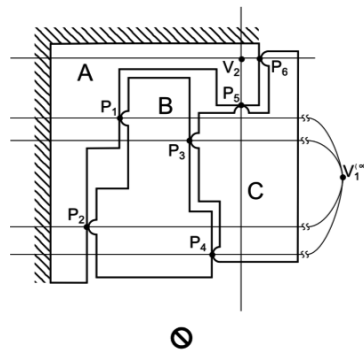
Table 5.5: 2-dimensional three-body conditions overview (4 of 4).

Condition 5.3.7: The constraint lines of two interfaces cannot all be parallel.

| Figure 5.3.7a | Figure 5.3.7b |

5.5 Remarks

5.5.1 Remark on infinitesimal tangential motion

In order to better understand Condition 5.3.6, it should be noted that two contact points with a virtual pivot allow an infinitesimal tangential motion, this is illustrated in Figure 5.5.1. The motions in Figure 5.5.1 are deliberately exaggerated to help illustrate the effect. In Condition 5.3.6, one radial motion of the bodies is redundantly constrained whereas one infinitesimal tangential motion is allowed.
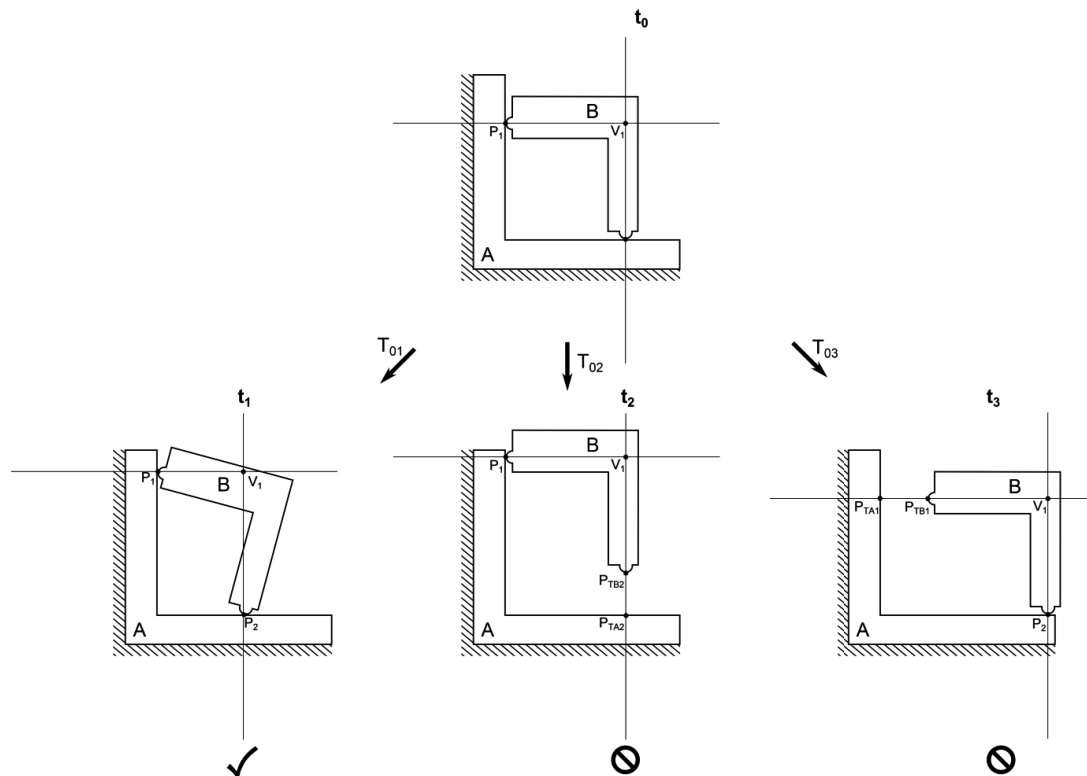
Figure 5.5.1: The motion allowed by an interface with a virtual pivot.

5.5.2   Sliding contact points

When two bodies with virtual pivots have a shared contact point this contact point can slide over the surfaces (Figure 5.5.2). This means that the contact point P_1 at t_0 and the contact point P_2 at t_1 are physically different.
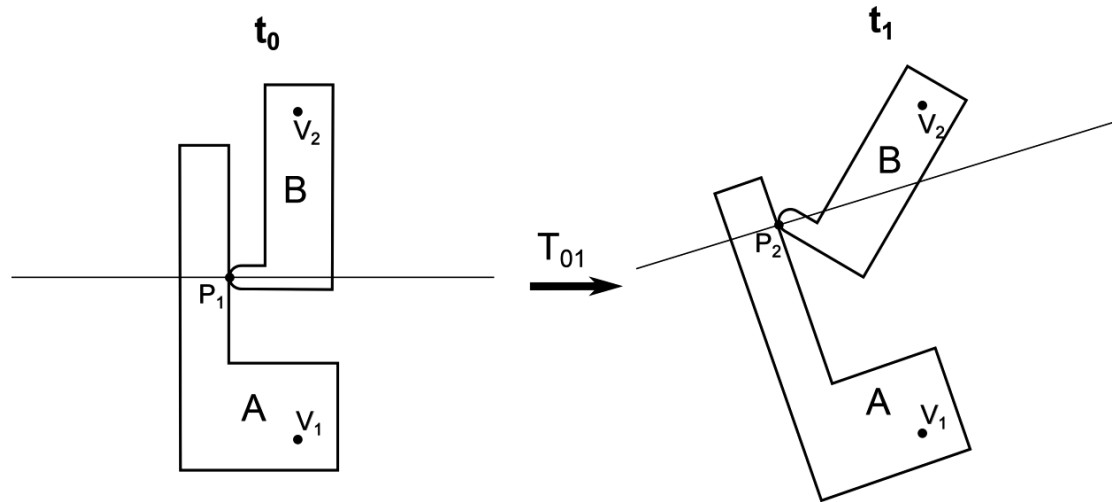
Figure 5.5.2: Contact point P_1 is different from P_2. This happens when two bodies have virtual pivots and share an interface.

5.6   Chapter summary

This chapter presented necessary conditions for 2-dimentional kinematic mounts: three necessary conditions for two-body kinematic mounts and seven conditions for three-body kinematic mounts.

Chapter 6 Classification and discussion of three-body 2-dimensional kinematic mounts

6.1 Problem statement

Propose a classification of the examples of Chapter 4 according to their orthogonal and parallel constraint lines.

By classification, we mean a set of non-equivalent configurations so that any kinematic mount is equivalent to an element of this set.

6.2 Definitions

6.2.1 Interface-pictogram

An *interface-pictogram* is a graphical representation of the constraint lines displaying relations between constraint lines of an interface (Figure 6.2.1). All interface-pictograms have to obey condition 5.3.2 and 5.3.3 (§5.3). The interface-pictogram does not display the actual distance between two constraint lines.
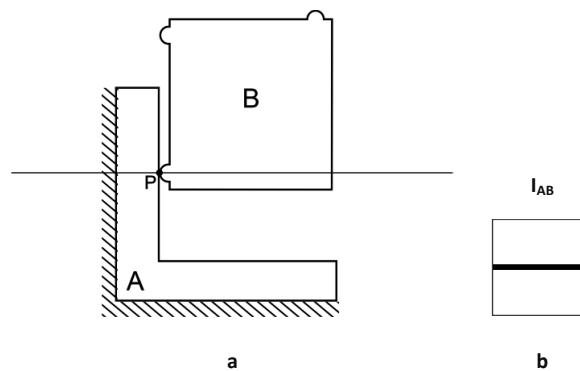
Figure 6.2.1: a) Two bodies A and B with Interface I_{AB} having one constraint line. b) The interface-pictogram of the Figure 6.2.1a.

6.2.2 Configuration-pictogram

A *configuration*-pictogram is the set of all interface-pictograms for a configuration (Figure 6.2.2). In the case of two bodies the configuration-pictogram and interface-pictogram are the same. All configuration-pictograms are equivalent under the equivalence relations mentioned in §6.3.1 and §6.3.2, in addition, all configuration-pictograms of three bodies have to obey Conditions 5.4.3, 5.4.5 and 5.4.6.

a   **b**
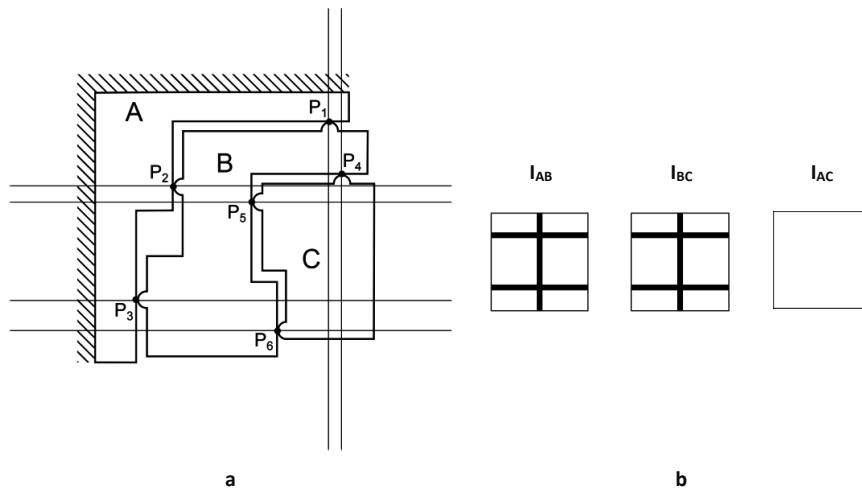
Figure 6.2.2: a) A three-body configuration. b) The configuration-pictogram of Figure 6.2.2a, consisting of two interface-pictograms with three constraint lines and one empty interface-pictogram.

6.2.3 Configuration-array

The *configuration-array* of a configuration is a 1 x 2 (for two bodies) or 3 x 2 array (for three bodies). It indicates the number of contact points of an interface and whether their constraint lines are parallel to the x or y-axis. The configuration-array of a configuration gives no information on the position of the contact points, only that they do not share the same constraint line. The rows of a configuration-array describe the interfaces (1st row I_{AB}, 2nd row I_{BC}, 3rd row I_{AC}). The first Column describes the number of constraint lines parallel to the x-axis. The second column, the number of constraint lines parallel to the Y-axis. All configuration-arrays have the equivalence relations mentioned in §6.3.1 and §6.3.2, in addition all configuration-arrays of three bodies have to obey 2-dimensional three-body conditions 3, 5 and 6 (§4.4).

a   **b**
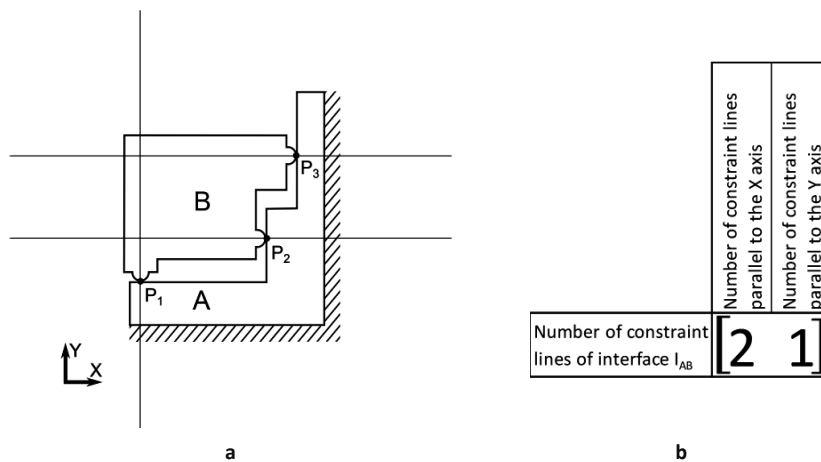
Figure 6.2.3: a) A two-body configuration. b) The 1 by 2 configuration-array of Figure 6.2.3a.
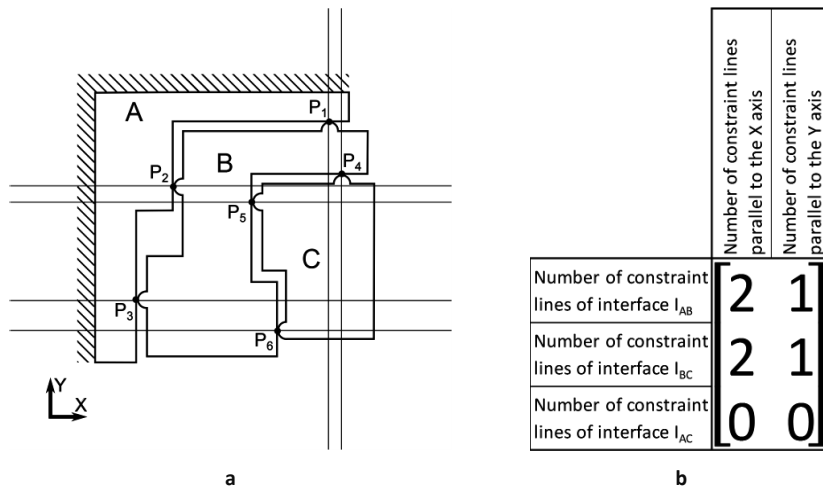
Figure 6.2.4: a) A three-body configuration. b) The configuration-array of Figure 6.2.4a, a 3 by 2 array.

6.2.4   Correspondence of configuration-pictogram and configuration-array

The configuration-pictogram and the configuration-array relay exactly the same information. This means that every configuration-pictogram has one configuration-array and vice versa.

Table 6.2.1: Example of correspondence of configuration-pictogram and configuration-array
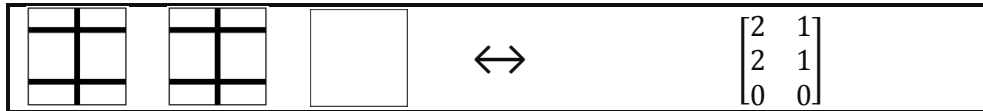
6.2.5   Configuration-representation and interface-representation.

The *configuration-representation* of a configuration is either the configuration-array or configuration-pictogram. For ease of use we will always display both. Note that in the case of a kinematic coupling the configuration-representation is the same as the *interface-representation*.
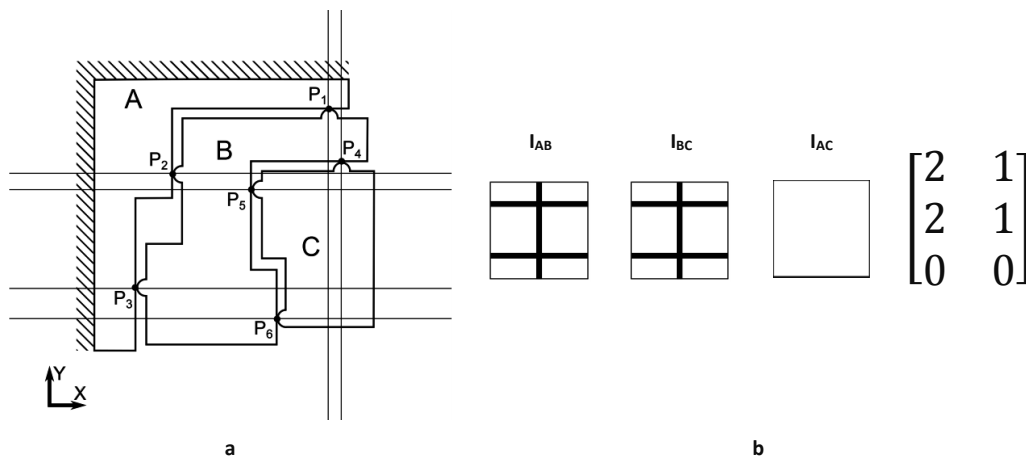
Figure 6.2.5: a) A three-body configuration. b) The configuration-representation of Figure 6.2.5a, consisting of the configuration pictogram and configuration-array

6.2.6 Relabeling

We define relabeling a configuration-representation as interchanging the names of the bodies (Figure 6.2.6)

t$_0$

T_{01}

t$_1$
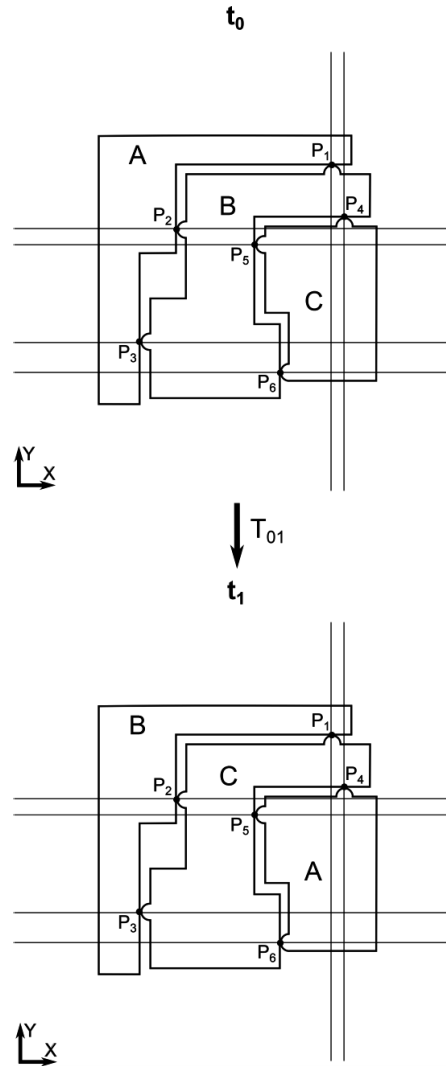
Figure 6.2.6: A configuration (t$_0$) and a relabelled configuration (t$_1$)

6.3 Equivalence relations

6.3.1 Rotational equivalence of a configuration-representation

Two configurations (t_0 and t_1 in Figure 6.3.1 a) are considered equivalent if one is a rotation of the other. In the case of this thesis due to the problem statement only rotations which are multiples of 90° are considered. Due to this we can also consider the configuration-representations (t_0 and t_1 in Figure 6.3.1 b) equivalent.
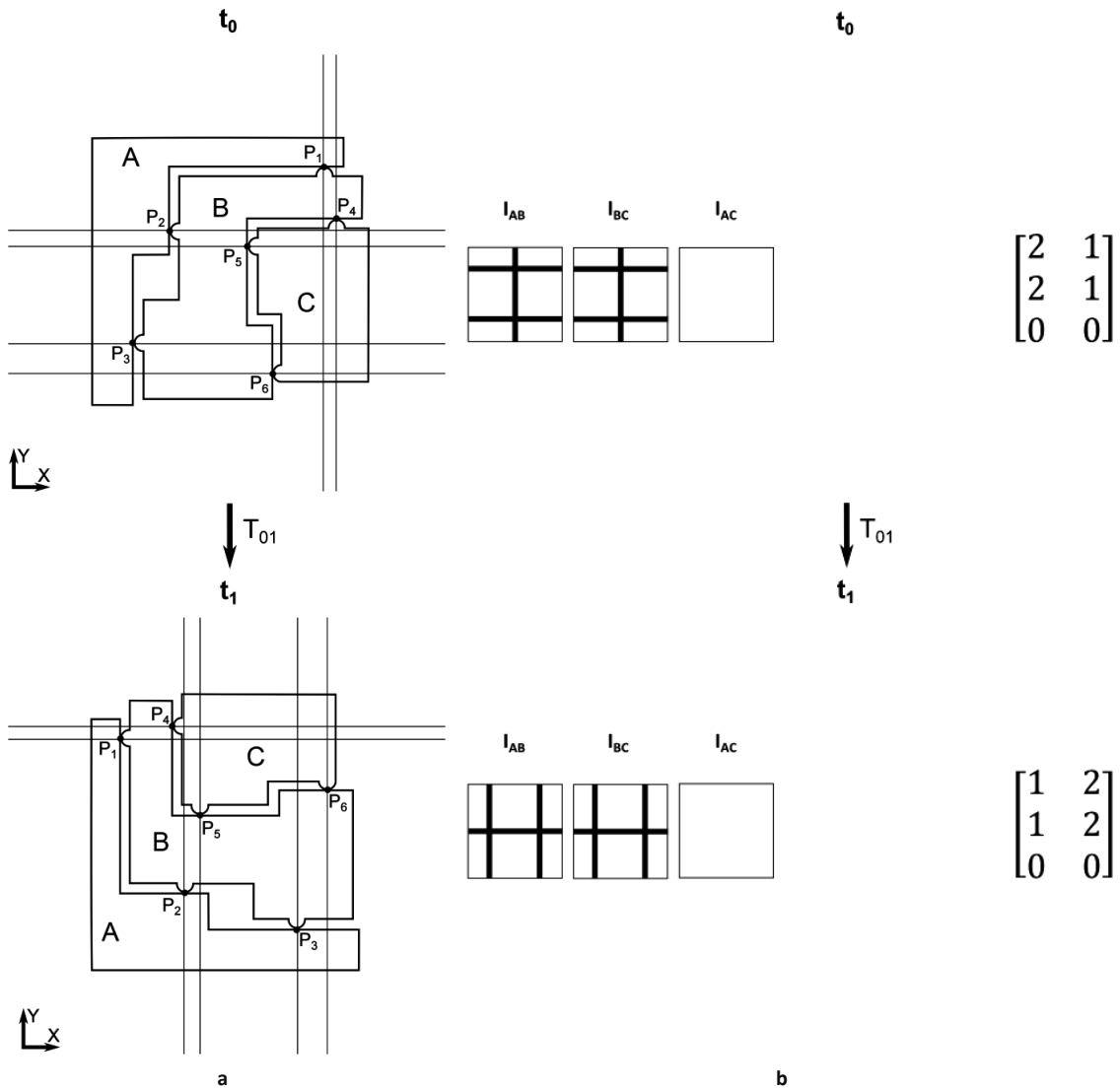
Figure 6.3.1: a) A three-body general configuration and its rotation. b) The configuration-representation and the configuration-representation of the rotated configuration-representation Figure 6.3.1a. We note that for the configuration-array the equivalence is simply a permutation of the columns.

6.3.2 Equivalence of a relabeled configuration-representation

We consider a relabelled configuration (t_1 in Figure 6.3.2) equivalent to the original configuration (t_0 in Figure 6.3.2). Due to this we also consider configuration-representations of these configurations equivalent (Figure 6.3.2).
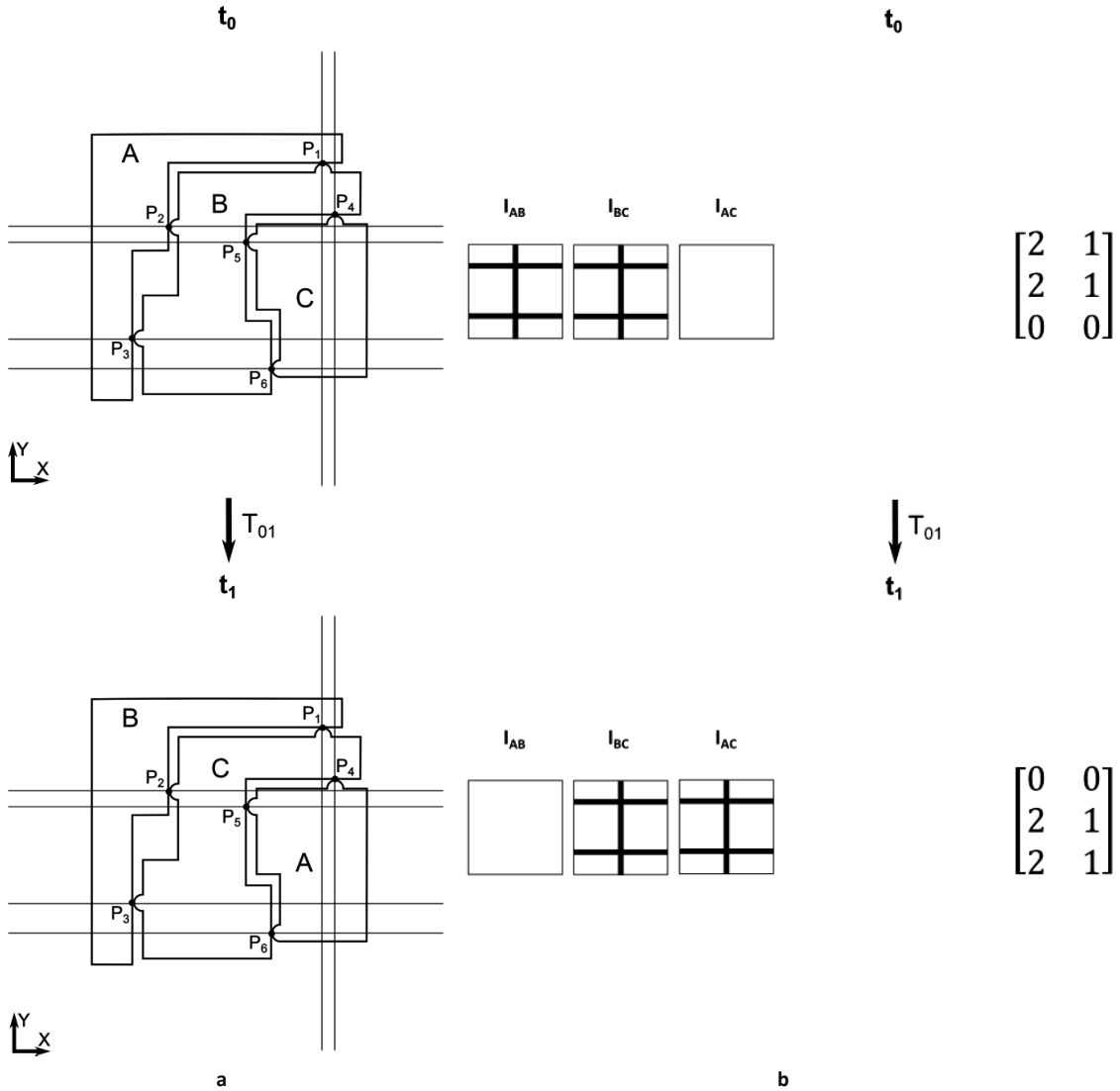
Figure 6.3.2: a) A three-body general configuration and its relabelled configuration. b) The configuration-representation (t_0) and its equivalent configuration-representation (t_1) of Figure 6.3.2a. We note that for the configuration-array the equivalence is simply a permutation of the rows.

6.4   Configuration representations

6.4.1   The configuration-representation of a two-body 2-dimensional kinematic mount.

The two-body configuration-representation satisfying the conditions of §5.2, is illustrated in Figure 6.4.1b. We conjecture that any other configuration-representation of a two-body 2-dimensional kinematic mount can be obtained by rotation (see also the equivalence relation in §6.3.1). Note that this kinematic mount is also a kinematic coupling.

<center>a   b</center>
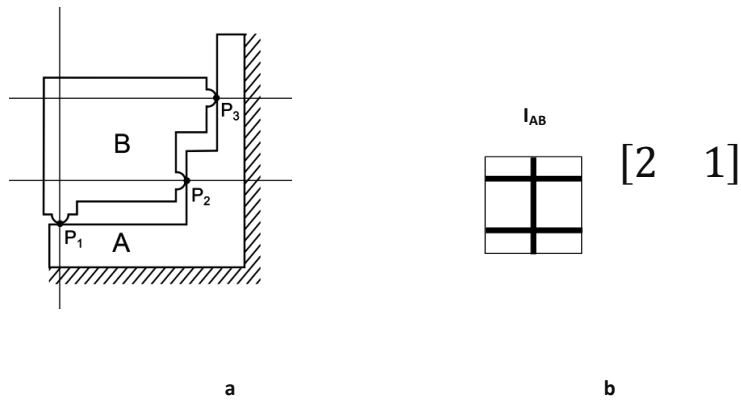
Figure 6.4.1: a) Example 4.2.1.1 of a two-body kinematic coupling. b) The configuration-representation of Example 4.2.1.1.

6.4.2   The nine configuration-representations of three-body 2-dimensional kinematic mounts.

The nine configuration-representations which are linked to the nine configuration-arrays that resulted from the conditions of §5.3 are visualized here with their example from Chapter 4

<center>a   b</center>
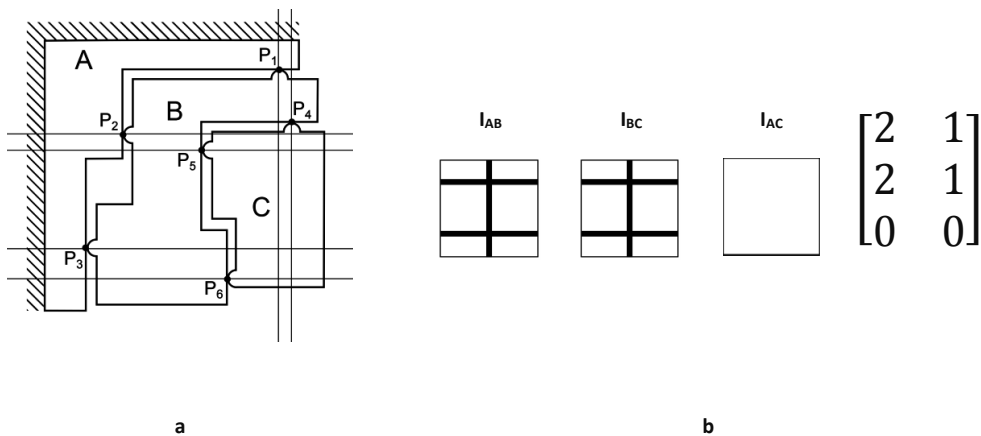
Figure 6.4.2: a) Example 4.2.2.1 of a three-body kinematic mount. b) The configuration-representation of the kinematic mount Example 4.2.2.1.

a   **b**
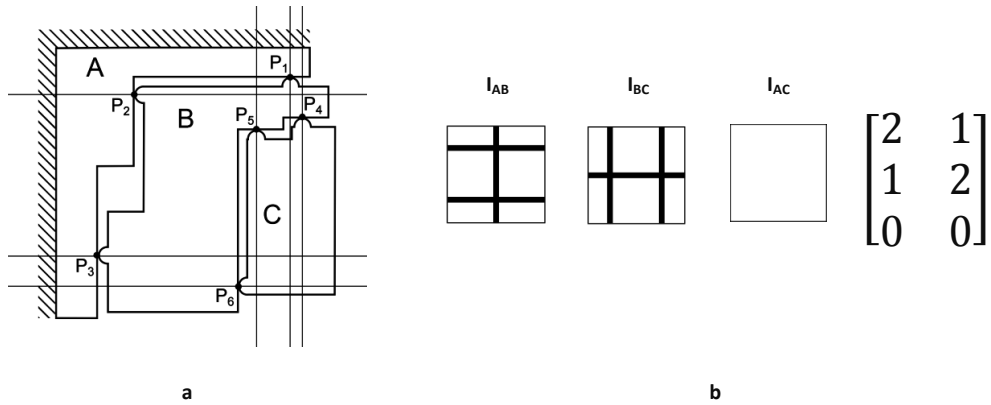
Figure 6.4.3: a) Example 4.2.2.2 of a three-body kinematic mount. b) The configuration-representation of the kinematic mount Example 4.2.2.2.

a   **b**
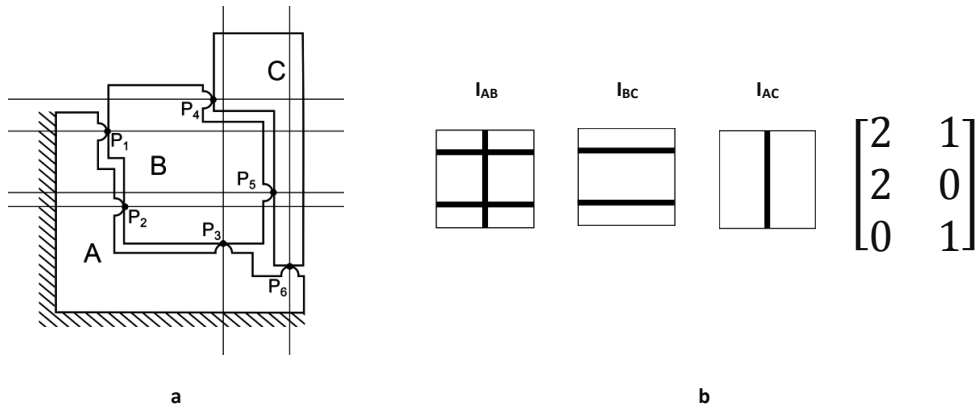
Figure 6.4.4: a) Example 4.2.2.3 of a three-body kinematic mount. b) The configuration-representation of the kinematic mount Example 4.2.2.3.

a   **b**
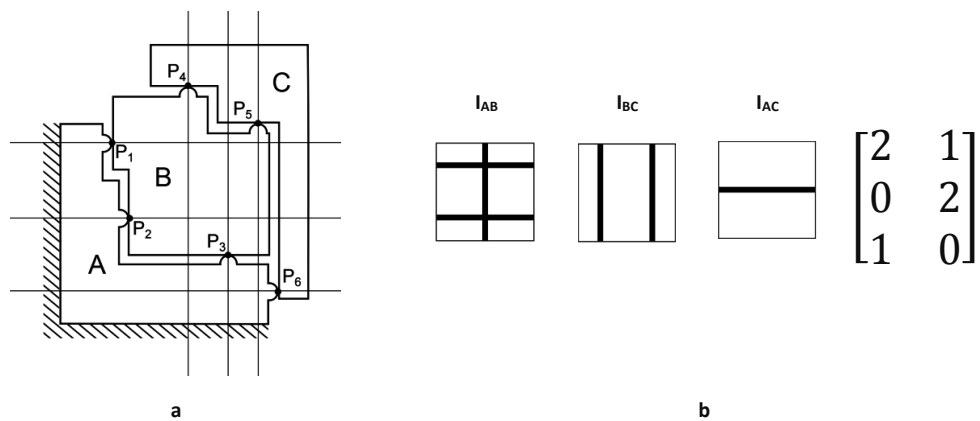
Figure 6.4.5: a) Example 4.2.2.4 of a three-body kinematic mount. b) The configuration-representation of the kinematic mount Example 4.2.2.4.

a   b
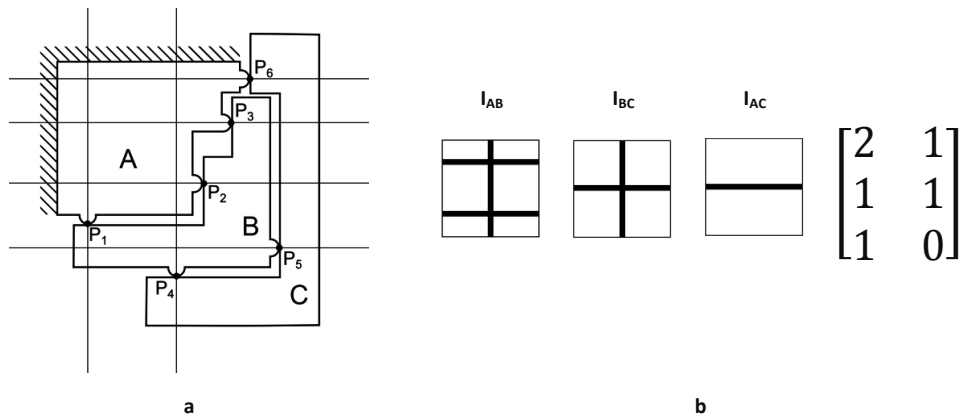
Figure 6.4.6: a) Example 4.2.2.5 of a three-body kinematic mount. In order to be a kinematic mount it must obey Condition 5.3.5 b) The configuration-representation of the kinematic mount Example 4.2.2.5.

a   b
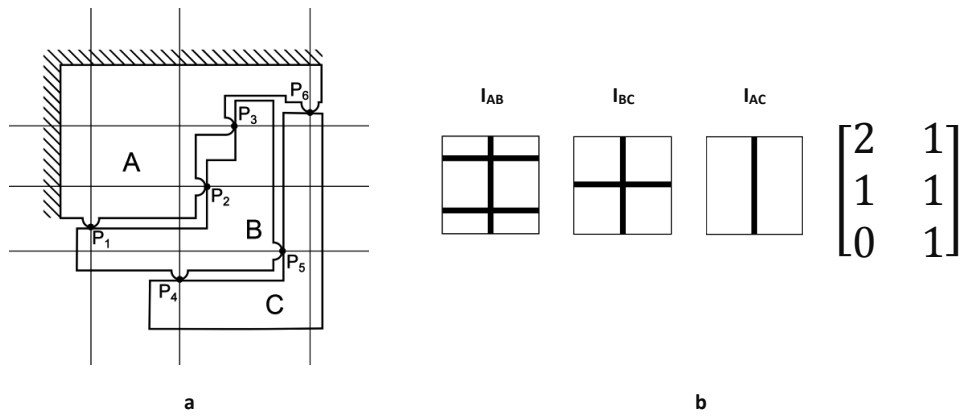
Figure 6.4.7: a) Example 4.2.2.6 of a three-body kinematic mount. In order to be a kinematic mount it must obey Condition 5.3.5 b) The configuration-representation of kinematic mount Example 4.2.2.6.

a   b
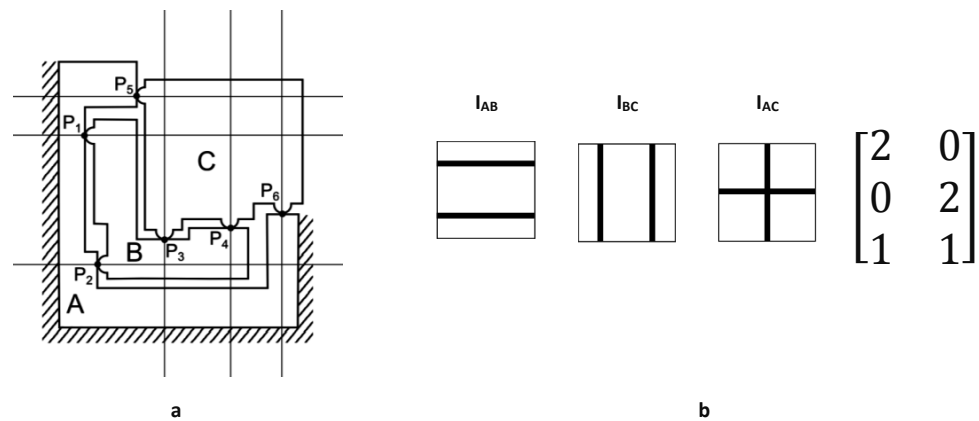
Figure 6.4.8: a) Example 4.2.2.7 of a three-body kinematic mount. b) The configuration-representation of kinematic mount Example 4.2.2.7.

a   **b**
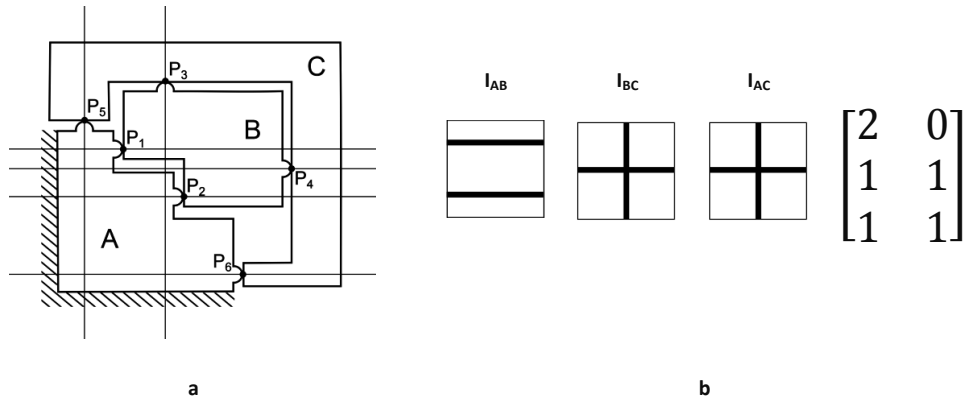
Figure 6.4.9: a) Example 4.2.2.8 of a three-body kinematic mount. In order to be a kinematic mount it must obey Condition 5.3.6 b) The configuration-representation of kinematic mount Example 4.2.2.8.

a   **b**
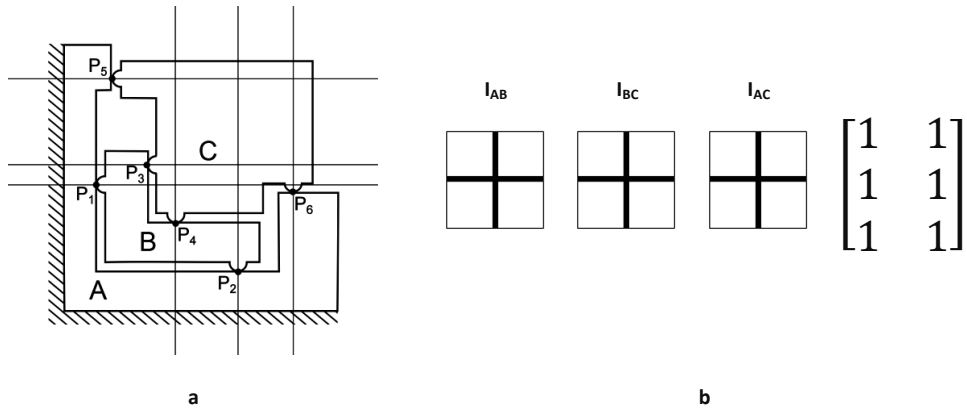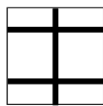
Figure 6.4.10: a) Example 4.2.2.9 of a three-body kinematic mount. In order to be a kinematic mount it must obey Condition 5.3.6 b) The configuration-representation of kinematic mount Example 4.2.2.9.
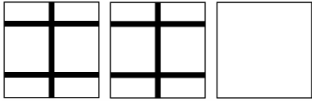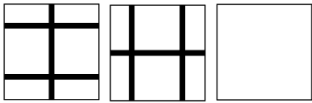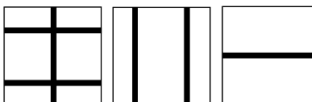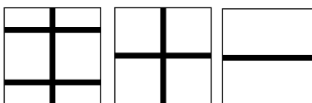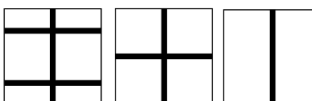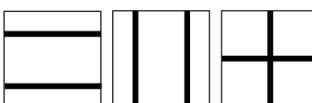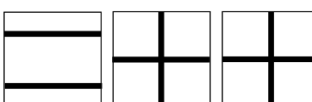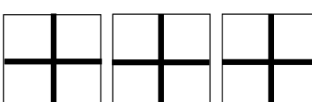
6.5 Conjectured list of all non-equivalent configuration-representations for two and three-body kinematic mounts

Table 6.5.1: Overview of the configuration-pictogram of two-body 2-dimensional kinematic mounts.

Two-body Configuration example	Configuration-representation	Applicable 2-dimensional two-body conditions		
		5.2.1	5.2.2	5.2.3
4.2.1.1	$\begin{bmatrix} 2 & 1 \end{bmatrix}$	✓	✓	✓

Table 6.5.2: Overview of the configuration-pictogram of three-body 2-dimensional kinematic mounts.

Three-body Configuration Example	Configuration-representation	Applicable 2-dimensional three-body conditions						
		5.3.1	5.3.2	5.3.3	5.3.4	5.3.5	5.3.6	5.3.7
4.2.2.1	$\begin{bmatrix} 2 & 1 \\ 2 & 1 \\ 0 & 0 \end{bmatrix}$	✓	✓	✓	✓			✓
4.2.2.2	$\begin{bmatrix} 2 & 1 \\ 1 & 2 \\ 0 & 0 \end{bmatrix}$	✓	✓	✓	✓			✓
4.2.2.3	$\begin{bmatrix} 2 & 1 \\ 2 & 0 \\ 0 & 1 \end{bmatrix}$	✓	✓	✓	✓			✓
4.2.2.4	$\begin{bmatrix} 2 & 1 \\ 0 & 2 \\ 1 & 0 \end{bmatrix}$	✓	✓	✓	✓			✓
4.2.2.5	$\begin{bmatrix} 2 & 1 \\ 1 & 1 \\ 1 & 0 \end{bmatrix}$	✓	✓	✓	✓	✓		✓
4.2.2.6	$\begin{bmatrix} 2 & 1 \\ 1 & 1 \\ 0 & 1 \end{bmatrix}$	✓	✓	✓	✓	✓		✓
4.2.2.7	$\begin{bmatrix} 2 & 0 \\ 0 & 2 \\ 1 & 1 \end{bmatrix}$	✓	✓	✓	✓			✓
4.2.2.8	$\begin{bmatrix} 2 & 0 \\ 1 & 1 \\ 1 & 1 \end{bmatrix}$	✓	✓	✓	✓		✓	✓
4.2.2.9	$\begin{bmatrix} 1 & 1 \\ 1 & 1 \\ 1 & 1 \end{bmatrix}$	✓	✓	✓	✓		✓	✓

6.6 Chapter summary

Chapter 4 presented examples of two and three-body 2-dimensional kinematic mounts and Chapter 5 gave conditions applying to these kinematic mounts. In this chapter, we gave a conjectured exhaustive set of non-equivalent configuration-representations for these kinematic mounts. Configuration-representations and this exhaustive set provide design guidelines to quickly select, identify and design a two or three-body 2-dimensional kinematic mount.

More specifically, this chapter introduced the configuration-representations notation as well as equivalence relations. We used these along with the conditions of Chapter 5 to classify 2-dimensional kinematic mounts into a total of 1 two-body configuration-representation and 9 three-body configuration-representations. We conjecture that this list consists of all non-equivalent configuration-representations of kinematic mounts.

6.7 Heuristic method used to derive the conjectured classification

We obtained our conjecture using a heuristic method not detailed in this thesis. This method generated all possible configuration-arrays consisting of non-negative integers with sum of entries equal to 3 or 6 then applied the conditions of Chapter 5 together with the equivalence relations of 6.3 to give the list of Section 6.5.

6.8 Perspectives

Our results for three 2-dimensional bodies can be generalized to more than three bodies. Moreover, non-orthogonal interfaces can be considered.

Chapter 7   Two and three-body 3-dimensional kinematic mounts

7.1   Problem statement

For two bodies:

> *Propose examples of kinematic mounts assembled with one interface whose contact points lie on the axes of a set of orthogonal coordinates, and whose constraints are parallel to one of these three orthogonal axes.*

For three bodies:

> *Propose examples of kinematic mounts assembled with up to three interfaces whose contact points lie on the axes of a set of orthogonal coordinates (we exclude the intersection point of these axes). All the constraint lines are parallel to one of the three orthogonal axes.*

7.2   Notation

We represent each contact point by a sphere. We indicate where the contact point touches or will touch by shading that hemisphere in black. There are two types of contact points, as illustrated in Figure 7.3.1.1.
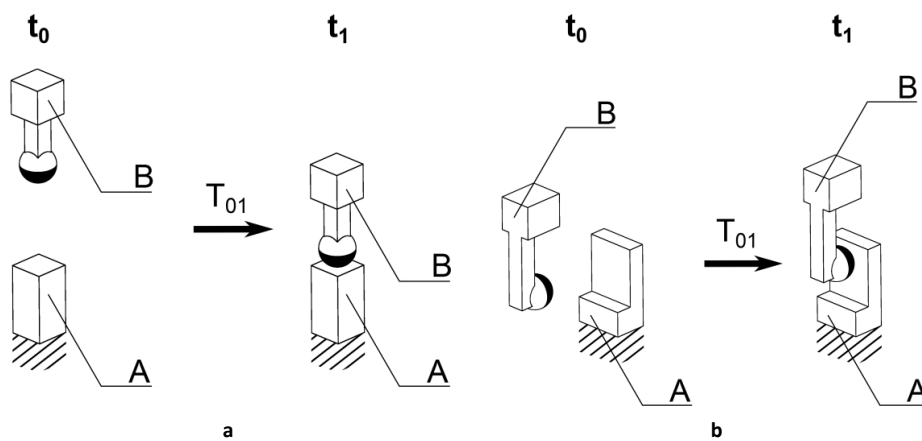
Figure 7.3.1.1: Contact points. a) The first type of contact point. b) The second type of contact point.

7.3   Definition

7.3.1   Configuration-array

The *configuration-array* of a configuration is a 1 by 2 array (for two bodies) or 3 by 2 array (for three bodies). It indicates the number of contact points of an interface and whether their constraint lines are parallel to the x, y or z-axis. The configuration-array of a configuration gives no information on the position of the contact points, only that they do not share the same constraint line. The rows of a configuration-array describe the interfaces (1st row I_{AB}, 2nd row I_{BC}, 3rd row I_{AC}). The first Column describes the number of constraint lines parallel to the x-axis. The second column, the number of constraint lines parallel to the y-axis. The third column, the number of constraint lines parallel to the z-axis. Two examples of configuration-arrays are illustrated in Figure 7.3.1.1 and Figure 7.3.1.2. All configuration-arrays of two bodies have to obey Conditions 8.3.2, 8.3.3 and 8.3.5 (§8.3). All configuration-arrays of three bodies have to obey Conditions 8.5.2 and 8.5.3 (§8.5). These conditions will be detailed in Chapter 8.
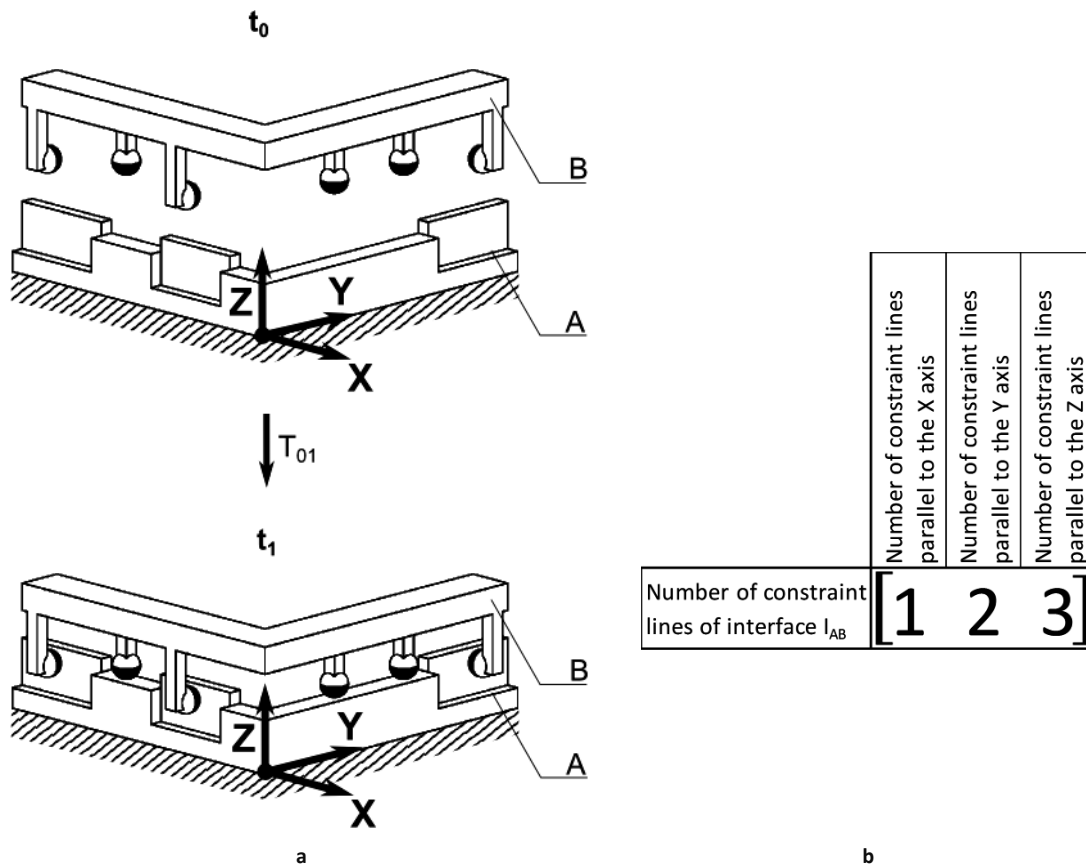
Figure 7.3.1.1: a) Two-body three axes example 7.4.1.2, b) The configuration-array of Two-body three axes Example 7.4.1.2.

t₀

C

Z

Y

X

A

B

↓ T₀₁

t₁

C

A

B
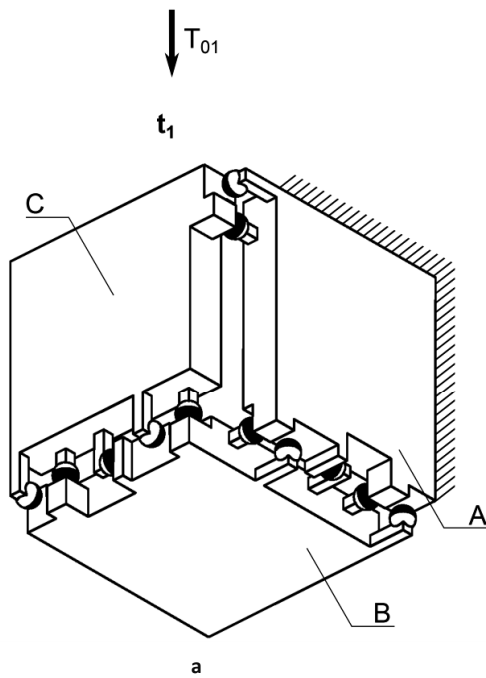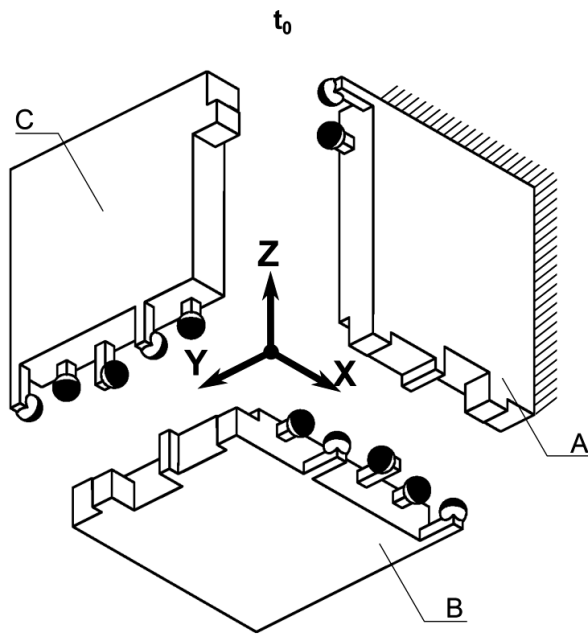
	Number of constraint lines parallel to the X axis	Number of constraint lines parallel to the Y axis	Number of constraint lines parallel to the Z axis
Number of constraint lines of interface I_{AB}	1	2	2
Number of constraint lines of interface I_{BC}	2	1	2
Number of constraint lines of interface I_{AC}	1	1	0

a   b

Figure 7.3.1.2: a) Three-body three axes example 7.4.2.1, b) The configuration-array of Three-body three axes example 7.4.2.1.

7.4 Examples of kinematic mounts and their configuration-array

In Section 7.4.1, we present examples of configurations of two bodies and in Section 7.4.2 we give examples of three bodies with a three perpendicular line interface. At the end of this chapter we offer an overview (Table 7.1 and 7.2) of these examples. We conjecture that these examples are exhaustive with respect to the problem statement 7.1.

7.4.1 Two examples of a two body 3-dimensional kinematic mount

$$[2 \quad 2 \quad 2]$$
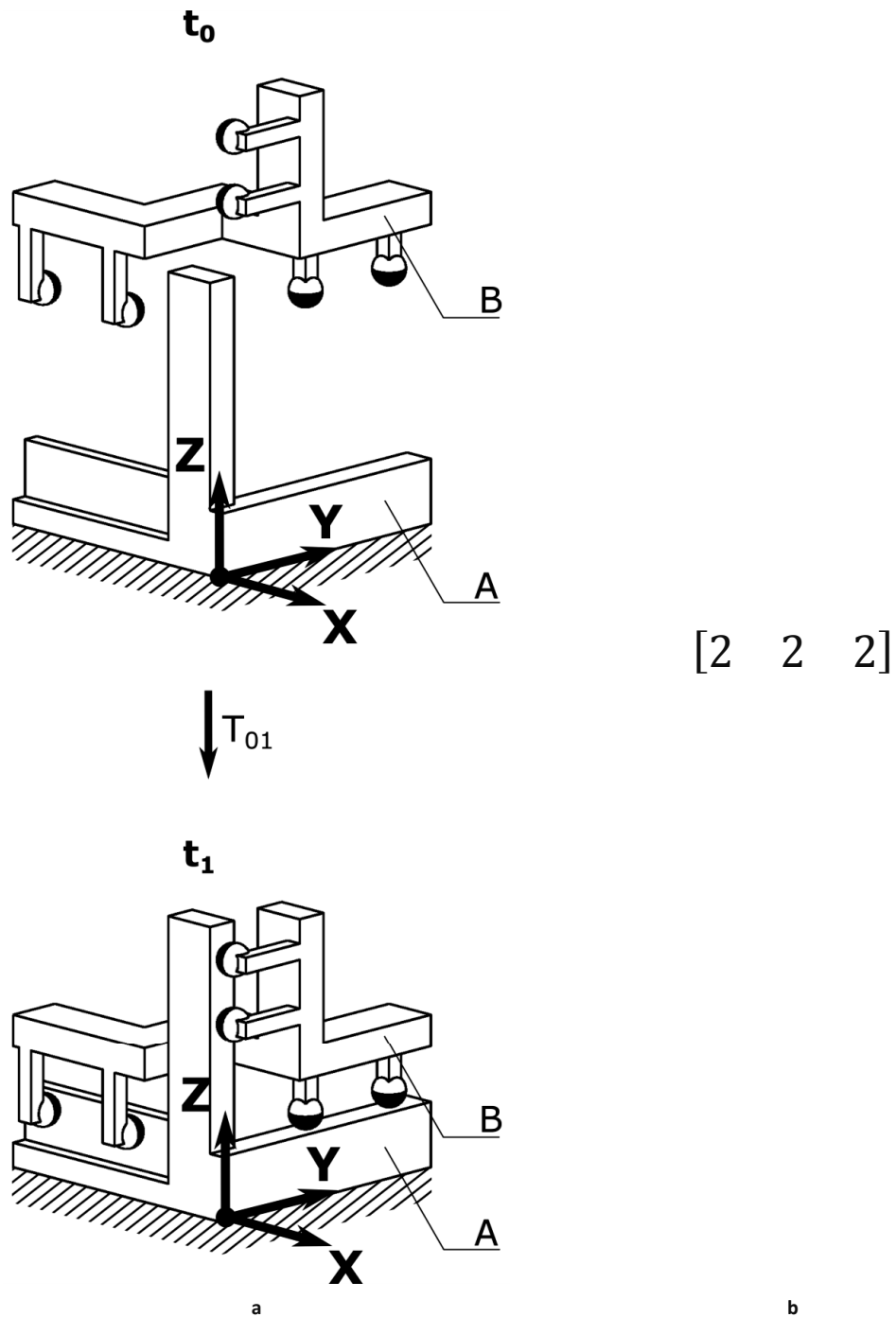
Figure 7.4.1.1: A kinematic mount with three pairs of parallel constraint lines Example 7.4.1.1. b) The configuration-array of Example 7.4.1.1.

$$\mathbf{t_0}$$

$$T_{01}$$

$$\begin{bmatrix} 1 & 2 & 3 \end{bmatrix}$$

$$\mathbf{t_1}$$

a
b
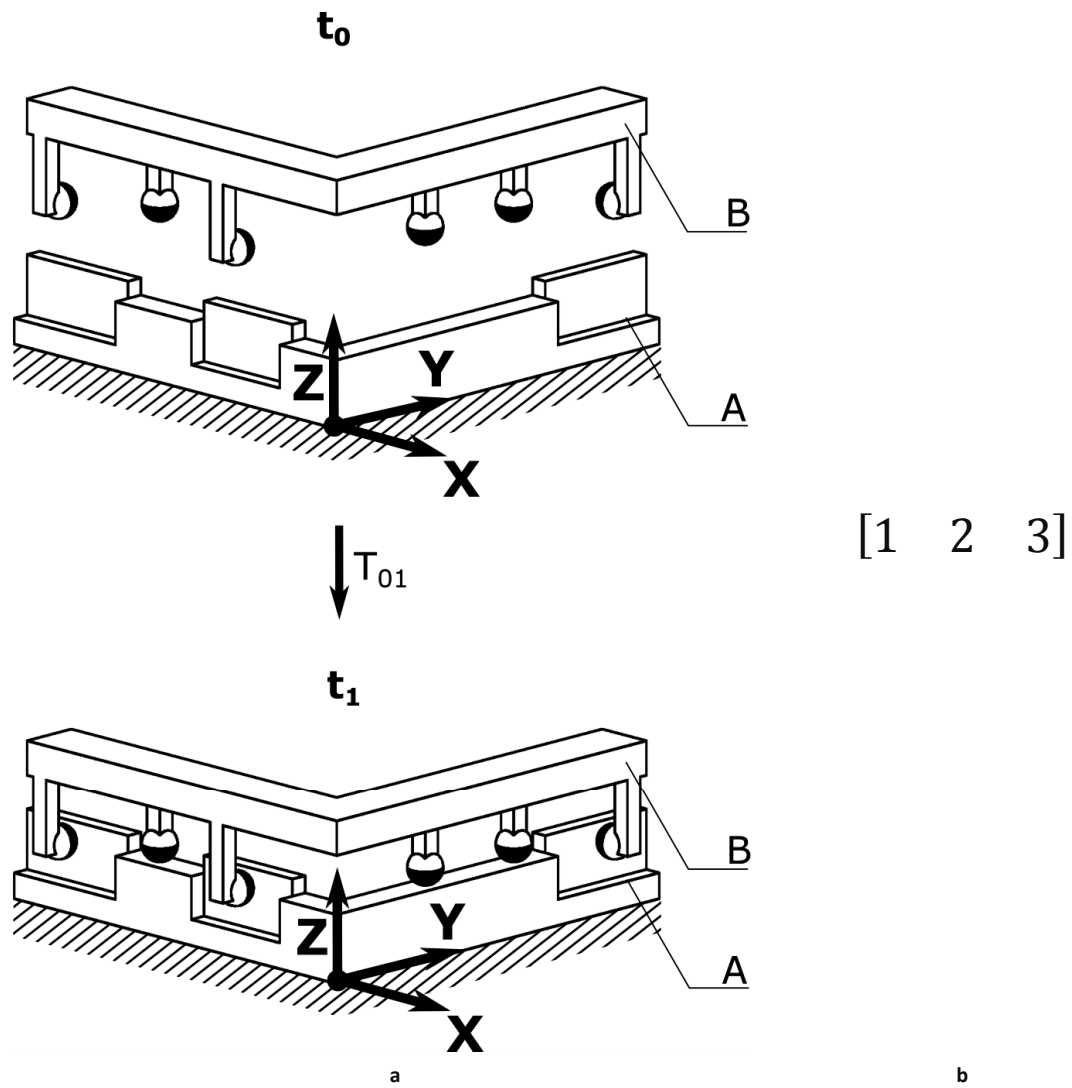
Figure 7.4.1.2: A kinematic mount with three sets of constraint lines. One set has three parallel constraint lines a second set has two parallel constraint lines and a third set has a single constraint line Example 7.4.1.2. b) The configuration-array of Example 7.4.1.2.

7.4.2 Seven examples of three body, three-perpendicular-line interface, 3-dimensional kinematic mounts
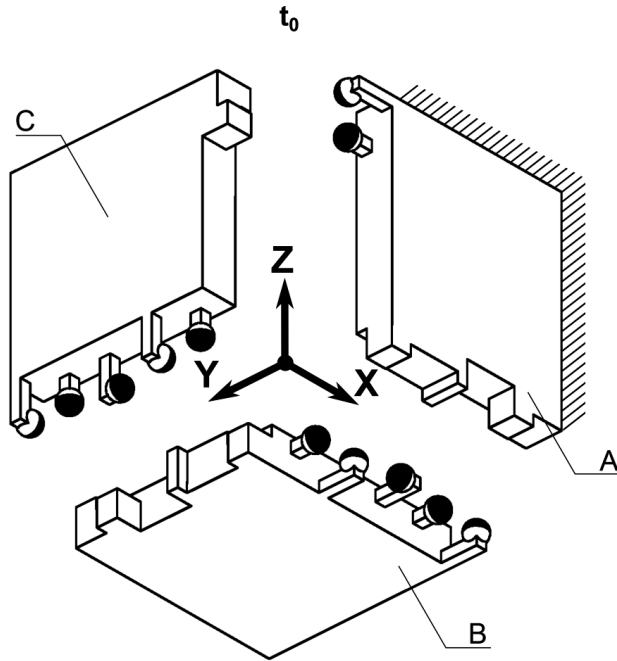
$$\begin{bmatrix} 1 & 2 & 2 \\ 2 & 1 & 2 \\ 1 & 1 & 0 \end{bmatrix}$$
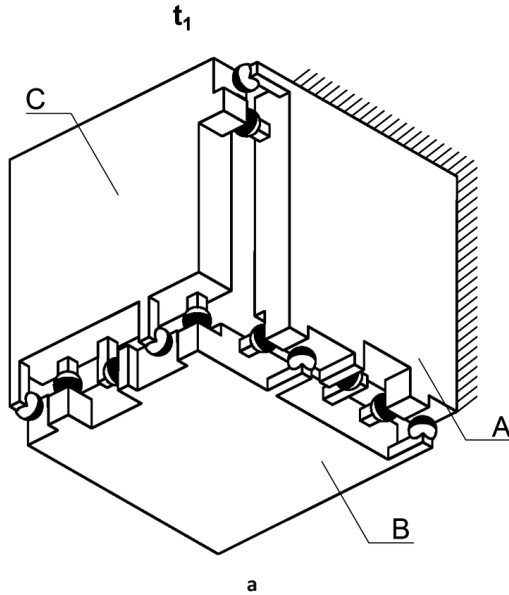
Figure 7.4.2.1: Three-body three axes Example 7.4.2.1. b) The configuration-array of the kinematic mount Example 7.4.2.1.
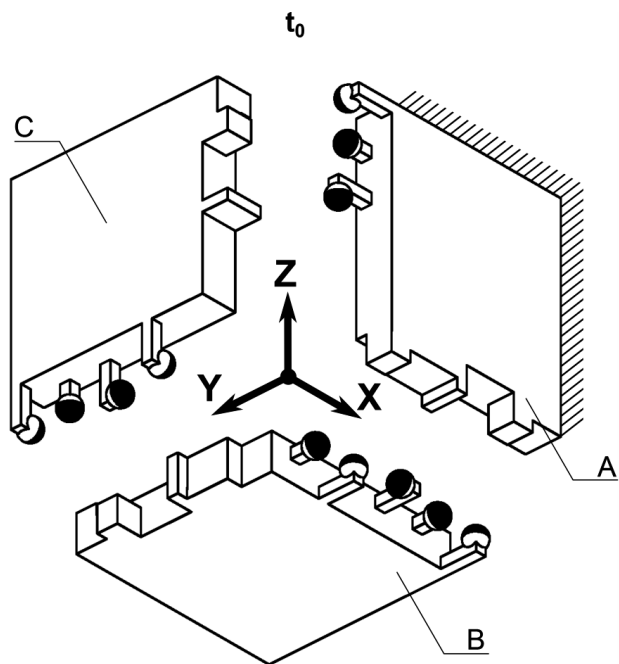
$$\begin{bmatrix} 1 & 2 & 2 \\ 2 & 1 & 1 \\ 1 & 1 & 1 \end{bmatrix}$$
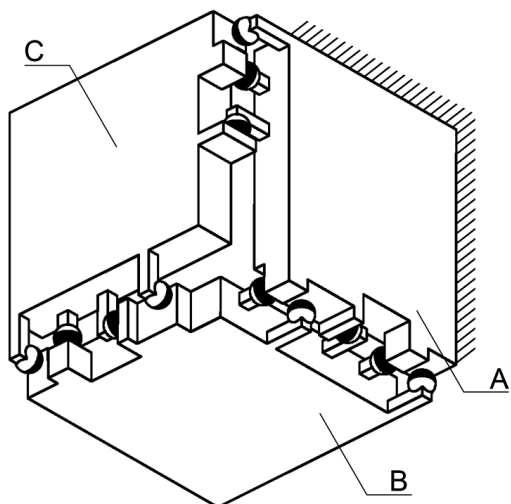
a   b

Figure 7.4.2.2: Three-body three axes Example 7.4.2.2. b) The configuration array of the kinematic mount Example 7.4.2.2.
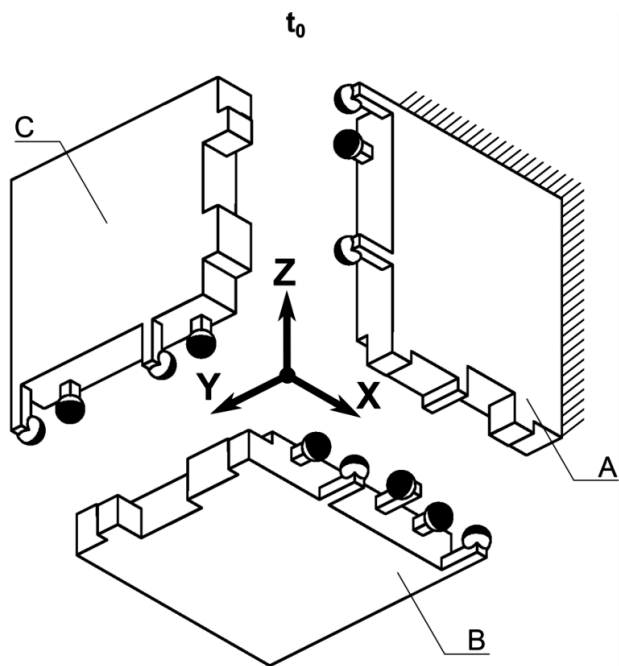
$$\begin{bmatrix} 1 & 2 & 2 \\ 2 & 0 & 2 \\ 1 & 2 & 0 \end{bmatrix}$$
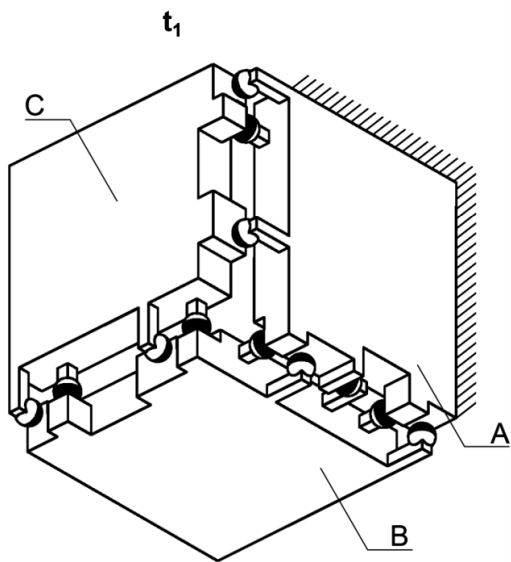
a   **b**

Figure 7.4.2.3: Three-body three axes Example 7.4.2.3. b) The configuration array of the kinematic mount Example 7.4.2.3.

t₀

$$\begin{bmatrix} 1 & 2 & 2 \\ 1 & 1 & 2 \\ 2 & 1 & 0 \end{bmatrix}$$

T_{01}

t₁
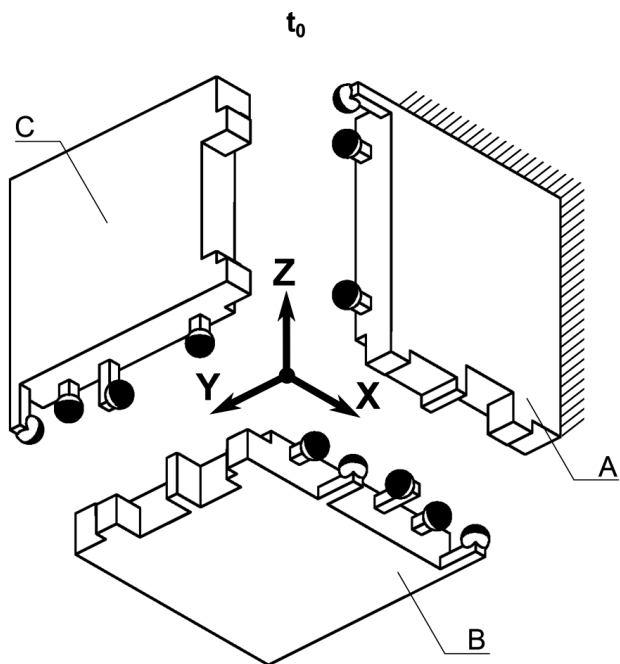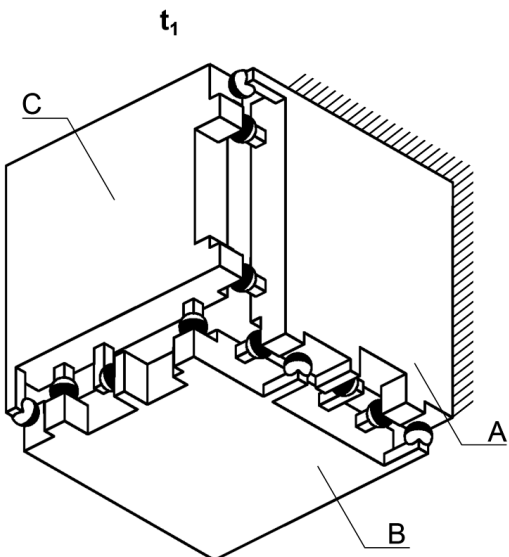
a   b

Figure 7.4.2.4: Three-body three axes Example 7.4.2.4. b) The configuration array of the kinematic mount Example 7.4.2.4.

t₀

$$\begin{bmatrix} 1 & 2 & 1 \\ 2 & 0 & 2 \\ 1 & 2 & 1 \end{bmatrix}$$

T₀₁

t₁
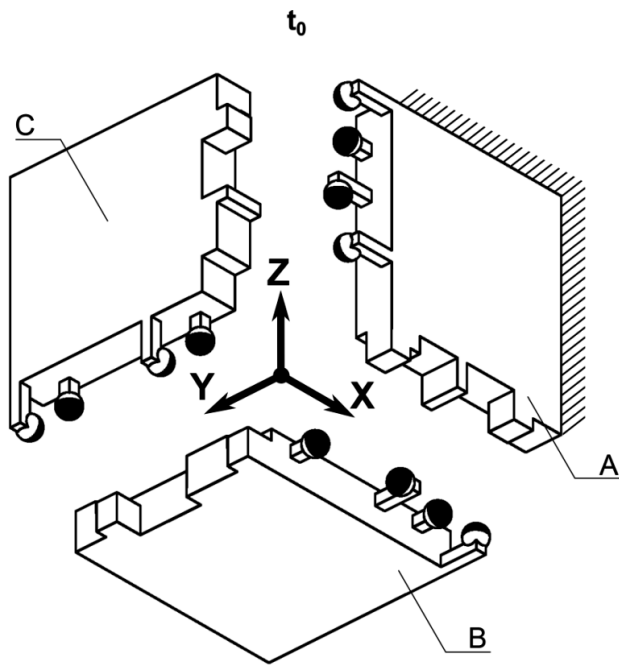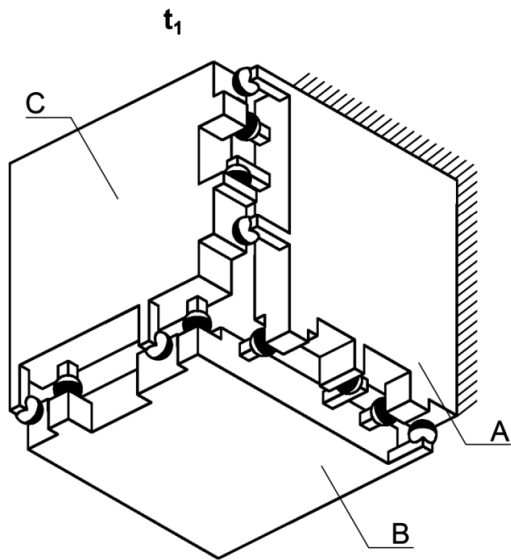
a   b

Figure 7.4.2.5: Three-body three axes Example 7.4.2.5. b) The configuration array of the kinematic mount Example 7.4.2.5.
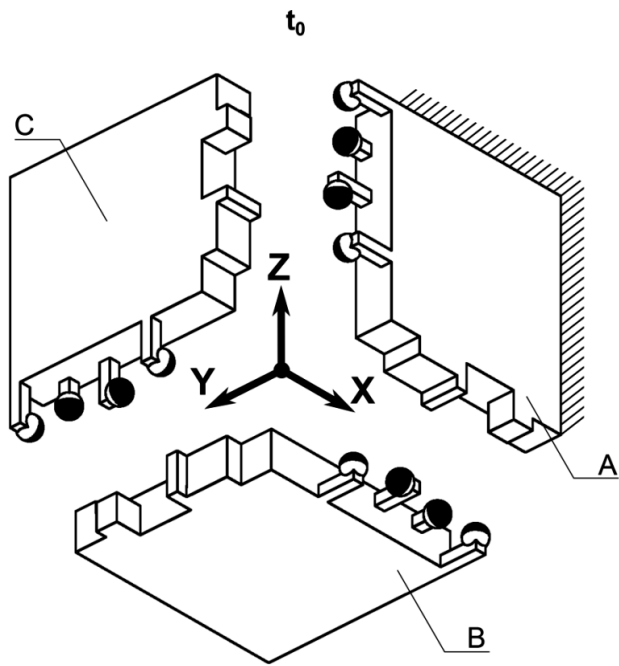
$$\begin{bmatrix} 1 & 1 & 2 \\ 2 & 1 & 1 \\ 1 & 2 & 1 \end{bmatrix}$$
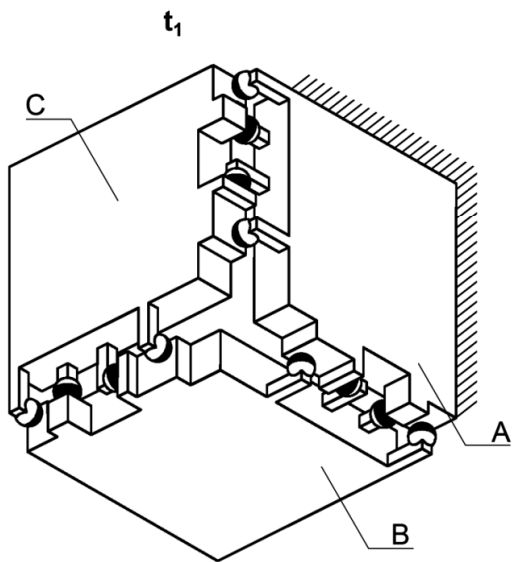
a   b

Figure 7.4.2.6: Three-body three axes Example 7.4.2.6. b) The configuration array of the kinematic mount Example 7.4.2.6.
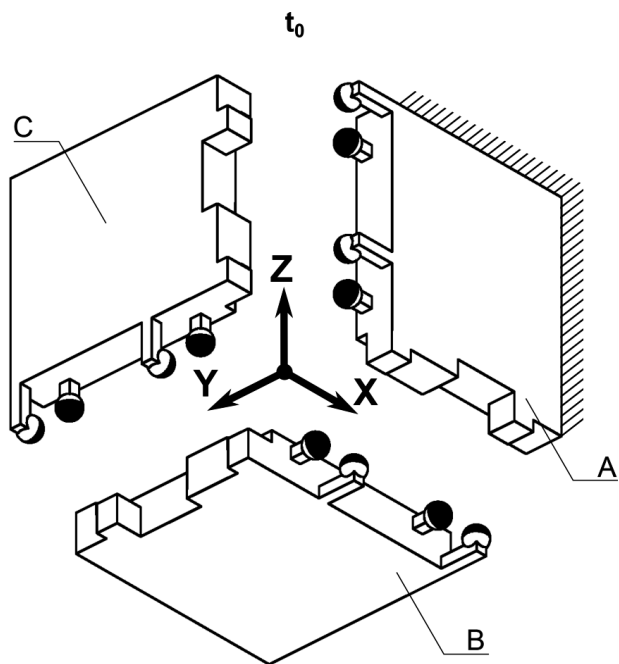
$$\begin{bmatrix} 0 & 2 & 2 \\ 2 & 0 & 2 \\ 2 & 2 & 0 \end{bmatrix}$$
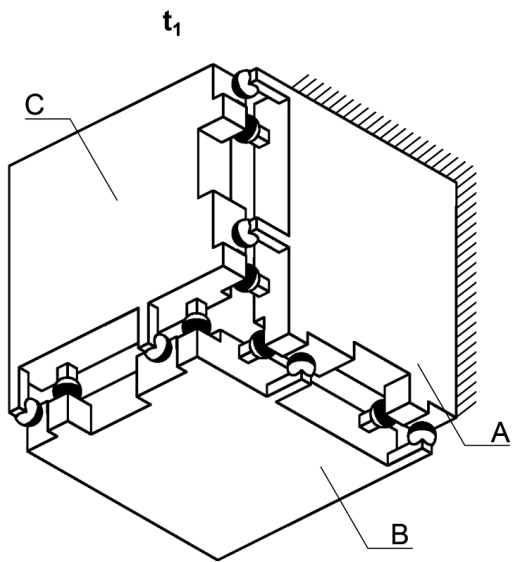
Figure 7.4.2.7: Three-body three axes Example 7.4.2.7. b) The configuration array of the kinematic mount Example 7.4.2.7.

7.5 Overview

Table 7.1: Two-body overview.

Example 7.4.1.1:

[2 2 2]

B

A
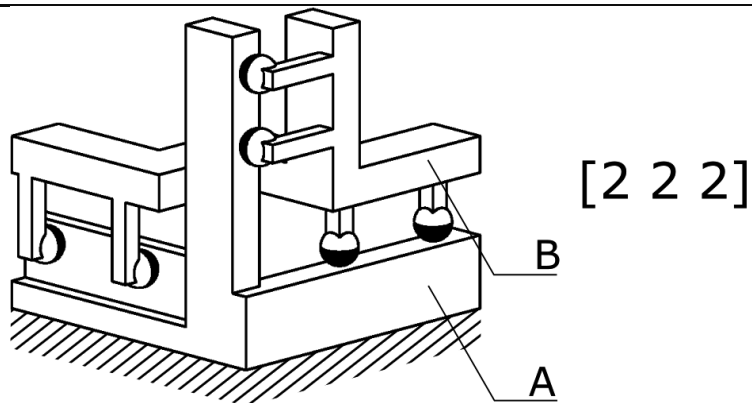
Figure 7.4.1.1

Example 7.4.1.2:

[1 2 3]

B

A
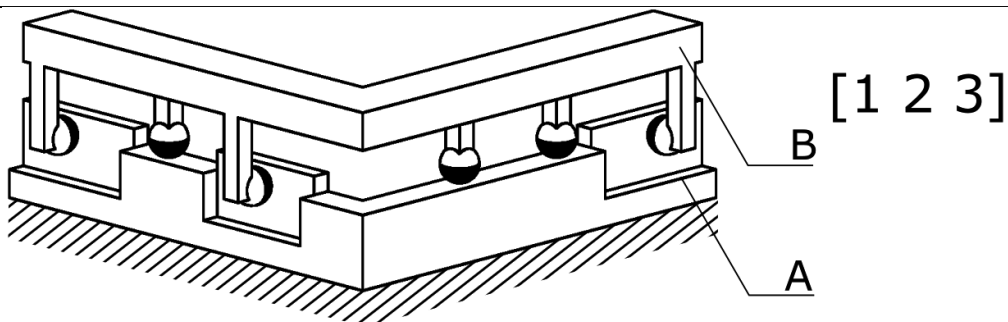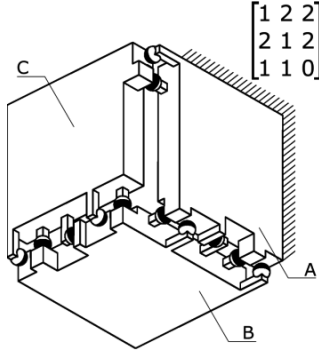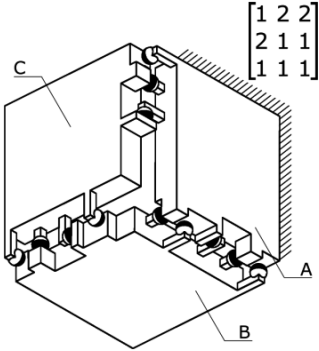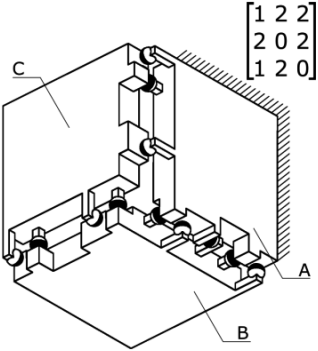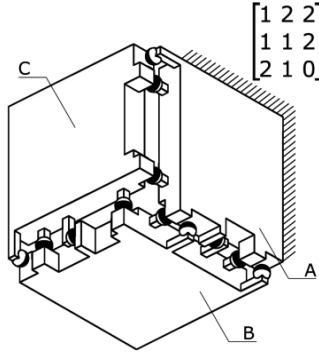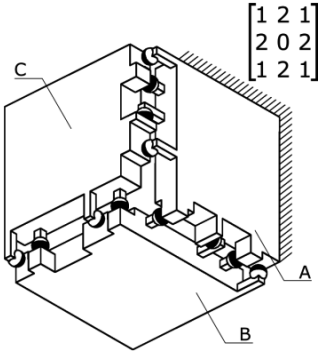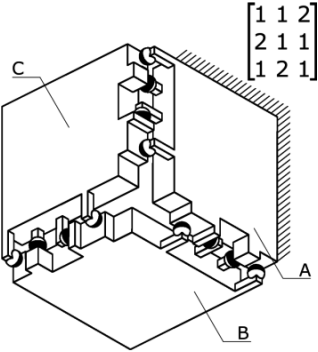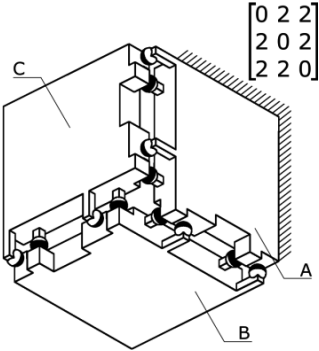
Figure 7.4.1.2

Table 7.2: Three-body overview.

Example 7.4.2.1	Example 7.4.2.2	Example 7.4.2.3
$\begin{bmatrix} 1 & 2 & 2 \\ 2 & 1 & 2 \\ 1 & 1 & 0 \end{bmatrix}$	$\begin{bmatrix} 1 & 2 & 2 \\ 2 & 1 & 1 \\ 1 & 1 & 1 \end{bmatrix}$	$\begin{bmatrix} 1 & 2 & 2 \\ 2 & 0 & 2 \\ 1 & 2 & 0 \end{bmatrix}$
Figure 7.4.2.1	Figure 7.4.2.2	Figure 7.4.2.3
Example 7.4.2.4	Example 7.4.2.5	Example 7.4.2.6
$\begin{bmatrix} 1 & 2 & 2 \\ 1 & 1 & 2 \\ 2 & 1 & 0 \end{bmatrix}$	$\begin{bmatrix} 1 & 2 & 1 \\ 2 & 0 & 2 \\ 1 & 2 & 1 \end{bmatrix}$	$\begin{bmatrix} 1 & 1 & 2 \\ 2 & 1 & 1 \\ 1 & 2 & 1 \end{bmatrix}$
Figure 7.4.2.4	Figure 7.4.2.5	Figure 7.4.2.6

Example 7.4.2.7
$\begin{bmatrix} 0 & 2 & 2 \\ 2 & 0 & 2 \\ 2 & 2 & 0 \end{bmatrix}$
Figure 7.4.2.7

Chapter 8   Conditions for two and three body 3-dimensional kinematic mounts

8.1   Problem statement

The problem statement of this chapter is:

> *Identify necessary conditions for the kinematic mounts of Chapter 7.*

8.2   Remark

We illustrate a constraint line in three dimensions by a dotted line. We illustrate parts of a plane on which constraint lines lie with a dash-dot line.

8.3   Some conditions for two-body kinematic mounts.

Condition 8.3.1:

A two-body kinematic mount requires six contact points (Figure 8.3.1).
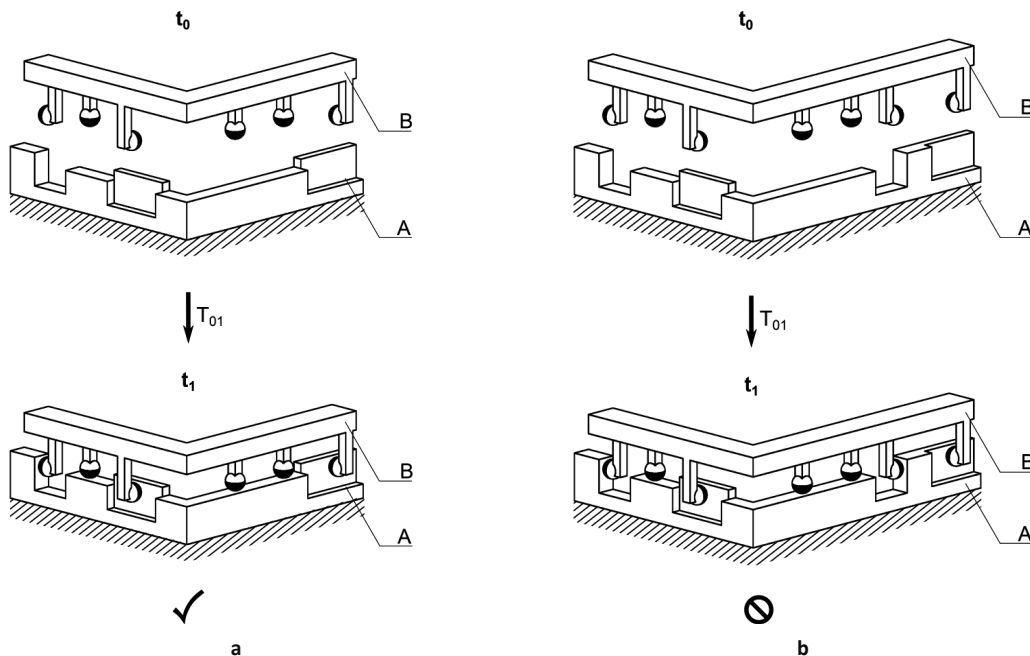
Figure 8.3.1: a) Two bodies require six contact points. b) This configuration is a kinematic mount, because it has seven contact points.

Condition 8.3.2:

An interface cannot have collinear constraint lines (Figure 8.3.2).
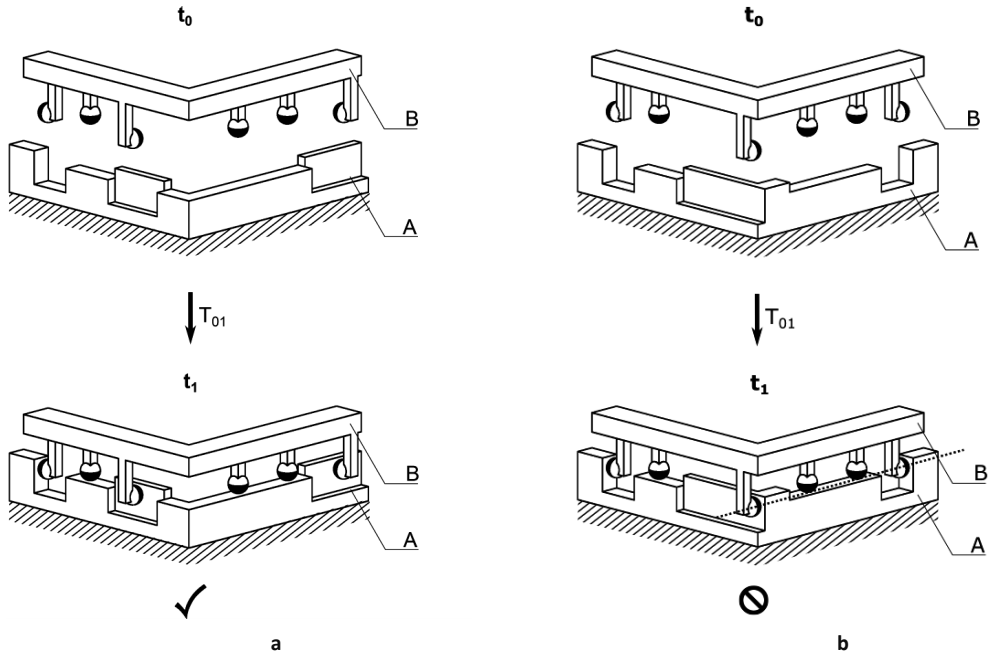
Figure 8.3.2: a) A configuration with no collinear constraint lines. b) A configuration that is not a kinematic mount because it has collinear constraint lines.

Condition 8.3.3:

An interface cannot have more than two coplanar parallel constraint lines (Figure 8.3.3).
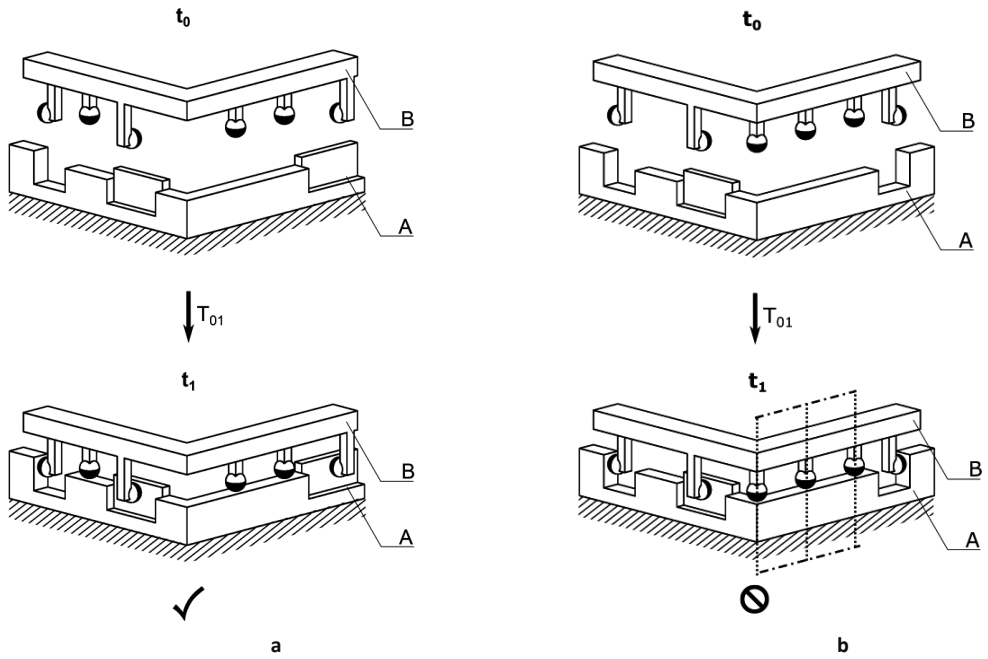
Figure 8.3.3: a) A configuration that has no more than two coplanar parallel constraint lines. b) A configuration that is not a kinematic mount as it has more than two coplanar parallel constraint lines.

Condition 8.3.4:

An interface cannot have more than three parallel constraint lines (Figure 8.3.4).
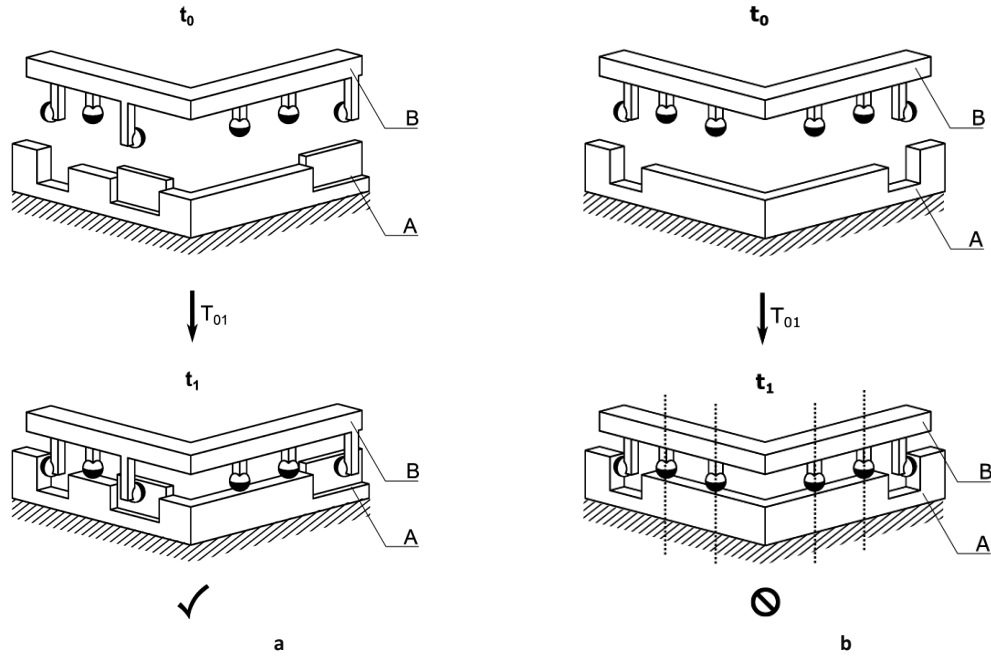
Figure 8.3.4: a) A configuration with three parallel constraint lines. b) A configuration that is not a kinematic mount because it has more than three parallel constraint lines.

Condition 8.3.5:

An interface cannot have more than three coplanar constraint lines (Figure 8.3.5).
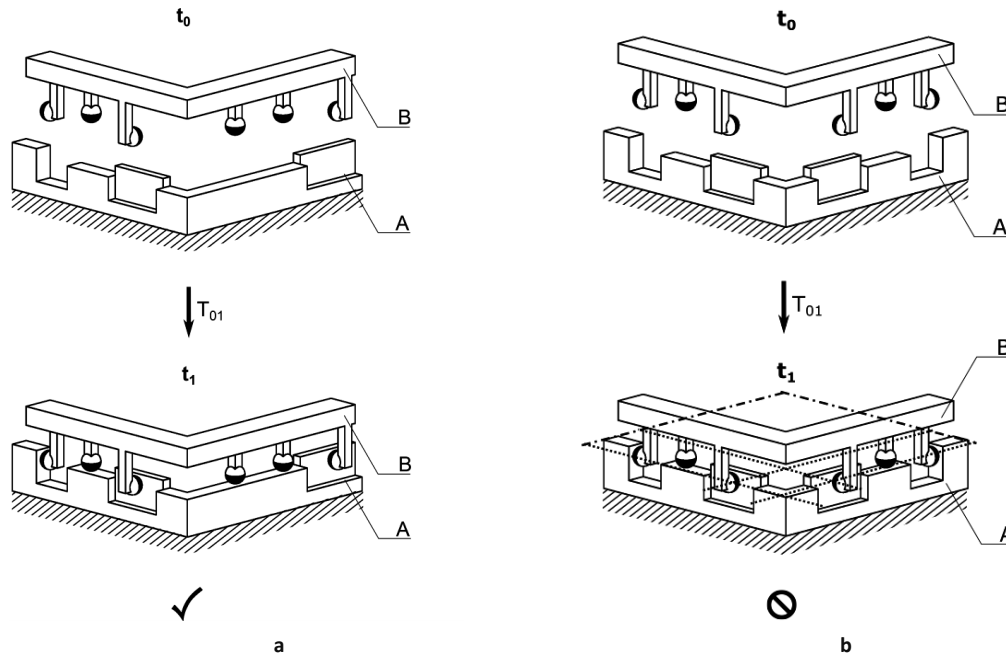
Figure 8.3.5: a) a Configuration with three coplanar constraint lines. b) A configuration that is not a kinematic mount because it has four coplanar constraint lines.

Condition 8.3.6:

An interface needs at least a set of three constraint lines which are not parallel to each other (Figure 8.3.6).
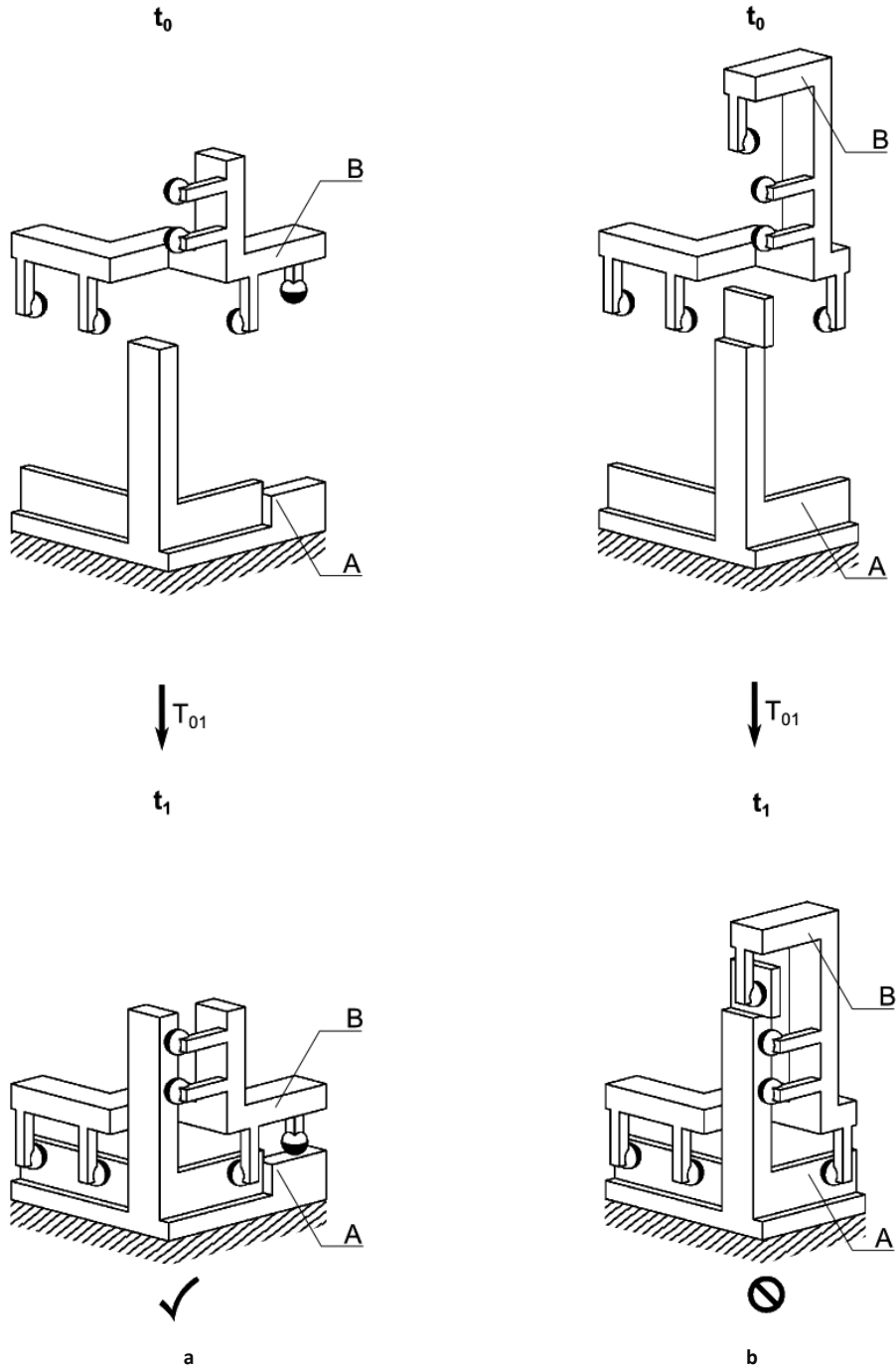
Figure 8.3.6: a) A configuration which has sets of three constraint lines that are not parallel to each other. b) A configuration that only contains sets of two constraint lines that are not parallel to each other. This configuration is not a kinematic mount.

8.4 Corollary for two-body kinematic mounts

Corollary 8.4.1:

Not more than five contact points can lie on a line (Figure 8.3.1).
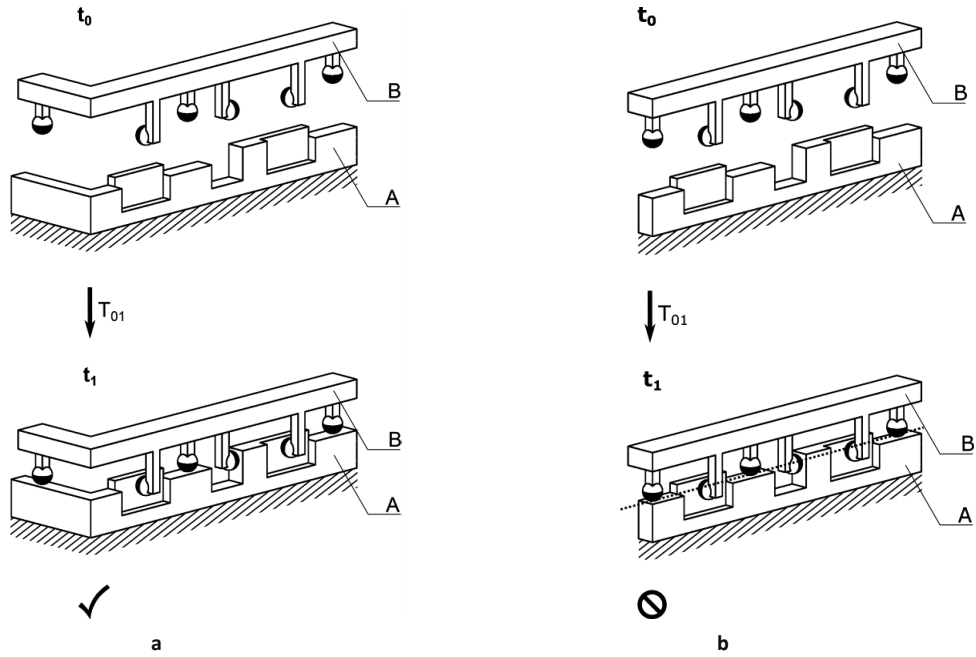
Figure 8.4.1: a) A configuration with five contact points that lie on a single line. b) This configuration is not a kinematic mount, because it has six contact points on a single line.

8.5 Some conditions for three-body kinematic mounts.

Condition 8.5.1:

A three-body kinematic mount requires twelve contact points (Figure 8.5.1).
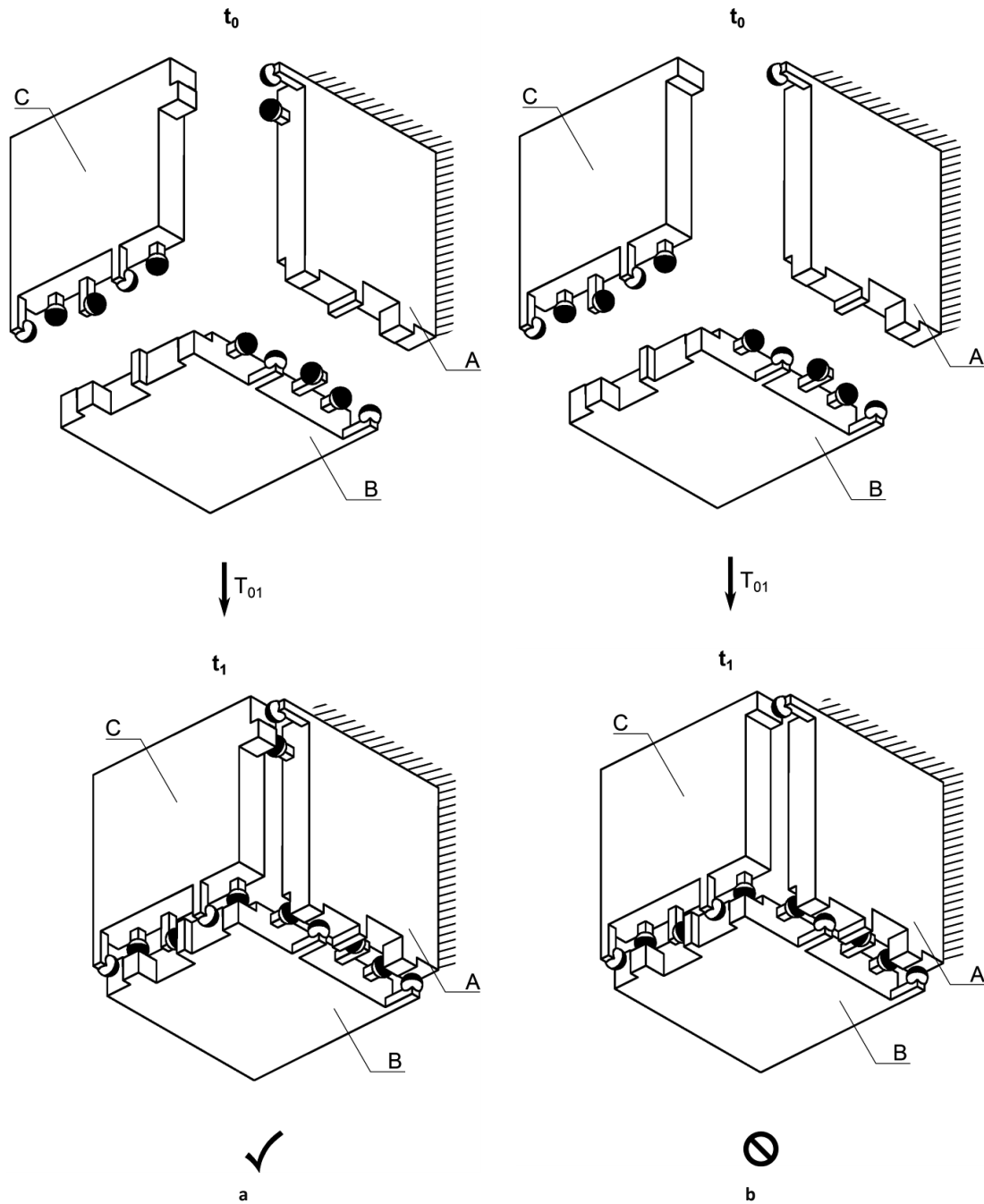
Figure 8.5.1: a) A configuration with twelve contact points. b) This configuration is not a kinematic mount, because it has eleven contact points.

Condition 8.5.2:

An interface cannot have collinear constraint lines (Figure 8.5.2).

t_0 t_0

T_{01} T_{01}

t_1 t_1

a **b**
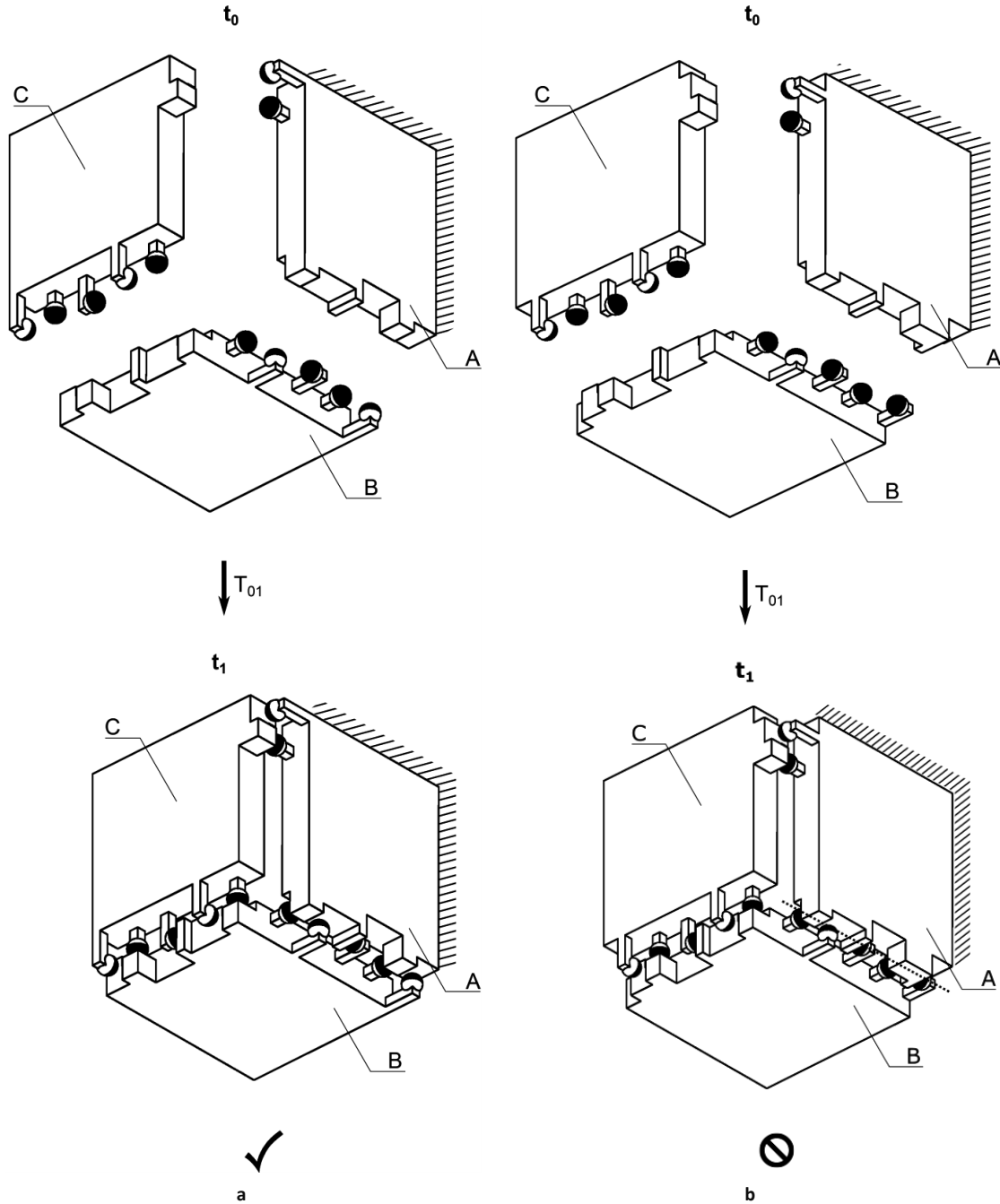
Figure 8.5.2: a) A configuration with no collinear constraint lines in its interfaces. b) This configuration is not a kinematic mount as the interface I_{AC} has two collinear constraint lines.

Condition 8.5.3:

An interface cannot have more than two parallel constraint lines (Figure 8.5.3).

t_0　　　　　　　　　　**t_0**

T_{01}　　　　　　　　**T_{01}**

t_1　　　　　　　　　　**t_1**

a　　　　　　　　　　　**b**
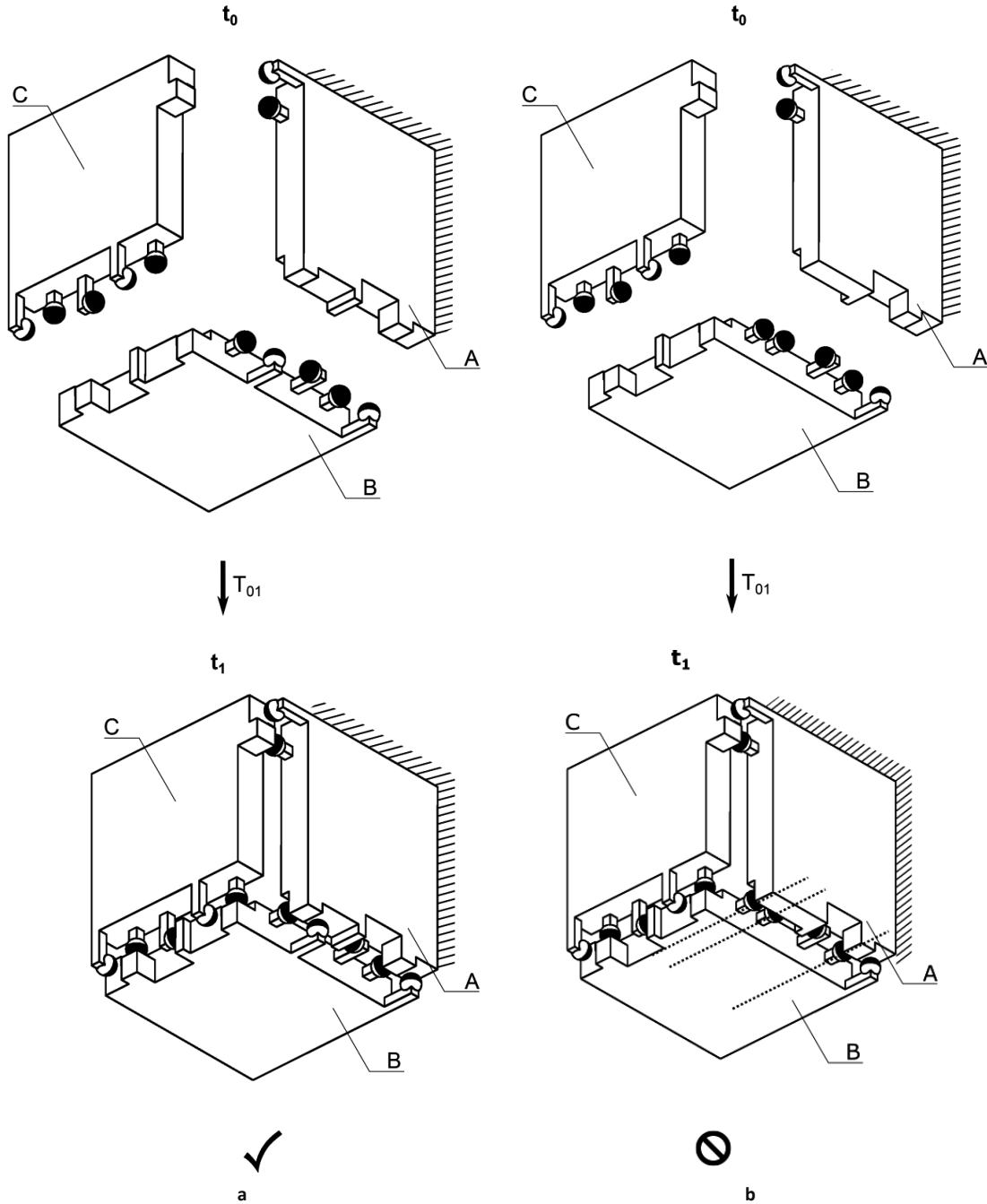
Figure 8.5.3: a) A Configuration where no interface has more than two parallel constraint lines. b) This configuration is not a kinematic mount as interface I_{AC} has three parallel constraint lines.

8.6   A conjecture for three-body kinematic mounts

Conjecture 8.6.1:

Every orthogonal axis has four constraint lines which are parallel to it (Figure 8.6.1).
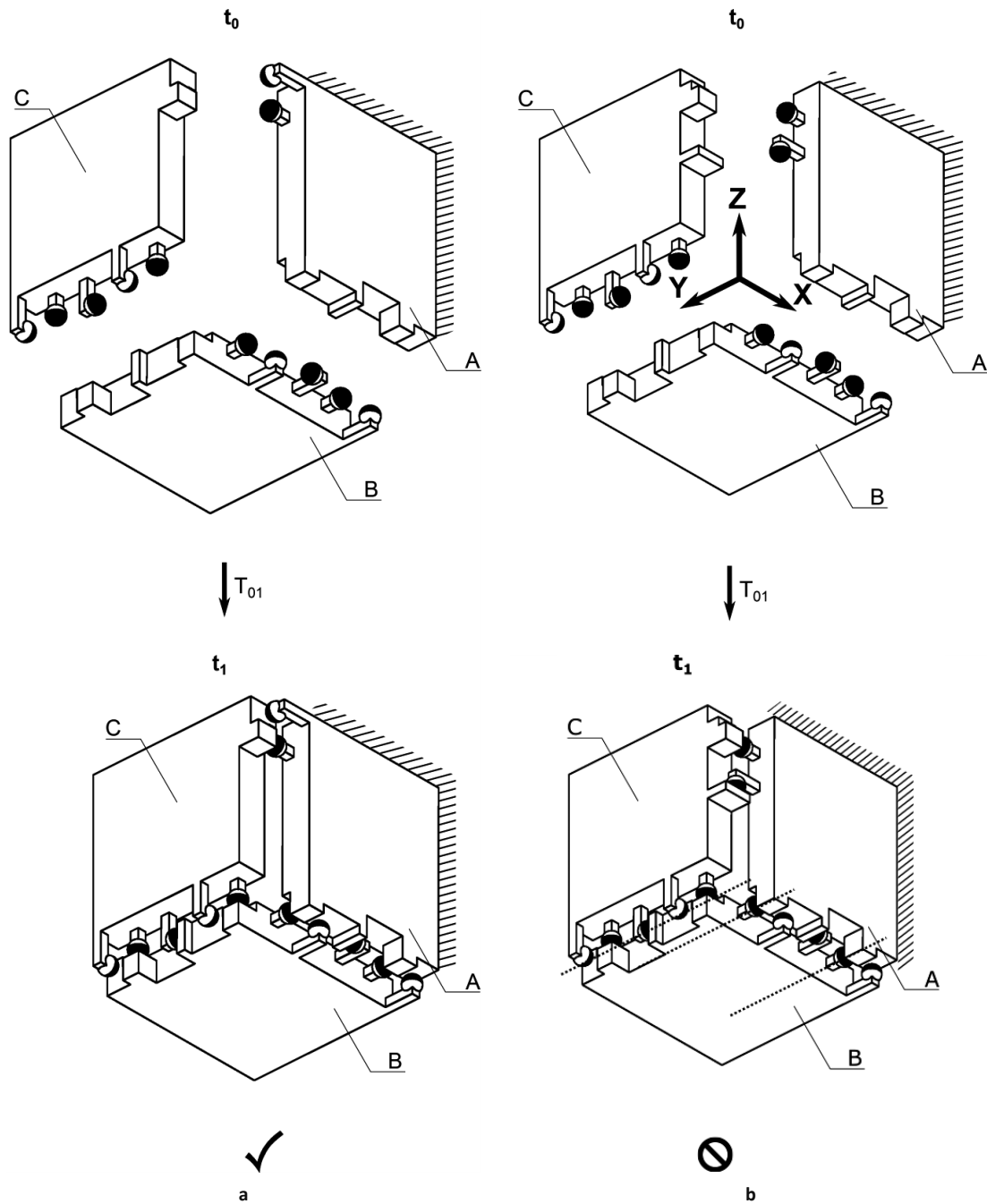
Figure 8.6.1: a) Every constraint is required exactly four times. b) This configuration is not a kinematic mount as it has three constraint lines parallel to the Y-axis.

8.7 Corollaries for three-body kinematic mounts

This section presents the two corollaries for three bodies. Both corollaries require Condition 8.5.2 and 8.5.3 and the problem statement of chapter 6. Corollary 8.7.1 uses Condition 8.5.1 in addition.

Corollary 8.7.1:

An interface requires at least two contact points.
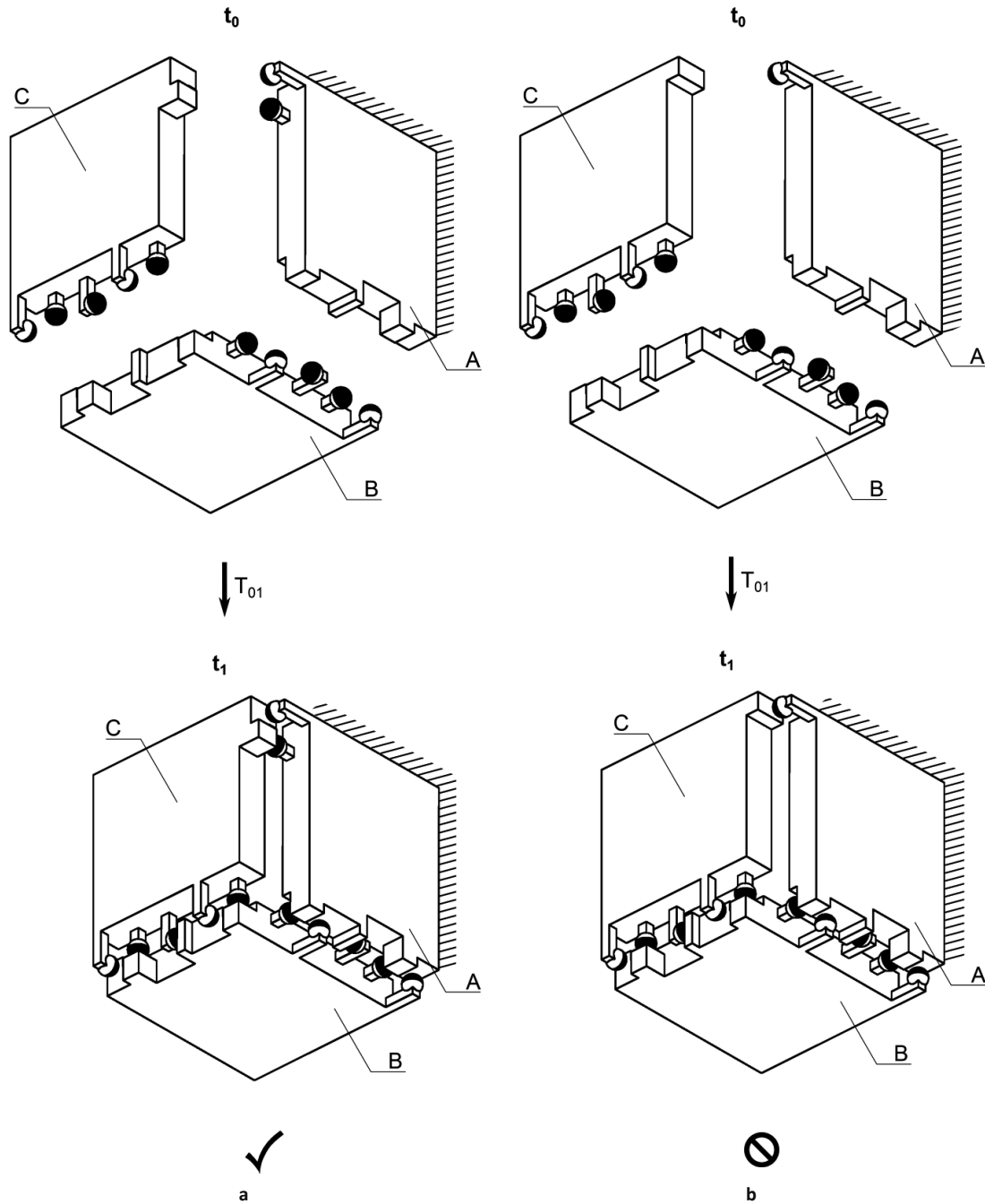
Figure 8.7.1: a) A configuration where every interface has at least two contact points. b) This configuration is not a kinematic mount, because it has only one contact point in interface I_{AC}.

Corollary 8.7.2:

An interface can have a maximum of five contact points.

t_0   **t_0**

T_{01} T_{01}

t_1   **t_1**

a   **b**
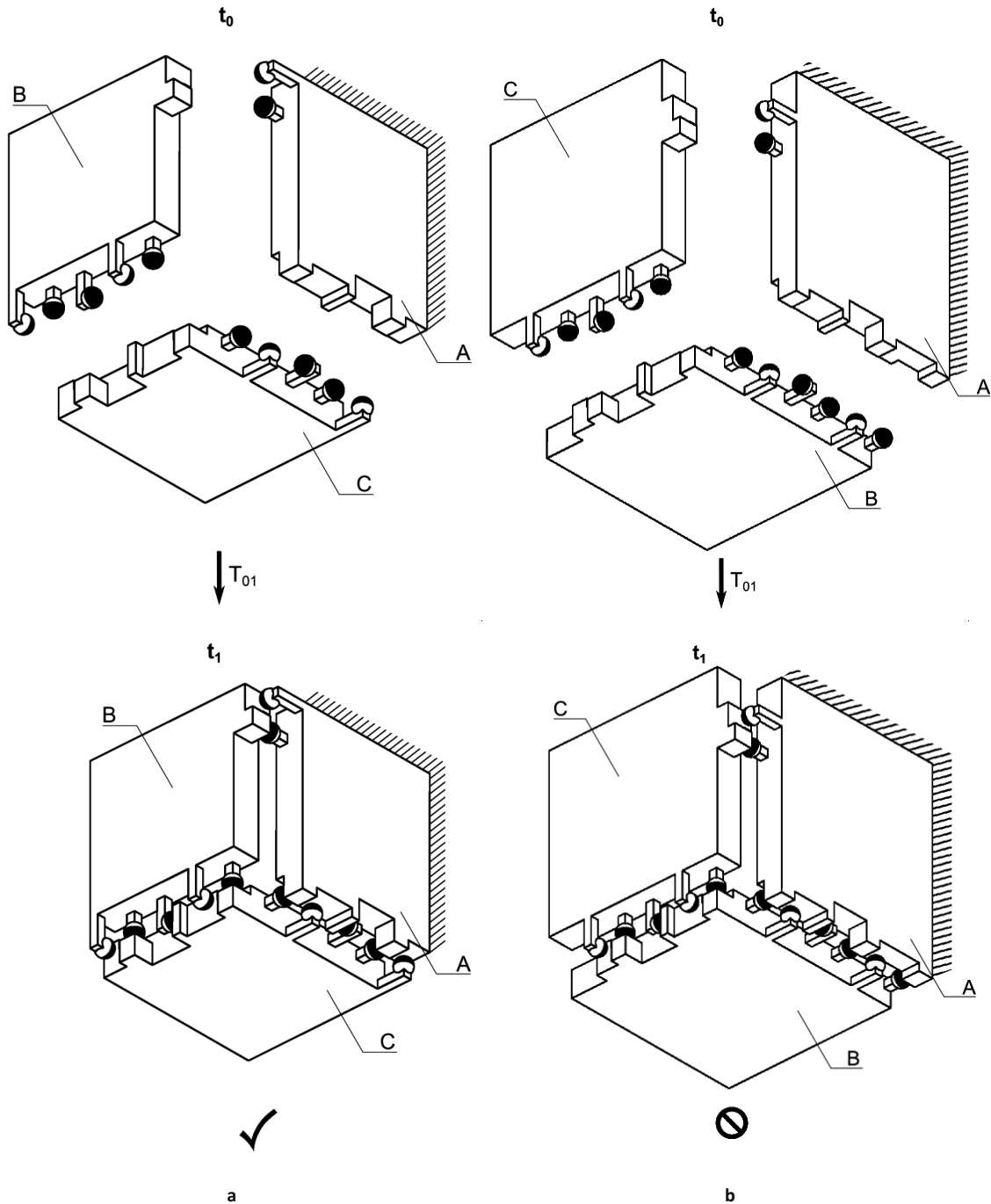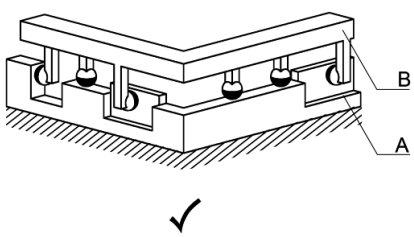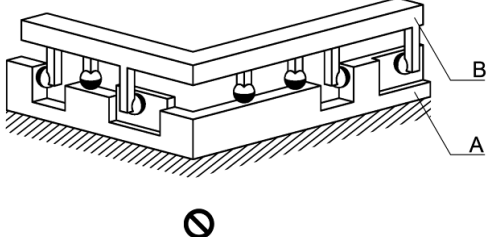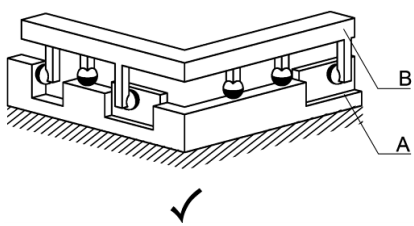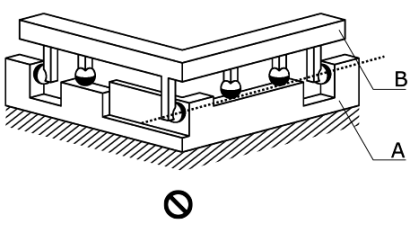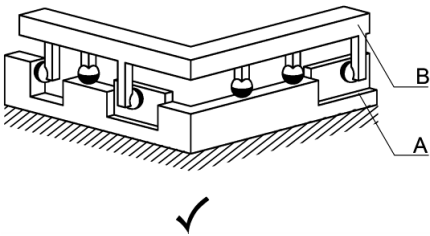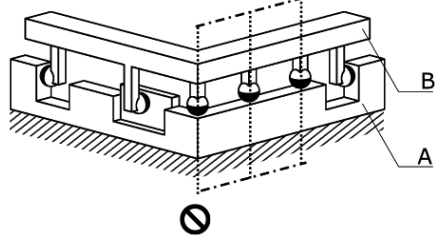
Figure 8.7.2: a) A configuration where every interface has less than six contact points. b) This configuration is not a kinematic mount, because it has six contact points in interface I_{AB}.

8.8 Overview
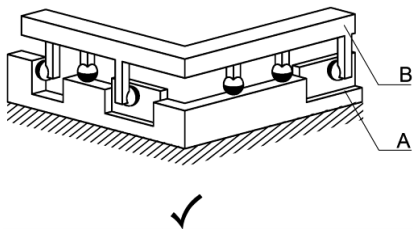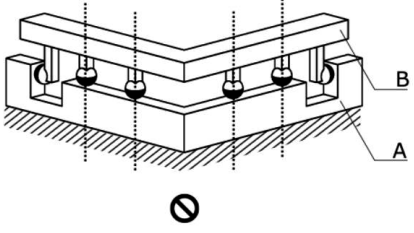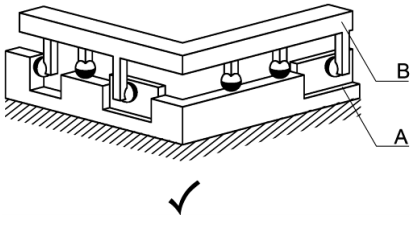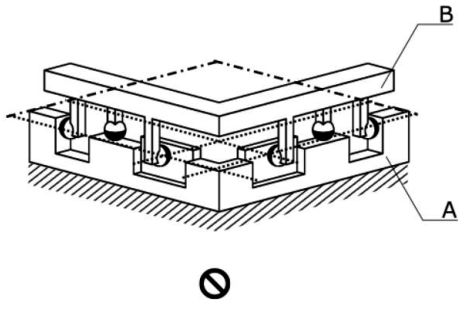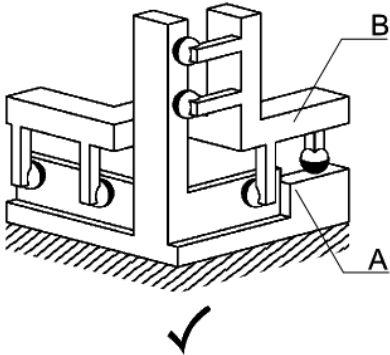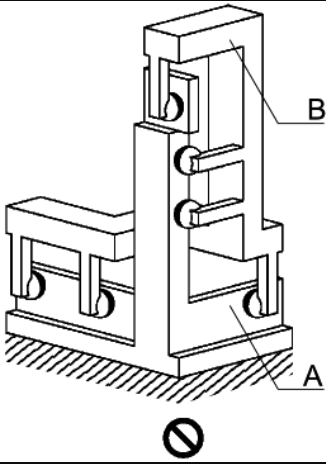
In this section we offer an overview of all the conditions in Table 8.1-8.4.

Table 8.1: Two-body conditions overview (1 of 2)

Condition 8.3.1: A two-body kinematic mount requires six contact points.	
Figure 8.3.1a	Figure 8.3.1b

Condition 8.3.2: An interface cannot have collinear constraint lines.	
Figure 8.3.2a	Figure 8.3.2b

Condition 8.3.3: An interface cannot have more than two coplanar parallel constraint lines.	
Figure 8.3.3a	Figure 8.3.3b

Table 8.2: Two-body conditions overview (2 of 2).

Condition 8.3.4: An interface cannot have more than three parallel constraint lines.	
Figure 8.3.4a	Figure 8.3.4b
Condition 8.3.5: An interface cannot have more than three coplanar constraint lines.	
Figure 8.3.5a	Figure 8.3.5b
Condition 8.3.6: An interface needs at least three constraint lines which are not parallel to each other	
Figure 8.3.6a	Figure 8.3.6b

Table 8.3: Three-body conditions and conjecture overview (1 of 2).
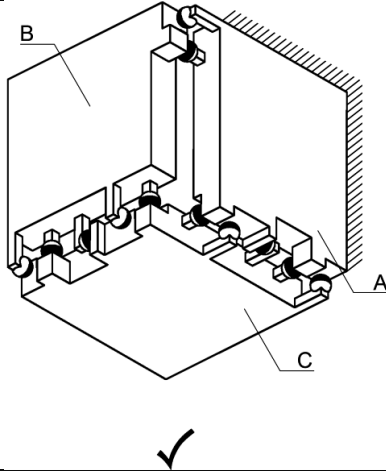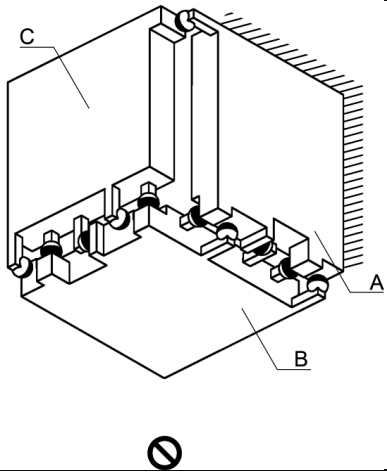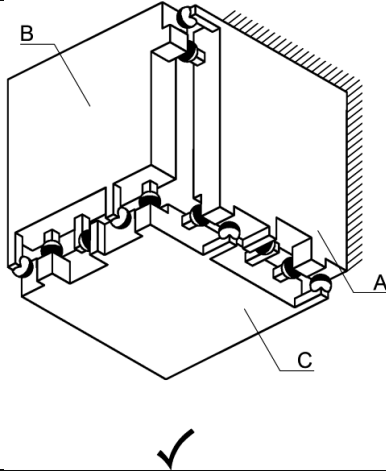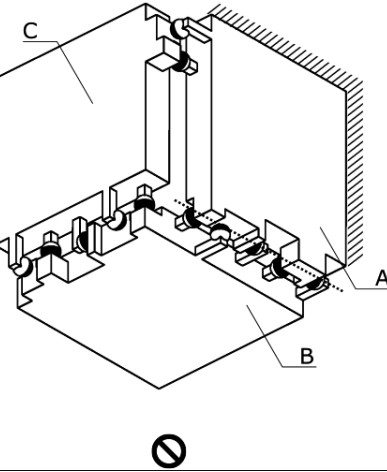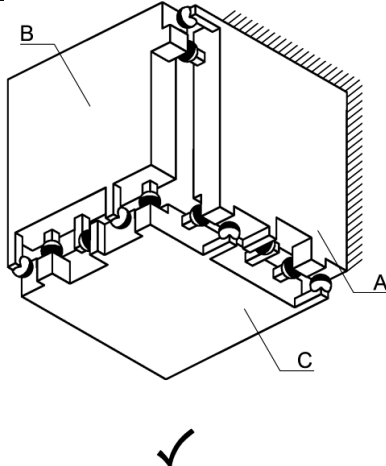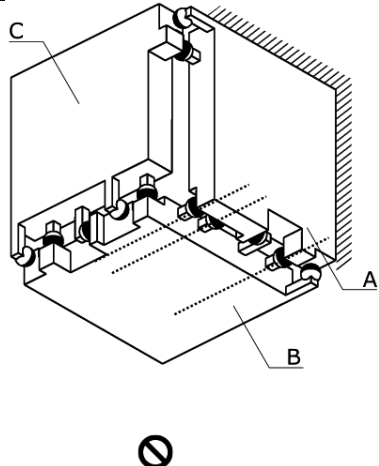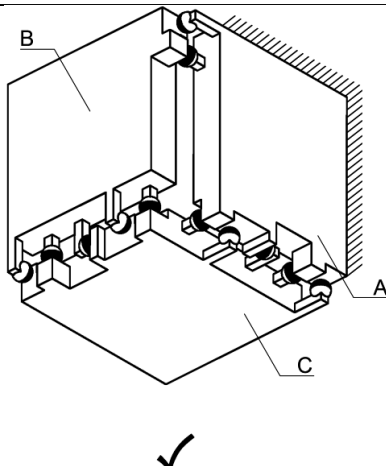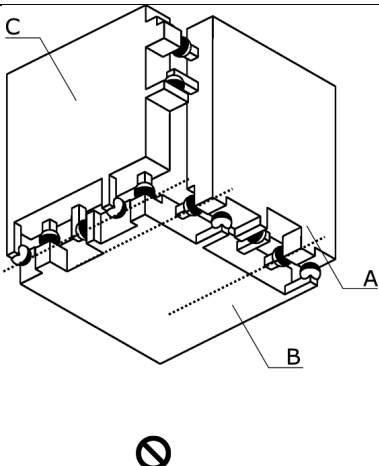
Condition 8.5.1: A three-body kinematic mount requires 12 contact points.	
Figure 8.5.1a	Figure 8.5.1b
Condition 8.5.2: An interface cannot have collinear constraint lines.	
Figure 8.5.2a	Figure 8.5.2b

Table 8.4: Three-body conditions and conjecture overview (2 of 2).

Condition 8.5.3: An interface cannot have more than two parallel constraint lines.	
Figure 8.5.3a	Figure 8.5.3b

Conjecture 8.6.1: Every orthogonal axis has four constraint lines parallel to it.	
Figure 8.6.1a	Figure 8.5.1b

8.9   Chapter summary

This chapter presents six conditions for two-body 3-dimensional kinematic mounts and four conditions for three-body 3-dimensional kinematic mounts. All conditions are conjectural, however some of them are known rules of thumb. We consider that Conjecture 8.6.1 is important as it appears to be non-trivial.

Chapter 9   Classification and discussion of three-body 3-dimensional kinematic mounts

9.1   Problem statement

Propose a classification of the examples of Chapter 7 according to their interface constraint lines.

By classification, we mean a set of non-equivalent configurations so that any kinematic mount is equivalent to an element of this set.

9.2 Definitions

9.2.1 Relabeling a configuration

We use the term *relabeling a configuration* to mean an interchange of the names of the axes for two bodies (Figure 9.2.1a) and for three bodies (Figure 9.2.1b). Relabeling for three bodies is done in order to guarantee that: (i) the interface between body A and B is always the x-axis, (ii) the interface between body B and C is always the y axis, (iii) The interface between body A and C is always the z-axis.
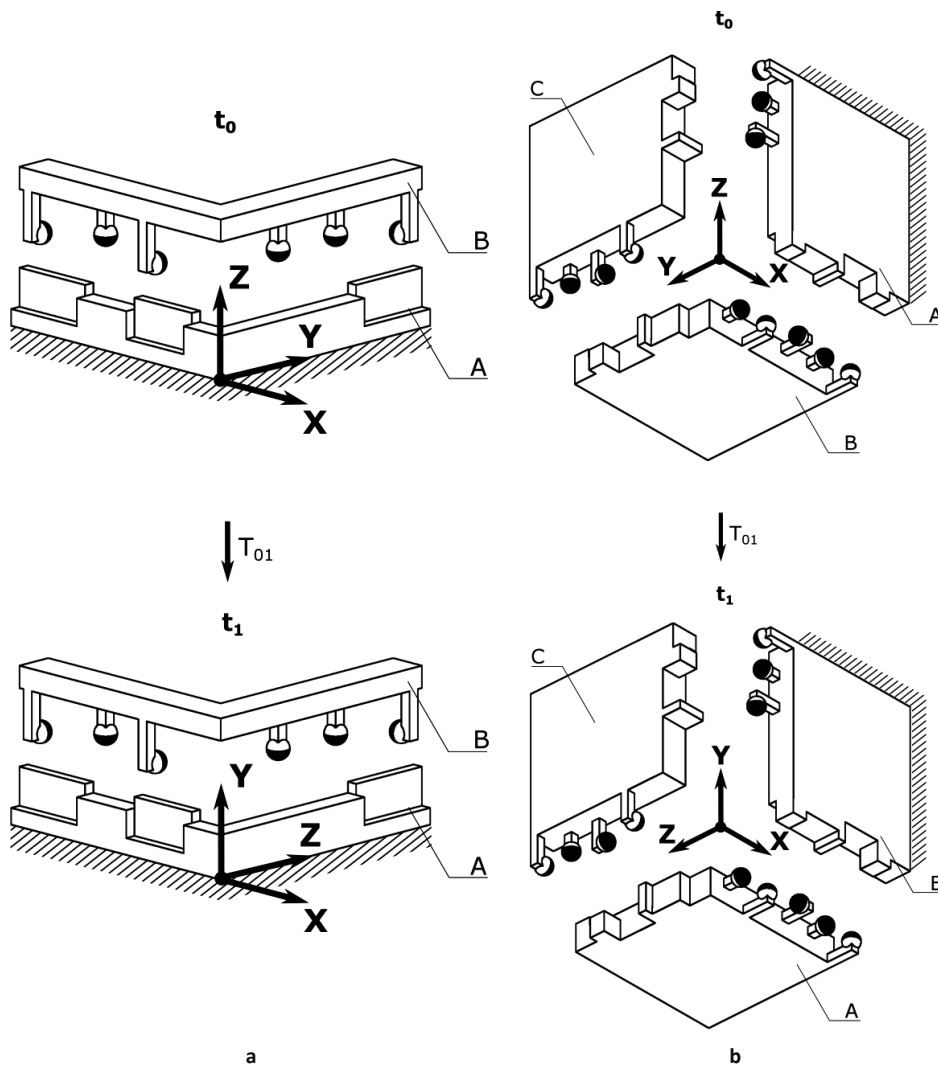
Figure 9.2.1: a) A two-body three axes configuration (t_0) and a relabeled two-body three axes configuration (t_1), where the Y and Z axes are interchanged. b) A three-body three axes configuration (t_0) and a relabeled three-body three axes configuration (t_1), where the Y and Z axes are interchanged.

9.2.2   Relabeling-matrix and relabeled configuration-array

Relabeling as in Section 9.2.1 induces a transformation of the configuration array, this transformation can be represented by a 3 by 3 matrix which we call the *relabeling-matrix*. This matrix encodes the correspondence between the configuration-array C_0 prior to relabeling and the configuration-array C_1 after relabeling. We note that relabeling-matrices are the permutation-matrices mentioned in [59]. We call the array of the relabeled configuration the *relabeled configuration-array*. For a two-body configurations (Figure 9.2.2a) this is done by right multiplication of the configuration-array with the relabeling-matrix (Figure 9.2.2b). For a three-body configuration (Figure 9.2.3a) this is done by left and right multiplication with relabeling-matrices (Figure 9.2.3b).
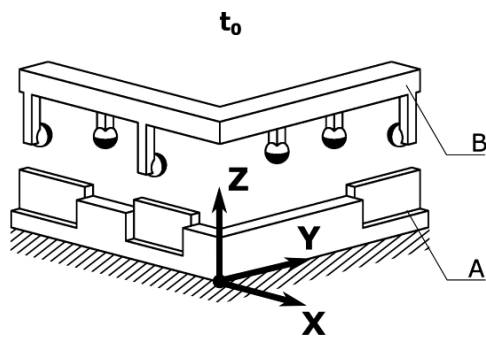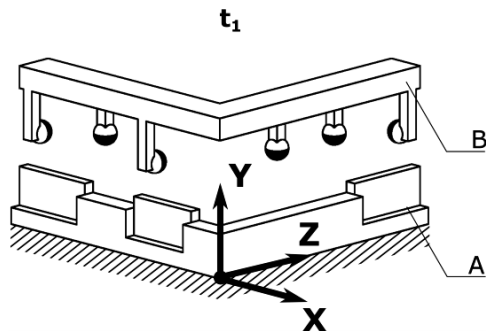
$$C_0 R_x = C_1$$

$$[1 \quad 2 \quad 3] \begin{bmatrix} 1 & 0 & 0 \\ 0 & 0 & 1 \\ 0 & 1 & 0 \end{bmatrix} = [1 \quad 3 \quad 2]$$

a

b

Figure 9.2.2: a) A two-body three axes configuration (t_0) and a relabeled two-body three axes configuration (t_1). b) The configuration array C_0 of the configuration at t_0 in Figure 9.2.2a is related, by post-multiplication with the relabeling-matrix R_x, to C_1.
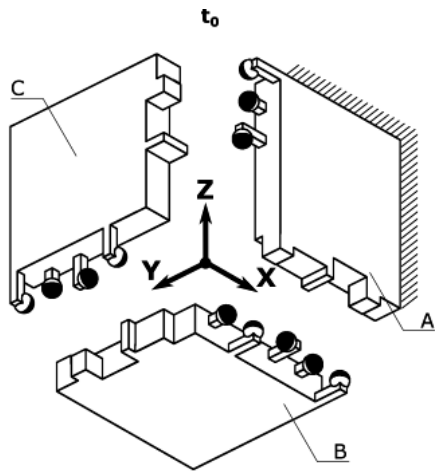
$$R_{xy}C_0R_{yx} = C_1$$

$$\begin{bmatrix} 0 & 0 & 1 \\ 1 & 0 & 0 \\ 0 & 1 & 0 \end{bmatrix}\begin{bmatrix} 1 & 2 & 2 \\ 2 & 1 & 1 \\ 1 & 1 & 1 \end{bmatrix}\begin{bmatrix} 0 & 1 & 0 \\ 0 & 0 & 1 \\ 1 & 0 & 0 \end{bmatrix} = \begin{bmatrix} 1 & 1 & 1 \\ 2 & 1 & 2 \\ 1 & 2 & 1 \end{bmatrix}$$

a   **b**
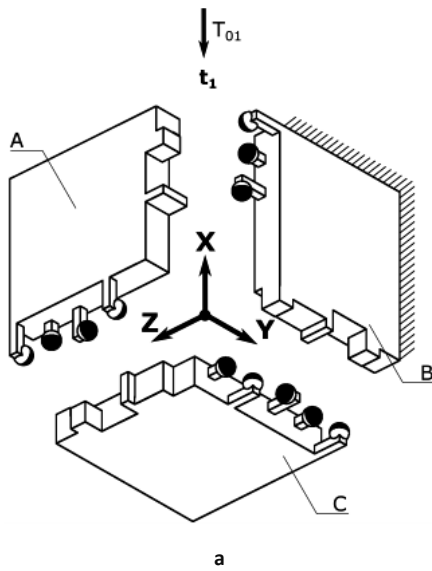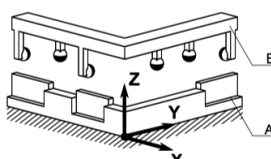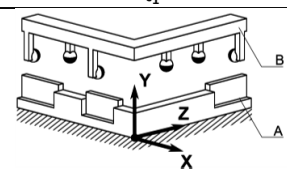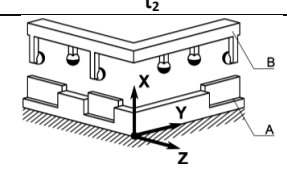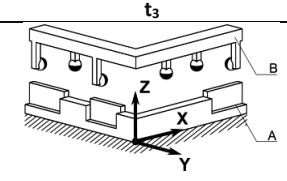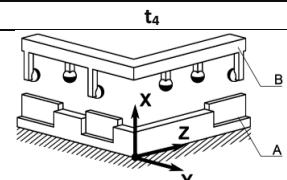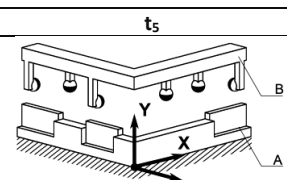
Figure 9.2.3: a) A three-body three axes configuration (t_0) and a relabeled three-body three axes configuration (t_1) b) The configuration array C_0 of the configuration at t_0 in Figure 9.2.3a is related by left and right multiplication by the relabeling-matrices R_{xy} and $R_{yx,}$, respectively to the configuration array C_1.

9.3 Equivalence relations

9.3.1 Relabeled configurations
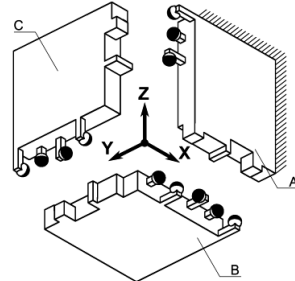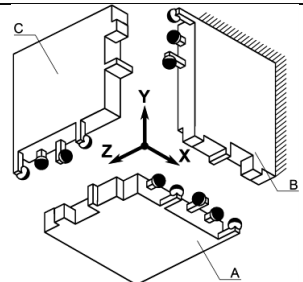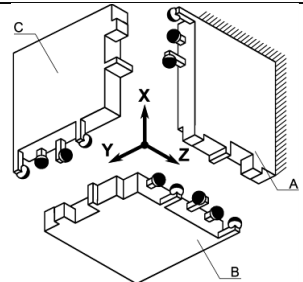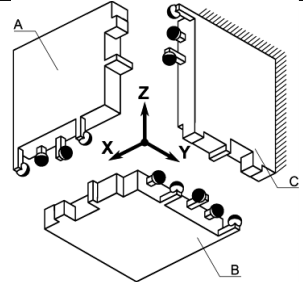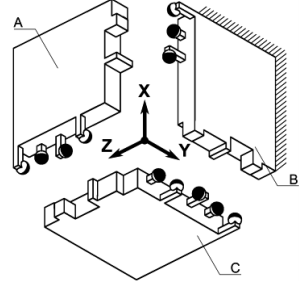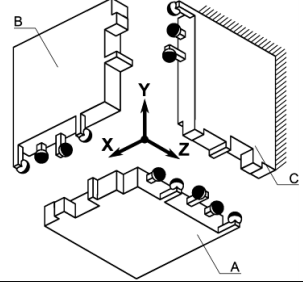
A configuration and a relabeled configuration are said to be equivalent if the configuration-array and relabeled configuration-array are related by one of the five possible sets of relabeling-arrays. This is illustrated for two bodies (Table 9.3.1) and three bodies (Table 9.3.2).

Table 9.3.1: A configuration-array of two bodies can be relabeled by relabeling-arrays into a relabeled-configuration-array. Relabeling comes down to all possible permutations of interchanging the names of the axes.

Original configuration	Relabeling	Relabeled configuration	Relabeled Configuration-array
t_0	C_0R_x	t_1	
$C_0 = [C_{11} \quad C_{12} \quad C_{13}]$ $[1 \quad 2 \quad 3]$	T_{01} $\longrightarrow$ $[1 \quad 2 \quad 3]\begin{bmatrix}1&0&0\\0&0&1\\0&1&0\end{bmatrix}$		$C_1 = [C_{11} \quad C_{13} \quad C_{12}]$ $[1 \quad 3 \quad 2]$
	C_0R_y	t_2	
	T_{02} $\longrightarrow$ $[1 \quad 2 \quad 3]\begin{bmatrix}0&0&1\\0&1&0\\1&0&0\end{bmatrix}$		$C_2 = [C_{13} \quad C_{12} \quad C_{11}]$ $[3 \quad 2 \quad 1]$
	C_0R_z	t_3	
	T_{03} $\longrightarrow$ $[1 \quad 2 \quad 3]\begin{bmatrix}0&1&0\\1&0&0\\0&0&1\end{bmatrix}$		$C_3 = [C_{12} \quad C_{11} \quad C_{13}]$ $[2 \quad 1 \quad 3]$
	C_0R_{yx}	t_4	
	T_{04} $\longrightarrow$ $[1 \quad 2 \quad 3]\begin{bmatrix}0&1&0\\0&0&1\\1&0&0\end{bmatrix}$		$C_4 = [C_{13} \quad C_{11} \quad C_{12}]$ $[3 \quad 1 \quad 2]$
	C_0R_{xy}	t_5	
	T_{05} $\longrightarrow$ $[1 \quad 2 \quad 3]\begin{bmatrix}0&0&1\\1&0&0\\0&1&0\end{bmatrix}$		$C_5 = [C_{11} \quad C_{12} \quad C_{13}]$ $[2 \quad 3 \quad 1]$
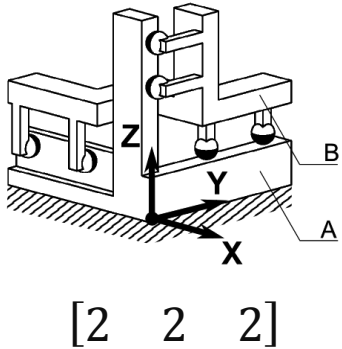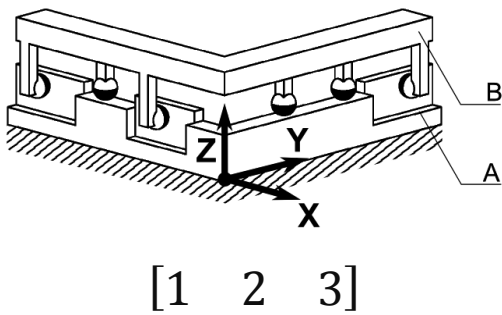
Table 9.3.2: A configuration-array of three bodies can be relabeled by relabeling-arrays into a relabeled configuration-array. The relabeling comes down to all possible permutations of the names of the axes.

Original configuration	Relabeling	Relabeled configuration	Relabeled Configuration-array
t_0	$R_x C_0 R_x$	t_1	
$$C_0 = \begin{bmatrix} C_{11} & C_{12} & C_{13} \\ C_{21} & C_{22} & C_{23} \\ C_{31} & C_{32} & C_{33} \end{bmatrix}$$ $$\begin{bmatrix} 1 & 2 & 2 \\ 2 & 1 & 1 \\ 1 & 1 & 1 \end{bmatrix}$$	$T_{01} \longrightarrow$ $$\begin{bmatrix} 1 & 0 & 0 \\ 0 & 0 & 1 \\ 0 & 1 & 0 \end{bmatrix}\begin{bmatrix} 1 & 2 & 2 \\ 2 & 1 & 1 \\ 1 & 1 & 1 \end{bmatrix}\begin{bmatrix} 1 & 0 & 0 \\ 0 & 0 & 1 \\ 0 & 1 & 0 \end{bmatrix}$$		$$C_1 = \begin{bmatrix} C_{11} & C_{13} & C_{12} \\ C_{31} & C_{33} & C_{32} \\ C_{21} & C_{23} & C_{22} \end{bmatrix}$$ $$\begin{bmatrix} 1 & 2 & 2 \\ 1 & 1 & 1 \\ 2 & 1 & 1 \end{bmatrix}$$
	$R_y C_0 R_y$	t_2	
	$T_{02} \longrightarrow$ $$\begin{bmatrix} 0 & 0 & 1 \\ 0 & 1 & 0 \\ 1 & 0 & 0 \end{bmatrix}\begin{bmatrix} 1 & 2 & 2 \\ 2 & 1 & 1 \\ 1 & 1 & 1 \end{bmatrix}\begin{bmatrix} 0 & 0 & 1 \\ 0 & 1 & 0 \\ 1 & 0 & 0 \end{bmatrix}$$		$$C_2 = \begin{bmatrix} C_{11} & C_{12} & C_{13} \\ C_{21} & C_{22} & C_{23} \\ C_{31} & C_{32} & C_{33} \end{bmatrix}$$ $$\begin{bmatrix} 1 & 1 & 1 \\ 1 & 1 & 2 \\ 2 & 2 & 1 \end{bmatrix}$$
	$R_z C_0 R_z$	t_3	
	$T_{03} \longrightarrow$ $$\begin{bmatrix} 0 & 1 & 0 \\ 1 & 0 & 0 \\ 0 & 0 & 1 \end{bmatrix}\begin{bmatrix} 1 & 2 & 2 \\ 2 & 1 & 1 \\ 1 & 1 & 1 \end{bmatrix}\begin{bmatrix} 0 & 1 & 0 \\ 1 & 0 & 0 \\ 0 & 0 & 1 \end{bmatrix}$$		$$C_3 = \begin{bmatrix} C_{33} & C_{32} & C_{31} \\ C_{23} & C_{22} & C_{21} \\ C_{13} & C_{12} & C_{11} \end{bmatrix}$$ $$\begin{bmatrix} 1 & 2 & 2 \\ 2 & 1 & 1 \\ 1 & 1 & 1 \end{bmatrix}$$
	$R_{xy} C_0 R_{yx}$	t_4	
	$T_{04} \longrightarrow$ $$\begin{bmatrix} 0 & 0 & 1 \\ 1 & 0 & 0 \\ 0 & 1 & 0 \end{bmatrix}\begin{bmatrix} 1 & 2 & 2 \\ 2 & 1 & 1 \\ 1 & 1 & 1 \end{bmatrix}\begin{bmatrix} 0 & 1 & 0 \\ 0 & 0 & 1 \\ 1 & 0 & 0 \end{bmatrix}$$		$$C_4 = \begin{bmatrix} C_{33} & C_{31} & C_{32} \\ C_{32} & C_{33} & C_{12} \\ C_{12} & C_{13} & C_{11} \end{bmatrix}$$ $$\begin{bmatrix} 1 & 1 & 1 \\ 2 & 1 & 2 \\ 1 & 2 & 1 \end{bmatrix}$$
	$R_{yx} C_0 R_{xy}$	t_5	
	$T_{05} \longrightarrow$ $$\begin{bmatrix} 0 & 1 & 0 \\ 0 & 0 & 1 \\ 1 & 0 & 0 \end{bmatrix}\begin{bmatrix} 1 & 2 & 2 \\ 2 & 1 & 1 \\ 1 & 1 & 1 \end{bmatrix}\begin{bmatrix} 0 & 0 & 1 \\ 1 & 0 & 0 \\ 0 & 1 & 0 \end{bmatrix}$$		$$C_5 = \begin{bmatrix} C_{22} & C_{23} & C_{21} \\ C_{32} & C_{33} & C_{31} \\ C_{12} & C_{13} & C_{11} \end{bmatrix}$$ $$\begin{bmatrix} 1 & 1 & 2 \\ 1 & 1 & 1 \\ 2 & 2 & 1 \end{bmatrix}$$
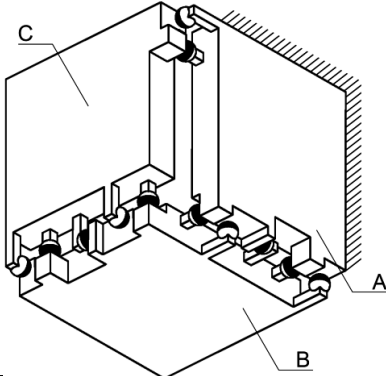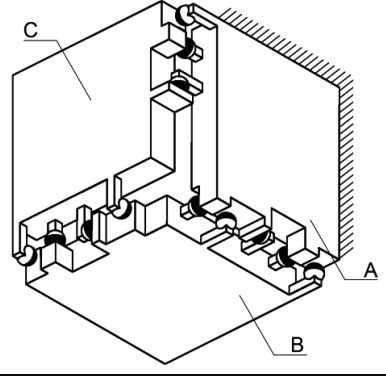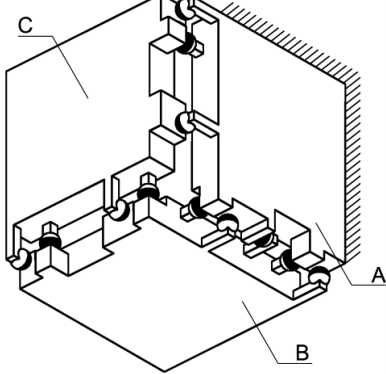
9.4 Conjecture: All non-equivalent configuration-arrays for two-body and three-body kinematic mounts

Table 9.4.1: Overview of the configuration-representations of the two-body kinematic mounts

Two-body configuration Example	Configuration-representation	Applicable two-body conditions					
		8.3.1	8.3.2	8.3.3	8.3.4	8.3.5	8.3.6
7.4.1.1	$\begin{bmatrix} 2 & 2 & 2 \end{bmatrix}$	✓	✓	✓	✓	✓	✓
7.4.1.2	$\begin{bmatrix} 1 & 2 & 3 \end{bmatrix}$	✓	✓	✓	✓	✓	✓

Table 9.4.2: Overview of the configuration-representations of the three-body kinematic mounts (1 of 3).

Three-body configuration Example	Configuration-representation	Applicable three-body conditions and conjecture			
		8.4.1	8.4.2	8.4.3	8.5.1
7.4.2.1	$\begin{bmatrix} 1 & 2 & 2 \\ 2 & 1 & 2 \\ 1 & 1 & 0 \end{bmatrix}$	✓	✓	✓	✓
7.4.2.2	$\begin{bmatrix} 1 & 2 & 2 \\ 2 & 1 & 1 \\ 1 & 1 & 1 \end{bmatrix}$	✓	✓	✓	✓
7.4.2.3	$\begin{bmatrix} 1 & 2 & 2 \\ 2 & 0 & 2 \\ 1 & 2 & 0 \end{bmatrix}$	✓	✓	✓	✓

Table 9.4.3: Overview of the configuration-representations of the three-body kinematic mounts (2 of 3).
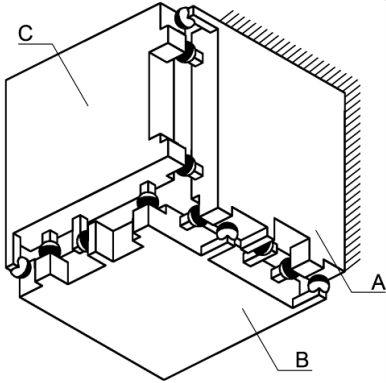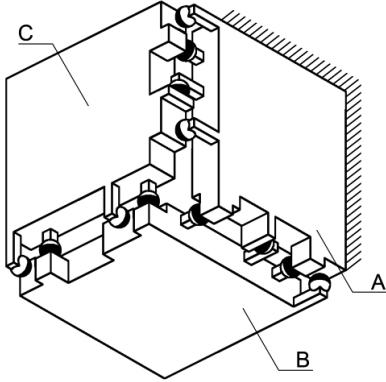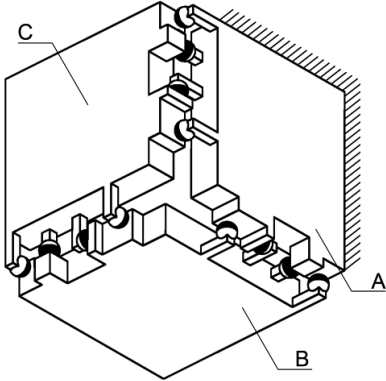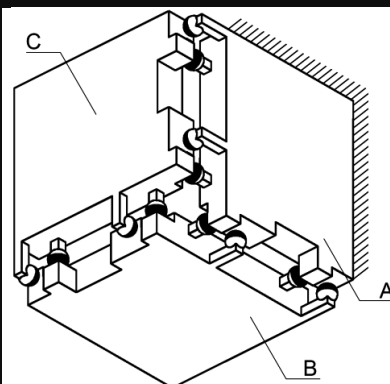
Three-body configuration Example	Configuration-representation	Applicable three-body conditions and conjecture			
		8.4.1	8.4.2	8.4.3	8.5.1
7.4.2.4	$\begin{bmatrix} 1 & 2 & 2 \\ 1 & 1 & 2 \\ 2 & 1 & 0 \end{bmatrix}$	✓	✓	✓	✓
7.4.2.5	$\begin{bmatrix} 1 & 2 & 1 \\ 2 & 0 & 2 \\ 1 & 2 & 1 \end{bmatrix}$	✓	✓	✓	✓
7.4.2.6	$\begin{bmatrix} 1 & 1 & 2 \\ 2 & 1 & 1 \\ 1 & 2 & 1 \end{bmatrix}$	✓	✓	✓	✓

Table 9.4.4: Overview of the configuration-representations of the three-body kinematic mounts (3 of 3).

Three-body configuration Example	Configuration-representation	Applicable three-body conditions and conjecture			
		8.4.1	8.4.2	8.4.3	8.5.1
7.4.2.7	$\begin{bmatrix} 0 & 2 & 2 \\ 2 & 0 & 2 \\ 2 & 2 & 0 \end{bmatrix}$	✓	✓	✓	✓

9.5   Chapter summary

In this chapter we introduced the configuration-representation notation and equivalence relations and used these together with the conditions specified in Chapter 8 to classify 3-dimensional kinematic mounts into a total of 2 two-body configuration-representations and 7 three-body configuration-representations. We conjecture that this list consist of all non-equivalent configuration-representations of kinematic mounts.

9.6   Heuristic method used to derive the conjectured classification

We obtained our conjecture using a heuristic method not detailed in this thesis. This method generated all possible configuration-arrays consisting of non-negative integers with sum of entries equal to 6 or 12 then applied the conditions of Chapter 8 together with the equivalence relations of 9.3 to give the list of Section 9.4.

Chapter 10   Demonstrators

10.1 Introduction

This chapter begins the applications which continue to Chapter 13. This chapter presents a physical demonstrator to complement the theory developed in the previous chapters.

10.2 Problem statements

Present demonstrators illustrating 2-dimensional Condition 5.3.6.

Present demonstrators of the seven three-body kinematic mounts of Chapter 9.

10.3 2-dimensional demonstrators

Two demonstrators illustrating Figures 5.3.6.1b and 5.3.6.2b were realized.

Figure 10.1 and Figure 10.2 illustrate how all contact points can stay in contact despite the fact that the bodies have different positions. This indicates the existence of a degree of freedom.

<div align="center">

a   b

</div>
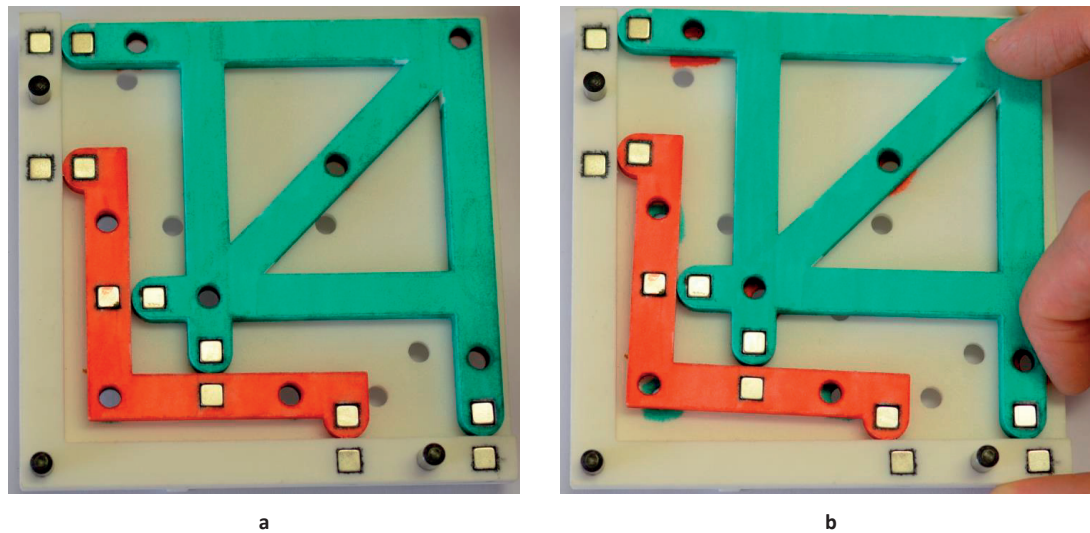
Figure 10.1: The demonstrator of Figure 5.3.6.1b. a) The demonstrator prior to applying a displacement with body C fixed. Note the hole in the bottom left corner. b) A small movement was applied to body A and we note that all points are still in contact. Note how the same holes at the bottom left overlaps in a different way.

| a | b |
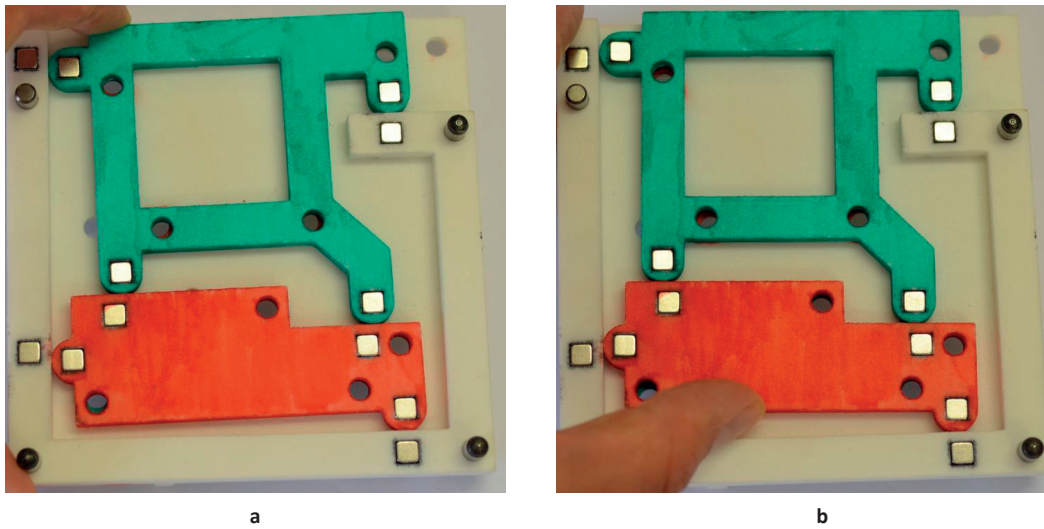
Figure 10.2: The demonstrator of Figure 5.3.6.2b. a) The demonstrator prior to applying a displacement with body C fixed. Note the hole in the bottom left corner. b) A small movement was applied to body A and we note that all points are still in contact. Note how the same holes at the bottom left overlaps in a different way.

10.4 3-dimensional demonstrators

We constructed demonstrators for all our examples of 3-dimensional three-body kinematic mounts. Each demonstrator is shown in a flat unassembled state and in its assembled state.

| a | b |
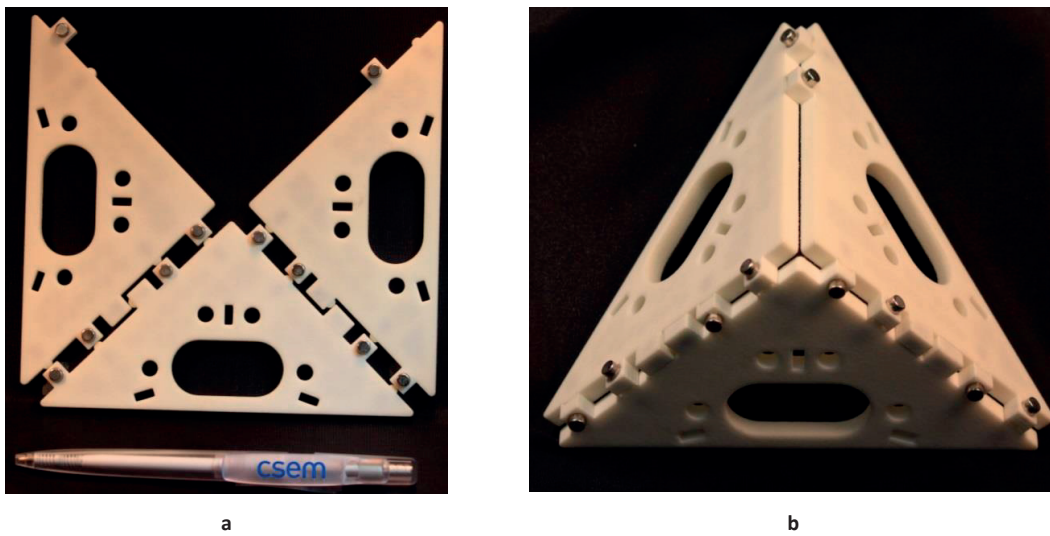
Figure 10.3: Demonstrator of Example 7.4.2.1. a) Unassembled. b) Assembled.
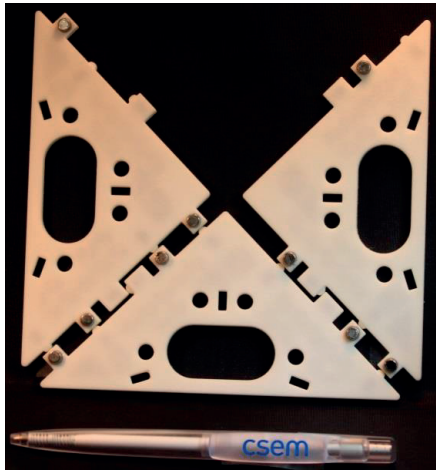
a
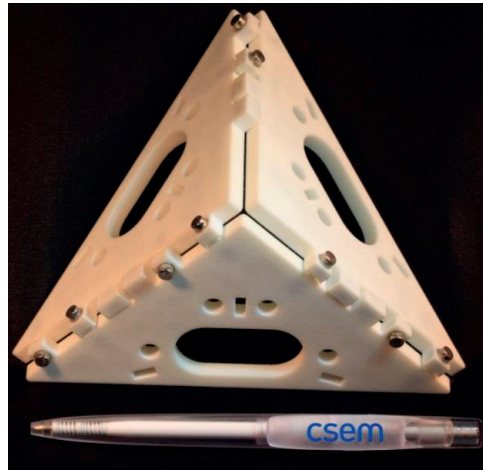
b

Figure 10.4: Demonstrator of Example 7.4.2.2. a) Unassembled. b) Assembled.
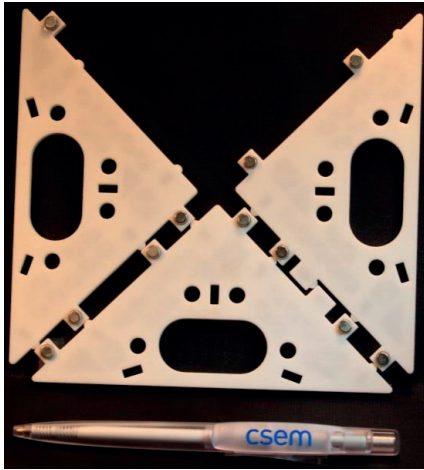
a
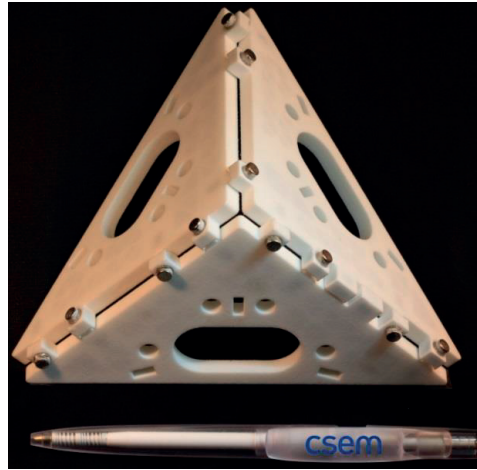
b

Figure 10.5: Demonstrator of Example 7.4.2.3. a) Unassembled. b) Assembled.
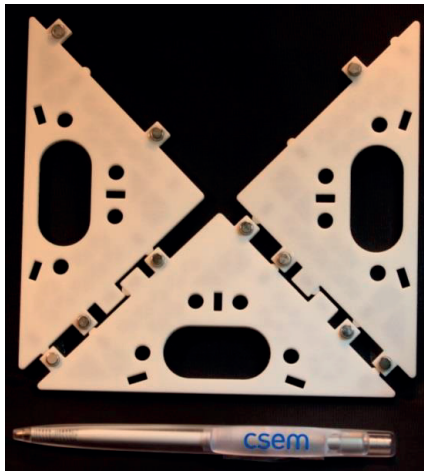
a
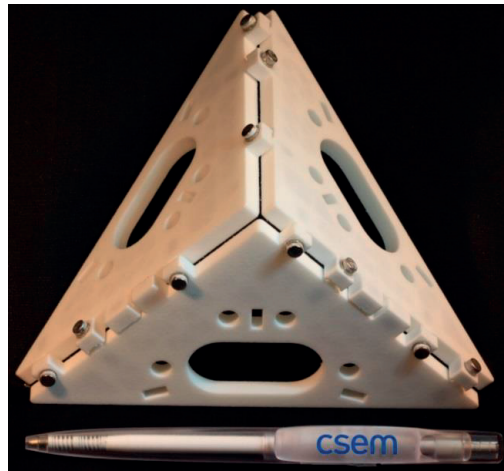
b

Figure 10.6Demonstrator of Example 7.4.2.4. a) Unassembled. b) Assembled.
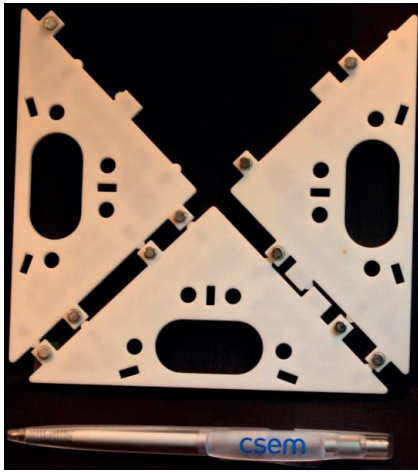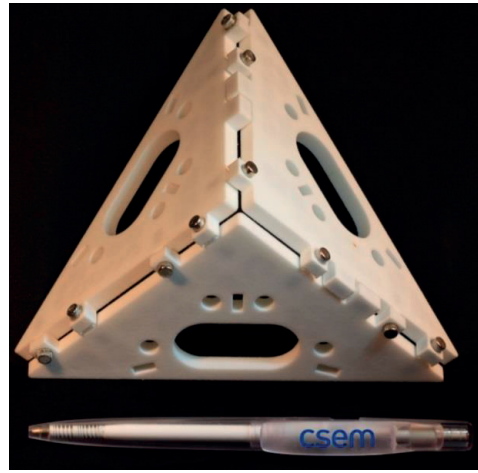
Figure 10.7: Demonstrator of Example 7.4.2.5. a) Unassembled. b) Assembled.
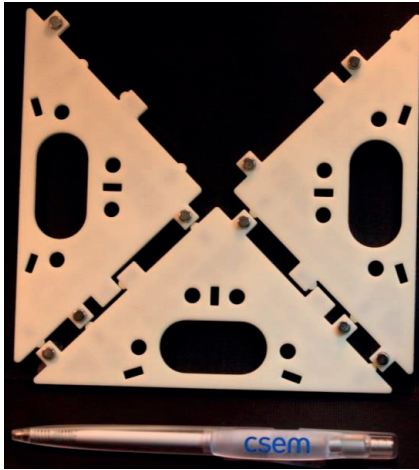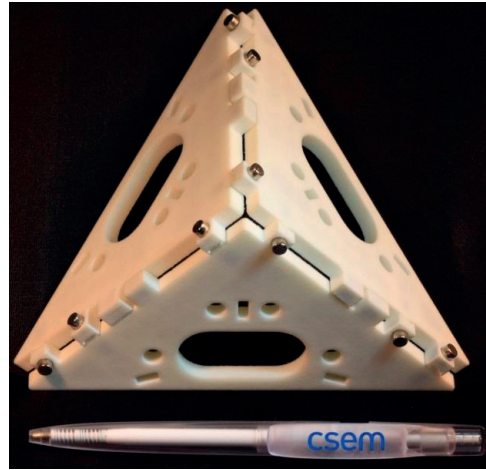
Figure 10.8: Demonstrator of Example 7.4.2.6. a) Unassembled. b) Assembled.
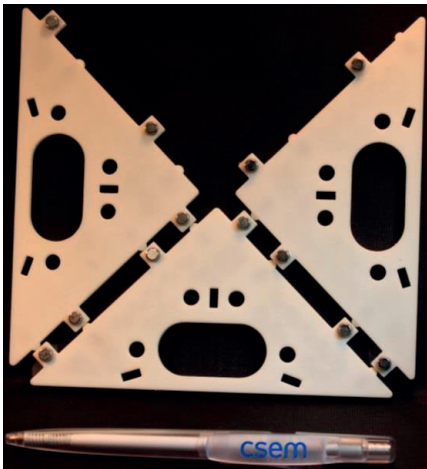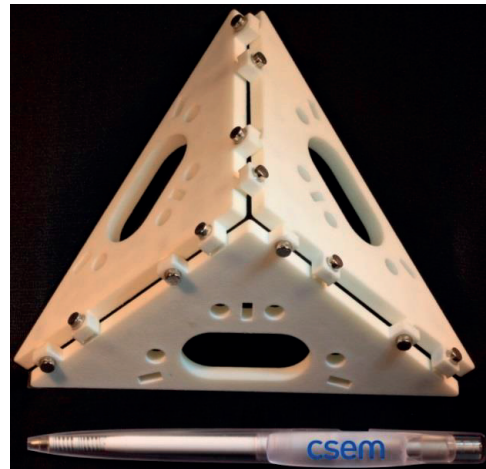
Figure 10.9: Demonstrator of Example 7.4.2.7. a) Unassembled. b) Assembled.

Chapter 11 Examples of nesting force and assembly methods.

11.1 Problem statement

Present the physical techniques used to apply nesting forces and enable assembly of 3-dimensional kinematic mounts.

11.2 Description

Five different methods for assembling kinematic mounts were utilized, consisting of two different approaches. The first approach is to apply a nesting force, such as compliance methods or magnets. The second is assembly via gluing, soldering or bolting.

11.3 Methods for applying a nesting force

11.3.1 Compliance-based nesting force

Two different compliant based assembly methods were used. The first involved integrating clips inside the bodies to be assembled. The second is to have the clips be separate parts.

11.3.1.1 *Integrated clips*

Integrated clips are simply small springs attached to a manipulation interface. An example of where we applied integrated clips is offered in Figure 13.4.4. Though integrated clips advantageously reduces the number of parts, they add complexity and limit how the bodies approach each other during assembly.
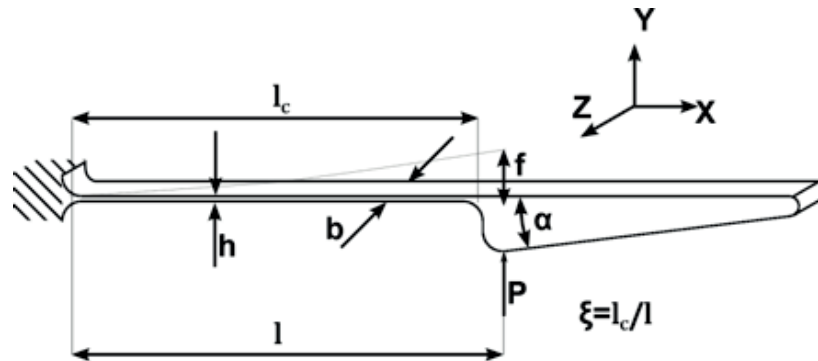
Figure 11.1: A schematic illustration of an integrated clip.

The design of integrated clips can be done using the formulas of Table 11.1. One simply has to make sure to not go over the maximum admissible displacement f_{adm} while ensuring that for the applied displacement x, there is sufficient force P=Kx to keep each body in place.

Table 11.1: Formulas for an integrated clip, see Henein [60].

K	P_{adm}	f_{adm}
$\dfrac{Ebh^3}{4l^3\xi(3-3\xi+\xi^2)}$	$\dfrac{\sigma_{adm}bh^2}{6l}$	$\dfrac{2\sigma_{adm}l^2\xi(3-3\xi+\xi^2)}{3Eh}$

E is the Young's modulus [Pa]; K is the rigidity of the leaf spring in [N/m]; P_{adm} is the admissible force in [N]; b is the width of the leaf spring [m]; f_{adm} is the maximum admissible displacement; h is the thickness of the leaf spring [m]; l is the length at which the force is applied in [m]; l_c is the length of the leaf spring in [m]; $\xi = \frac{l_c}{l}$ is a dimensionless design parameter; σ_{adm} is the admissible stress of the material [Pa]

Care should be taken with the angle of the clip tip angle α which should be smaller than the angle of friction for optimal positioning of the part within the clip without damaging it. In addition one has to limit the movements of the clip in order to avoid fracture.

11.3.1.2 *Separate Clips*
An alternative technique is to use separate clip springs, as illustrated in Figures 11.2 and 11.3. These clips are separate parts added to the bodies to provide the force keeping them together. When all the clips are assembled onto the bodies they behave as a rigid body, as illustrated in Figure 11.3f.

a

b

Figure 11.2: a) a single clip in neutral position b) a single clip in open position. It can be displaced further, up to a hard mechanical stop.
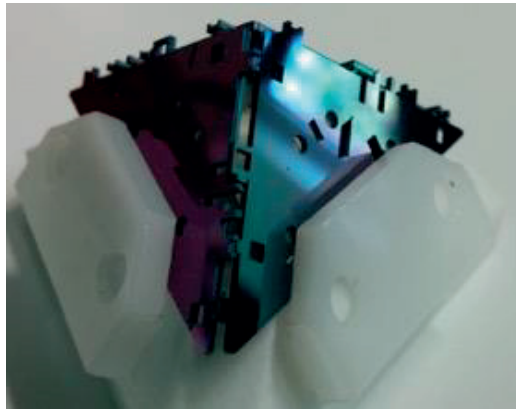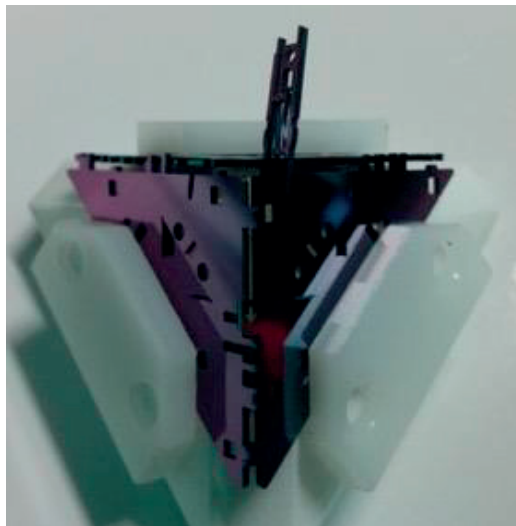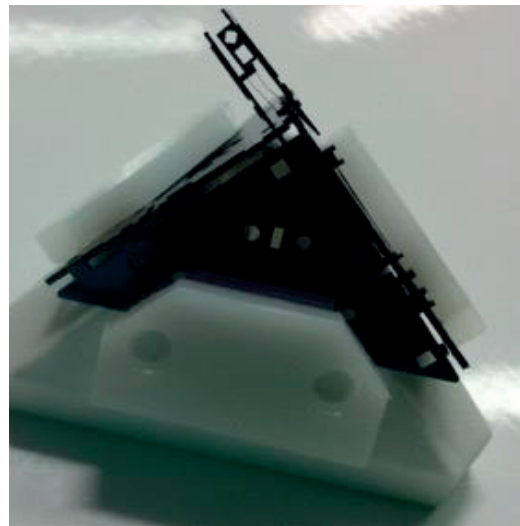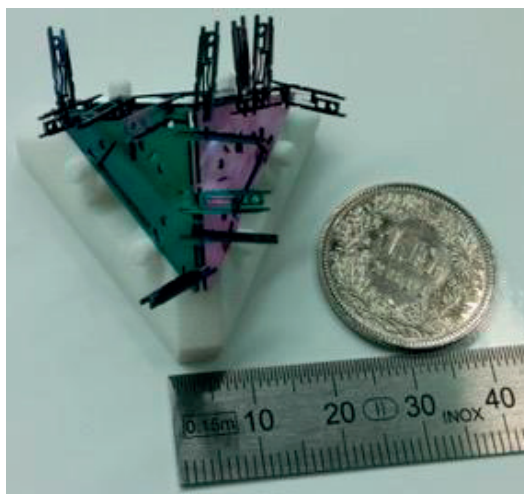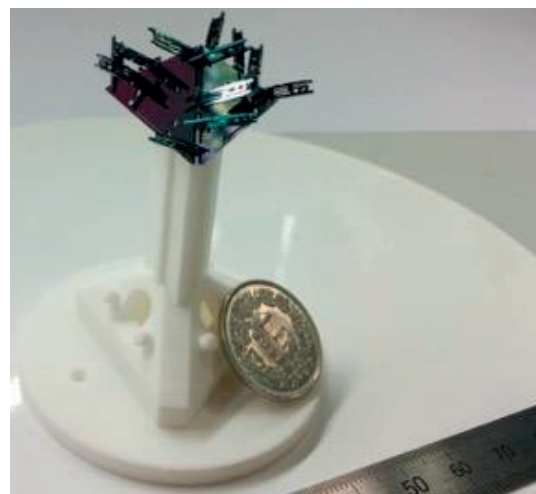
Figure 11.3: The assembly of three Silicon parts by means of Silicon clips. a) Illustrates the Silicon pieces pre-aligned on a plastic support. b),c),d) show the mounting of a single clip. e) and f) Illustrate the final mounted part with clips on it.

Sizing separated clips is analogous to the case of the simple linear guide, with the exception that the force is not applied at the center of the two leaf springs, so assembly is maintained by tensile and compressive forces of the leaf springs. An illustration of the load case is given in Figure 11.4.
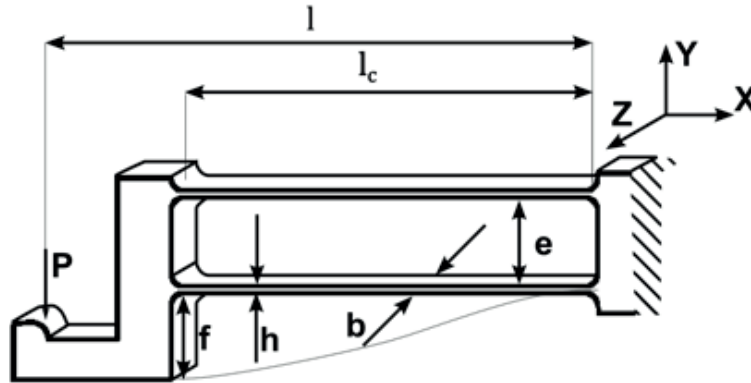
Figure 11.4: The linear guide used for separate clips.

The formulas of Table 11.2, taken from Henein [60], were used as a first approximation for the relation between the force and displacement. Note that the further the force is away from the middle of the leaf spring, the less valid the equations of Table 11.2.

Table 11.2: Formulas for a separate clip based on a simple linear guide.

K_{lin}	M_{adm}	P_{adm}	f_{adm}
$\dfrac{24EI}{l^3\xi^3}$	$\dfrac{\sigma_{adm}bh^2}{6}$	$\dfrac{\sigma_{adm}bh^2}{6l}$	$\dfrac{\sigma_{adm}l^2\xi^3}{24Eh}$

E is Young's modulus [Pa]; K is the rigidity of the leaf spring in [N/m]; M_{adm} is the admissible moment in [Nm]; P_{adm} is the admissible force in [N]; b is the width of the leaf spring [m]; f_{adm} is the maximum admissible displacement; h is the thickness of the leaf spring [m]; l is the length at which the force is applied in [m]; l_c is the length of the leaf spring in [m]; $\xi = \frac{l_c}{l}$ is a dimensionless design parameter; σ_{adm} is the admissible stress of the material.

In addition, care was taken to consider the buckling of the leaf spring in compression so as not to exceed the buckling limit. Formulas can be found in Henein [60].

As before, the clip tip angle α should be smaller than the angle of friction for optimal positioning of the part within the clip without damaging it. In addition one has to limit the movements of the clip such that it doesn't break.

11.3.2 Magnets

Another method for producing nesting force is by means of pairs of small magnets localized at each contact point. By using small magnets inside the body, approach of the bodies during pre-alignment is less constrained as there is no longer any geometric barrier. Gluing magnets in the bodies is less complex than adding clips at every contact. Magnets also take up less volume. Figure 11.5 shows an example configuration using twelve pairs of small magnets.

| a | b |
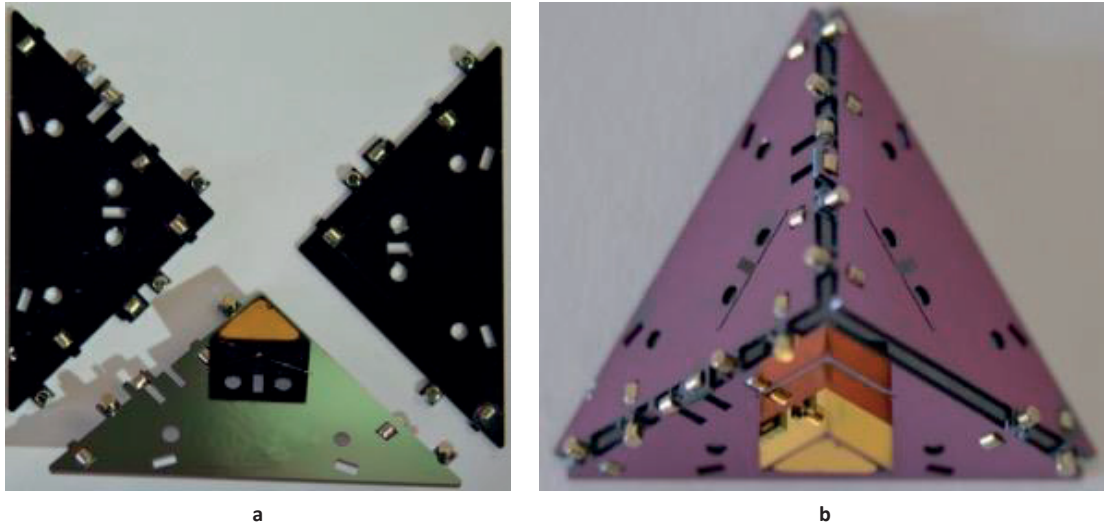
Figure 11.5: The assembly of three Silicon parts by means of cylindrical Ø1 by 1 mm magnets.

11.3.2.1 Magnets for Silicon bodies
The magnet nesting force method was applied to the Silicon bodies used in the experiments of Chapter 12. In order to give a better example we will further describe the details to this application.

The mass of a Silicon part with magnets and prisms is 0.55 grams so a force of 6 mN is applied by gravity. A body is always held up by three magnets. In the measured prototype we used 12 pairs of S-01-01-N magnets, having 1mm diameter, 1 mm length and N45 magnetization. The gap size between the magnets in assembled state is 1.3mm with a force of 17 mN. When the magnets are at 2 mm distance of each other a force of 6 mN is exerted. These values were calculated with the supplier's online calculator and verified by means of FEM simulations.

The effect of magnet misalignment on the nesting force was examined using finite element analysis. The result was that a rotation of 0 to 10 degrees around the point in the middle of the two magnets has a negligible effect on force variation. The maximum offset (1mm) between the axes results in about a 15% diminution of the nesting force. Both are not problematic due to the relatively large safety factor.

11.4 Permanent attachment methods of Silicon bodies.

In contrast with the methods described above, the force between the parts is much more dependent on the type of surface used. In addition care has to be taken to minimalize misalignment.

11.4.1 Gluing

Two types of glues were used: epoxy and UV glue. Both glues are used for Silicon assembly so were natural candidates. For our application the NORDSON EFD PERFORMUS III fluid dispenser was used for both glues to locally apply a defined amount of glue, see Figure 11.6a.

Gluing requires careful consideration of the interface as it can misalign the bodies since it adds a thin layer dependent on viscosity (~85μm Figure 11.6a for the epoxy glue). The offset caused by the glue layer can be minimized by isolating the glues using well-defined glue cavities (cf. Figure 11.6b).
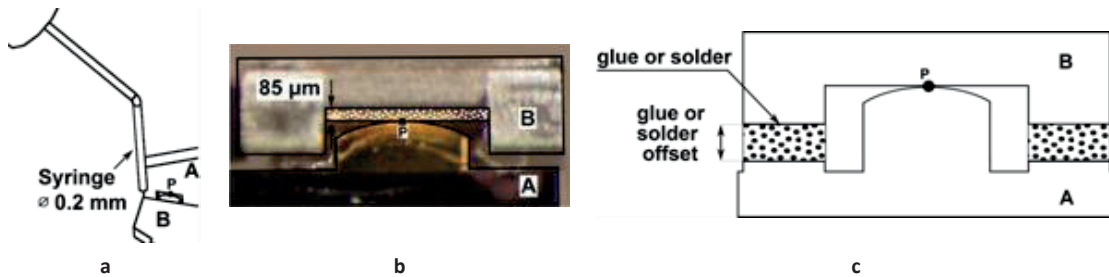
Figure 11.6: a) Application of a glue or solder at contact point P between two bodies A and B. b) Measured gap between two bodies A and B at a contact point P. c) Example of a more efficient contact point design with glue cavities

The first glue was EPO-TEK® 353ND epoxy glue. This epoxy glue is a two component glue with a viscosity of 3 to 5 Pa s (at 23°C) and it typically requires curing at 80°C for 30 minutes. The lap shear strength of this glue is at least 13.7 MPa and the die shear strength is at least 35 MPa. In addition a set of first tests resulted in all die-shear strength values being higher than 37 MPa. This epoxy requires a heating step and a time period less suited for constructing prototypes.

The second glue was Norland UV Glue NOA 61. This glue consists of a photopolymer that cures with UV light (peak sensitivity at 365 nm), a full cure of $3J/cm^2$ is recommended. It is cured using the Omnicure LX300 LED UV spot curing system using a 3mm lens at a 10 mm working distance (4000 mW/Cm^2 at 365 nm). The viscosity of the UV glue is 0.3-0.45 Pa s. The UV glue has the advantage that it can be applied at room temperature and locally exposed to UV light for about 30 seconds for a typical bond area. It can be disassembled when soaked in Methylene Chloride. The minimum tensile strength is 19.3 MPa. For optimum adhesion about 1 week of aging is required, this can be shortened to 12 hours at 50°C. In general the UV glue lends itself well to prototype construction.

11.4.2 Soldering

A solder paste, Loctite RA10 was used in the assembly of Silicon components. The Silicon components each have a gold layer of 200 nm, deposited by PVD. The solder composition is Sn62/Pb36/2Ag.The solder is composed of small balls of diameters between 38 and 53 μm. It has a viscosity of 500 Pa s and thus requires a larger syringe for application. Once the solder is applied to an assembly the entire assembly has to be put in an oven at 180°C. A larger variation in the gap size was observed with the solder (Figure 11.7). The offset caused by the solder can be minimized similar to glues with a well-defined solder cavity (cf. Figure 11.6b). The lowest measured shear strength of the solder is 9.83 MPa the damage indicated an adhesive failure of the gold layer, implying that the gold rather than the solder provides the limit.

Figure 11.7: a) Application of solder at a contact point between two bodies causing an offset of 130μm. b) Another contact point of the same assembly with an offset of 180 μm.

11.4.3 Bolting

An attempt to use M1 bolts was also made. To ensure a correct stress distribution and minimize play, a plain washer and a spring washer were used (Figure 11.8a). One of the critical factors in using a bolt is knowledge of the correct total tightening torque as this determines the equivalent stress felt by the bolt and the thread and the initial force determining the stress in the Silicon bodies. In order to be able to calculate this, the values of Table 11.3 used, the geometric parameters are illustrated in Figure 11.8b and c.
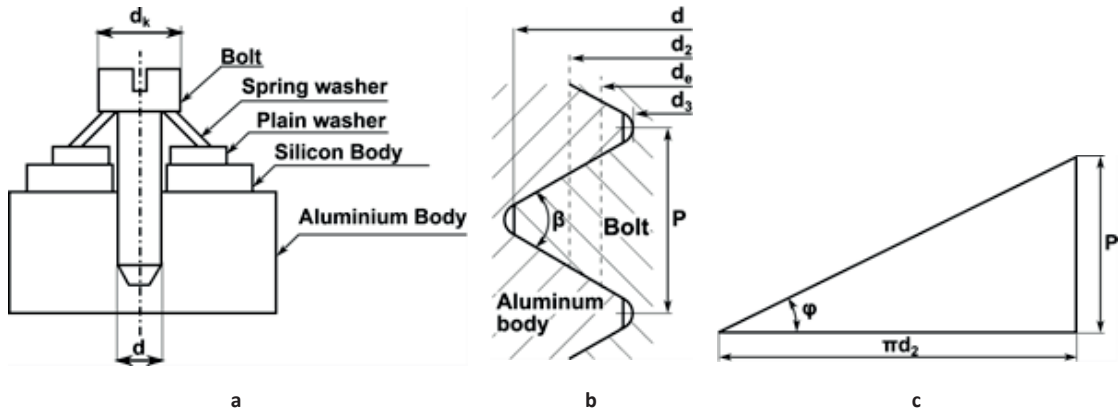
Figure 11.8: A bolted assembly of three parts.

Table 11.3: Values of the bolt assemblies properties. The formulas are taken from [61]. The material data comes from [62].

Property	Value
Bolt nominal diameter	$d = 1\ mm$
Bolt head diameter	$d_k = 2\ mm$
Thread pitch	$P = 0.25\ mm$
Pitch diameter (ISO thread)	$d_2 = d - 0.649519P = 0.84mm$
Root diameter (ISO thread)	$d_3 = d - 1.226869P = 0.69mm$
Effective diameter	$d_e = \dfrac{d_2 + d_3}{2} = 0.77\ mm$
Effective tensile stress Area	$A_e = \left(\dfrac{\pi}{4}\right)d_e^2 = 0.4602mm^2$
Thread profile angle (ISO thread)	$\beta = 60°$
Coefficient of friction (assumption)	$\mu = 0.15 \pm 0.05$
Pitch angle	$\phi = \mathrm{atan}\left(\dfrac{P}{\pi d_2}\right) = 0.095\ rad$
Effective friction angle	$\rho_e = \mathrm{atan}\left(\dfrac{\mu}{\cos\left(\dfrac{\beta}{2}\right)}\right) = 0.175 \pm 0.056\ rad$
Static load safety coefficient	$C = 0.9$
Bolt yield stress (Stainless steel A2-70 from Bossard [62])	$\sigma_{0.2} = 450\ MPa$

Taking the formulas provided by van Beek [61] and rewriting them we can calculate the initial tensile force F_i as a function of the yield stress $\sigma_{0.2}$ substituted in the Von-Mises stress

$$F_i < \frac{C\sigma_{0.2}}{\sqrt{\left(\left(\frac{1}{A_t^2} + 192\left(\frac{d_2 \tan(\phi + \rho_e)}{\pi d_3^3}\right)^2\right)\right)}}$$

11.1

Assuming that the friction experienced by the bolt acts at the bolt head diameter d_k the head torque M_h is

$$M_h = \frac{\mu F_i d_k}{2}$$

11.2

The torque to overcome the thread friction M_t is

$$M_t = \frac{d_2 F_i \tan(\phi + \rho_e)}{2}$$

11.3

The tightening torque M_{tot} is

$$\begin{aligned} M_{tot} &= M_h + M_t \\ &= 0.023 \, for \, \mu = 0.1 \\ &= 0.028 \, for \, \mu = 0.15 \\ &= 0.032 \, for \, \mu = 0.2 \end{aligned}$$

11.4

These values are of the same order of magnitude as the M1 tightening torque of 19.5 mNm recommended by Tohnichi [63], a company specialized in tools and measurements related to torque.

A Petit Pierre SA torque screwdriver was used to apply torques between 5 and 55 mNm. It was observed for bolting a single part that there was no damage or problems when applying 30 mNm. However, it was important to keep the surface of the plain washer polished to avoid high local stress concentrations in the Silicon body. Simple Silicon bodies on aluminum were successful. In addition a similar assembly was tried on three identical and perpendicular Silicon components with intermediate Silicon parts which proved unsuccessful as tightening the bolts caused the parts to rotate then break due to internal stress. Unfortunately, no more parts were available for testing the assembly and it would be interesting to test the assembly with a smaller torque limit.
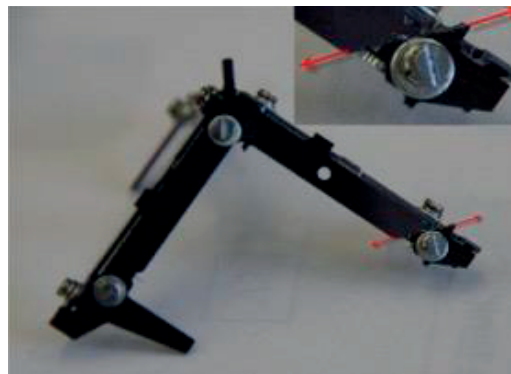
Figure 11.9: A bolted assembly of three parts, with a fracture along the red line.

11.5 Discussion

We evaluate our methods by criteria ranked from 1 to 5, where 1 represents the worst value and 5 the best.

11.5.1 A case study

In order to be able to discuss the criteria, we focus on a three-body kinematic mount (cf. Figure 11.10a) applied to the sugar-cube sized delta robot (Figure 11.10b).
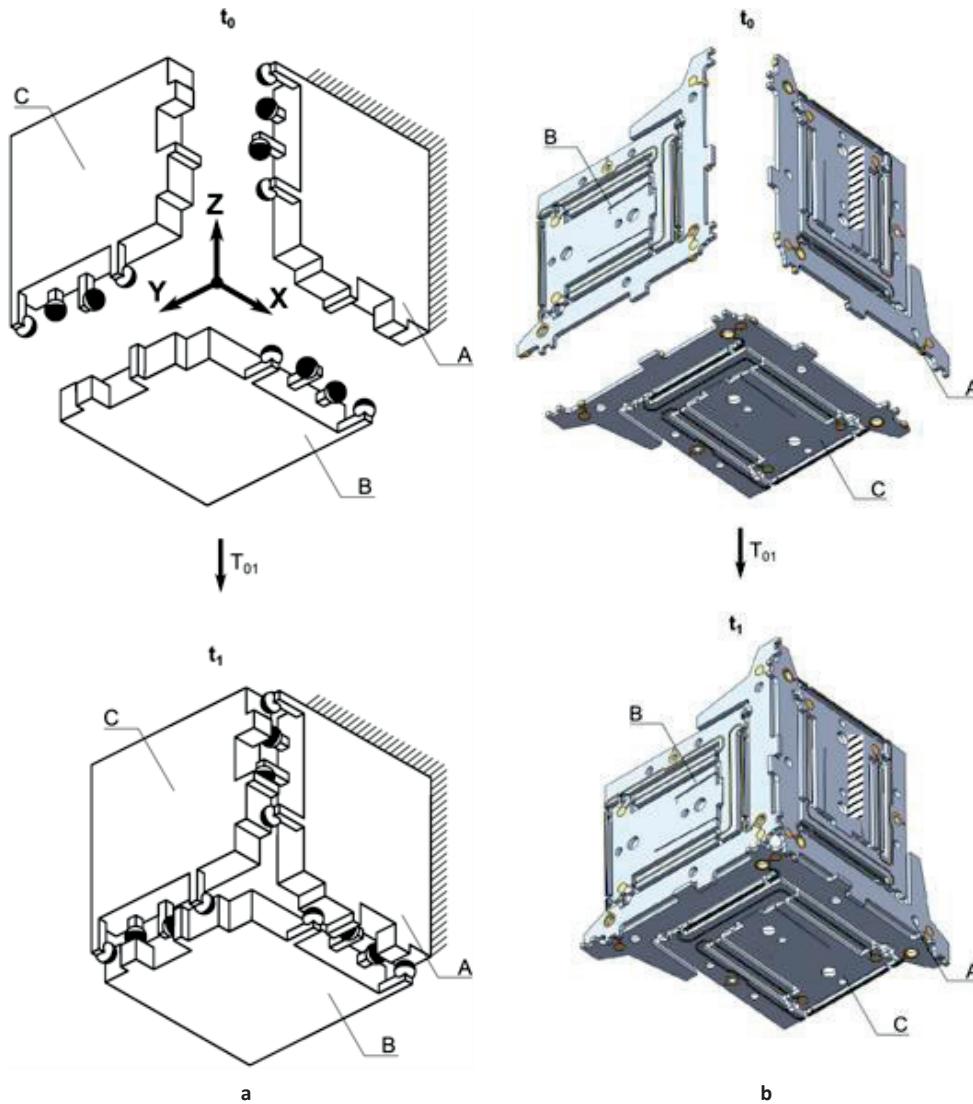
Figure 11.10: a) kinematic mount example 7.3.2.6, b) kinematic mount example 7.3.2.6 implemented in a sugar-cube size delta robot (20 x 20 x 20 mm).

Each part has a typical size of 27x27x0.545 mm. The parts are created using photolithography and DRIE, and depending on the attachment procedure steps as gold deposition or additional surface depths can be required.

The sugar cube sized delta robot will be further discussed in Chapter 13.
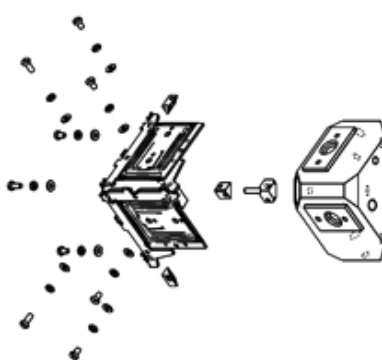
11.5.2 Definition of criteria
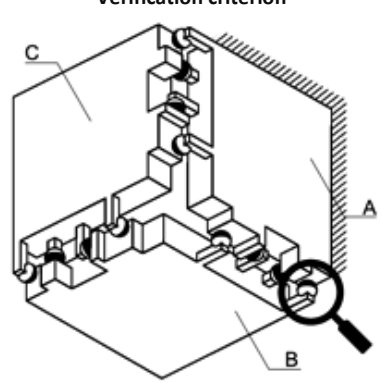
The criteria are divided into two categories, those that apply to the assembly in general and those that apply to bodies or contact points.

11.5.2.1 Assembly

Time criterion

Definition:	The amount of time required to assemble three slabs of Silicon perpendicular to each other.

Value	Meaning
1	The assembly time of the parts takes 4 hours
2	The assembly time of the parts takes 3 hours
3	The assembly time of the parts takes 2 hours
4	The assembly time of the parts takes 1 hour
5	The assembly time of the parts takes less than 1 hour

Assembly complexity criterion

Definition:	The amount of additional parts in the assembly and the unique jigs in the assembly and their complexity.

Value	Meaning
1	The assembly requires a complex assembly jig and/or more than 48 additional parts.
2	The assembly requires only a simple assembly jig and 48 or less additional parts
3	The assembly requires only a simple assembly jig and 24 or less additional parts.
4	The assembly requires only a simple assembly jig and 12 or less additional parts.
5	The assembly requires only a simple assembly jig and no additional parts.

Verification criterion

Definition:	The amount of effort required to verify whether an assembly has been correctly assembled.

Value	Meaning
1	The assembly method makes it very hard to verify a correct assembly.
2	The assembly method makes it hard to verify a correct assembly.
3	The assembly method makes it a bit harder to verify a correct assembly.
4	The assembly method can be verified optically under a microscope as without the assembly method
5	The assembly method can be verified more easily than with a microscope for a correct assembly.

Cost criterion
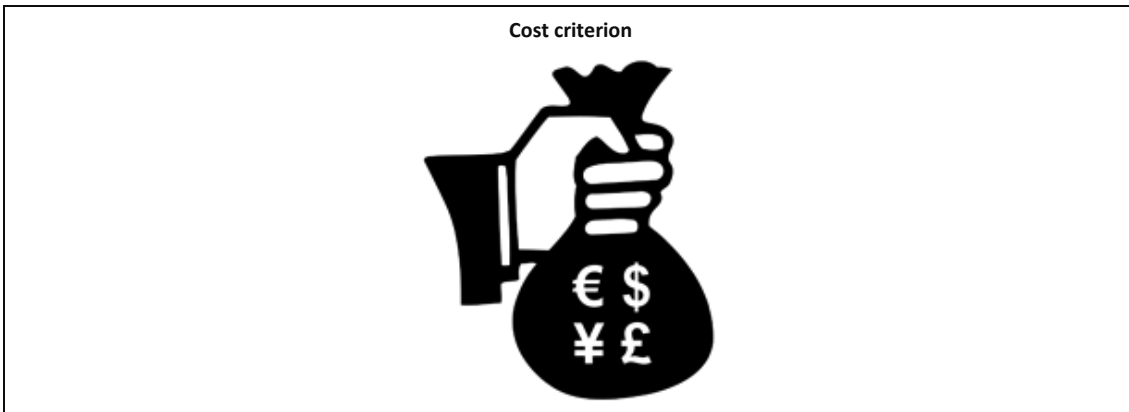
Definition:	The material cost of the assembly method. This does not include operator hours or added fabrication steps and does not include costs of jigs or tools.

Value	Meaning
1	The assembly method adds more than 5000€ of cost per assembly.
2	The assembly method adds more than 1000€ of cost per assembly.
3	The assembly method adds more than 500€ of cost per assembly.
4	The assembly method adds more than 100€ of cost per assembly.
5	The assembly method adds little to no extra cost.

Risk of damage criterion
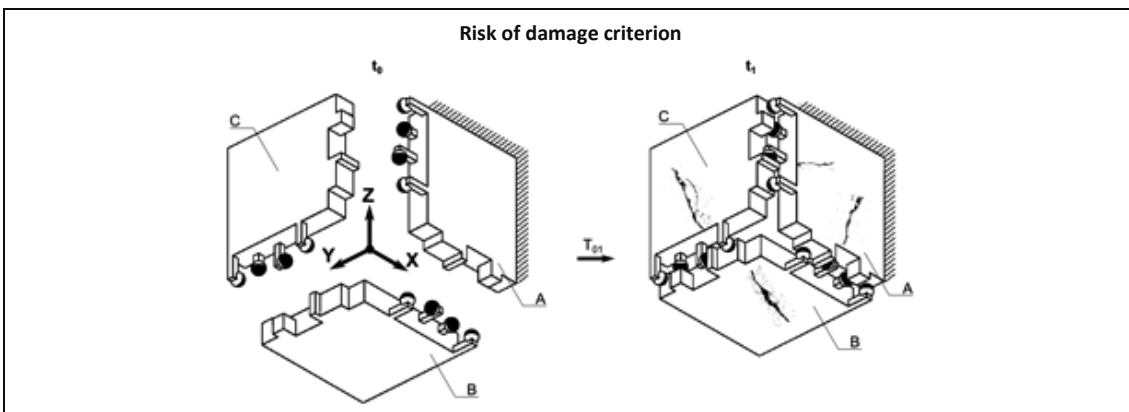
Definition:	The chance of parts getting damaged by the assembly method.

Value	Meaning
1	The assembly method has a high risk of damaging the parts
2	The assembly method has a significant risk of damaging the parts
3	The assembly method has a risk of damaging the parts
4	The assembly method has a small risk of damaging the parts
5	The assembly method has no risk of damaging the parts.

Disassembly criterion
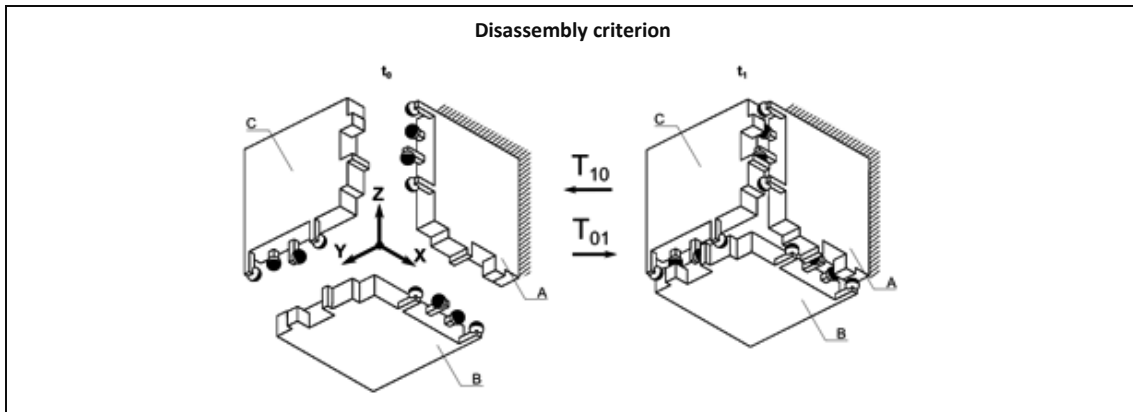
Definition:	The degree to which Silicon parts can be assembled and disassembled repeatedly without change or damage to the parts.

Value	Meaning
1	The parts cannot be disassembled non-destructively.
2	The parts can be disassembled within 1 day, with significant damage or change.
3	The parts can be disassembled within 1 day, with little to no damage or change.
4	The parts can be disassembled within 30 minutes, with ease with little to no damage or change.
5	The parts can be disassembled within 1 minute, with ease without any damage or change.

Aesthetic criterion
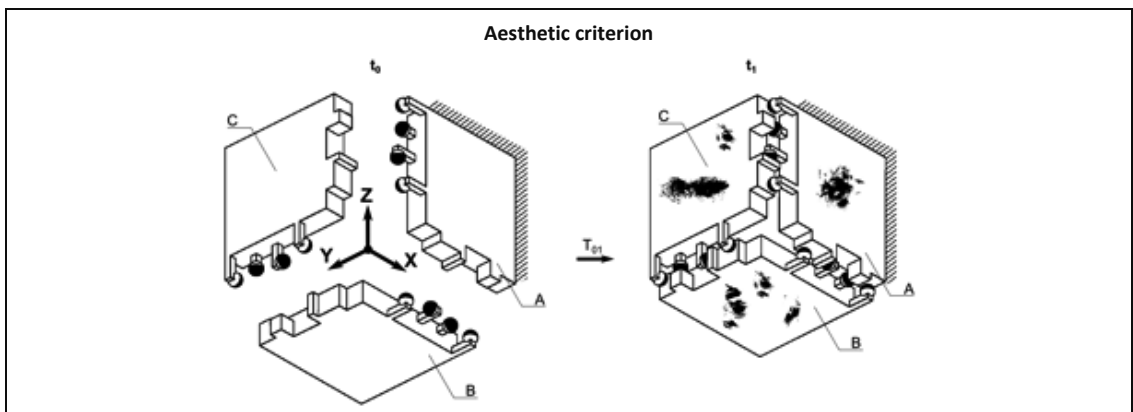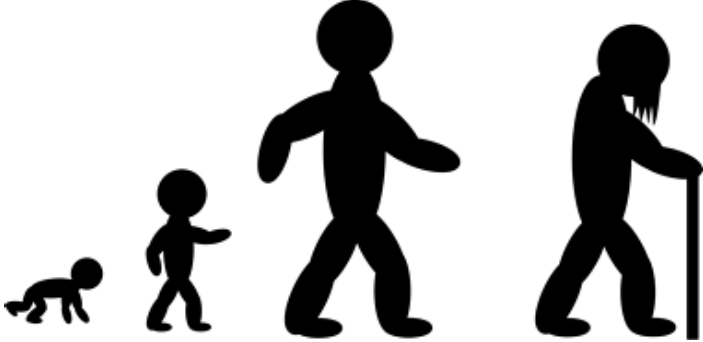
Definition:	The amount in which the part perception is changed with respect to a part without that assembly method.

Value	Meaning
1	The assembly looks significantly less nice with the assembly method.
2	The assembly looks less nice with the assembly method.
3	The assembly looks slightly less nice with the assembly method.
4	The assembly looks the same with the assembly method.
5	The assembly looks better with the assembly method.
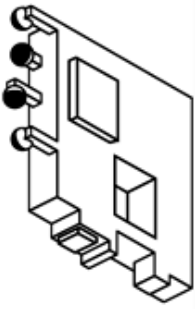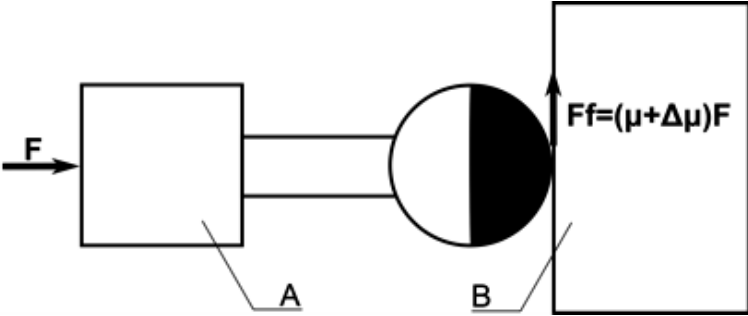
Training criterion

Definition:	The amount of experience and preparation required for the operator to assemble the parts correctly. By preparation we mean the act of getting all components and jigs together to start an assembly in addition to understanding the methodology.

Value	Meaning
1	The assembly method is not intuitive and requires 4 or more hours of preparation.
2	The assembly method is significantly less intuitive and requires at least 3 hours of preparation
3	The assembly method is less intuitive and requires at least 2 hours of preparation.
4	The assembly method is intuitive but requires at least 1 hour of preparation
5	The assembly method is very intuitive and requires nearly no preparation.

Maturity criterion

Definition:	The degree to which the process is deemed ready for industry and can be automated.

Value	Meaning
1	The process requires a large effort to become mature and to be automated.
2	The process requires significant effort to become mature and automated.
3	The process requires effort to be developed and automated. Typically a development of half a year
4	The process requires some effort to become mature and automated. Typically a development of 3 months
5	The process is easily automated and is mature. Typically a development of 1 month

11.5.2.2 Body and contact point

Body complexity criterion	
Definition:	The required changes to the Silicon parts to allow the assembly method. We evaluate this in terms of changed surface area and the added manufacturing steps. This excludes parts that serve as connectors even though they can also be made of Silicon.
Value	**Meaning**
1	The parts require a change to more than 4 mm² and adds other steps to the fabrication process.
2	The parts require a change within 4mm² and adds other steps to the fabrication process.
3	The parts require a change within 4mm² and adds no other steps to the fabrication process.
4	The parts require a change within 1mm² and adds no other steps to the fabrication process.
5	No changes have to be made to the parts.

Contact point friction criterion	
Definition:	The change of the coefficient of friction at the contact interface with the assembly method.
Value	**Meaning**
1	The friction coefficient is significantly higher than without the assembly method.
2	The friction coefficient is higher than without the assembly method.
3	The friction coefficient is slightly higher than without the assembly method.
4	The friction coefficient is equal to without the assembly method.
5	The friction coefficient is lower than without the assembly method

In the contact point friction criterion figure: $F_f = (\mu + \Delta\mu)F$

Contact point fatigue criterion

Definition:	The capability of the assembly method to survive cyclic loading at 80% of the connection strength in tensile load.

Value	Meaning
1	The assembly method survives less than 10^3 loading cycles
2	The assembly method survives between 10^3 and 10^4 loading cycles
3	The assembly method survives less than 10^4 and 10^5 loading cycles
4	The assembly method survives less than 10^5 and 10^6 loading cycles
5	The assembly method survives more than 10^6 loading cycles

Contact point alignment criterion

Definition:	The amount of added uncertainty introduced by the assembly method in a kinematic mount. We evaluate this by the added 3σ position uncertainty of a single contact point along its constraint line

Value	Meaning
1	The assembly method has a 3σ position uncertainty of more than 10µm
2	The assembly method has a 3σ position uncertainty of less than 10µm
3	The assembly method has a 3σ position uncertainty of less than 5µm
4	The assembly method has a 3σ position uncertainty of less than 1µm
5	No additional position uncertainty

Contact point nesting force criterion	
Definition:	The amount of force that has to be applied to detach a single contact point. We assume here that the assembly method takes up a surface area of 1 mm^2.
Value	**Meaning**
1	The assembly requires a stress lower than 1 MPa to break the nesting force.
2	The assembly requires a stress lower than 5 MPa to break the nesting force.
3	The assembly requires a stress lower than 10 MPa to break the nesting force.
4	The assembly requires a stress lower or equal to 50 MPa to break the nesting force.
5	The assembly requires a stress higher than 500 MPa to break the nesting force.

Contact point nesting volume criterion	
Definition:	The volume of the attachment compared to the parts without the attachment.
Value	**Meaning**
1	The assembly method requires more than 10 mm^3 per contact point.
2	The assembly method requires less than 10 mm^3 per contact point.
3	The assembly method requires less than 5 mm^3 per contact point.
4	The assembly method requires less than 1mm^3 per contact point.
5	The assembly method requires less than 0.1mm^3 per contact point.

11.5.3 Discussion

Table 11.4 evaluates the assembly methods in terms of the criteria defined in Section 11.5.2. The main result is that using integrated clips or magnets are preferred assembly methods. Epoxy glues and soldering score low due to the time required for prototyping, as in this thesis. Though bolting scores rather high, it is noted that, due to limited parts, no successful assembly was achieved using this method. UV gluing proved to be a versatile assembly method easily applicable to bodies at the cost of contact point alignment. Compensating for alignment adds complexity. One could add further weight to the contact point alignment criterion resulting in more preference for clips and magnets. The evaluation of robotic and automated assembly is left for future work.

Table 11.4: Comparison matrix of the assembly methods.

		Method						
Criterion		Integrated clips	Separate clips	Magnets	UV gluing	Epoxy gluing	Soldering	Bolting
Assembly	Time	5	4	3	5	1	1	2
	Assembly complexity	5	4	3	5	5	5	2
	Verification	4	4	4	4	4	5	4
	Cost	4	3	5	5	5	5	5
	Risk of damage	5	5	3	5	4	3	2
	Demountable	4	4	5	3	3	3	3
	Aesthetics	4	1	2	3	3	2	2
	Training required	5	4	5	4	3	4	3
	Maturity	5	4	4	5	5	5	2
Body & contact point	Body Complexity	4	5	5	3	3	2	5
	Contact point friction	4	4	4	2	2	1	4
	Contact point fatigue	5	5	5	2	3	3	5
	Contact point alignment	5	5	5	2	2	1	5
	Contact point nesting force	2	2	2	4	4	3	5
	Contact point nesting volume	3	1	5	5	5	5	3
	Total	**64**	**55**	**60**	**57**	**52**	**48**	**52**

Chapter 12 Positioning error measurements

This chapter presents the results of positioning error measurements made on 3-dimensional three-body kinematic mounts.

12.1 Problem statement

Estimate 6 DOF positioning error by conducting measurements on two and three-body 3-dimensional kinematic mounts.

12.2 First experiment

The first experiment was conducted with milled parts and custom contact spheres and flats. Measurement was carried out by the 3D Coordinate-Measuring Machine (CMM) equipped with a low force 3D touch probe [64]. The specific machine on which these tests were carried out is named "micro-CMM'' and is located at the Swiss Federal Institute of Metrology (METAS), Bern, Switzerland. A two-body and a three-body kinematic mount were manufactured and tested and their performance was compared experimentally. The measurements were done at METAS in order to achieve a reliable order of magnitude, to save time and to have a traceable measurement. The setup 3-D uncertainty is known to be within 50 nm and variables such as temperature, humidity, cleanliness and vibration are readily observed in the setup. A detailed discussion of the setup can be found in Küng [64]. Figure 12.2.1 shows the micro-CMM, its touch probe and measuring stylus.

a   b
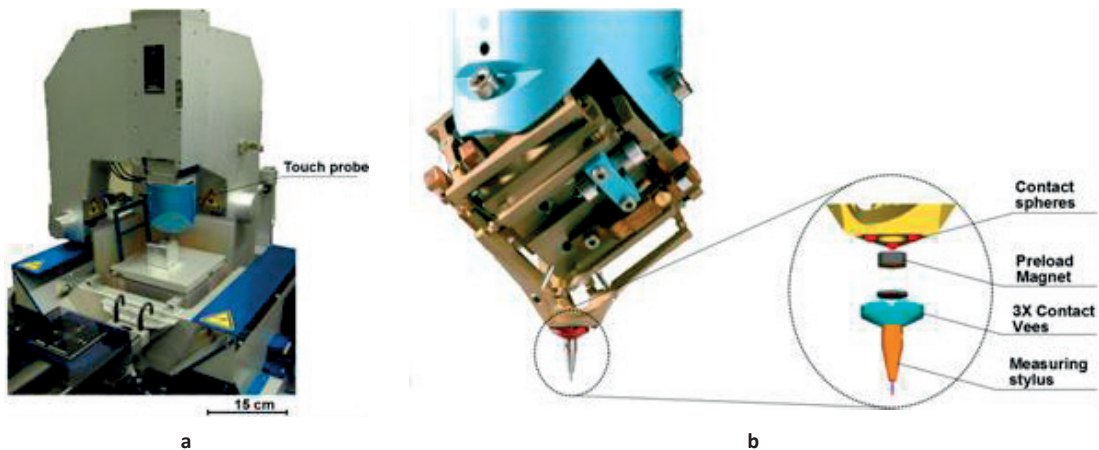
Figure 12.2.1: a) the micro-CMM and its touch probe, b) the touch-probe of the micro-CMM with the measuring stylus mounted on top of it. The measuring stylus is kept in place using a kinematic mount.

12.2.1 Considerations for the first experiment

The distances between the centers of the spheres in both the three-body and two-body configuration are the same. In addition both use the same means of measurement, styli measured by the micro-CMM. For the contact materials, a Silicon nitride sphere is used in contact with a hardened polished steel slab. The hardened polished steel slabs were water cut

from standard gauge blocks (Mitutoyo 1mm thickness) and have a roughness R_a of 50 nm. The Silicon nitride spheres are grade 3 spheres with a R_a roughness of 10 nm (Supplied by Ceratec).

The combination of materials is comparable to the materials used by Slocum [15], though no specific mention of the roughness was made in this paper. We used a readily available oil lubricant (Balzers-Pfeiffer öl P3) between the contacts in order to reduce friction.

Gluing the ceramic spheres to the components was done by epoxy adhesive Loctite EA 9483, recommended by Henkel. For the hardened metal a cyanoacrylate Loctite 480 was used. To make sure the glue did not misalign the spheres or hardened steel slabs we used small glue sockets.

A major constraint for the design was the limited measurement volume, namely 80 x 80 x 38 mm^3. In addition, the actual available place for mounting equipment for manipulation was limited to a volume of 110 x 110 x 50 mm^3.

In order to reduce thermal effects for the two-body kinematic mount a lever system connected to a plastic handle was used. In the case of the three-body kinematic mount plastic handles are used for manipulating.
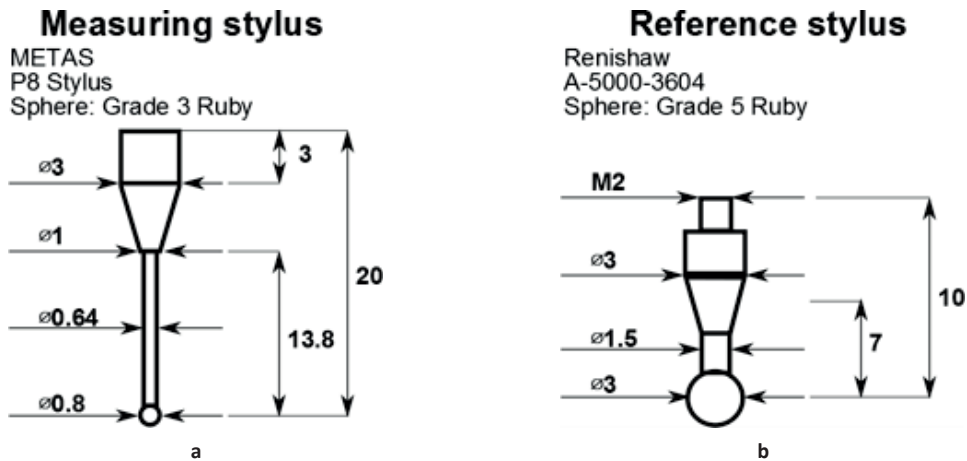
Figure 12.2.2: a) The specifications of the measuring stylus, which was mounted on the touch probe during the measurements. All dimensions are in mm. b) The specifications of the reference styli, on which the measurement was performed. All measurements are in mm.

The measurements were performed with METAS and their touch probe which had their P8 calibrated 0.8 mm diameter grade 3 ruby stylus mounted on it (Figure 12.2.2a). We call this stylus the *measuring stylus.* The measurements were performed for the two and three-body configuration on respectively 6 and 9 reference styli (3 per body) (Figure 12.2.2b). The reference-styli have a 3 mm diameter and are grade 5 with a ruby tip (Renishaw A-5000-3604).

The disturbance forces applied by measuring with the touch probe are below 0.5 mN. Magnets within the micro-CMM, are not allowed as it could result in damage to the probe. The applied nesting forces per contact point are 90 mN for the two-body configuration, by using the mobile body B its mass. In addition, we wished to stay as close as possible to the discussed theoretical configurations therefore it was chosen to keep the contact points on a single line. This including the limited volume and the requirement of keeping the bodies sufficiently rigid resulted in the different preload. For the three-body case they are not equal between the inner and outer contacts the nesting forces here are 2.47 N and 0.92 N respectively for a contact closer to the nesting force and a contact further away.

12.2.2 Configurations of the first experiment

The schematic figures of the configurations of first experiment are illustrated in Figure 12.2.3 and Figure 12.2.7.
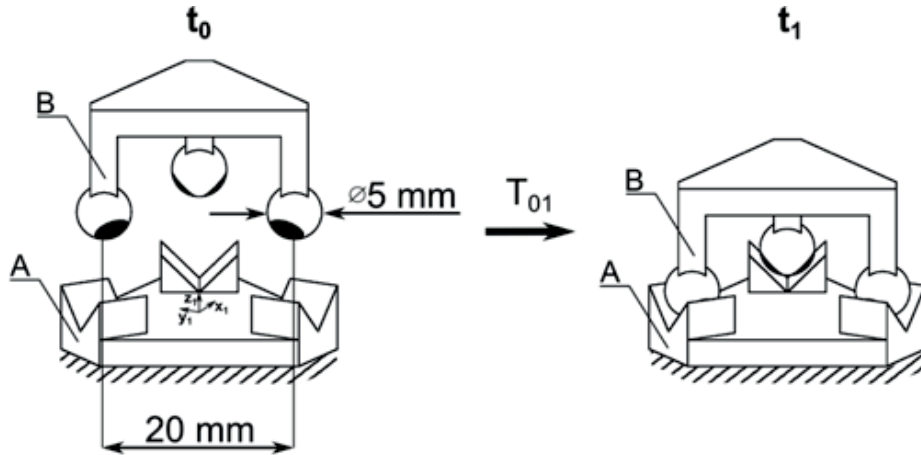
Figure 12.2.3: a) Three-Vee kinematic Mount.

The layout of the two-body kinematic Mount is shown in Figure 12.2.4. The principal components are the two bodies, where body B has the spheres glued into it and body A has the contact flats glued into it. Both bodies have three reference styli of which we measure the centers of the spheres mounted on top of these styli. In order to measure the positioning error, we manipulate body B with respect to body A using a *manipulation lever* having a limited range of motion.
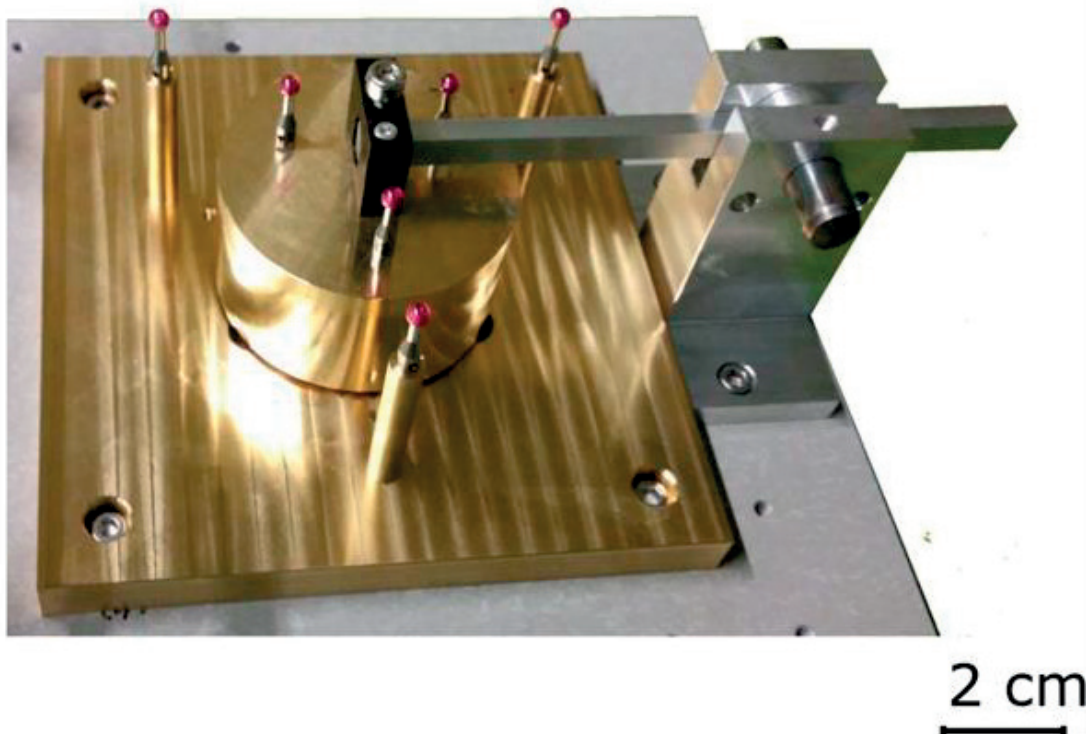
Figure 12.2.4: Constructed two-body kinematic Mount. The nesting force is applied by means of the mass of the mobile body B.
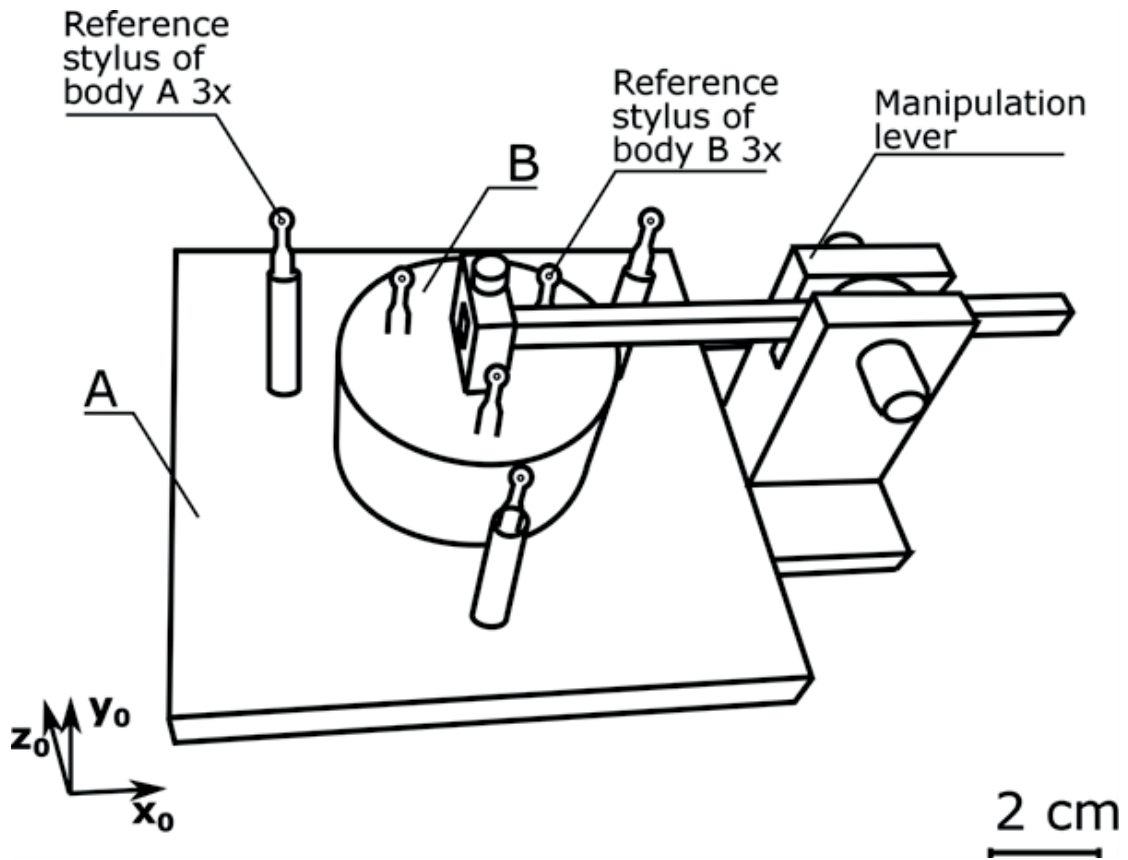
Figure 12.2.5: Layout of the Constructed version of the two-body kinematic mount. Illustrating the reference styli of bodies A and B and the manipulation lever used to displace the body.
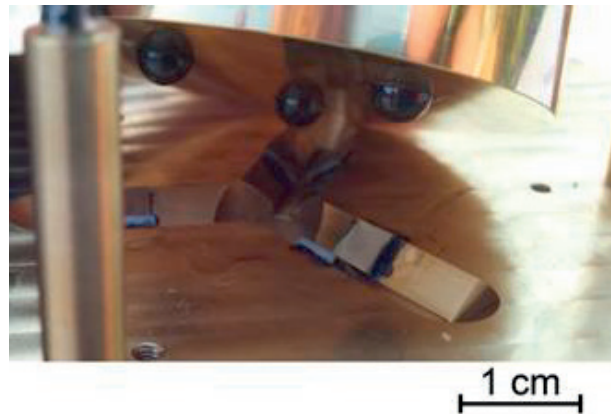
Figure 12.2.6: The contact spheres and contact flats of the two-body kinematic mount.
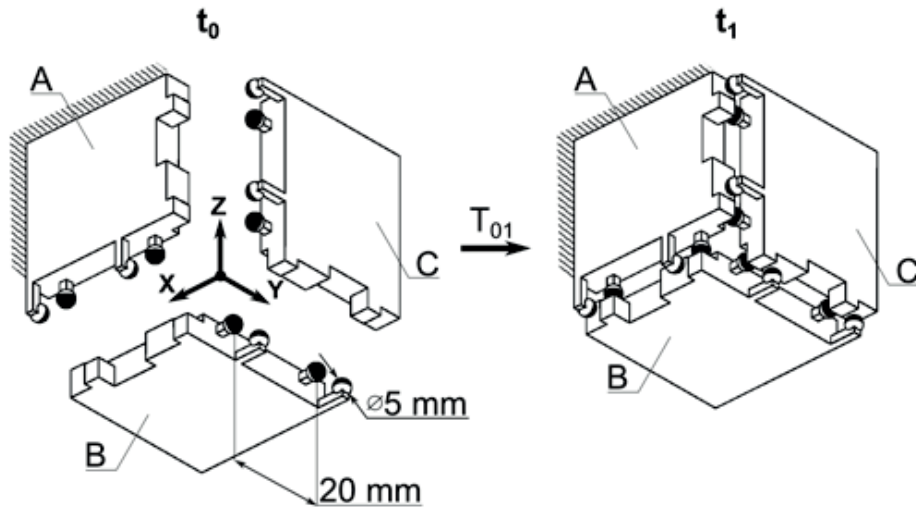
Figure 12.2.7: a) Three-body kinematic mount of Example 7.4.2.7.

The layout of the three-body kinematic mount is shown in Figure 12.2.8. The principal components are the three bodies of which each have spheres and contact flats glued into them. Each of the three bodies has three reference styli of which we measure the centers of the spheres mounted on top of these styli. In order to examine the positioning error we manipulate body B and C with respect to body A by means of a manipulation handles. The movement is limited by preloaded springs.
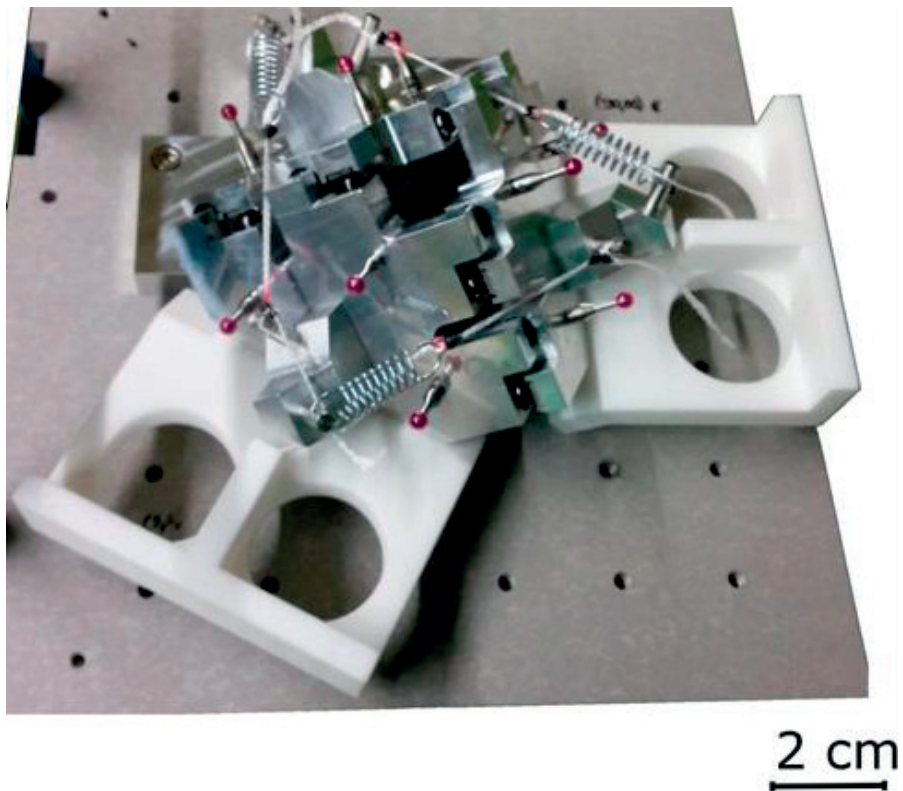
Figure 12.2.8: Realized version of the three-body kinematic mount
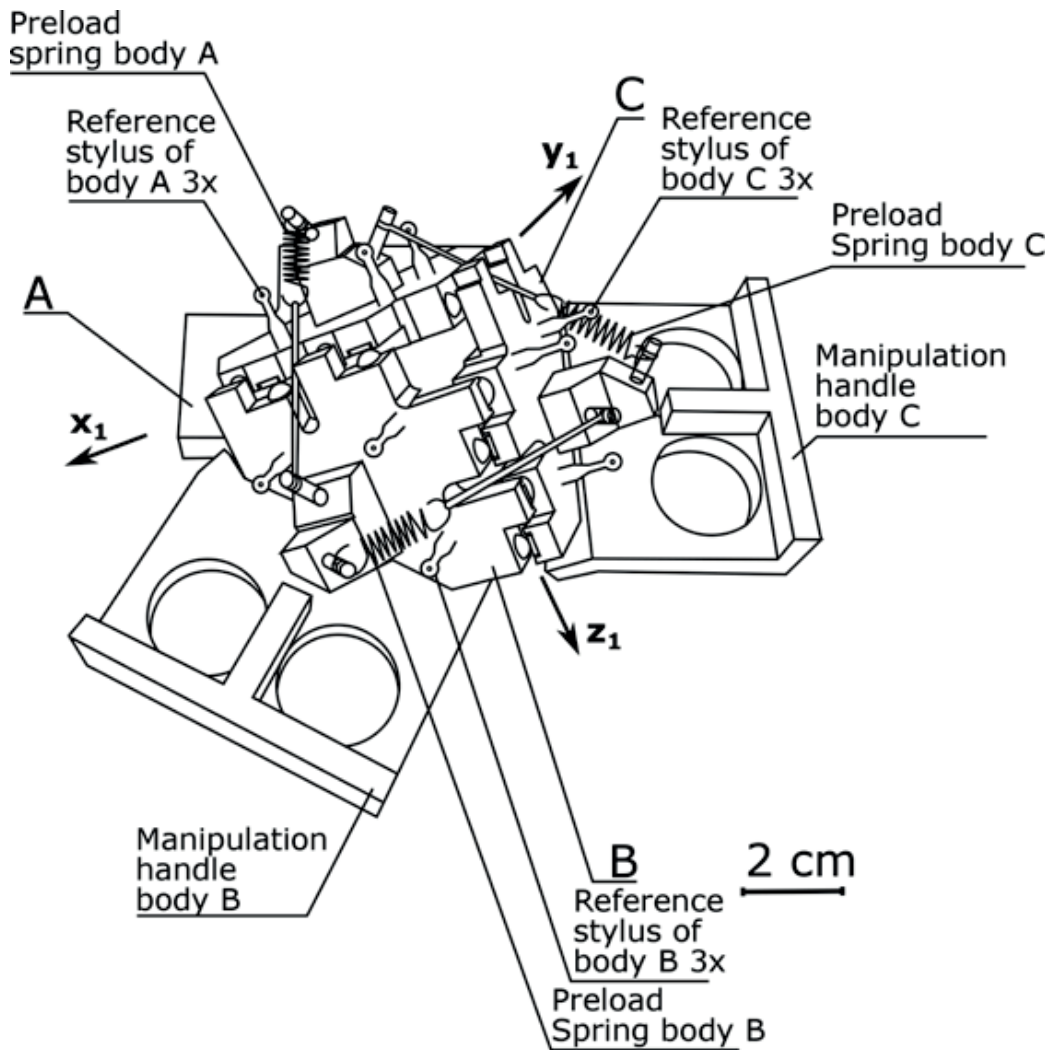
Figure 12.2.9: a) Layout of the realized version of the three-body kinematic mount. The nesting force is applied by means of three preload springs. b) The three-body kinematic mount as a schematic. Body A is fixed, Body B and body C are mobile. They are positioned by using the manipulation handles. The measurements are conducted by measuring the spheres of the styli on bodies A, B and C.

Figure 12.2.10: A contact sphere and contact flat of the three-body kinematic mount in contact.

12.2.3 The measurement procedure for two bodies

For each measurement, we measure three points on each body, as illustrated by the top view in Figure 12.2.11. This figure shows both bodies and the points which lie in the center of the spheres mounted on the styli.
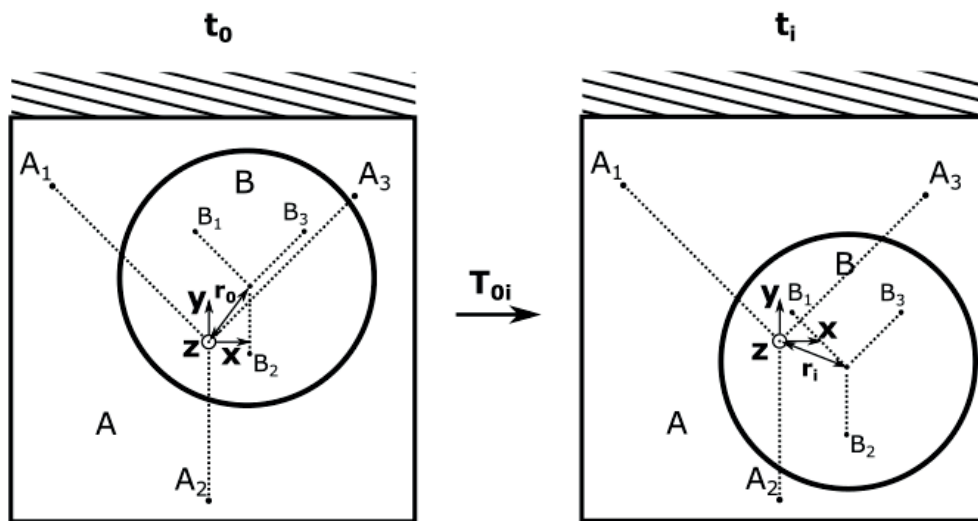
Figure 12.2.11: Schematic top view of the two-body setup. The two bodies are body A and B, by measuring the spheres mounted on the styli of the bodies we measure the position of the points at the center of the spheres A_1 to A_3 and B_1 to B_3. From these two sets of three points we can calculate their incenters and the relative angle between the planes. In this image we illustrate both the initial measurement (t_0) with the distance r_0 between the incenters and another measurement (t_i) with a distance r_i between the incenters. Between each measurement this the manipulation lever is moved so that it lifts body B by its handle. The upward movement removes the contact points between body A and B. The body is placed in contact again using the same lever, for a new measurement.

The manipulation of putting the contact points in and out of position is displayed in Figure 12.2.13.
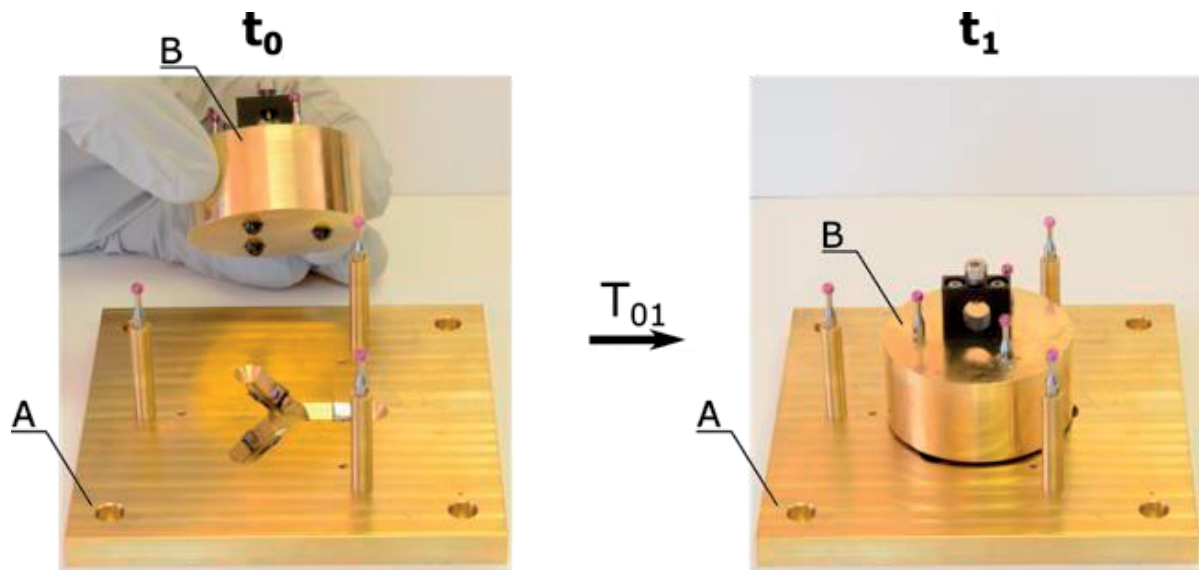
Figure 12.2.12: The two-body kinematic mount in unaligned and aligned position.
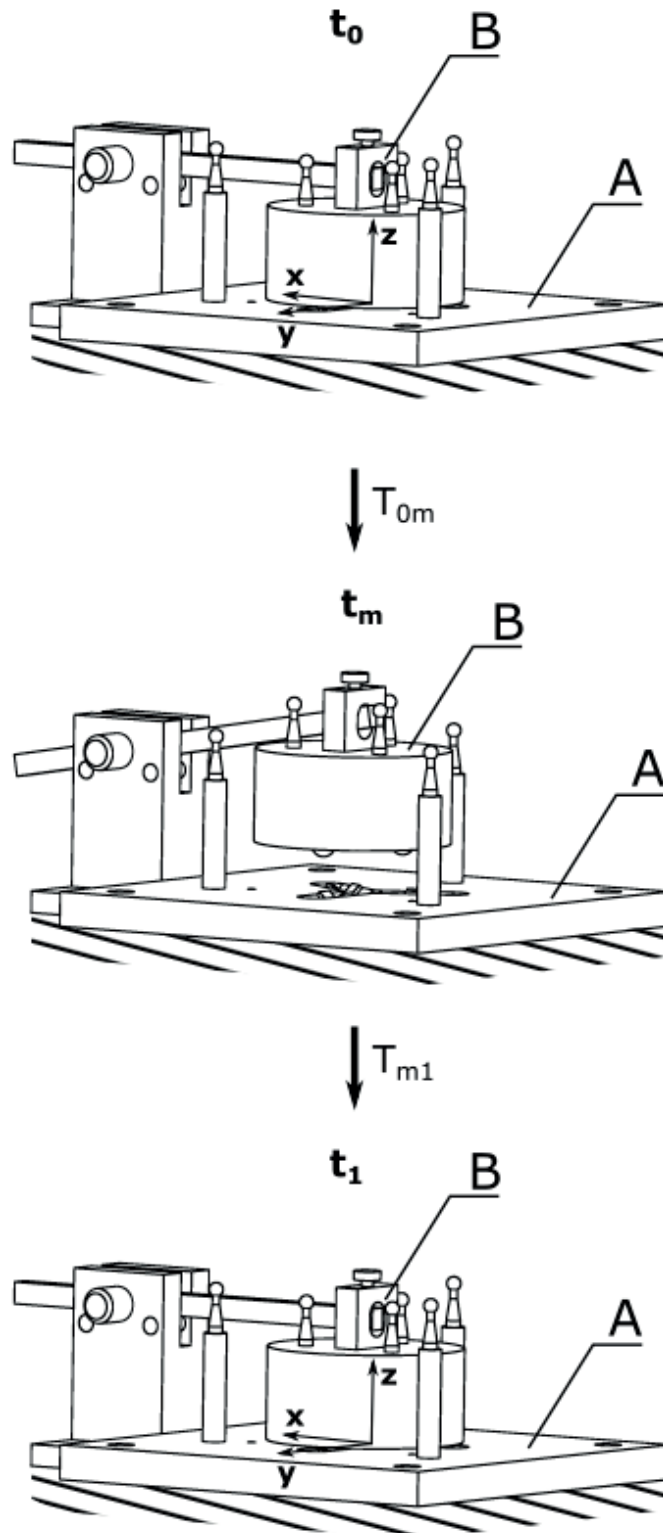
Figure 12.2.13: This figure shows how body B is manipulated with use of the manipulation lever to be in and out of contact with body A. Before every positioning error measurement, we used the manipulation lever to go out and into contact.

12.2.4 Measurement procedure for three bodies

For each measurement, we measure three points in each body, as illustrated by the top view in Figure 12.2.14. This figure shows the three bodies and the points lying at the sphere centers mounted on the styli.
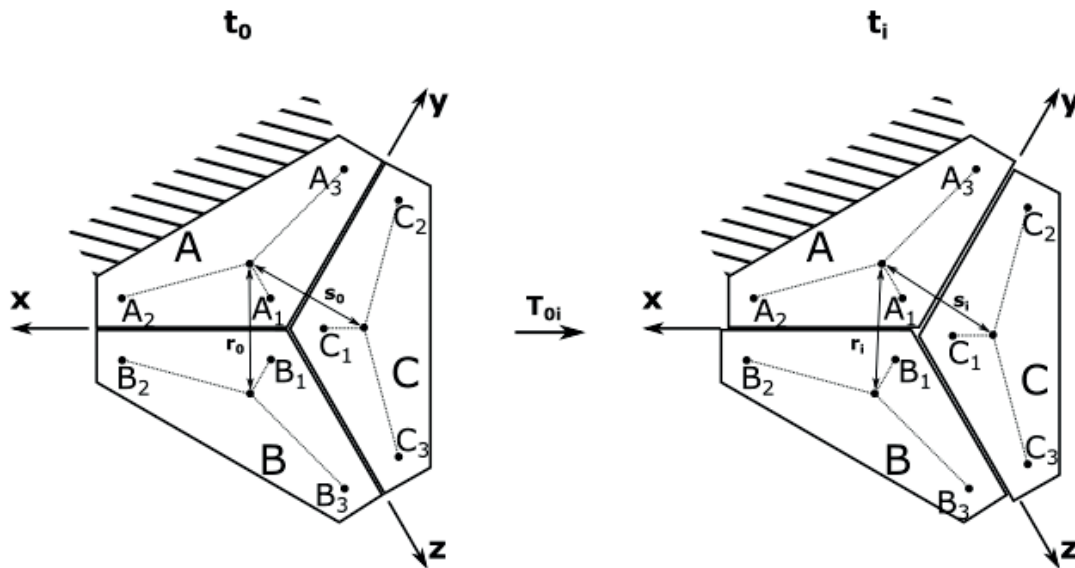
Figure 12.2.14: Schematic top view of the three-body setup. The three bodies are body A, B and C, by measuring the spheres mounted on the styli of the bodies we measure the position of the points at the center of the spheres A_1 to A_3, B_1 to B_3 and C_1 to C_3. After this the manipulation handle is used to manipulate the parts in and out of aligned state for a new series of measurements. For each measurement we compare the distances between the incenters r_i and s_i of the three bodies with the reference incenters r_0 and s_0. In addition we also look at the relative change in angle of the points B_1 to B_3 and C_1 to C_3 with respect to A_1 to A_3

The manipulation of putting the contact points in and out of position is displayed in Figure 12.2.16.
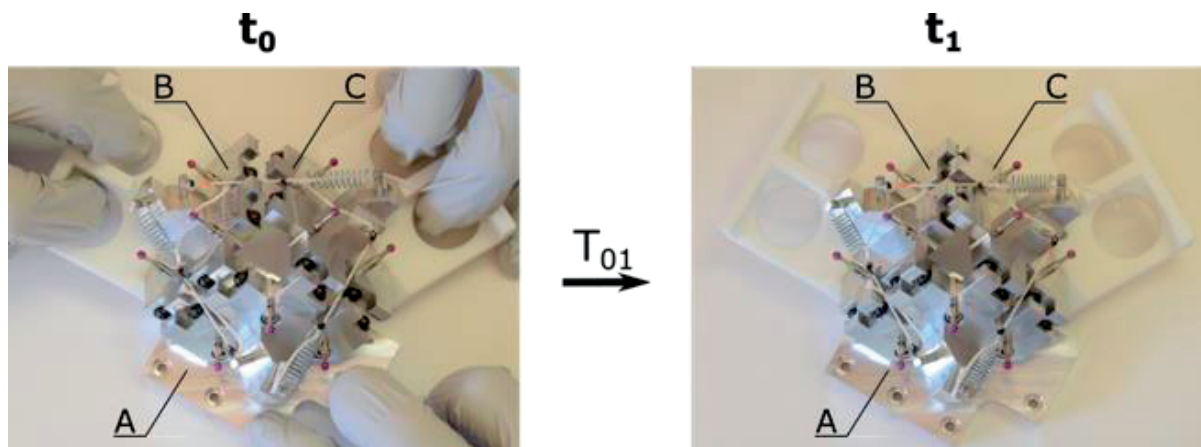
Figure 12.2.15: The three-body kinematic mount in unaligned and aligned position.
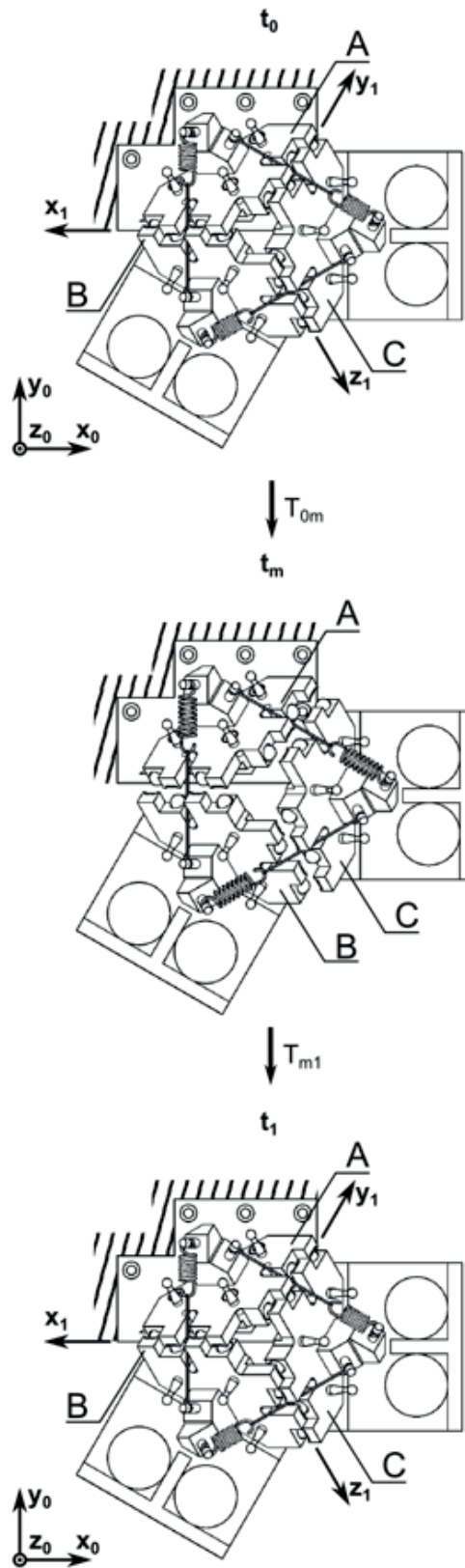
Figure 12.2.16: This figure shows how body B and C are manipulated with use of the manipulation handles to be in and out of contact with body A. Before every positioning error measurement we use the manipulation handles to go out and into contact.

12.2.5 Results of the first experiment

We tabulated the average and extreme values of the position measurements. We indicate the measurement here by a normalized axis and the angular rotation around this axis.

12.2.5.1   Two-body kinematic mount

For the two-body kinematic mount a total of **10 positioning error measurements** were done. An additional measurement was done in order to have a reference measurement, implying that the bodies were not displaced in between the measurement. The measurements measured the centers of the three reference styli we choose to analyze the incenter of the triangle defined by these three sphere centers. The reference zero point is the incenter defined by the centers of the three contact spheres.

Table 12.2.1: The ten measurements and their minimum, maximum and average.

Measurement nr.	Linear position				Rotational axis – and angle			
	Displacement vector components			Displacement	Normalized rotation vector components			Angle
	X Xi-X1 μm	Y Yi-Y1 μm	Z Zi-Z1 μm	D ri-r0 μm	Xr	Yr	Zr	α μrad
0	0	0	0	0	0	0	0	0
1	0.075	0.056	-0.15	0.177	-0.64	-0.62	0.46	5
2	0.054	-0.073	-0.02	0.093	-0.31	-0.56	0.77	6
3	0.106	-0.221	-0.036	0.248	0.58	-0.4	0.72	5
4	0.073	-0.028	-0.036	0.086	-0.53	-0.57	0.63	6
5	0.079	-0.05	-0.031	0.098	-0.48	-0.6	0.64	6
6	0.09	-0.175	-0.03	0.2	0.03	-0.75	0.66	5
7	0.102	-0.213	-0.047	0.241	0.2	-0.68	0.7	4
8	0.108	-0.192	-0.044	0.225	0.1	-0.74	0.67	4
9	0.122	-0.196	-0.045	0.236	0.06	-0.73	0.68	4
Minimum	0.054	-0.221	-0.15	0.086	-0.64	-0.75	0.46	4
Maximum	0.122	0.056	-0.02	0.248	0.58	-0.4	0.77	6
Average	0.09	-0.122	-0.049	**0.178**	-	-	-	**5**

12.2.5.2   Three-body kinematic mount

For the three-body kinematic mount a total of **3 positioning error measurements** were done. An additional measurement was done in order to have a reference measurement, implying that the bodies were not displaced in between the measurement. The limited number of measurements is primarily due to time and cost.

Table 12.2.2: The three measurements and their average.

| | | | Linear position | | | | Rotational axis – and angle | | | |
| | | | Displacement vector components | | | Displacement | Normalized rotation vector components | | | Angle |
		Measurement nr.	X Xi-X1 µm	Y Yi-Y1 µm	Z Zi-Z1 µm	D ri-r0 µm	Xr	Yr	Zr	α µrad
Body	B	0	0	0	0	0	0	0	0	0
		1	-0.805	-0.025	0.553	0.977	-0.87	-0.32	-0.38	53
		2	0.809	0.022	-0.169	0.827	0.80	0.59	0.05	30
		Average	0.002	-0.002	0.192	**0.902**	-	-	-	**42**
	C	0	0	0	0	0	0	0	0	0
		1	0.017	0.828	0.006	0.828	-0.75	-0.66	-0.06	29
		2	-0.020	0.573	0.158	0.595	0.64	0.76	0.14	32
		Average	-0.001	0.701	0.082	**0.712**	-	-	-	**31**
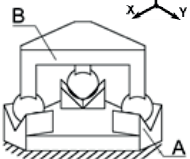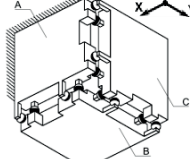
12.2.6 Comparison and discussion

The measurements show that the kinematic mount example 7.3.2.7 has a positioning error on the order of a micron and an angular error on the order of tens of microrads.

The average positioning error of the three-body mount is between 4 and 5 times larger than for the Three-Vee coupling and the rotation angle error is between 6.2 and 8.5 times larger.

The number of experiments performed is too low to provide reliable statistical analysis but indicates the correct order of magnitude.

Table 12.2.3: Average displacement and change of angle of the measured configurations.

		Average		
		Three-Vee	Example 7.3.2.7	
			Body	
			B	C
Degree of Freedom (DOF)	D	0.178 µm	0.902 µm	0.712 µm
	α	5 µrad	42 µrad	31 µrad
Number of measurements		10	3	

12.3 Experiment on Silicon parts

The second experiment was conducted with Silicon bodies and a custom setup. This experiment considered four configurations: a two-body configuration and 3 three-body configurations. After presenting the configurations, we introduce the custom setup which makes use of three interferometers and two autocollimators.

12.3.1 Second experiment configurations

To test the kinematic mounts, Silicon pieces of size 2 x 2 x 0.545 mm were made in [100] type Silicon wafers. The pieces contained three holes as illustrated in Figure 12.3.1. For a two-body reference in Silicon we used Silicon parts with three-rectangular holes. These rectangular holes combined with precision steel spheres give us an indication of an obtainable two-body alignment.
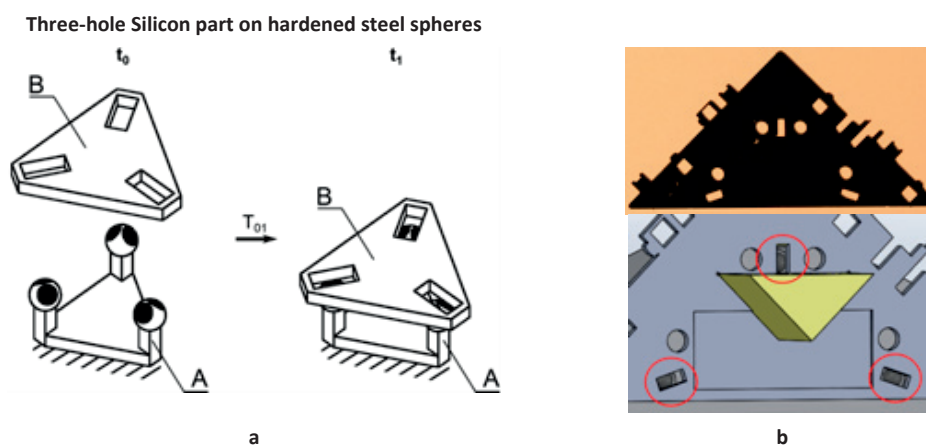
Figure 12.3.1: a) An illustration showing the three-spheres of body A which in contact with the rectangular holes of body B constrain all degrees of freedom b) An image of the part with its three holes, and a CAD impression of the balls in contact with the rectangular holes.

The Silicon bodies have contact points oriented perpendicular or parallel to the wafer flat implying a [110] crystalline orientation for the in plane contacts and a [100] orientation for the out of plane contacts. An example of the parts assembled with magnets and prisms for the experiment is offered in Figure 12.3.2. Due to financial and production constraints three configurations were tested, these are illustrated in their tested orientation in Figure 12.3.3.
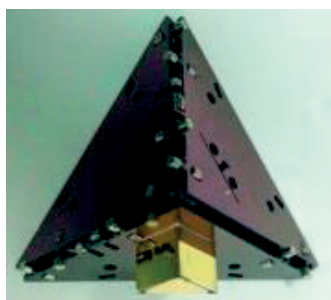
Figure 12.3.2: The Silicon bodies assembled using magnets.
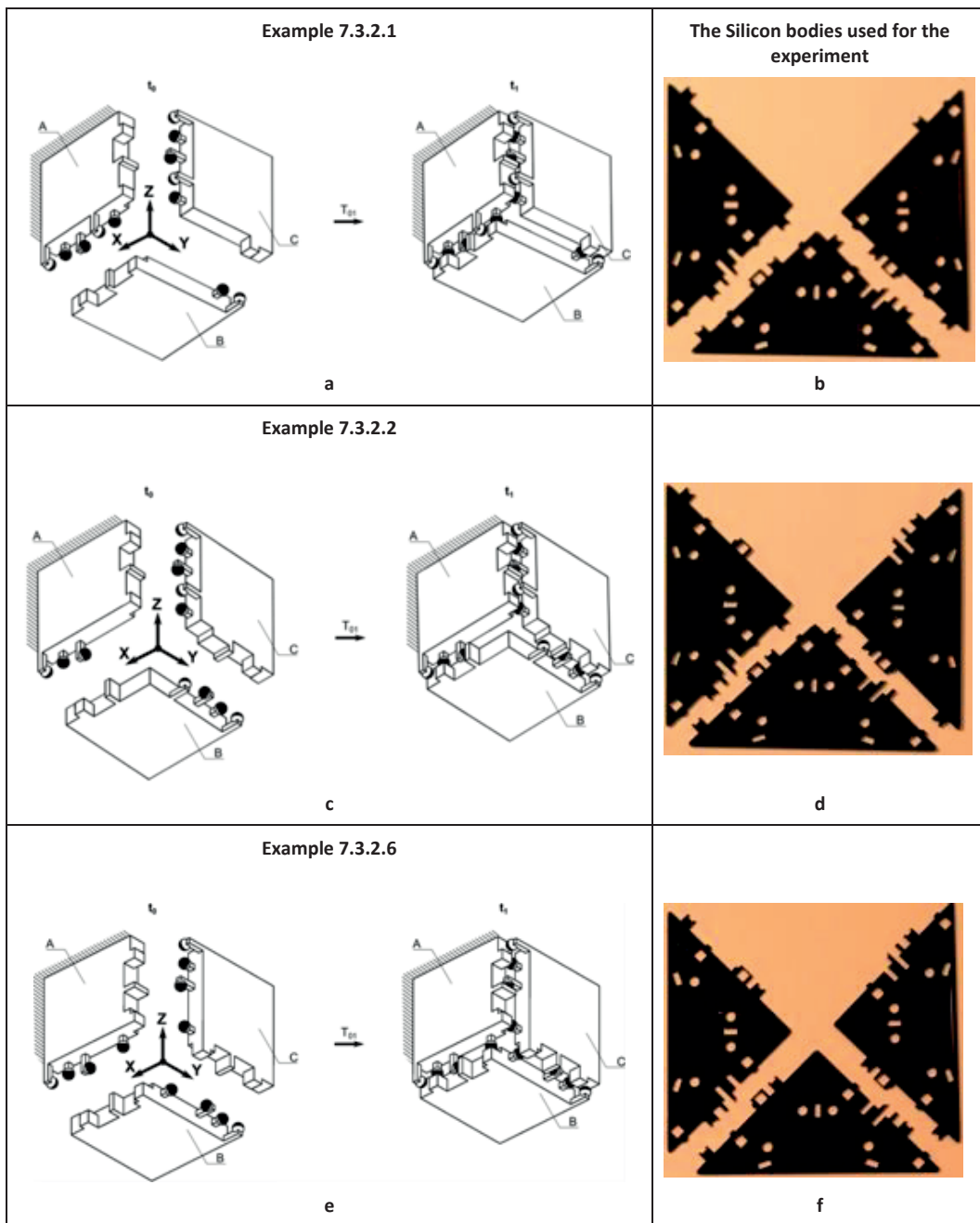
Figure 12.3.3: a) Example 7.3.2.1 in its tested orientation, b) the Silicon bodies of Example 7.3.2.1. c) Example 7.3.2.2 in its tested orientation, d) The Silicon bodies of Example 7.3.2.2. e) Example 7.3.2.6 in its tested orientation, f) The Silicon bodies of Example 7.3.2.6

12.3.2 The 6 DOF measurement setup for measuring Silicon kinematic mounts

12.3.2.1 Two-body hole coupling

In order to have a reference measurement for two-body alignment a kinematic coupling using rectangular holes and spheres was used as illustrated in Figure 12.3.4a. Though this is not exactly the same as the three-Vee coupling, it does consist of 6 contact points organized in a similar way and offers thus a first approximation of a three-Vee coupling in Silicon. In future work it would be interesting to use KOH-etching for creating a more Vee like contact. The measurement of the two-body hole coupling consisted of the Silicon part on 3 hard metallic spheres Figure 12.3.4. The practical implementation is shown in Figure 12.3.4b and Figure 12.3.5.
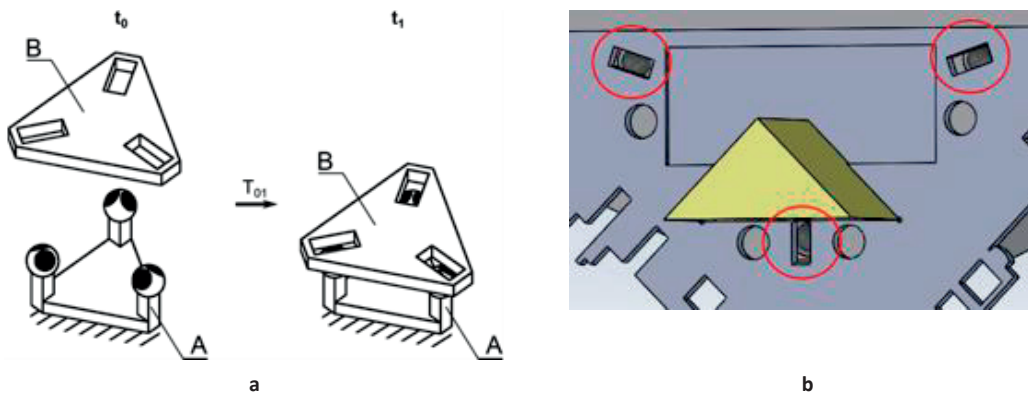
Figure 12.3.4: a) The two-body hole coupling measured as a reference configuration. b) The contact points with the metal spheres on the Silicon part.

Figure 12.3.5a illustrates the two contact points per sphere which are at a 90 degree angle. Figure 12.3.5b shows how the preload is applied by means of a dead mass applied to the part. Note that the mass is guided in a through hole for stability.
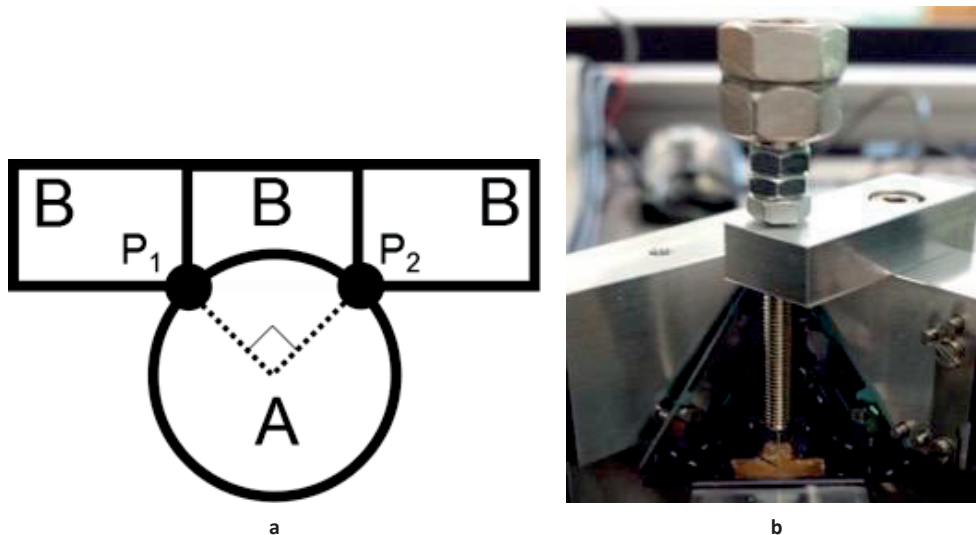
Figure 12.3.5: a) The contact points of the metal sphere (body A) with the Silicon part (body B). The angle between the contact points P_1 and P_2 is 90 degrees. b) The nesting force is applied to the Silicon part with a dead load on top of the autocollimator prism.

12.3.2.2   *Three-body coupling*

In order to measure the positioning error of the previously fabricated Silicon pieces a custom setup was designed. The setup, illustrated in Figure 12.3.6, is based on three Fabry-Perot interferometers (Attocube fps3010) with a 25 picometer resolution and two autocollimators (Möller-Wedel 10/500) with a 5 µrad resolution. In order to prevent parasitic reflections of the autocollimators two black 3D printed plates with holes were designed. The overall measuring resolution of the setup in a controlled environment is 6 nm and 5 µrad. The difference between the specified resolution of the interferometer and measured resolution is due to the limited temperature stability in the room.

a

b
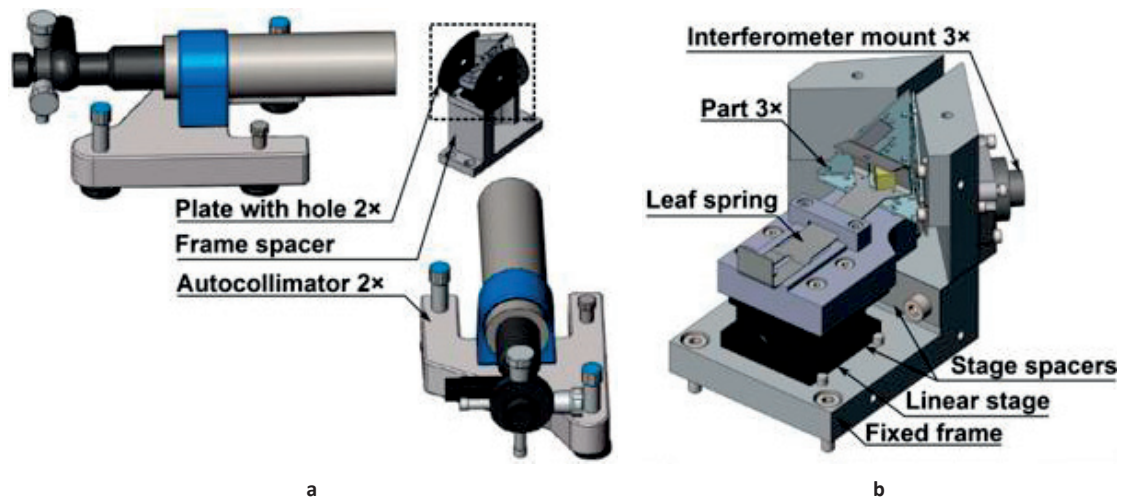
Figure 12.3.6: a) A general view of the measurement setup with its two autocollimators, frame spacer to put the setup at the height of the autocollimators and plates with holes to block parasitic reflections. b) A zoomed view of the parts mounted on the frame spacer. First there is a fixed frame with dowel pins for aligning the linear stage. To calibrate the stroke and height there are additional stage spacers. The leaf spring can detach the part with the prism from the other two allowing for repeated measurement. On the linear guide the part is mounted on a total of three balls glued into pockets for the alignment.

In order to guarantee the alignment of the three interferometers with an accepted reflection angle range (0.075° to 0.295°), each of them is mounted on a membrane containing three leaf springs (Figure 12.3.8). This membrane allows for laser angle adjustment of the interferometers non-axial angles. The membrane itself is illustrated in Figure 12.3.7.
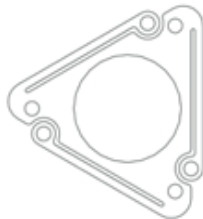
Figure 12.3.7: The interferometer mount membrane.

a

b
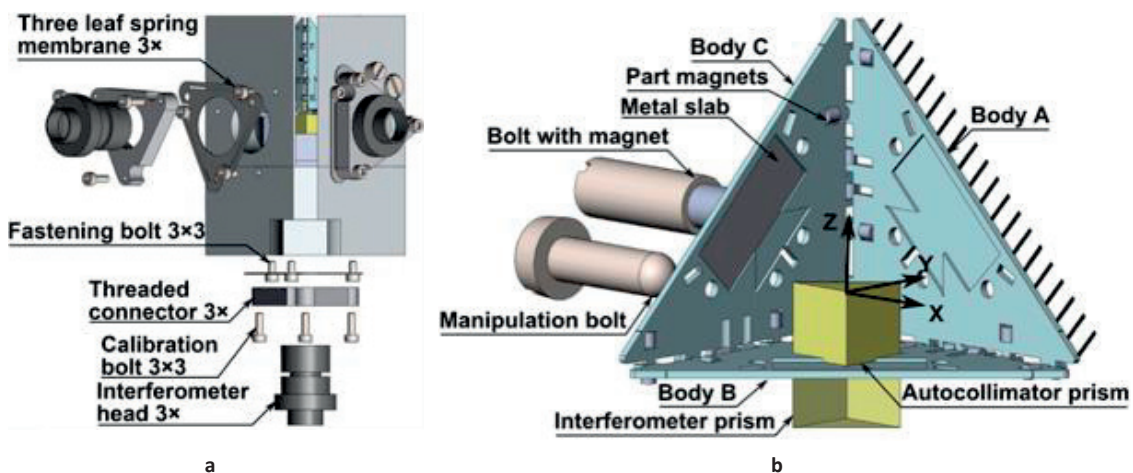
Figure 12.3.8: a) The back view of the measurement setup, it shows the leaf spring membrane that carries the interferometer mount and all fastening and calibration bolts. b) The three bodies as in their mounted state in an experiment. Body A is the body that is fixed. Body C always has its contact points in contact with body A the other degrees of freedom are blocked by the fixed frame when not in contact with body B. The nesting force to keep body C in contact the manipulation bolt is applied by the bolt with magnet. In order to pre-align the part the manipulation bolt is used.

The setup is placed in a controlled environment (temperature, cleanliness) and mounted on an anti-vibration table. Each Silicon body has small NdFeB magnets glued onto it. With these magnets the bodies, when brought into pre-alignment, precisely align themselves as the configurations of bodies form a kinematic mount. The Silicon bodies are shown in Figure 12.3.8b.

12.3.3 The measurement procedure

Body A (Figure 12.3.8b) is always fixed on the setup frame. In the unaligned state, bodies B and C are constrained to the setup and, in the aligned state, they are constrained to body A.

Body B has a metal slab incorporated and is kept in position prior to alignment by body A and by a manipulation bolt.

The force keeping body B in position comes from a magnet mounted on a bolt, which attracts the metal slab. The position of the manipulation bolt can be modified so as to fix the body to the setup frame or to allow the bodies to align themselves.

Body C holds two prisms of size 5mm x 5mm x 5mm. These prisms are used as reflective flat orthogonal references for measurement with the autocollimator and interferometer.

Body C is fixed with respect to a linear guide mounted on the setup using a leaf spring (unaligned state). By moving the linear guide and removing the leaf spring, the body is allowed to align with respect to the other two bodies (aligned state).

A measurement consists of setting the sensors to zero in an aligned state, after which the bodies are unaligned and realigned to measure the difference in position.

12.3.4 Results of the first experiment

We computed the standard deviation of the position measurements and 99.7 % of the data was within three standard deviations. Moreover, we compute the 95% confidence interval of the standard deviation.

12.3.4.1 Silicon two body hole coupling
38 measurements were performed successfully to analyze the positioning error of all six DOFs (X, Y, Z, R_x, R_y and R_z), with results shown in Table 12.3.1.

Table 12.3.1: The standard deviation of position and its 95% confidence interval for all six Degrees of Freedom of a two-body hole coupling. The two-body hole kinematic coupling is composed of a Silicon part in contact with three metallic spheres.

38 measurements	Standard deviation of position	95 % Confidence Interval of the standard deviation of position		Standard deviation of position	95 % confidence interval of the standard deviation of position
X	0.040 μm	[0.040 0.032] μm	R_X	32 μrad	[26 42] μrad
Y	0.17 μm	[0.14 0.22] μm	R_Y	54 μrad	[44 70] μrad
Z	0.20 μm	[0.16 0.27] μm	R_Z	15 μrad	[12 19] μrad

12.3.4.2   Silicon three-body kinematic mount example 7.3.2.1
27 measurements were performed successfully to analyze the positioning error of all six DOFs (X, Y, Z, R_x, R_y and R_z), with results given in Table 12.3.2.

Table 12.3.2: The standard deviation of position and its 95% confidence interval for all six Degrees of Freedom of a Silicon three-body kinematic mount of Example 7.3.2.1 as illustrated in Figure 12.3.3a.

27 measurements	Standard deviation	95 % Confidence Interval of the standard deviation		Standard deviation	95 % confidence interval of the standard deviation
X	2.3 µm	[2 5.5] µm	**R_X**	360 µrad	[280 500] µrad
Y	2.2 µm	[1.7 3.1] µm	**R_Y**	300 µrad	[230 410] µrad
Z	1.6 µm	[1.2 2.2] µm	**R_Z**	400 µrad	[310 550] µrad

12.3.4.3   Silicon three-body kinematic mount example 7.3.2.2
23 measurements were performed successfully to analyze the positioning error of all six DOFs (X, Y, Z, R_x, R_y and R_z), with results given in Table 12.3.3.

Table 12.3.3: The standard deviation of position and its 95% confidence interval for all six Degrees of Freedom of a Silicon three-body kinematic mount of Example 7.3.2.2 as illustrated in Figure 12.3.3c.

23 measurements	Standard deviation	95 % Confidence Interval of the standard deviation		Standard deviation	95 % confidence interval of the standard deviation
X	0.95 µm	[0.72 1.4] µm	**R_X**	730 µrad	[560 1000] µrad
Y	3.4 µm	[2.6 4.8] µm	**R_Y**	88 µrad	[68 125] µrad
Z	3.1 µm	[2.4 4.4] µm	**R_Z**	300 µrad	[230 430] µrad

12.3.4.4   Example 7.3.2.6
33 measurements were performed successfully to analyze the positioning error of all six DOFs (X, Y, Z, R_x, R_y and R_z)., with results given in Table 12.3.4.

Table 12.3.4: The standard deviation of position and its 95% confidence interval for all six Degrees of Freedom of a Silicon three-body kinematic mount of Example 7.3.2.2 as illustrated in Figure 12.3.3e.

33 measurements	Standard deviation	95 % Confidence Interval of the standard deviation		Standard deviation	95 % confidence interval of the standard deviation
X	0.28 µm	[0.22 0.38] µm	**R_X**	18 µrad	[14 24] µrad
Y	0.098 µm	[0.078 0.13] µm	**R_Y**	16 µrad	[12 21] µrad
Z	1.8 µm	[1.4 2.5] µm	**R_Z**	9 µrad	[7.2 12] µrad

12.3.5 Comparison and discussion

An overview of the results is presented in Table 12.3.5. When we compare the three-hole coupling to the kinematic mounts, we note that the kinematic mounts that are not symmetric, Example 7.3.2.1 and Example 7.3.2.2, have significantly worse performance in terms of their angular error. The translational positioning error is of the same level for Example 7.3.2.6 and the Three-Vee coupling; this is most likely attributed to the symmetry of both configurations. The variation of angular error does not allow to clearly distinguish between Example 7.3.2.6 and the Three-hole coupling, the reason being that the resolution limit of the autocollimators is 5μrad. This means that for future measurements it would be interesting to allow even better angular resolution measurements. Generally speaking, micron-level positioning error is obtained and symmetric configurations seem to be the most interesting for further investigation.

Table 12.3.5: the standard deviation of the degrees of freedom of the measured configurations.

		Standard Deviation			
		Two-body hole coupling	Example 7.3.2.1	Example 7.3.2.2	Example 7.3.2.6
Degree of Freedom (DOF)	X [μm]	0.040	0.95	3.0	0.29
	Y [μm]	0.17	3.4	2.2	0.074
	Z [μm]	0.20	3.1	1.6	1.8
	Rx [μrad]	32	730	360	15
	Ry [μrad]	54	88	300	16
	Rz [μrad]	15	300	400	8.7

12.4 Conclusions and recommendations

Our measurements show that kinematic mounts, and especially symmetric kinematic mounts, are promising for sub-micron and micron level positioning error of three-body systems. Our main recommendation is to automate the measurement setup thereby increasing the number of measurements per configuration and collecting more statistical data regarding the performance of the configurations.

Chapter 13   Applications

13.1 Problem statement

Present prototypes of kinematic mount applications.

13.2 Context of the applications

The thesis was done at the Centre Suisse d'Electronique et de Microtechnique (CSEM), Neuchâtel Switzerland, where work was carried out within a research program on the assembly of Silicon components and their integration into micromechanical systems. The research project addresses precision engineering and mechatronics at the centimeter scale using Silicon and motivated the applications discussed in this chapter.

| a | b | c |
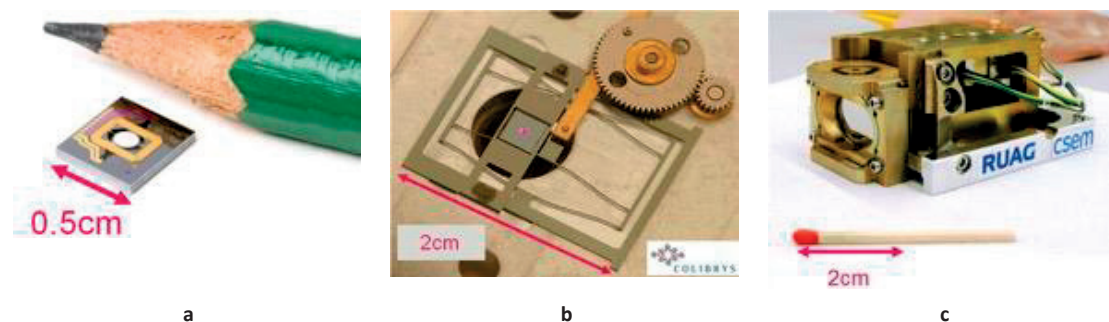
Figure 13.2.1: a) A typical two axes MEMS mirror device, actuated using a voice coil, image courtesy of MicroVision, Inc. b) An example of Silicon technology applied to a linear guide obscuring a sensor, courtesy of CSEM and Colibrys. c) An example of classical precision engineering used for another beam steering device, courtesy of CSEM and RUAG space.

Advantages of Silicon include its high mechanical stability, having no hysteresis, extremely high precision tolerances, the possibility for batch manufacturing, flexibility in 2.5D design, and the possibilities of actuator and sensor integration. Silicon components have notably been used in the watch industry (Figure 13.2.2).
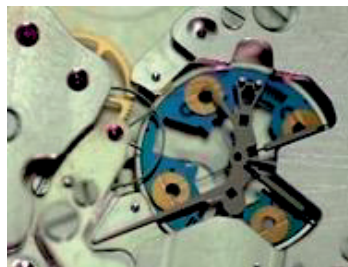
Figure 13.2.2: The Genequand regulator, developed by CSEM and Vaucher Manufacture Fleurier, uses Silicon components to obtain a mechanical watch with significantly increased autonomy.

Silicon is a brittle material (its ultimate strength is its yield strength), so care must be taken to avoid damaging parts and rendering them unusable. In order to address this, CSEM has conducted tests with Silicon flexures having different geometries and surface treatments, see Figure 13.2.3a.

| a | b | c |
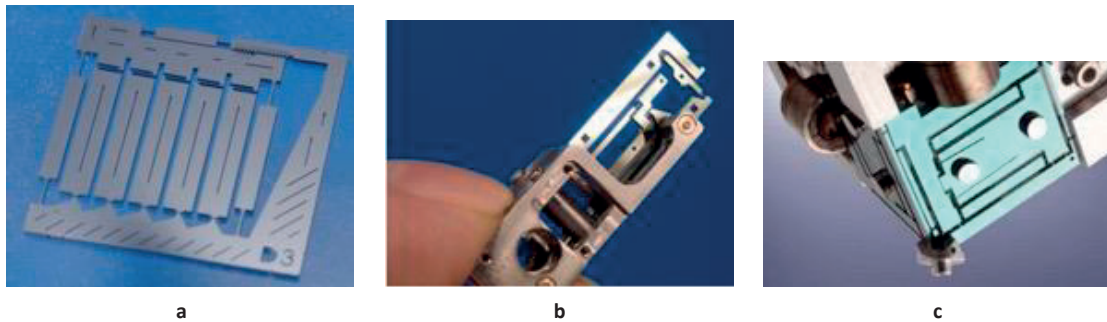
Figure 13.2.3: a) A test sample of CSEM used to test flexures with different geometry, size and surface treatments [66]. b) A Silicon microbalance, of which the entire mechanism is made in Silicon using flexures [67]. c) A sugar-cube size delta robot manufactured by CSEM [66].

Another challenge of using Silicon is the integration and precision assembly of Silicon parts into mechatronic structures, see Figure 13.2.3b and Figure 13.2.3c. In some cases this also means addressing the limits of Silicon assembly, as Silicon components are made with photolithography and Deep Reactive-Ion Etching (DRIE) resulting typically of only stacking 2-D layers. More complex assemblies such as Figure 13.2.3c are not typically done.

Kinematic design is a factor in reliable, precise and repeatable Silicon assembly. This is how the kinematic mounts of this thesis apply to repeatable deterministic assembly without adding significant process complexity.

13.3 Sugar cube delta robot

13.3.1 Context

The applications of this thesis started with the manufacture of the first Silicon sugar-cube sized delta robot, see Figure 13.2.3c.

13.3.2 Actuation and sensing of the demonstrator

Two different versions were realised: one with ultra-sonic piezo actuators and one without. The newer prototype did not contain a sensor, but a previous version had used CSEM's ICYcam a 6 DOF position sensor. The novel sugar-cube size delta robot permits integration of this sensor as well as several other optical principles, as desired.

13.3.3 Mechanism assembly

13.3.3.1   Prior art
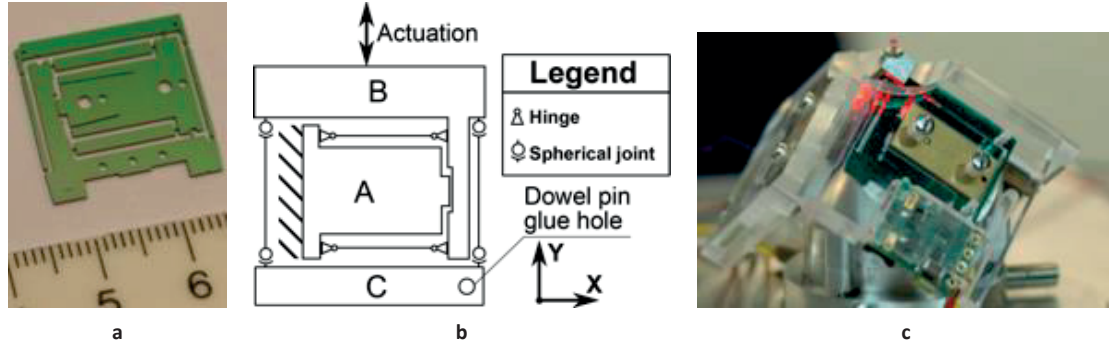
Figure 13.3.1: a) one of the parts used in the assembly of the old sugar-cube size delta robot. b) The kinematics of a single slab. Body A is fixed. Body B is connected by a parallelogram bar mechanism to body A and can translate along the Y axis, this translation is blocked by the actuator in our case an ultra-sonic piezo actuator from PI. Body C is blocked in the rotation around Z and the translation along Y. By coupling three slabs together orthogonally we can get a delta robot kinematics. c) Illustrates a sugar-cube size delta robot using ultrasonic piezo actuators.

Assembly of the components proved challenging as the parts were only aligned using loose fitting dowel pins and glue at the delta robot's head. Moreover, removing the Silicon parts from the wafer was difficult due to rigid attachments which resulted in forces too high to be safely applied to the components and the result was broken parts prior to actual assembly.

13.3.3.2   Wafer release

In order to prevent damage during fabrication, the parts are attached to the wafer to block all degrees of freedom. The challenge is to have these attachments compliant enough to allow for release of the part without damaging it. The attachments should, however also be rigid enough to block forces exerted on the part during production, so that the part remains attached to the wafer and does not detach in the etching baths.

13.3.3.3   Mechanism release

In order to prevent damage during assembly the parts are attached to each other blocking all degrees of freedom of the mechanisms inside them. The challenge is to have these attachments compliant enough to allow for release of the parts without damaging the mechanism due to excessive force during mechanism release. The attachments should, however also be rigid enough to block forces exerted on the part during production, so that the parts remain attached to each other and do not detach in the etching baths.

13.3.3.4 Kinematic mount

In order to allow a correct alignment and easier assembly, a kinematic mount was used to assemble the sugar-cube size delta robot.
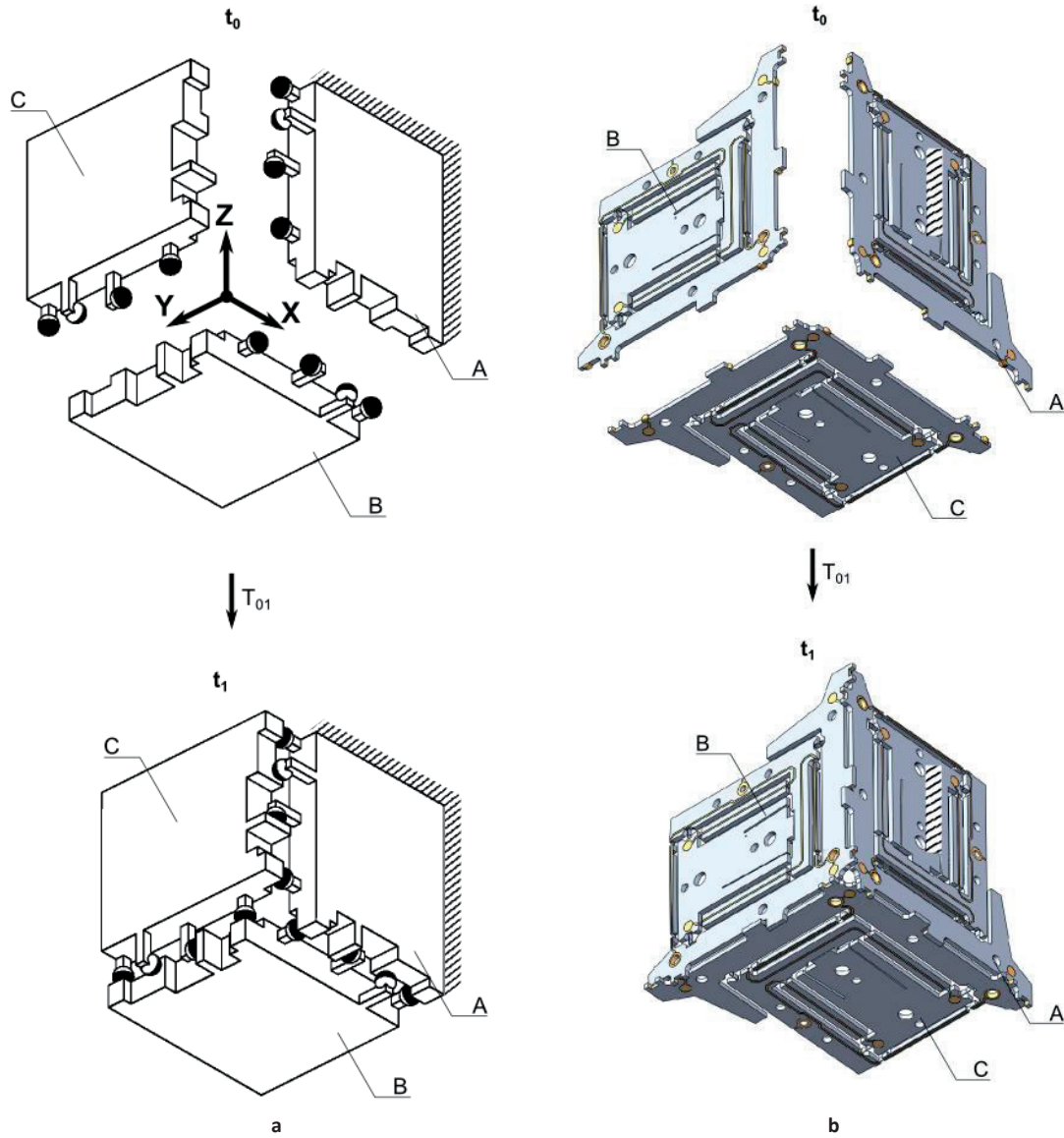
Figure 13.3.2: a) A test sample of CSEM used to test flexures with different geometry, size and surface treatments [66]. b) A Silicon micro-balance, of which the entire mechanism is made in Silicon using flexures [67]. c) A sugar-cube size delta robot manufactured by CSEM [66].
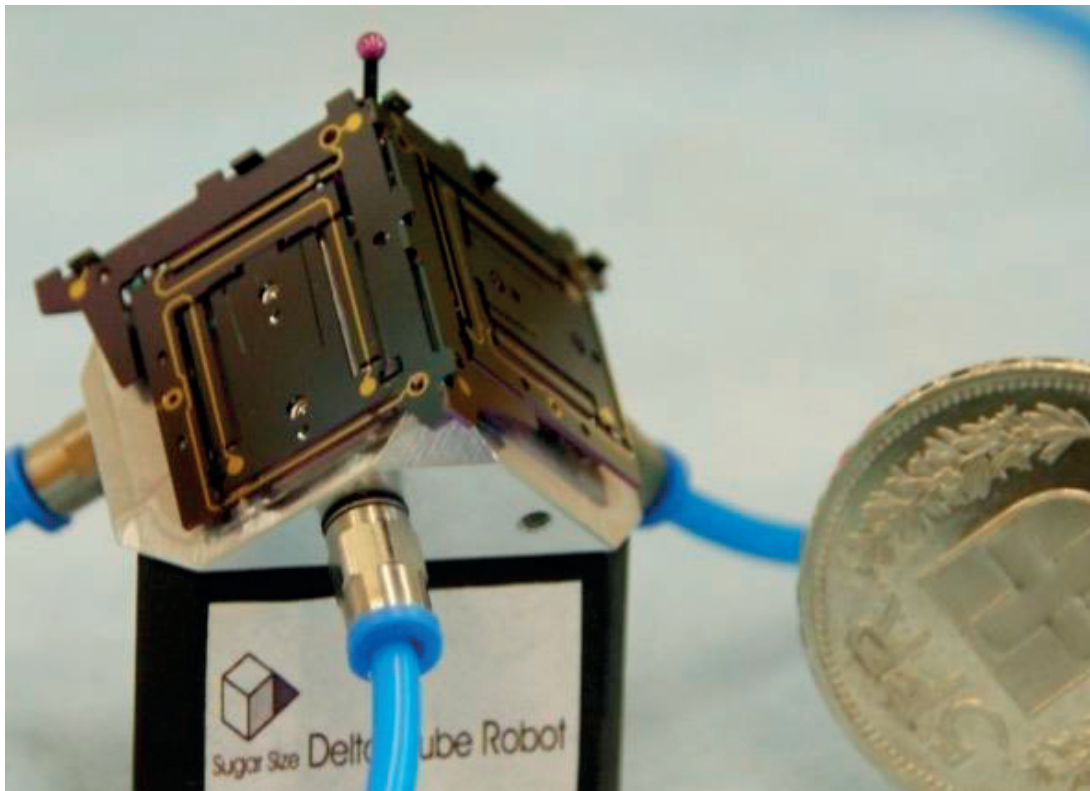
Figure 13.3.3: A sugar-cube size delta robot manufactured by CSEM and assembled and designed as part of this thesis [66] using a kinematic mount for easy assembly.

13.3.3.5   *Nesting force/assembly method*

In order to assemble the sugar-cube sized delta robot, a temporary nesting force was applied by a combination of gravity and a vacuum applied with a pneumatic jig and base.
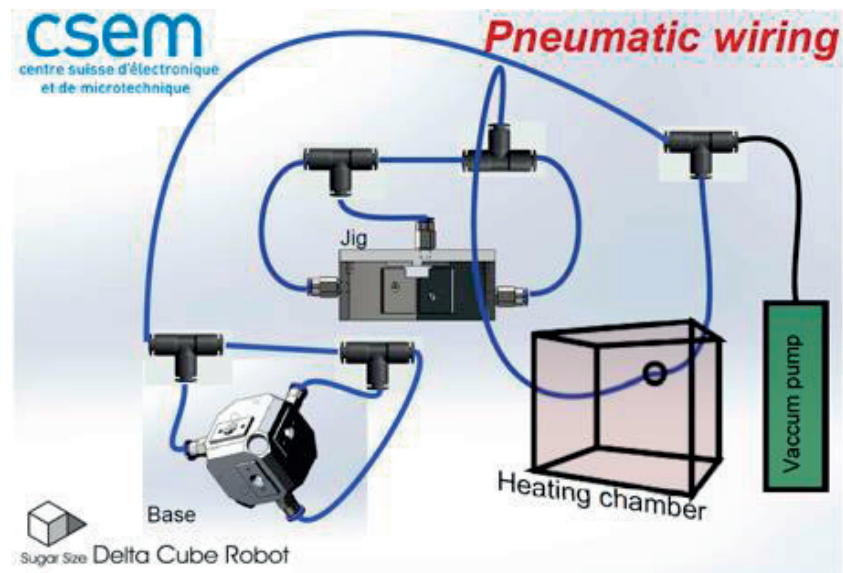
Figure 13.3.4:The assembly jig and base used for the preload and attachment of the sugar cube delta robot. Allowing for epoxy gluing, Uv gluing and soldering, of the sugar cube delta robot.

13.3.3.6   Demonstrator specifications

The final assembly allowed for ±0.6 mm translation along a set of Cartesian axes along the connected edges of the slabs. The total size of the robot is 27x27x27 mm.

13.4 Tip tilt piston mirror

The methodology of Silicon assembly was further implemented on a tip tilt piston mirror mechanism (TTPmm). The manufacturing and the kinematic decomposition and assembly are further described in this section.

13.4.1 Kinematics

As for the sugar-cube delta-robot, the kinematic structure of a tip tilt piston mirror mechanism was divided into a set of slabs, in this case 4. The mechanism resides in 3 identical monolithic Silicon slabs hereafter referred to as "the flexure slabs". These mechanism slabs are coupled to the fourth brick, a Silicon part with a gold deposited mirror. The flexure slabs have multiple functionalities: decoupling the actuators while allowing for less demanding tolerances between flexure slab, frame and actuator; providing a translation of the integrated mirror frame.

The kinematic structure of a single flexure slab is displayed in Figure 13.4.1.Each flexure slab contains a mirror frame; constraining the mirror in axial with respect to a linear guide and a tangential blocking the rotation along the mirrors normal axis and in plane translations of the mirror. The linear guide is interconnected with an actuator decoupling allowing for over constraints, resulting from either an imperfect actuator, geometry or assembly, to have no significant effect on the functionality.
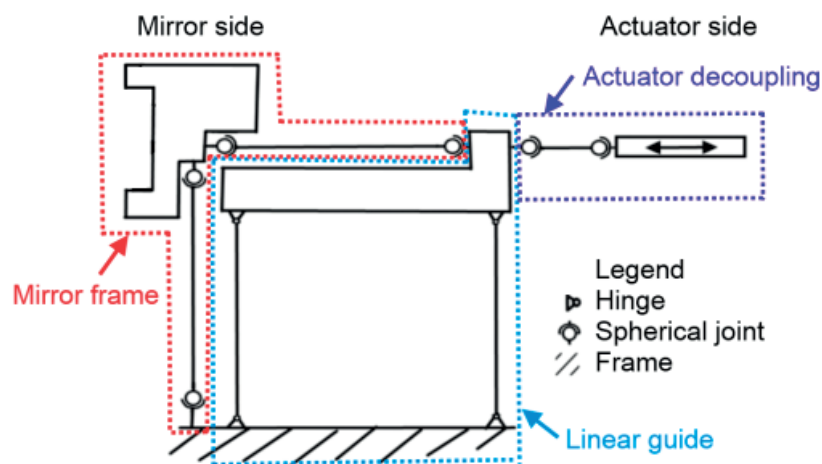
Figure 13.4.1: kinematics of a flexure slab.

The implemented design of the TTPmm is capable of +/- 4 degree (Tip and Tilt) rotations in the mirror plane; the (Piston) translation range out of the mirror plane is +/- 0.6 mm.

13.4.2 Assembly

For the assembly, each of the three flexure slabs constrains the mirror in 2 DOFs: 1 axial and 1 tangential. Our alignment method achieves isostatic positioning of the mirror. The flexure slabs are fixated to a metal frame. The assembly is illustrated in Figure 13.4.2
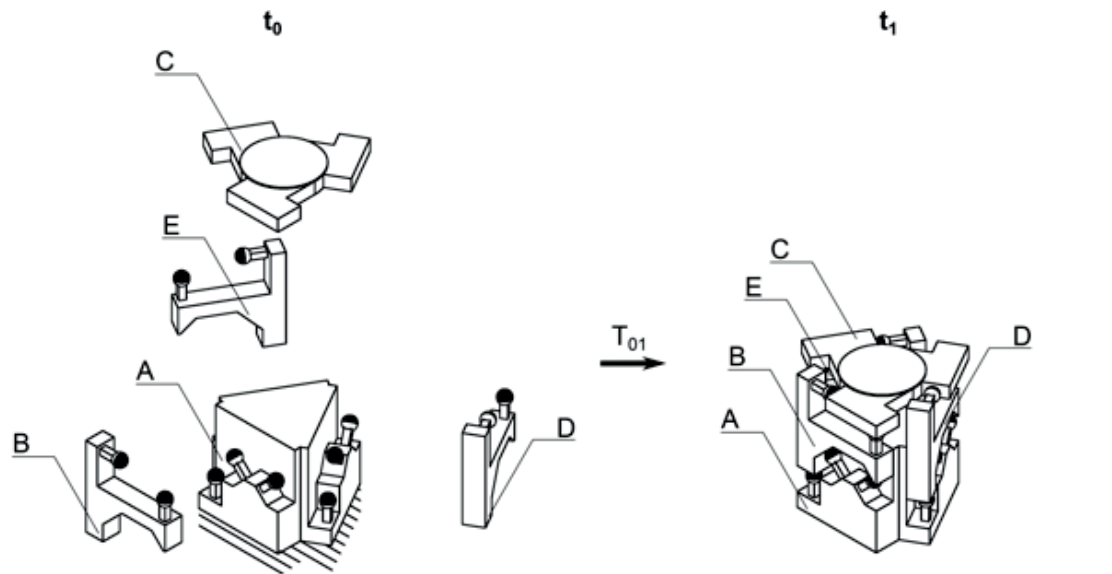
Figure 13.4.2: Assembly of the tip tilt mirror. Bodies B, D and E are the flexure steps which are aligned with respect to dowel pins that are part of body A. Lastly the mirror itself, body C, is mounted on the flexure slabs.

The entire assembly fits in a 40x40x42 mm³ rectangular volume and is shown in Figure 13.4.2. The actuators are in turn coupled to the Silicon rods to provide the actuation. The flexure slabs are fixated with either gluing or soldering. To allow for soldering the flexure slabs and the mirror have a gold coating on their interfaces.
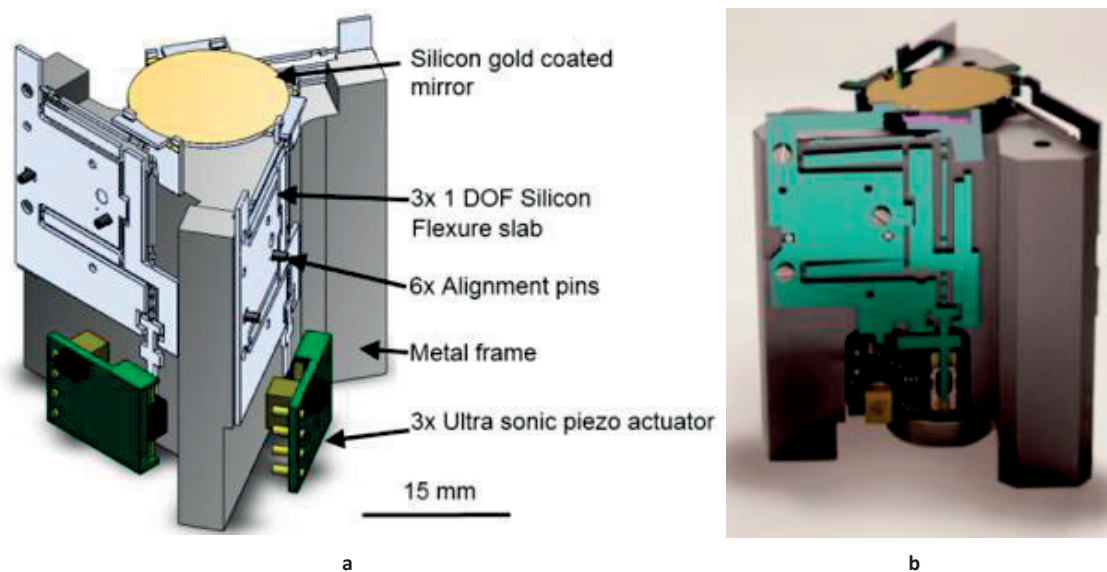
Figure 13.4.3: a) The layout of the tip Tilt Piston Mirror Mechanism. b) The realised version of the Tip Tilt Piston Mirror Mechanism.

13.4.3 Actuation and sensing

The TTPmm allows for various actuation and sensing possibilities, in this case the actuation was realized using the same ultrasonic piezo actuators as implemented in the sugar cube delta robot. Sensing functions are not directly implemented in the current design. A first approach is to use an optical measurement system based on the mirror itself to characterize its displacements. Finite element analysis showed that the lowest eigenfrequency was a 580 Hz out of plane mode of the linear guide of the flexure slabs.

13.4.4 Novel version

Following a first version of the the tip tilt piston mirror, a novel version was made incorporating piezo strain gauges which allows direct sensing of the mirror position. In this version, the integrated clips used for nesting force are clearly visible at the top of the mirror.
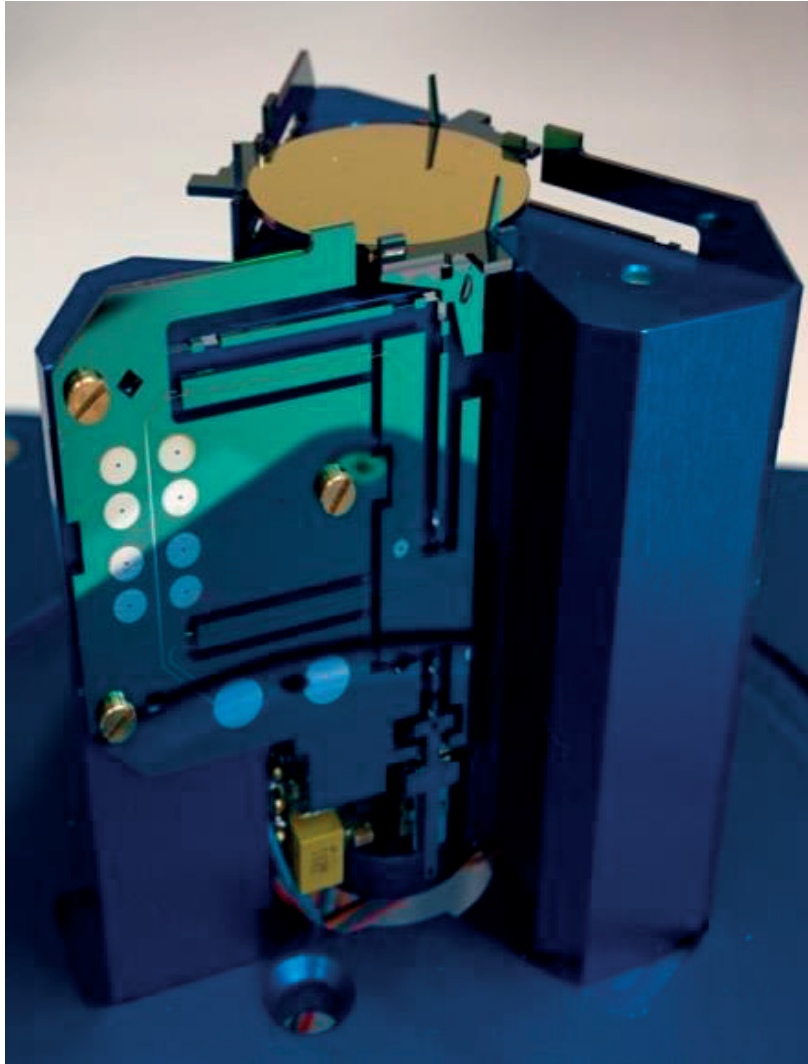
Figure 13.4.4: Tip Tilt Piston Mirror Mechanism incorporating strain gauges and integrated clips for mounting the mirror.

13.5 Capsense

A third demonstrator was made to show that kinematic mounts can be used for more complex assembly. The demonstrator consists of eight bodies, of which four Silicon slabs having a parasitic linear guide, consisting of four flexures and differential capacitive sensors. The remaining four bodies are present for the assembly phase.
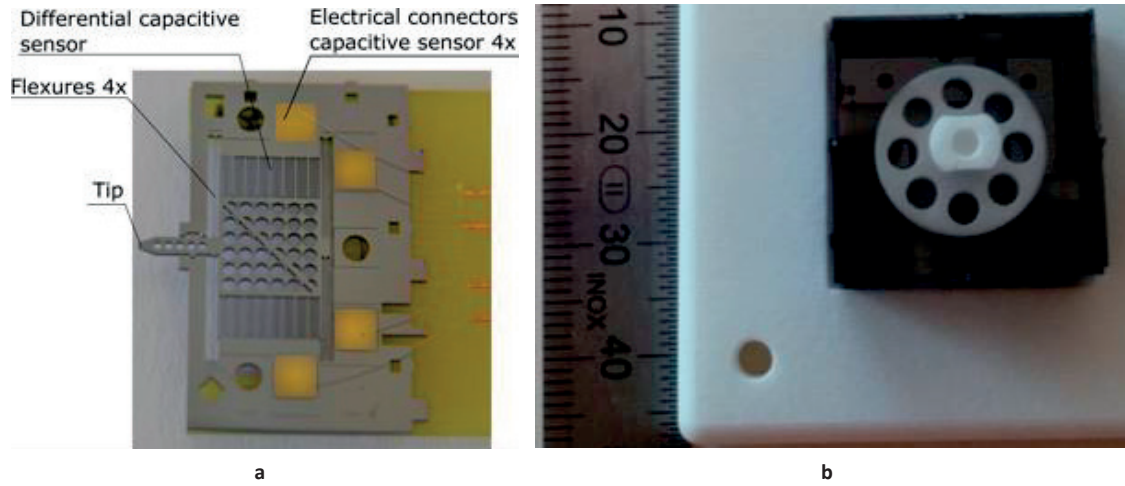
Figure 13.5.1: a) A single Capsense part. b) The assembled Capsense parts.
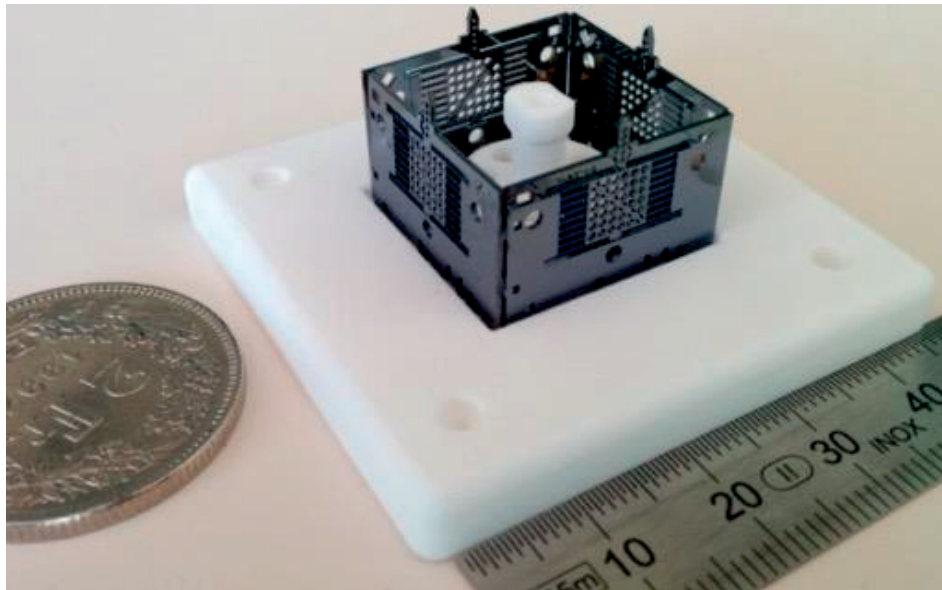
Figure 13.5.2: The assembled Capsense bodies.

An example of how to carry out such a complex assembly with the kinematic contacts can be seen in Figure 13.5.3.
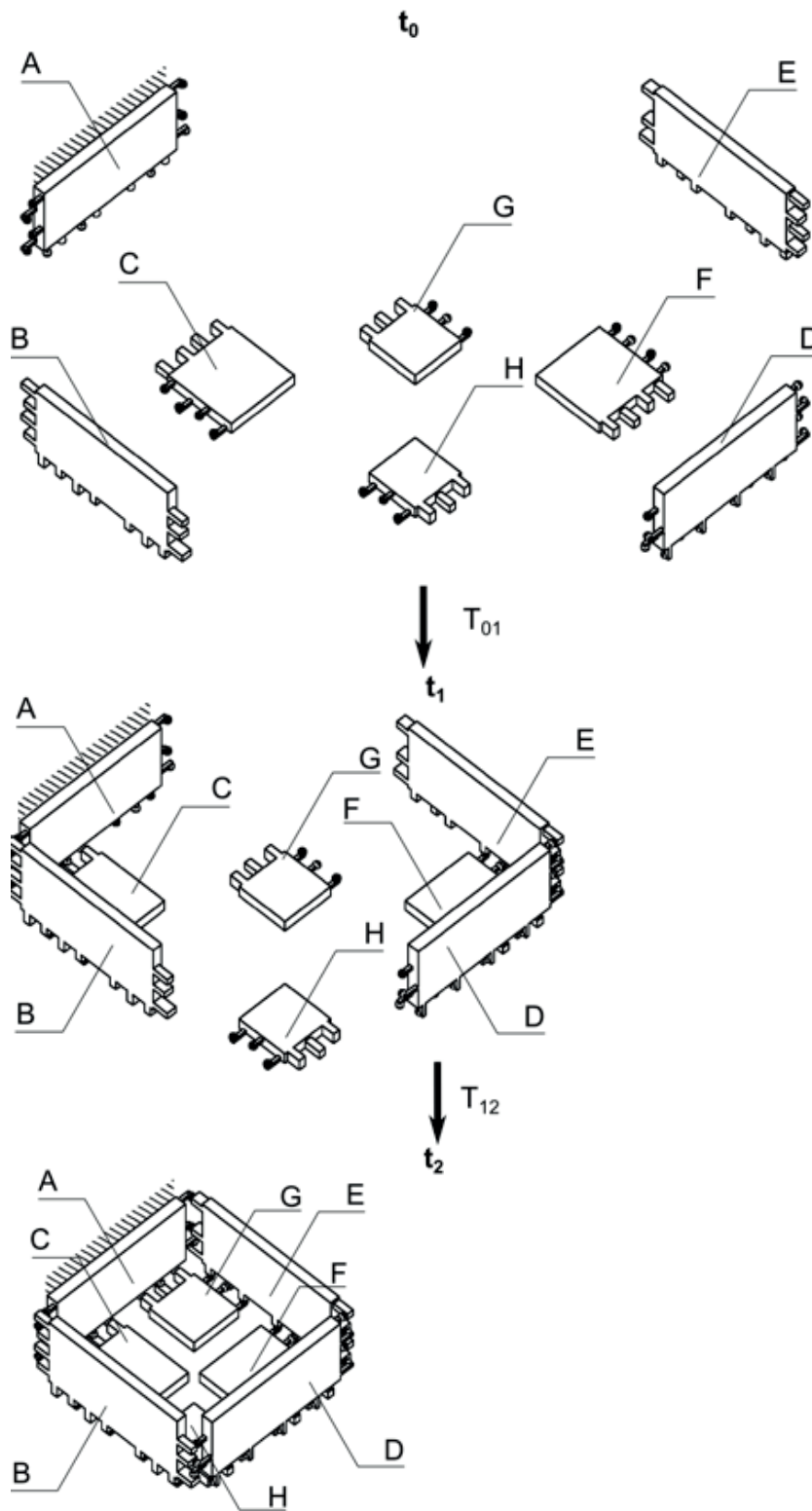
Figure 13.5.3: The assembly of the Capsense brick consists of A, B and C which form a three-body kinematic mount and D,E and F which form another three-body kinematic mount. When the three body-kinematic mounts (ABC and DEF) are assembled they form a two-body kinematic mount with respect to each other. Lastly parts G and H form two separate kinematic mounts with ABCDEF.

13.6 LIDAR module for a satellite removing space debris.

A further application was a LIDAR part for a satellite aimed at identifying and removing space debris. LIDAR is a technology that measures distance by using laser light to illuminate an object of interest. There are three different modules to be assembled orthogonally due to limited space within the satellite: the first is an electronics module, the second an optics module and the third a laser module. Kinematic mounts are desirable here in order to have a deterministic assembly preventing blocking or jamming during assembly.

| a | b | c |
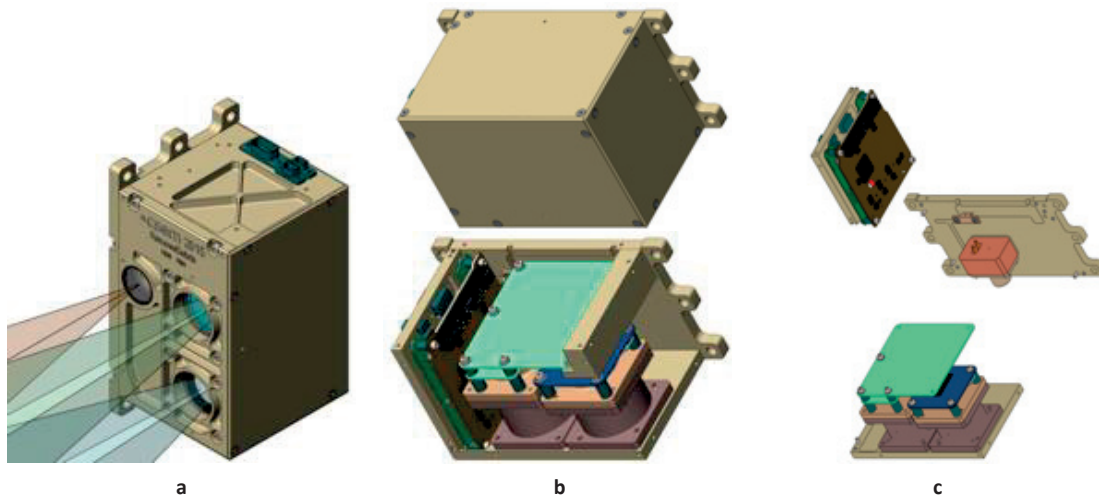
Figure 13.6.1: a) The LIDAR module, b) The LIDAR module back view with the plates and with the plates removed exposing the modules. C) The disassembled modules.

The kinematic mount used is illustrated in Figure 13.6.3. In order to have a relatively easy assembly, we chose to compromise determinism and realise the kinematic mount concept using contact lines and surfaces instead of contact points. For each interface two contact points were realized using dowel pins and slightly larger slotted holes. The remaining two contact points were realized by means of two long but narrow flat on flat surfaces. The nesting force and attachment was realized using two bolts per interface. Half of an interface is illustrated in (Figure 13.6.2).
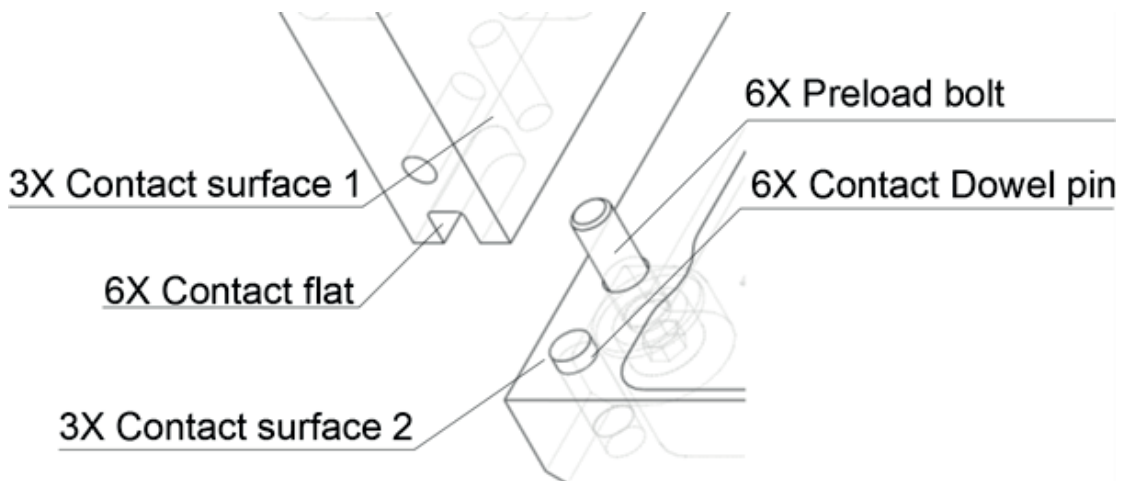
Figure 13.6.2: A contact point realised with a dowel pin and and a contact flat. In addition the two contact surfaces are also put into contact. In total there is 6 preload bolt
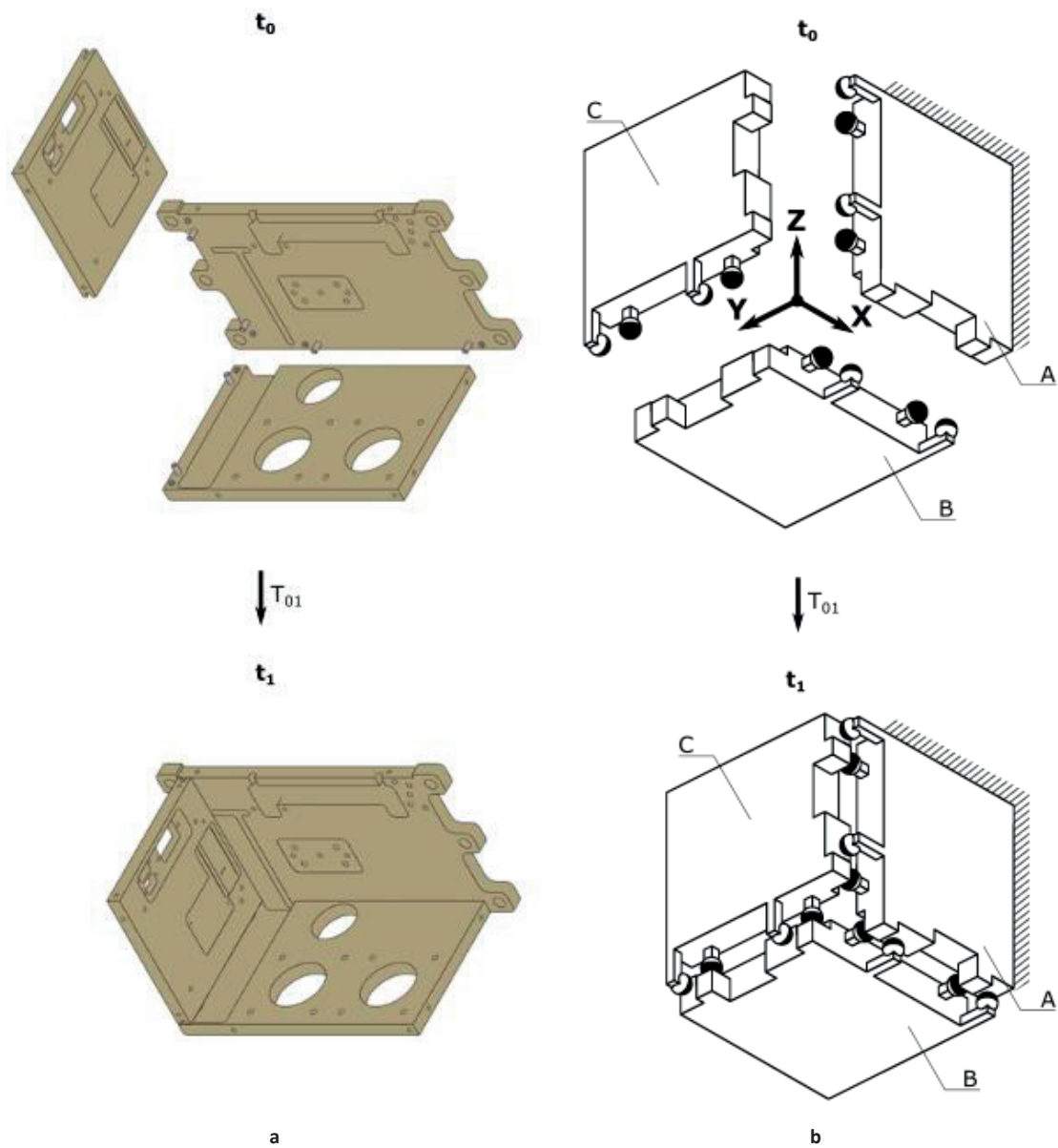
Figure 13.6.3: a) The slabs of the satellite prior and after assembly. b) The kinematic mount concept at the basis of the basis of the applied concept.

13.7 Chapter summary

This chapter introduced four separate applications of kinematic mounts. For the sugar cube delta robot, the author was responsible for the alignment method, conductive tracks and assembly. The tip tilt piston mirror was designed and assembled by the author. The Capsense was also fully designed and assembled by the author. The LIDAR module was designed by an engineer from CSEM based on the kinematic mount example 7.4.2.7 presented in this thesis. The Silicon part fabrication of the sugar cube delta robot, tip tilt piston mirror and Capsense was done at the CSEM foundry.

Chapter 14 Conclusion

14.1 Overview

Kinematic design has been used for 250 years with most of recent research dealing with the development of tools for analysis of kinematic assemblies and detailing the possibilities of two-body interfaces. No significant work has been made to generalize kinematic couplings to more than two bodies. This thesis develops the theory and application of three-body kinematic mounts, the three-body generalization of kinematic couplings, by providing design rules and a catalogue that will allow scientists and engineers to investigate and apply kinematic mounts.

The first part of the thesis deals with theory. It starts with establishing rigorous definitions to establish a rigorous foundation for kinematic mounts. With these definitions in place, examples of 2-dimensional and 3-dimensional mounts of two and three bodies are given. Conditions satisfied by these configurations are then presented. The theoretical part finishes by presenting sets of non-equivalent configurations which we conjecture give a complete classification of two and three-body kinematic mounts, up to rotation and relabeling.

The second part consists of applications. This part starts by describing a set of 3D-printed demonstrators providing hands-on verification of the three-body 3-dimensional kinematic mounts presented in the theoretical part. This is followed by examples of nesting force implementation and assembly methods for kinematic mounts. In the subsequent chapter, experiments are performed to determine the positioning error of the three-body 3-dimensional kinematic mounts presented in the theoretical part of the thesis. These experiments, applied to both micro-machined Silicon parts and classically machined parts, show that a micron level positioning error is achieved. The thesis thus validates the performance of three-body kinematic mounts. Finally, several applications of kinematic mounts are given in robotic, optical, measurement and satellite systems. Although the main focus of the applications is on Silicon micro-assembly, indications are given on a wider range of applications of kinematic mounts

14.2 Contributions

The original contributions of this thesis are:

Theoretical contributions:

- State of the art review of essential knowledge in the field of kinematic couplings.

- Rigorous problem statement for the design of two-body and three-body kinematic mounts.

- Rigorous limitation of the scope of research to three-body kinematic mounts whose contact points lie exclusively on three convergent orthogonal lines and whose constraint lines are parallel to these lines.

- An exhaustive catalogue of three-body kinematic mounts consisting of seven non-equivalent configurations in 3D and nine non-equivalent configurations in 2D.

- Pictogram and an array representations of the nine configurations of three-body kinematic mounts.

- An exhaustive set of four conditions satisfied by three-body 3-dimensional kinematic mounts.

- An exhaustive set of seven conditions satisfied by three-body 2-dimensional kinematic mounts.

Practical contributions:

- Realization of a two-body kinematic mount and a three-body kinematic mount in metal, and precise measurement of their positioning error on a 3D coordinate measurement machine at the Swiss Federal Institute of Metrology. Positioning error of 0.2 microns and 5 μradian achieved with two-body kinematic mounts. Positioning error of 1 micron and 50 μradian achieved with three-body kinematic mounts.

- Realization of three-body kinematic mounts in Silicon by Deep Reactive Ion Etching processes and experimental measurement of their positioning error.

- Realization of 3D printed demonstrators giving an intuitive validation of non-trivial theoretical conditions.

- Physical implementation of nesting forces and assembly methods allowing for the physical construction of kinematic mounts.

- Physical realizations in robotics, optics and aerospace using new innovative kinematic mounts.

- Experimental observation that the symmetric configuration of three-body kinematic mounts made in Silicon perform significantly better than the non-symmetric configurations.

- Experimental observation that nesting forces applied with magnets are most effective and practical for use.

14.3 Limitations and perspectives

No formal proof for the exhaustivity of the conditions nor the exhaustivity of the catalogue of three-body kinematic mounts is given in this thesis. This work could be expanded by establishing a rigorous proof of the conditions for kinematic mounts, especially Conjecture 8.5.1.

Experimental validation was limited by time and budget: no statistical measurement of positioning error could be made on classically machined two-body and three-body kinematic mounts. More precise experiments on all kinematic mount configurations and their positioning repeatability performance would be interesting. These experiments will allow to determine which configuration would be more suitable for positioning repeatability. This is already an issue for two-body kinematic mounts. In that field, there is a definite preference for using the Three-Vee coupling, but there is no significant experimental data published validating this. A detailed comparative research between a Three-Vee coupling and a Tetrahedron-Vee-Flat coupling would be interesting.

In this thesis, the contact points of three-body kinematic mounts all lie on three orthogonal convergent lines. The study could be widened to contact points located anywhere in space. In order to accomplish this extension, the work of Hopkins on Freedom and Constraint Topologies provides an interesting starting point. This work offers an exhaustive catalogue of possible topologies for the interfaces between two bodies. This could therefore be a first step to a general exhaustive analysis of all possible kinematic mounts consisting of three bodies.

The theory could be further advanced by not just considering contact points, but also contact lines, resulting in quasi-kinematic mounts.

The analysis of the generated configurations was done using screw theory. This was left out of the thesis as it was not the main novelty of this work. It also appears that invariant theory could be applied to provide rigorous proofs of our conjectures.

The next step, after fully describing all mounts for three bodies, is to continue work for more than three bodies.

For applications requiring kinematic mounts suitable for heavy loads, it is interesting to further explore stiffness issues for kinematic mounts, as they limit their applicability.

Though a first experimental validation was done, it would be advantageous to develop an automated experimental setup to characterize the wear effects as well as the positioning repeatability over larger number of alignment cycles. With such an automated setup it would be also interesting to investigate the fatigue limits of kinematic mounts due to wear.

Another topic for research would be kinematic mount interchangeability. This has been investigated for kinematic couplings and generalizing this work to kinematic mounts could be interesting for applications in which numerous components are interchanged.

Another interesting consideration is surface interfaces and their influence on the performance of mounts. This includes factors such as roughness, friction coefficient and lubrication. Though the general consensus is that it is best to have a lubricated smooth surface with a low friction coefficient, a better determination of their effects will help designers.

If kinematic mounts interfaces are further studied, this could lead to normalized standards for kinematic mounts interfaces for applications which would allow for easily interfacing of assembly line components.

14.4 Final remarks

Kinematic design has become common practice in many areas of precision engineering. Though kinematic couplings are applied in many domains it is remarkable that kinematic mounts with three bodies touching each other have not been studied in depth. It is the goal of this work to generalize kinematic couplings to three body kinematics mounts, and so empower designers and scientists with new concepts of alignment. As many assemblies consist of far more than three parts, this work is just scratching the surface of an unopened treasure trove in kinematic design. We hope that this work encourages the use of kinematic design in applications where it can help attain the required positioning errors.

Appendix A: Mechanical drawings related to the first experiment

This appendix contains the drawings of the prototypes realized in the first experiment for reference.

Appendix A.1: Drawings of the two-body kinematic mount for the first experiment.

COUPE D-D

D

1		Version initiale		11.02.2016	SDr		
Rév.	Zone	Description / Modification		Date	Dessiné	Contrôlé	Approuvé

Traitement :

Matière : POM noir

Ces plans sont la propriété du CSEM. Ils ne doivent pas ,sans notre autorisation écrite être copiés, reproduits ou communiqués à des tiers.

Acronyme projet / Produit

Cotes en mm

csem centre suisse d'électronique et de microtechnique

Dénomination

outil levage

Poids (g) :

Format	Echelle
A4	2:1

Tol. gén. selon ISO 8015
Longueur/angle : ISO 2768-1-f
Forme/position : ISO 2768-2-K

Casser les angles :
0.1 ... 0.3 mm
Rugosité gén. :

N° dessin

Johan_101DE-01

Rév. 1

Feuille 1 de 1

COUPE D-D

3 pièces

Rév.	Zone	Description / Modification		Date	Dessiné	Contrôlé	Approuvé
1		Version initiale		11.02.2016	SDr		

Traitement :

Ces plans sont la propriété du CSEM. Ils ne doivent pas, sans notre autorisation écrite être copiés, reproduits ou communiqués à des tiers.

Matière : Laiton

Acronyme projet / Produit

Cotes en mm

Dénomination

entretoise palpeur

Poids (g) :

csem centre suisse d'électronique et de microtechnique

Format	Echelle
A4	2:1

Tol. gén. selon ISO 8015
Longueur/angle : ISO 2768-1-f
Forme/position : ISO 2768-2-k

Casser les angles :
0.1 ... 0.3 mm
Rugosité gén. :

N° dessin

Johan_103DE-01

Rév.	Feuille
1	1 de 1

1		Version initiale			10.03.2016	SDr		
Rév.	Zone	Description / Modification			Date	Dessiné	Contrôlé	Approuvé

Traitement :

Matière : Alu 6082

Ces plans sont la propriété du CSEM. Ils ne doivent pas ,sans notre autorisation écrite être copiés, reproduits ou communiqués à des tiers.

Acronyme projet / Produit

Cotes en mm

csem centre suisse d'électronique et de microtechnique

Dénomination

Levier

Poids (g) :

Format	Echelle
A4	1:1

Tol. gén. selon ISO 8015
Longueur/angle : ISO 2768-1-f
Forme/position : ISO 2768-2-K

Casser les angles :
0.1 ... 0.3 mm
Rugosité gén. : N7

N° dessin **Johan_115DE-01**

Rév.	Feuille
1	1 de 1

Appendix A.2: Drawings of the three-body kinematic mount of the first experiment.

DETAIL L
SCALE 10 : 1

SECTION S-S
SCALE 1 : 1

VIEW D
SCALE 1 : 1

SECTION P-P
SCALE 1 : 1

DETAIL E
SCALE 2 : 1

Tout les congés sont fait avec
une fraise de 4 sauf si indiqué.

Nr. de pièce: 2		Date: 04.03.2016		Dessiné: JKs

Traitement :	Matière : Aluminium			
Ces plans sont la propriété du CSEM. Ils ne doivent pas, sans notre autorisation écrite être copiés, reproduits ou communiqués à des tiers.	Acronyme projet / Produit			Cotes en mm
	Dénomination		Polds (g) :	
csem centre suisse d'électronique et de microtechnique	Pièce mobile trois corps		Format A3	Echelle
Tol. gén. selon ISO 8015 Cote, forme : ISO 2768-fH Cote < 0.5mm : ±0.03mm	Rugosité gén. :	Casser les angles : d>5mm : 0.1..0.3 mm d<5mm : 0.02..0.05mm	N° dessin **Johan_105DE-01**	Rév. **1**	Feuille de

16

5 X 45°

7 X 45°

12

5.50 X 45°

1

5

H

SECTION H-H

4

∅3

7

18

H

2 X ∅2 H7 +0.01 0

6

M3x0.5

I

I

6

4

8

3

2.50

6

7.50

8.25

4

SECTION I-I

Nr. de pièce: 3   Date: 07.03.2016   Dessiné: JKs

Traitement :

Matière : Aluminium

Ces plans sont la propriété du CSEM. Ils ne doivent pas, sans notre autorisation écrite être copiés, reproduits ou communiqués à des tiers.

Acronyme projet / Produit

Cotes en mm

csem centre suisse d'électronique et de microtechnique

Dénomination

Poids (g) :

Bloque de precharge

Format A3   Echelle

Tol. gén. selon ISO 8015 Cote, forme : ISO 2768-fH Cote < 0.5mm : ±0.03mm

Rugosité gén. :

Casser les angles : d>5mm : 0.1..0.3 mm d<5mm : 0.02..0.05mm

N° dessin

Johan_106DE-01

RÉV. 1   Feuille de

Nr. de pièce: 6   Date: 07.03.2016   Dessiné: JKs

Traitement :

Ces plans sont la propriété du CSEM. Ils ne doivent pas, sans notre autorisation écrite être copiés, reproduits ou communiqués à des tiers.

csem centre suisse d'électronique et de microtechnique

Matière : Acier

Acronyme projet / Produit

Dénomination

Goupille de precharge

Cotes en mm

Poids (g) :

Format   Echelle

Tol. gén. selon ISO 8015
Cote, forme : ISO 2768-fH
Cote < 0.5mm : ±0.03mm

Rugosité gén. :

Casser les angles :
d>5mm : 0.1..0.3 mm
d<5mm : 0.02..0.05mm

N° dessin   **Johan_107DE-01**

Rév.   **1**

Feuille de

165

SECTION D-D

SECTION G-G

54.74° ±5°

Nr. de pièce: 1   Date: 10.03.2016   Dessiné: JKs

Traitement :		Matière : Aluminium		
Ces plans sont la propriété du CSEM. Ils ne doivent pas, sans notre autorisation écrite être copiés, reproduits ou communiqués à des tiers.		Acronyme projet / Produit		Cotes en mm
csem centre suisse d'électronique et de microtechnique		Dénomination	Poids (g) :	
		Base de fixation incliné	Format A3	Echelle
Tol. gén. selon ISO 8015 Coté, forme : ISO 2768-fH Cote < 0.5mm : ±0.03mm	Rugosité gén. : Casser les angles : d>5mm : 0.1..0.3 mm d<5mm : 0.02..0.05mm	N° dessin **Johan_108DE01**	Rév. **1**	Feuille de

Bibliography

[1] H. Soemers, *Design Principles: For Precision Mechanisms*. T-Pointprint, 2011.

[2] J. C. Maxwell, *The Scientific Papers of James Clerk Maxwell: Volume 2*, Reissue edition. Cambridge University Press, 2011.

[3] A. H. Slocum, *Precision Machine Design*. Society of Manufacturing Engineers, 1992.

[4] T. N. Whitehead, *The design and use of instruments and accurate mechanisms; underlying principles,*. New York, 1934.

[5] R. V. Jones, *Instruments and Experiences: Papers on Measurement and Instrument Design*, 1 edition. Chichester West Sussex ; New York: Wiley, 1988.

[6] S. T. Smith and D. G. Chetwynd, *Foundations of Ultra-Precision Mechanism Design*, Reprint edition. CRC Press, 1994.

[7] J. Philips, *Freedom in Machinery*. Cambridge: Cambridge University Press, 2007.

[8] M. Bassière and E. Gaignebet, *Métrologie générale, théorie de la mesure, les instruments et leur emploi*. Dunod, 1966.

[9] J. E. Furse, "Kinematic design of fine mechanisms in instruments," *J. Phys. [E]*, vol. 14, no. 3, p. 264, 1981.

[10] D. L. Blanding, *Exact Constraint: Machine Design Using Kinematic Processing*. New York: ASME Press, 1999.

[11] F. (Franz) Reuleaux and A. B. W. (Alexander B. W. Kennedy, *Kinematics of machinery, outlines of a theory of machines;* London, Macmillan, 1876.

[12] W. T. B. Kelvin and P. G. Tait, *Treatise on Natural Philosophy*, 2nd edition. Cambridge; 2009: Cambridge University Press, 2009.

[13] L. C. Hale, "Principles and techniques for designing precision machines," 1999.

[14] C. Evans, *Precision engineering: an evolutionary view*. Cranfield Press, 1989.

[15] A. H. Slocum and A. Donmez, "Kinematic couplings for precision fixturing — Part 2: Experimental determination of repeatability and stiffness," *Precis. Eng.*, vol. 10, no. 3, pp. 115–122, Jul. 1988.

[16] J. Ziegert and V. Tymianski, "Air bearing kinematic couplings," *Precis. Eng.*, vol. 31, no. 2, pp. 73–82, Apr. 2007.

[17] K. C. Godtfred, "Toy building brick," US3005282 A, 24-Oct-1961.

[18] M. L. Culpepper, "Design of quasi-kinematic couplings," *Precis. Eng.*, vol. 28, no. 3, pp. 338–357, Jul. 2004.

[19] R. S. Woodbury, *Studies in the History of Machine Tools*. Cambridge, Mass: The MIT Press, 1973.

[20] David Wilkinson, "Screw Threading Machine (metal lathe).", USX220 I1, 14 DEC 1798

[21] J. B. Hopkins and M. L. Culpepper, "Synthesis of precision serial flexure systems using freedom and constraint topologies (FACT)," *Precis. Eng.*, vol. 35, no. 4, pp. 638–649, Oct. 2011.

[22] R. S. (Robert S. Ball, *A treatise on the theory of screws*. Cambridge : University Press, 1900.

[23] D. E. Whitney, *Mechanical Assemblies: Their Design, Manufacture, and Role in Product Development*, 1 edition. New York: Oxford University Press, 2004.

[24] I. Sherrington and E. H. Smith, "Design and performance assessment of a Kelvin clamp for use in relocation analysis of surface topography," *Precis. Eng.*, vol. 15, no. 2, pp. 77–85, 1993.

[25] A. H. Slocum, "Design of three-groove kinematic couplings," *Precis. Eng.*, vol. 14, no. 2, pp. 67–76, Apr. 1992.

[26] A. H. Slocum, "Kinematic couplings for precision fixturing—Part I: Formulation of design parameters," *Precis. Eng.*, vol. 10, no. 2, pp. 85–91, Apr. 1988.

[27] P. Schmiechen and A. Slocum, "Analysis of kinematic systems: a generalized approach," *Precis. Eng.*, vol. 19, no. 1, pp. 11–18, 1996.

[28] C. H. Schouten, P. C. J. N. Rosielle, and P. H. J. Schellekens, "Design of a kinematic coupling for precision applications," *Precis. Eng.*, vol. 20, no. 1, pp. 46–52, Jan. 1997.

[29] R. R. Vallance, C. Morgan, and A. H. Slocum, "Precisely positioning pallets in multi-station assembly systems," *Precis. Eng.*, vol. 28, no. 2, pp. 218–231, Apr. 2004.

[30] M. Barraja and R. R. Vallance, "Tolerancing kinematic couplings," *Precis. Eng.*, vol. 29, no. 1, pp. 101–112, Jan. 2005.

[31] A. J. Hart, A. Slocum, and P. Willoughby, "Kinematic coupling interchangeability," *Precis. Eng.*, vol. 28, no. 1, pp. 1–15, Jan. 2004.

[32] M. L. Culpepper, M. V. Kartik, and C. DiBiasio, "Design of integrated eccentric mechanisms and exact constraint fixtures for micron-level repeatability and accuracy," *Precis. Eng.*, vol. 29, no. 1, pp. 65–80, Jan. 2005.

[33] G. Spinnler, *Conception des machines: principes et applications. Statique*. PPUR presses polytechniques, 1997.

[34] R. G. K. M. Aarts, J. P. Meijaard, and J. B. Jonker, "Flexible multibody modelling for exact constraint design of compliant mechanisms," *Multibody Syst. Dyn.*, vol. 27, no. 1, pp. 119–133, Nov. 2011.

[35] B. Gregerson, G. Gallagher, and B. Wiseman, "300 mm microenvironment pod with door on side," US 5944194 A, 31-Aug-1999.

[36] A. Slocum, "Kinematic couplings: A review of design principles and applications," *Int. J. Mach. Tools Manuf.*, vol. 50, no. 4, pp. 310–327, Apr. 2010.

[37] James E. Holliday, Gary M. Gallagher, "Enclosed sealable purgible semiconductor wafer holder," US5755332 A, 26-May-1998.

[38] William J. Fosnight, Anthony C. Bonora, Raymond S. Martin, Perry Peterson, "SMIF pod including independently supported wafer cassette," US6398032 B2, 04-Jun-2002.

[39] William J. Fosnight, Anthony C. Bonora, Raymond S. Martin, Jay Tatro, "Evacuation-driven SMIF pod purge system," US5988233 A, 23-Nov-1999.

[40] James Nigg, Ralph Henderer, "Modular carrier for semiconductor wafer disks and similar inventory," US6779667 B2, 24-Aug-2004.

[41] Alexander H. Slocum, Matthew J. Van Doren, Scott Ziegenhagen II Rodney, Don Sauer, "Modular system," US5733024 A, 31-Mar-1998.

[42] "Passively activated valve for carrier purging," US6056026 A, 02-May-2000.

[43] Barry Gregerson, Boyd Wittman, "Reinforced semiconductor wafer holder," US5476176 A, 19-Dec-1995.

[44] Kelly Peterson, Brian Wiseman, Gary Gallagher, Barry Gregerson, "Shipping and transport cassette with kinematic coupling," US6010009 A, 04-Jan-2000.

[45] Yutaka Endo, Nobuyoshi Tanno, "Substrate storage cassette positioning device and method," WO1999040623A1, 13-Aug-2002.

[46] Gregory W. Bores, Michael C. Zabka, "Wafer carrier having a low tolerance build-up," US6520338 B2, 18-Feb-2003.

[47] Rodney C. Ow, Karl Mathia, "Wafer carrier adapter and method for use thereof," US6165268 A, 26-Dec-2000.

[48] John Burns, Matthew A. Fuller, Jeffery J. King, Martin L. Forbes, Mark V. Smith, "Wafer container and door with vibration dampening latching mechanism," US7182203 B2, 27-Feb-2007.

[49] "Wafer support attachment for a semi-conductor wafer transport container," US6811029 B2, 02-Nov-2004.

[50] "Wafer container having electrically conductive kinematic coupling groove, support surface with electrically conductive kinematic coupling pin, transportation system, and method," US6389706 B1, 21-May-2002.

[51] Martin Peiter, Clinton Haris, "Wafer container having electrically conductive kinematic coupling groove to detect the presence of the wafer container on a support surface, the support surface, and method," US6389707 B1, 21-May-2002.

[52] A. J. Stein, D. L. Trumper, and R. J. Hocken, "A metrological atomic force microscope," presented at the ASPE pointinspace 2002, 2002.

[53] C. Werner, *A 3D translation stage for metrological AFM*. Eindhoven: Technische Universiteit Eindhoven, 2010.

[54] A. J. Hart, A. Slocum, and J. Sutin, "Segmented and shielded structures for reduction of thermal expansion-induced tilt errors," *Precis. Eng.*, vol. 28, no. 4, pp. 443–458, Oct. 2004.

[55] X. Yu, N. Mingyang, W. Zhang, S. Yongxin, and Q. Shuo, "Analysis and experiments of the thermal–optical performance for a kinematically mounted lens element," *Appl Opt 53*, 2014.

[56] W. Rudin, *Principles of Mathematical Analysis*, 3rd Edition. McGraw-Hill, 1976.

[57] H. S. M. Coxeter and S. L. Greitzer, *Geometry Revisited*. MAA, 1967.

[58] N. J. A. Sloane, "A000041 - OEIS," *The On-line encyclopedia of integer sequences*. [Online]. Available: https://oeis.org/A000041. [Accessed: 23-Mar-2016].

[59] E. W. Weisstein, "Permutation Matrix." [Online]. Available: http://mathworld.wolfram.com/PermutationMatrix.html. [Accessed: 26-Mar-2016].

[60] S. Henein, *Conception des structures articulées à guidages flexibles de haute précision*. Lausanne: EPFL, 2000.

[61] A. van Beek, *Advanced Engineering Design: Lifetime Performance and Reliability*. TU Delft, 2006.

[62] "Technical resources for fasteners | Bossard Group." [Online]. Available: http://www.bossard.com/en/application-engineering/technical-resources.aspx. [Accessed: 01-Dec-2015].

[63] "Tohnichi Torque Technical Data." [Online]. Available: http://www.tohnichi.com/torque-technical-data.asp. [Accessed: 01-Dec-2015].

[64] A. Küng, F. Meli, and R. Thalmann, "Ultraprecision micro-CMM using a low force 3D touch probe," *Meas. Sci. Technol.*, vol. 18, no. 2, p. 319, 2007.

[65] *The European Magazine: And London Review*. Philological Society of London, 1789.

[66] S. Henein, F. Barrot, S. Jeanneret, L. Giriens, M. Gumy, S. Droz, and M. Toimil, "Silicon Flexures for the Sugar-Cube Delta Robot," presented at the EUSPEN 2011, 2011.

[67] S. Henein, F. Barrot, A. Dommann, P. Walter, P. Schwab, S. Droz, C. Verjus, and T. Overstolz, "Silicon flexure-based micro-balance for batch weighing," presented at the EUSPEN, San Sebastian, 2009.

[68] "Dividing Engine | Time and Navigation." [Online]. Available: http://timeandnavigation.si.edu/multimedia-asset/dividing-engine. [Accessed: 12-May-2016].

[69] J. Ramsden, Description of an engine for dividing mathematical instruments. London : Commissioners of Longitude, 1777.

[70] L. C. Hale and A. H. Slocum, "Optimal design techniques for kinematic couplings," Precis. Eng., vol. 25, no. 2, pp. 114–127, Apr. 2001.

[71] J. B. Hopkins, J. J. Vericella, and C. D. Harvey, "Modeling and generating parallel flexure elements," Precis. Eng., vol. 38, no. 3, pp. 525–537, Jul. 2014.

Curriculum Vitae

Johan Kruis

Rue des Berthoudes 70, Apt. 13	Nationality: Dutch
2000, Neuchâtel (NE) Switzerland	Date of Birth: August 10, 1987
johankruis@hotmail.com	Marital status: Single

Education

2012 - 2016	**CSEM & EPFL - Swiss Center for Electronics and Microtechnology & Swiss Federal Institute of Technology in Lausanne** (Switzerland), Doctoral school: Microsystems and Microelectronics
2009 - 2011	**TU/E - Eindhoven University of Technology in Eindhoven** (the Netherlands), M.Sc. in Mechanical Engineering, specialization Micro and Nano Scale Engineering
2008 - 2009	**TU/E - Eindhoven University of Technology in Eindhoven** (the Netherlands), Pre-master program Mechanical Engineering
2004 - 2008	**Fontys - Fontys University of Applied Sciences in Eindhoven** (the Netherlands), B.Eng. in Mechanical Engineering, specialization: Mechanical Design and Innovation
1999 - 2004	**WereDi - Havo in Valkenswaard** (the Netherlands), specialization: Science & Technology, extra subject: Computer Science

Employment History

	CSEM & EPFL - Ph.D. thesis in Neuchâtel (Switzerland), Precision Mechanisms group (CSEM) and Patek Philippe Chair in Micromechanical and Horological Design (Instant-Lab)
March 2012 until August 2016	A thesis concerning novel kinematic interfaces for two- and three-body systems requiring micron-level position repeatability. The results are an exhaustive solution catalogue, a set of necessary conditions, various silicon metal and 3D Printed demonstrators, including the experimental verification.
	Three side projects for the watch industry. Subjects: Patent research (2 months), Spring design (3 months), Silicon attachment design (1 month).
September 2010 until December 2011	**TU/e & EPFL - Master thesis in Eindhoven and Lausanne** (the Netherlands and Switzerland), Micro and Nano Scale Engineering lab (MNSE at TU/E) and robotic systems laboratory (LSRO2 at EPFL)
	The design, realization and testing of an actuated lens suspension for high dynamics micron resolution 3D printing in glass using a femtosecond laser.

April 2010 until July 2010	**TU/e - Master internship in Eindhoven** (the Netherlands), Constructions and Mechanisms Group
	An analytical optimization of five designs for a mechanical touch probe for 3D position measurements with submicron accuracy.
January 2008 until June 2008	**ASML - Bachelor thesis in Veldhoven** (the Netherlands)
	Design of a test-rig for lifetime testing the alignment contacts of the wafer handling robot in a vacuum environment.
February 2007 until July 2007	**Philips Applied Technologies – Bachelor internship in Eindhoven** (the Netherlands)
	An optimization study of a novel ablation-free manufacturing process for lens-arrays in polymers using a Nd-YAG laser.
	References available upon request

Patent & Publications

Patent:

- Kruis J. et al., "Method for freeing a micromechanical part and a micromechanical part comprising sacrificial fasteners", WO2013093108 A1, 27-Jun-2013.

First author publications:

- Kruis J. et al., "6 DOF repeatability measurement setup for measuring position of assembled silicon parts with nanometric resolution", EUSPEN 2015, Leuven.

- Kruis J. et al., "Mesoscale Systems for Medical and Surgical Applications", Atelier SMYLE 2013, Besançon.

- Kruis J. et al., "Design and fabrication of a novel centimeter scale three dimensional silicon tip, tilt and piston mirror mechanism", EUSPEN 2013, Berlin.

- Kruis J. et al., "Design of a miniature laser scanning head for high-bandwidth, low-amplitude beam steering", ISOT 2012, Paris.

Third author publication:

- Cosandier F. et al., "A three device silicon based platform for micro-assembly and characterization", EUSPEN 2016, Nottingham.

Skills

Languages: Dutch (native), English (fluent), French (fluent B2), German (B1), Spanish (A2)

Software: Solidworks, Unigraphics, Matlab, Mathematica, Comsol, NX Nastran, ANSYS, Microsoft Office.

Hobbies & Interests

- Bouldering, Hiking, Badminton, Skiing
- Board games, Role playing games
- Piano